

Determining the role of ASPM in human brain size regulation.

Maram Aljuhni

Submitted in accordance with the requirements for the degree of
Doctor of Philosophy

The University of Leeds

School of Medicine

Department of Ophthalmology and Neuroscience

May, 2019

The candidate confirms that the work submitted is her own and that appropriate credit has been given where reference has been made to the work of others

This copy has been supplied on the understanding that it is copyright material and that no quotation from the thesis may be published without proper acknowledgement

© 2019 The University of Leeds
and Maram Aljuhni

Acknowledgements

My sincerest gratitude is toward my principle supervisor, Dr. Jacquelyn Bond, for giving me the opportunity to work on this interesting and vital project. Her knowledge and experience accompanied with continuous guidance have had a considerable impact on the completion of this thesis at all levels.

I would like to express my special thanks towards my co-supervisors Dr. Sandra Bell and Dr. Ewan Morrison for their assistance and encouragement provided throughout the course of this study.

I am very grateful toward my country, The Kingdom of Saudi Arabia, for providing me with the financial assistance and my family for their continued support, this study would not have been possible without their support.

It is my pleasure to thank all the staff and students who provided a friendly and supportive environment which in turn had a great impact on the progress of this study.

Abstract

Autosomal recessive primary microcephaly (MCPH) is a disease consisting of a small brain and associated intellectual disability. The most common cause of MCPH is mutation of the abnormal spindle-like micro tubule-associated gene (*ASPM*, formerly known as abnormal spindle-like microcephaly-associated gene) at the *MCPH5* locus. This thesis studies the function of *ASPM*, mitotic alterations due to homozygous *ASPM* mutation and identifies *ASPM* C-terminal interactants.

ASPM siRNA KD studies confirmed previously identified roles for *ASPM* in spindle pole focusing, spindle/cleavage furrow orientation, spindle assembly and cytokinesis. Roles for *ASPM* in maintaining nuclear and centrosome structure, centrosome biogenesis, mitotic progression, microtubule organisation, and abscission were identified as being microtubule associated. A novel role for *ASPM* in actin organisation was identified. In *MCPH5* patient fibroblast cells carrying the homozygous nonsense *ASPM* mutation *3663delG*, a low level of full length *ASPM* protein was observed suggesting transcriptional read-through was occurring. *ASPM*^{3663delG} was mis-localised to the cytoplasm suggesting it has a reduced ability to either travel to the mitotic spindle pole or become associated at the pericentrosomal matrix. In the patient fibroblast cells carrying *ASPM*^{3663delG} and *ASPM*^{9984+1G>T} homozygous mutations microtubule defects caused a variety of aberrant mitotic phenotypes which induced an increase in the duration of mitosis. These defects included prometaphase (*ASPM*^{3663delG}) or metaphase (*ASPM*^{9984+1G>T}) arrest, spindle mis-orientation and abscission failure and a decrease in the incidence of proliferation. Therefore MCPH arises

from a combination of mitotic abnormalities rather than a single aberration, which together result in a reduction in neural progenitor cell number. It is proposed that the single *MCPH5* small brain phenotype arising in patients carrying homozygous nonsense *ASPM* mutations may be the result of transcriptional read-through.

ASPM C-terminus has been shown to be required for *ASPM* spindle pole localisation, microtubule organisation and cytokinesis. Microtubule actin cross-linking factor 1 (MACF1) was identified as a candidate *ASPM* interacting protein from a yeast-2 Hybrid screen of the *ASPM* C-terminus against a foetal brain cDNA library. The MACF1-*ASPM* association was validated by co-immunoprecipitation (co-IP). MACF1 was shown to be associated with microtubules during interphase and was dependent upon *ASPM* for this localisation. MACF1 mitotic localisation was consistent with *ASPM* localisation at the minus ends of spindle microtubules and pericentrosomal matrix from prometaphase to early telophase. In patient cells carrying an *ASPM* C-terminal mutation MACF1 protein levels were proportional to *ASPM* expression. The alteration in the *ASPM*-MACF1 association due to *ASPM* mutation or *ASPM* reduction may account for the changes in actin organisation, microtubule associated forces, spindle mis-orientation and abscission observed in this research study.

Table of Contents

Acknowledgements	I
Abstract	II
Table of Contents	IV
List of Figures.....	VII
List of Tables	XII
Abbreviations.....	XIII
Chapter 1 : General introduction.	1
1.1. Neurogenesis.....	1
1.2. Microcephaly.....	6
1.3. Yeast 2-hybrid (Y2H) assay to identify protein interactions.....	37
1.4. Hypothesis and Aims	40
Chapter 2 : Materials and methods	42
2.1. Cell culture.....	42
2.2. Immunofluorescence (IF) and microscopy.....	47
2.3. Cryptic splice site investigation	50
2.4. Determination of protein expression by Immunoblotting.....	53
2.5. Protein interaction studies.....	57
2.6. Statistical analysis.....	58
Chapter 3 : Investigation into the effect of siRNA mediated <i>ASPM</i> knockdown upon mitosis.....	59
3.1 Introduction	59
3.2 Hypothesis	60
3.3 Objectives.....	60
3.4 Methods	61

3.5 Results.....	62
3.6 Discussion.....	95
Chapter 4 : Comprehensive analysis of the effect of <i>ASPM</i> mutation upon cellular mitosis.	104
4.1 Introduction	104
4.2 Hypothesis.	106
4.3 Objectives.	106
4.4 Methods	107
4.5 Results.....	108
4.5.5.1.2 Analysis of the effect of <i>ASPM</i> mutations on interphase microtubule distribution.	127
4.6 Discussion	151
Chapter 5 : Investigation of Novel <i>ASPM</i> -C-terminal interacting partners.	164
5.1 Introduction	164
5.2 Hypothesis.	174
5.3 Objectives.	174
5.4 Methods	174
5.5 Results.....	175
5.6 Discussion	206
Chapter 6 : Final conclusion and future work	216
Future work.....	225
Chapter 7 : References	229
Chapter 8 : Appendix.....	257

Appendix 1: Primary Antibodies employed in this project.	257
Appendix 2: Secondary Antibodies employed in this project.....	258
Appendix 3: The expression of ASPM in paraformaldehyde fixed cell.	259
Appendix 4: Homo sapiens - abnormalspindles vs Human Fetal Brain_RP1 Results Summary.....	260

List of Figures

Figure 1.1: Neurogenesis in human brain development.....	3
Figure 1.2: Symmetric and Asymmetric cell division is mitotic spindle orientation-dependant.	6
Figure 1.3: Sketch of the head circumference measurement of an unaffected child compared to a child of similar age, sex and ethnic background with microcephaly.	8
Figure 1.4: MRI images of microcephalic brain in patients with <i>MCPH5</i> mutation.	12
Figure 1.5: Genomic structure of ASPM.....	17
Figure 1.6: ASPM protein domain organisation Putative functional domains are shown;	20
Figure 1.7: ASPM distribution and localisation. Confocal images of U2OS cells.	23
Figure 1.8: CITK, NuMA and UBE3A regions involved in the interaction with ASPM C-terminus (CTR).	34
Figure 1.9: Schematic of the Yeast-two-Hybrid system.....	39
Figure 3.1: <i>ASPM</i> siRNA mediated KD leads to a significant reduction in ASPM protein level.....	63
Figure 3.2: ASPM protein cellular localisation in U2OS cells during interphase, mitosis and cytokinesis.	64
Figure 3.3: <i>ASPM</i> siRNA mediated KD causes a reduction of ASPM protein level in the nucleus and cytoplasm during interphase.....	66
Figure 3.4: <i>ASPM</i> siRNA mediated ASPM KD knocks down the ASPM protein at the spindle pole during metaphase.	67
Figure 3.5: 72 hr <i>ASPM</i> siRNA treatment efficiently decreases ASPM protein at the midbody during cytokinesis.	68
Figure 3.6: <i>ASPM</i> siRNA mediated ASPM KD in U2OS cells causes aberrant interphase nuclei.....	70

Figure 3.7: <i>ASPM</i> siRNA mediated KD results in interphase centrosomal alterations.	73
Figure 3.8: <i>ASPM</i> siRNA mediated KD induced low density, disorganised and clustered microtubules.	75
Figure 3.9: <i>ASPM</i> siRNA mediated KD induced redistribution of the actin network.	78
Figure 3.10: <i>ASPM</i> siRNA mediated KD induced increase in centrosomes number during mitosis and decrease in mitotic cell number.	81
Figure 3.11: <i>ASPM</i> siRNA mediated KD results in decrease in cell division and increase in frequency of prometaphase-metaphase cells.	83
Figure 3.12: <i>ASPM</i> siRNA mediated KD using U2OS cells induces mitotic spindle misorientation leading to an increase in asymmetric cell division.	86
Figure 3.13: <i>ASPM</i> siRNA mediated KD in U2OS cells induces an increase in the time taken to complete each stage of mitosis and in the occurrence of apoptosis.	88
Figure 3.14: <i>ASPM</i> siRNA mediated KD Histone H2B-GFP HeLa cells results in metaphase arrest and cytokinesis failure and causes aberrant nuclear interphase phenotype.	92
Figure 4.1: Effect of <i>ASPM</i> mutations <i>ASPM</i> ^{3663delG} and <i>ASPM</i> ^{9984+1T>G} on <i>ASPM</i> protein size and level of expression.	111
Figure 4.2: The <i>ASPM</i> 3663delG mutation does not result in the generation of a cryptic splice donor site in exon 15.	113
Figure 4.3: <i>ASPM</i> protein cellular localisation in <i>ASPM</i> ^{WT} fibroblast cells during interphase, metaphase and cytokinesis.	115
Figure 4.4: Analysis of <i>ASPM</i> localization in patient fibroblast cells during interphase.	117
Figure 4.5: Analysis of <i>ASPM</i> localization in patient fibroblasts during metaphase.	119
Figure 4.6: Analysis of <i>ASPM</i> integral intensity at the spindle poles of <i>ASPM</i> ^{WT} and <i>ASPM</i> ^{3663delG} fibroblast cells.	120
Figure 4.7: Analysis of <i>ASPM</i> localisation in <i>ASPM</i> ^{3663delG} and <i>ASPM</i> ^{9984+1T>G} cells in comparison to <i>ASPM</i> ^{WT} cells during cytokinesis.	122

Figure 4.8: Analysis of interphase nuclear, microtubule and centrosomal phenotypes of <i>ASPM</i> ^{WT} fibroblast cells.	124
Figure 4.9: Effect of <i>ASPM</i> mutations on nuclear interphase phenotypes.	126
Figure 4.10: Effect of <i>ASPM</i> mutations on MT organization.....	128
Figure 4.11: Analysis of the effect of <i>ASPM</i> mutations on actin structure and distribution.....	131
Figure 4.12: Effect of <i>ASPM</i> mutations on centrosome number and centrosome structure during interphase.	133
Figure 4.13: Analysis of nuclear, spindle pole, centrosome and microtubule organisation in <i>ASPM</i> ^{WT} fibroblast cells during mitosis.	134
Figure 4.14: Analysis of the effect of <i>ASPM</i> mutations on spindle pole number during prometaphase.	137
Figure 4.15: Analysis of the effect of <i>ASPM</i> mutations on spindle pole number and position during anaphase and telophase.	140
Figure 4.16: Analysis of the effect of <i>ASPM</i> mutations on cytokinesis.....	143
Figure 4.17: Analysis of the effect of <i>ASPM</i> mutations on frequency of mitosis and mitotic stage distribution.....	145
Figure 4.18: Analysis of the effect of <i>ASPM</i> mutations on division orientation and period of mitosis explored by live cell imaging.	148
Figure 5.1 <i>ASPM</i> C-terminal Y2H bait design.	165
Figure 5.2. A schematic representation of the full-length SRGAP2 protein and isoforms showing the active domains.	170
Figure 5.3. A schematic representations of full-length GCC2 protein with binding domains..	171
Figure 5.4. A schematic diagram of full-length MACF1 Wild-type protein with binding domains.....	173
Figure 5.5: Expression of <i>ASPM</i> in a panel of human cell lines by western blot.	177
Figure 5.6: Protein levels of <i>ASPM</i> in a panel of human cell lines by optimised <i>ASPM</i> western blot.	178

Figure 5.7: Protein levels of SRGAP2 in a panel of human cell lines determined by western blotting.	179
Figure 5.8 Protein levels of GCC2 in a panel of human cell lines by Western blot.	180
Figure 5.9: Identification by WB of MACF1 protein level in a panel of human cell lines.	182
Figure 5.10: Total protein levels of SRGAP2 in <i>MCPH5</i> patient cell lines measured by WB are significantly lower in lysates from <i>MCPH5</i> patient cell lines than in control cell lines.	184
Figure 5.11: Expression of MACF1 in HDF Neo and <i>MCPH5</i> patient cell lines detected by western blot.	186
Figure 5.12: ASPM C-terminal fragments for GST pull downs design.	188
Figure 5.13: GST Western blot of GST-ASPM C-terminal fragment fusion protein expression.	189
Figure 5.14: GST-ASPM pull down for SRGAP2 in synchronized.	191
Figure 5.15: Co-IP of ASPM and MACF1 in U2OS cells and HDF Neo cell and patient cell line lysates.	194
Figure 5.16: Co-IP of ASPM and MACF1 in <i>ASPM</i> siRNA mediated KD U2OS cell lysates.	195
Figure 5.17: Mitotic localisation of MACF1 in untreated U2OS cells.	197
Figure 5.18: MACF1 localises to the pericentrosomal matrix of the metaphase spindle pole.	198
Figure 5.19: MACF is decreased and redistributed in <i>ASPM</i> siRNA treated interphase U2OS cells.	199
Figure 5.20 MACF1 is associated with the MTs but is reduced in <i>ASPM</i> siRNA U2OS cells.	200
Figure 5.21: MACF1 and α -tubulin were absent from the Flemming body but remained in the central spindle of <i>ASPM</i> siRNA treated U2OS cells during cytokinesis.	201
Figure 5.22: Comparison of MACF1 localization and intensity WT and patient fibroblast cells in interphase.	203

Figure 5.23: MACF1 localization in *ASPM*^{WT}, *ASPM*^{9984+1T>G} and *ASPM*^{3663delG} cells during metaphase is mostly associated with the MT.....204

Figure 5.24: MACF1 and α -tubulin were absent from the midbody in *ASPM*^{3663delG} and *ASPM*^{9984+1T>G} cells during late telophase and cytokinesis. 205

Figure 8.1: ASPM is expressed at the periphery of a proportion of PFA fixed interphase U2OS cells.....262

List of Tables

Table 1.1: Disorders that cause congenital or postnatal microcephaly. Examples of genetic and syndromic disorders and pathologies which cause primary microcephaly.	9
Table 1.2: Disorders that cause congenital or postnatal microcephaly. Examples of genetic and syndromic disorders and pathologies which cause secondary microcephaly.	10
Table 1.3: MCPH loci and the associated <i>MCPH</i> genes.	14
Table 3.1: Comparison of the effect of siRNA mediated ASPM depletion on mitotic spindle position and cytokinesis in <i>ASPM</i> siRNA, RNAiMAX, <i>NT1</i> siRNA treated U2OS cells.	88
Table 3.2: The correlation between mitotic phenotypes and nuclear outcomes in <i>ASPM</i> siRNA, RNAiMAX, <i>NT1</i> siRNA treated HeLa cells.	94
Table 4.1: Comparison of interphase phenotype analysis between <i>ASPM</i> ^{WT} , <i>ASPM</i> ^{3663delG} and <i>ASPM</i> ^{9984+1T>G} cells.	149
Table 4.2: Comparison of mitotic phenotype analysis between <i>ASPM</i> ^{WT} , <i>ASPM</i> ^{3663delG} and <i>ASPM</i> ^{9984+1T>G} cells.	150
Table 4.3: Comparison of cytokinesis phenotype between <i>ASPM</i> ^{WT} , <i>ASPM</i> ^{3663delG} and <i>ASPM</i> ^{9984+1T>G} cells.	150
Table 5.1: ASPM C-terminal interactant list using Y2H screen ranked by confidence rating.	168
Table 5.2. The relative intensity (RI) of protein bands in arbitrary units (AU) after normalization to the density of β -actin (loading control).	182
Table 6.1: summary table of all cell lines and proteins used for each assay in this investigation.	228

Abbreviations

Ab	Antibody
ASP	Drosophila abnormal spindle, orthologue to ASPM
ASPM	Abnormal Spindle-like Microcephaly associated
bp	Base pair
BSA	Bovine serum albumin
CCD	charge-coupled device
CH	Calponin homology
CITK	Citron kinase
co-IP	Co-immunoprecipitation
C-Terminal	Carboxy terminal
°C	Degree centigrade
ddH ₂ O	Sterile distilled deionized water
DEPC	Diethylpyrocarbonate
dH ₂ O	Sterile distilled water
DMEM	Dulbeccos Modified Eagles Media
DMSO	Dimethyl sulfoxide
DNA	Deoxyribonucleic acid
dNTP	Deoxyribonucleotide triphosphate
DTT	Dithiothreitol
ECACC	European Collection of Authenticated Cell Cultures
EDTA	Ethylenediaminetetraacetic acid
FCS	Foetal calf serum
GCC2	GRIP and coiled-coil domain-containing protein2
GST	Glutathione-S-Transferase
HCl	Hydrochloric acid
HEPES	N-2-Hydroxyethylpiperazine-N-2-ethane sulphonic acid
hr	Hour

IF	Immunofluorescence
IQ	Isoleucine Glutamine
Kb	Kilobase pair
L	Litre
LDS	Lithium dodecyl sulphate
MACF1	Microtubule-actin cross-linking factor
MCPH	Autosomal recessive primary microcephaly
MT	Microtubule
MW	Molecular weight
min	Minutes
NaCl	Sodium chloride
ng	Nanogram
nm	Nanometre
NPC	Neuroprogenitor cell
NP40	Nonidet P-40
NSC	Neural stem cell
N-Terminal	Amino terminal
NuMA	Nuclear mitotic apparatus
OFC	Occipito-frontal head circumference
OD	Optical density
PBS	Phosphate buffer saline
PCR	Polymerase chain reaction
PEG	Polyethylene glycol
PFA	Paraformaldehyde
RNA	Ribonucleic acid
rpm	Revolutions per minute
RT	Room Temperature
RT-PCR	Reverse transcriptase PCR
s	Seconds

SD	Standard deviations
SDS	Sodium dodecyl sulphate
SDS-PAGE	Sodium dodecyl sulphate-polyacrylamide gel electrophoresis
siRNA	Short Interfering RNA
SRGAP2	SLIT-ROBO Rho GTPase-activating protein 2
T25/T75	25cm ² and 75cm ² tissue culture flasks
TAE	Tris acetate EDTA buffer
TBS	Tris Buffered Saline
TGN	Trans-Golgi network
TE	Tris (hydroxymethyl) aminoethane-ethylene diamine tetracetic acid
Trp	Tryptophan
UV	Ultraviolet
WB	Western Blotting
WT	Wild type
Y2H	Yeast two-hybrid

Chapter 1 : General introduction.

1.1. Neurogenesis.

Neurogenesis is a highly controlled developmental process by which neurons are generated via neural stem cells (NSCs). Neurogenesis takes place in all eukaryotes with the exception of Placozoa and Porifera (Kandel *et al.*, 2000).

Neurogenesis in mammalian brain development

Homo sapiens brain is a complex organ that made up from specialized nerves and together with spinal cord makes up the central nervous system (Drake *et al.*, 2004). Human brain has three major divisions, each has a vital function (Chédotal *et al.*, 2010). The three major parts of human brain are: the forebrain (including the cerebrum, thalamus and hypothalamus), midbrain (including various cranial nerve nuclei) and hindbrain (including medulla, pons and cerebellum) (Figure 1.1A) (Nieuwenhuys *et al.*, 2014). The forebrain is the largest region of the brain composed of cerebral cortex that serves as the outer layer of the cerebrum. Human brain size is considered relatively larger compared to most other animal families (Evans *et al.*, 2004) which is mainly resulted from the increase of the lateral expansion instead of increasing of the cortex thickness that folds and ridges to form gyri and sulci that can fit in the skull (Zhang *et al.*, 2016). The cerebral cortex is divided lengthwise into a left and right hemisphere which are connected by a thick cable-like bundle of nerve fibers called the corpus callosum for left-right hemisphere communication. Each of the two hemispheres consist of four lobes: frontal, temporal, parietal and occipital (Drake *et al.*, 2004; Palastanga *et al.*, 2006). Each lobe has a specific

function involved in the movement and sensory processes such as somatosensory perception (touch), vision, hearing and other critical functions such as memory, language, reasoning, emotion, intellect and personality (Palastanga *et al.*, 2006).

The central nervous system including brain and spinal cord is the largest part of the complex nervous system that controls most bodily and mental functions (Bueno, *et al* 2016). The central nervous system of vertebrates and invertebrates is developed from a single cell layer composed of neural stem cells (NSCs) that have the ability to proliferate, obtain area characteristics and differentiate into different cell types (Paridaen, *et al* 2014; Homem *et al.*, 2015; Sun *et al.*, 2017). NSC types are; neuroepithelial cells (NECs) which have the ability to potentially give rise to neurons, and radial glial cells (RGCs) that self-renew and give rise to glia and neurons. Neurons and glia are the building blocks of the central nervous system (Bergström *et al*, 2012; Götz *et al.*, 2015). Most neurons and glia are produced early during embryonic development in a series of steps called neurogenesis and gliogenesis respectively (Urbán *et al.*, 2014). The neurogenesis process in mammals is highly regulated throughout early embryonic neural development frequently up until early postnatal stages, nevertheless it persists in adult with low production in certain areas in the brain called germinal regions or neurogenic niches (stem cells activity regulators) (Ming Song, 2011). Based on their location, young born neurons migrate toward a proper distant positions to differentiate and participate in central nervous system development (Sidman *et al*, 1973; Jiang *et al*, 2016; Dudok *et al.*, 2017). Various types of functional neurons in human embryonic brain are produced in week three of brain development via neuroepithelial cells (early

stem cells) that line the ectoderm (germ layer) as a single sheet. These primary progenitors elongate apically and basally to form bipolar cells known specifically as RGC that generate large numbers of highly specialized undivided neurons (Zhang *et al.*, 2008; Arai *et al.*, 2017). Neurogenesis in the adult brain takes place in two germinal regions; the subventricular zone (SVZ) which is situated subjacent to the lateral ventricle, and in the subgranular zone (SGZ) which is located within the dentate gyrus of the hippocampus between the hilus and the granular cell layer (Figure 1.1B) (Bond *et al.*, 2015). Radial glial cells proliferate at a lower rate and for longer periods than early embryonic NSCs to give rise to highly specialized neurons that contribute to the striatum in the SVZ zone and dentate gyrus in the SGZ zone (Urbán *et al.*, 2014).

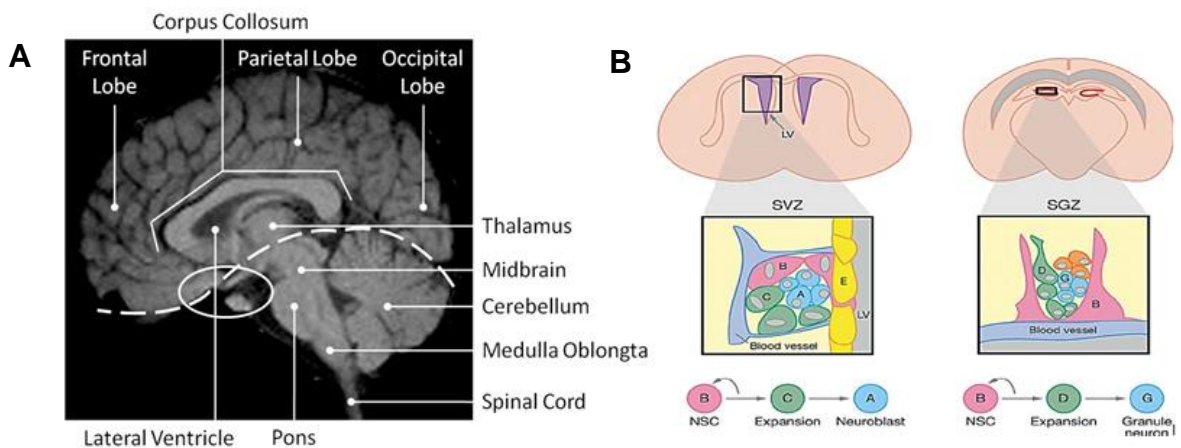


Figure 1.1: Neurogenesis in human brain development. **A.** drawing displaying different structures within the human brain using magnetic resonance imaging of 11-year-old female brain. The midbrain and hindbrain (below) are separated from the forebrain by dotted line *adapted from* (Bond *et al.*, 2002). **B.** Neurogenesis in brain of adult humans. Neural stem cell (B) in the subventricular zone (SVZ) and the subgranular zone (SGZ) lining the ependymal cells (E) differentiate to give rise to transient expanding cells (C) which in turn further produce neuroblast cells (A) and granule neuron (G) respectively *adapted from* (Li *et al.*, 2005).

Symmetric and asymmetric neural cell division

Neural stem cells have a unique characteristic in their ability to self-replicate, yet they also have the ability to differentiate irreversibly into progeny (Doe, et al., 2008; Chen et al., 2013; Tweedellet et al., 2017). The division of neuroepithelial cells is distinctive in terms of determining the fate of cells which regulate nervous system development and function (Egger *et al.*, 2010). In general, there are two distinct types of cell division by which neuroepithelial cells proliferate and differentiate: These are symmetric and asymmetric cell division (Willardsen, et al., 2011; Paridaenet al., 2014). Based on the type of division, the progenitor pool is either maintained at the same size and the brain is developed or the progenitor pool is expanded (Santoro *et al.*, 2016). Symmetric (proliferative) division increases progenitor cell number by giving rise to two identical progenitor cells (Hardwick *et al.*, 2015). However asymmetric (neurogenic) cell division maintains precursor cell number by generating one progenitor cell and contributes to the formation of the brain by producing one post mitotic neuron which migrates to the required layer of the developing brain (Gómez *et al.*, 2014; Xu *et al.*, 2017). At the onset of neurogenesis during embryonic brain development, primary neuroepithelial cells divide symmetrically at the ventricular surface to increase stem cell pools. However, later in brain development NPCs undergo asymmetric cell division to generate neurons that migrate to form the layers of the developing brain (Hardwick *et al.*, 2015).

The type of NPC division performed is dependent upon the orientation of the mitotic spindle and subsequent cleavage furrow positioning (Figure 1.2) with respect to the apical-basal polarity of neuroepithelial cells (Uzquiano *et al.*,

2018). In proliferative divisions, the division plane cleaves parallel to this polarity axis, whereas in neurogenic divisions the division plane cleaves perpendicular to the polarity axis (Knust et al., 2007; Egger et al., 2008; Ragkousi et al., 2014; Matsuzaki et al., 2015). In *Drosophila* the orientation of the mitotic spindle and positioning of the cleavage furrow were already identified to determine the type of cell division in neuroblasts (Betschinger et al., 2003; Rolls et al., 2003) and intestinal stem cells (Goulas et al., 2012; Guo Ohlstein, 2015) and in intestinal stem cells in mice (Clevers, et al., 2013). The balance between the number of symmetric and asymmetric divisions and therefore the orientation of the mitotic spindle and cleavage furrow is key to the resulting size of the brain (Wilcock et al., 2007; Uzquiano et al., 2018). Several studies revealed a correlation between spindle orientation defects and human diseases, particularly diseases of the brain (Fish, et al., 2006; Godin et al., 2010; Higgins et al., 2010; Lizarraga et al., 2010). One approach to explore the connection between spindle orientation defects and developmental brain disorders is to study autosomal recessive primary microcephaly (MCPH), a condition where the size of the developing brain and therefore prenatal head circumference is significantly reduced.

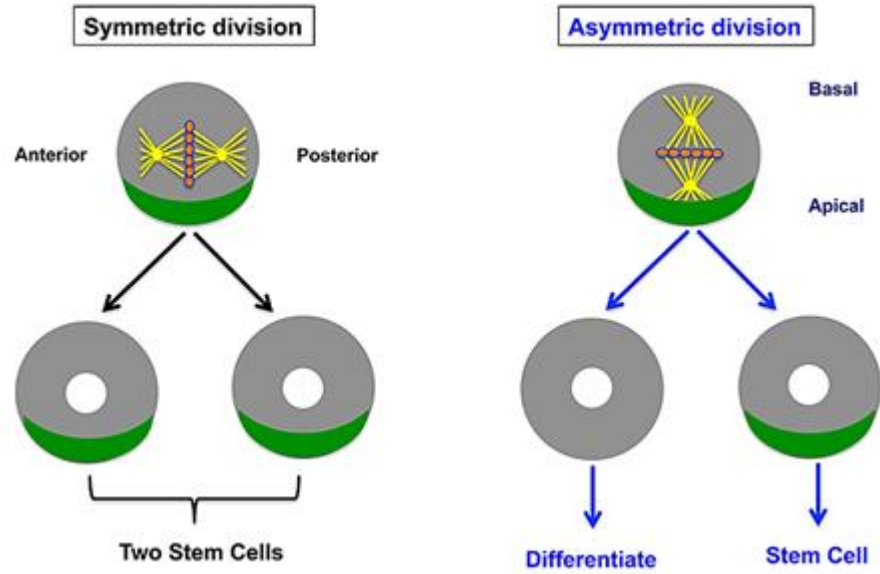


Figure 1.2: Symmetric and Asymmetric cell division is mitotic spindle orientation-dependant. The symmetrical division produce 2x identical stem cells when the mitotic spindle is oriented perpendicular to the polarity axis. Asymmetric division forms 1x stem cells and 1x non-mitotic neuron when the mitotic spindle is oriented parallel to the polarity axis taken from (Berika *et al.*, 2014).

1.2. Microcephaly.

Microcephaly is a medical condition in which the brain does not grow appropriately resulting in a smaller brain and therefore smaller head (circumference) than normal (Figure 1.3). It is associated with mild to severe mental retardation and usually a delay in motor and speech function (Passemaid *et al.*, 2013). Microcephaly is clinically identified by a reduced head circumference, which can be diagnosed using occipitofrontal circumference (OFC). Moderate microcephaly is defined as head circumference more than two standard deviations (SD) (Hanzlik *et al.*, 2017) and severe microcephaly is defined as head circumference more than three SD (Harris *et al.*, 2015) below the ethnic, sex and age matched mean (Vinken *et al.*, 1969) and in some cases

resulting in a value ranged from 4 to 14 SD below the mean (Bond, et al., 2002). In the general population the occurrence of microcephaly is around 2% (mild/moderate) and 0.1% (severe microcephaly) (Hanzlik et al., 2017). Microcephaly pathogenesis is heterogeneous. It can result from genetic alterations or an intrauterine infection in the early stages of pregnancy, the result of, for instance, rubella, toxoplasmosis (a parasite), cytomegalovirus (CMV, HHV-5) or Zika virus that can interfere with brain growth and development (Panchaud *et al.*, 2016). Alternative reasons for microcephaly encompass considerable exposure to X-rays within the first and second trimester of pregnancy, or foetal exposure to alcohol (Zuccolo *et al.*, 2016).

Microcephaly can be primary (congenital microcephaly) which is present at birth, can be genetic or non-genetic and can be diagnosed using ultrasound scan (La Torre *et al.*, 2006); or secondary microcephaly, that develops after birth (Woods, 2004; Leibovitz *et al.*, 2016). Primary microcephaly can be caused by genetic factors and malformations occurring during embryonic development such as in Amish lethal microcephaly and holoprosencephaly (Table 1.1), reviewed by (Naveed *et al.*, 2018). The consequences of the small brain are neurodevelopmental defects leading to impaired learning and memory function (Jayaraman *et al.*, 2018). Secondary microcephaly is characterized by postnatal normal head size but a failure of subsequent development such as in GLUT1 deficiency syndrome-1 and Rett syndrome (Table 1.2) (Opitz *et al.*, 1990; Harris *et al.*, 2015).

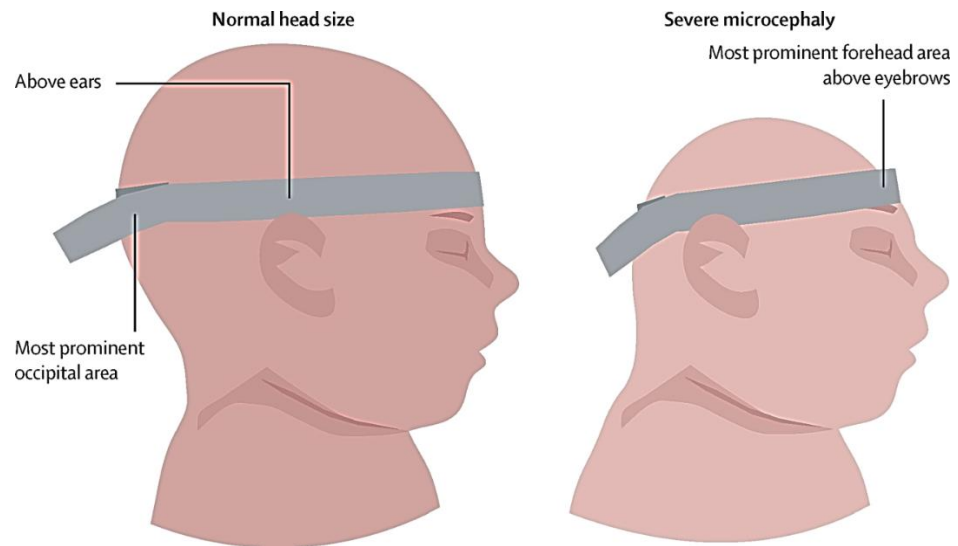


Figure 1.3: Sketch of the head circumference measurement of an unaffected child compared to a child of similar age, sex and ethnic background with microcephaly. The head circumference was measured using a measuring tape that cannot be stretched. Left, a child with typical head size and right, a child with microcephaly. Picture adapted from (Devakumar *et al.*, 2018).

Table 1.1: Disorders that cause congenital or postnatal microcephaly. Examples of genetic and syndromic disorders and pathologies which cause primary microcephaly.

Disorder characterised by a primary microcephaly	Chromosome	Gene	Description	Ref, MIM #
Holoprosencephaly 1; HPE1	21q22.3	<i>HPE1, CDON</i>	Human forebrain malformation that causes primary microcephaly and failure in cerebral hemisphere separation.	(Collins <i>et al.</i> , 1993; Walsh, 1999) #236100
Microlissencephaly 1;	17p13.3	<i>TUBA1A, NDE1</i>	Group of rare brain disorders that cause primary microcephaly and seizures	(Pilz <i>et al.</i> , 1999; Kato e Dobyns, 2003) #607432
Microcephaly, Amish Type; MCPHA	17q25.1	<i>SLC25A19</i>	Severe autosomal recessive metabolic disorder that causes extreme microcephaly, increase in the urinary organic acid 2-ketoglutarate and early death.	(Kelley <i>et al.</i> , 2002; Rosenberg <i>et al.</i> , 2002) #607196
Nijmegen Breakage Syndrome; NBS	8q21.3	<i>NBS1</i>	Known as Berlin breakage syndrome. Autosomal recessive congenital chromosomal instability syndromes that cause primary microcephaly, immunodeficiency and growth retardation	(Weemaes <i>et al.</i> , 1981; Saar <i>et al.</i> , 1997) #251260
Primary Autosomal Recessive Microcephaly	23 genetic loci with 1q31.3, 8p23.1 being the most common	<i>ASPM, MCPH1</i>	Primary microcephaly. Mutation in these genes cause diminished brain size.	(Bond <i>et al.</i> , 2002b; Trimborn <i>et al.</i> , 2004; Woods <i>et al.</i> , 2005a) *605481, *607117
Schizencephaly	10q26.11, 7q36.3	<i>COL4A1, EMX2, SHH</i>	An extremely rare congenital birth defect that causes primary microcephaly, psychomotor retardation and polymicrogyria.	(Brunelli <i>et al.</i> , 1996; Walsh, 1999) #269160

Disorder characterised by a secondary microcephaly	Chromosome	Gene	Description	Ref, MIM #
Basal Ganglia Calcification, Idiopathic, Childhood-Onset; IBGC	14q	Absence of Calcium or parathyroid hormone	Congenital neuropsychiatric disorder that causes microcephaly and hypertonicity of the muscles.	(Hallervorden, 1950; Geschwind <i>et al.</i> , 1999) %114100
GLUT1 Deficiency Syndrome 1; GLUT1DS1	1p34.2	SLC2A1	Neurologic genetic metabolic disorder affecting the nervous system that causes acquired microcephaly and spasticity.	(Wang <i>et al.</i> , 2000; Pascual <i>et al.</i> , 2004) #606777
Rett Syndrome; RTT	Xq28	MECP2	Rare neurodevelopmental disorder that causes microcephaly and seizures	(Ferlini <i>et al.</i> , 1990; Moog <i>et al.</i> , 2003) #312750

Table 1.2: Disorders that cause congenital or postnatal microcephaly. Examples of genetic and syndromic disorders and pathologies

Autosomal Recessive Primary Microcephaly (MCPH).

Autosomal recessive primary microcephaly (MCPH) is a rare neurodevelopmental disorder. MCPH is a congenital disorder, arising due to recessive mutations in genes. It is a congenital autosomal recessive syndrome, which is distinguished by a decrease in the size of the brain, particularly affecting the cerebral cortex of the brain (Aicardi, et al., 1998). It occurs early during pregnancy with static developmental aberrations (Qazi et al., 1973; Rosenberg *et al.*, 2002; Mahmood *et al.*, 2011). MCPH results in intellectual disability as a result of the substantial reduction in the functional capacity of a small brain, which is generally mild to moderate, but can be a severe disability (Barbelanne et al., 2014). The most affected part of the brain is the cerebral cortex which displays a substantial reduction in size (Figure 1.4) (Zaqout *et al.*, 2017). Magnetic resonance imaging (MRI) of MCPH patients revealed a normal central nervous system architecture, with a simplified anterior gyral pattern and no sign of a neuronal migration disorder (NMD) (Bond *et al.*, 2002; Vermeulen *et al.*, 2010).

Individuals with MCPH display an OFC of >3 standard deviations below the ethnically matched, age and sex related mean (Roberts, *et al.*, 2002; Pulvers *et al.*, 2015). The decrease in head circumference (HC) is reported to be detectable using ultrasound by week 32 of pregnancy (La Torre *et al.*, 2006). Initially, the clinical diagnostic phenotype that characterised MCPH was microcephaly with no evidence of other neurological disorders such as epilepsy or seizures (Jackson *et al.*, 2002; Roberts, *et al.*, 2002). However after the discovery of multiple MCPH genes it was reported that a higher frequency of

seizures and epilepsy was seen in individuals with some genetic forms of MCPH (Shen *et al.*, 2005; Woods *et al.*, 2005). The majority of affected individuals have a belated grasp of language and speech proficiency. Motor capabilities like walking, sitting and standing are also impaired (Genetics Home Reference, 2014). The offspring of consanguineous relationships, such as those from Northern Pakistan, Jordan, Saudi Arabia and the Yemen (Bond *et al.*, 2002), are at increased risk of MCPH due to gene mutations inherited from a common ancestor (Bond *et al.*, 2003; Woods *et al.*, 2005).

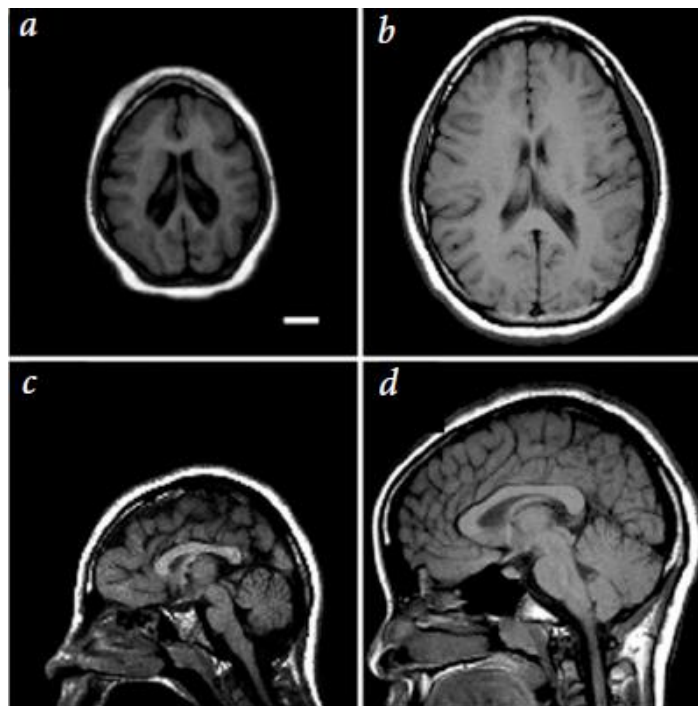


Figure 1.4: MRI images of microcephalic brain in patients with *MCPH5* mutation. Axial (a) and Sagittal (c) brain images from a 13-year-old female with *MCPH5* mutations. Axial (b) and Sagittal (d) brain images from a 11-year-old female with normal brain development (control) adapted from (Bond *et al.*, 2002).

1.2.2 Molecular Genetics of MCPH.

Individuals diagnosed with MCPH have recessive genetic mutations inherited from parents who each have one copy of a mutated gene but do not demonstrate MCPH signs or symptoms (Kloepfer *et al.*, 1964; Faheem *et al.*, 2015). Initially, MCPH was mapped by homozygosity in 5 recessive loci that were associated with primary microcephaly in different families (Jamieson *et al.*, 1999; Jamieson *et al.*, 2000; Pattison *et al.*, 2000). To date, at least 23 *MCPH* genes (*MCPH* loci 1-23) have been identified: (in order) Microcephalin, *WDR62*, *CDK5RAP2*, *CASC5*, *ASPM*, *CENPJ*, *STIL*, *CEP135*, *CEP63*, *CEP152*, *PHC1*, *CDK6*, *ZNF335*, *SASS6*, *MFSD2A*, *ANKLE2*, *CIT*, *WDFY3*, *COPB2*, *KIF14*, *NCAPD2*, *NCAPD3* and *NCAPH* (Jackson *et al.*, 1998; Jamieson *et al.*, 1999; Pattison *et al.*, 2000; Ohta *et al.*, 2002; Roberts, *et al.*, 2002; Hung *et al.*, 2004; Bond *et al.*, 2005; Kumar *et al.*, 2009; Nicholas *et al.*, 2009; Bilguvar *et al.*, 2010; Kaindl, 2014), see Table 1.3. Most of these MCPH proteins are associated with the centrosome or pericentrosomal matrix during mitosis, play critical roles in centriolar biogenesis or duplication, mitosis and cytokinesis (Evans *et al.*, 2005) and affect cell-cycle checkpoints (Sir *et al.*, 2011). The most common cause of MCPH is mutation of the Abnormal Spinde-like Microcephaly associated (*ASPM*) gene at the *MCPH5* locus. *ASPM* mutations represent 40-50% of MCPH cases in the Northern Pakistani population (Roberts, *et al.*, 2002; Zhong *et al.*, 2005). It has been suggested that MCPH arises due to a decrease in neural progenitor cell number (Bond *et al.*, 2002).

Table 1.3: MCPH loci and the associated MCPH genes.

Locus	Chromosome	Gene	Protein	Location	Proposed Function	References
MCPH1	8p23.1	<i>MCPH1</i>	Microcephalin	Nucleus/ Chromatin/ centrosome	DNA repair, chromosome condensation and telomerase repression	(Jackson <i>et al.</i> , 1998; Jackson <i>et al.</i> , 2002; Trimborn <i>et al.</i> , 2004; Lin, S. Y. <i>et al.</i> , 2005; O'driscoll <i>et al.</i> , 2006; Peng <i>et al.</i> , 2009; Shi <i>et al.</i> , 2012)
MCPH2	19q13.12- q13.2	<i>WDR62</i>	WD-repeat- containing protein 62	Nucleus, centrosomal during mitosis	Mitotic progression	(Bilguvar <i>et al.</i> , 2010; Nicholas <i>et al.</i> , 2010; Yu <i>et al.</i> , 2010; Kousar <i>et al.</i> , 2011; Novorol <i>et al.</i> , 2013; Chen <i>et al.</i> , 2014; Xu <i>et al.</i> , 2014)
MCPH3	9q33.2	<i>CDK5RAP2/ CEP215</i>	Cyclin-dependent kinase 5 regulatory subunit-associated protein 2	Centrosome/ Midbody	Microtubule function, maturation of centrosome and spindle checkpoint function	(Moynihan <i>et al.</i> , 2000; Bond <i>et al.</i> , 2005; Graser <i>et al.</i> , 2007; Fong <i>et al.</i> , 2008; Fong <i>et al.</i> , 2009; Zhang <i>et al.</i> , 2009)
MCPH4	15q15- q21.1	<i>CASC5/ KNL1</i>	Cancer susceptibility candidate 5	Centrosome	Kinetochores assembly, spindle assembly checkpoint function and chromosome segregation	(Jamieson <i>et al.</i> , 1999; Genin <i>et al.</i> , 2012; Ghongane <i>et al.</i> , 2014)
MCPH5	1q31.3	<i>ASPM</i>	Abnormal spindle- like, microcephaly associated protein	Peri- centrosomal/ Midbody	Spindle and cleavage furrow orientation, cytokinesis, spindle assembly, mitotic progression, differentiation and, dsDNA break repair and is a positive regulator of Wnt signalling	(Pattison <i>et al.</i> , 2000; Bond <i>et al.</i> , 2002; Bond <i>et al.</i> , 2003a; Kouprina, N., Pavlicek, A., Collins, N. K., Nakano, M., Noskov, V. N., Ohzeki, J., <i>et al.</i> , 2005; Zhong <i>et al.</i> , 2005; Fish, Kosodo, <i>et al.</i> , 2006; Van Der Voet, , <i>et al.</i> , 2009; Higgins <i>et al.</i> , 2010; Buchman <i>et al.</i> , 2011; Kato <i>et al.</i> , 2011; Kim <i>et al.</i> , 2011; Singhmaret al., 2011; Xu <i>et al.</i> , 2012; Novorol <i>et al.</i> , 2013; Connolly <i>et al.</i> , 2014; Fujimori <i>et al.</i> , 2014)
MCPH6	13q12.12	<i>CENPJ/ CPAP</i>	Centromeric protein J	Centrosome/ Midbody	Centriole length, microtubule assembly and spindle positioning	(Leal <i>et al.</i> , 2003; Hung <i>et al.</i> , 2004; Chen, <i>et al.</i> , 2006; Schmidt, <i>et al.</i> , 2009; Buchman <i>et al.</i> , 2011; Tang <i>et al.</i> , 2011; Lee <i>et al.</i> , 2014)
MCPH7	1p33	<i>STIL</i>	SCL/TAL1-	Peri-	Control of cell cycle and	(Kumar <i>et al.</i> , 2009; Kitagawa <i>et al.</i> , 2011;

			interrupting locus protein	centrosomal	organization of spindle, pro-centriole formation	Tang <i>et al.</i> , 2011)
MCPH8	4q12	<i>CEP135</i>	Centrosomal protein 135kD	Centrosome	Microtubule organization and centriole structure	(Ohta <i>et al.</i> , 2002; Hussain <i>et al.</i> , 2012; Roque <i>et al.</i> , 2012)
MCPH9	15q15-q21.1	<i>CEP152</i>	Centrosomal protein 152kD	Centrosome	Centriole duplication and assembly	(Guernsey <i>et al.</i> , 2010; Sir <i>et al.</i> , 2011; Brown <i>et al.</i> , 2013; Sonnen <i>et al.</i> , 2013)
MCPH10	3q22.2	<i>CEP63</i>	Centrosomal protein 63kD	Centrosome	Centriole biogenesis, centrosome localization and genome maintenance	(Loffler <i>et al.</i> , 2011; Brown <i>et al.</i> , 2013)
MCPH11	12p13.31	<i>PHC1</i>	Polyhomeotic-like protein 1	Nucleus	Involved in maintaining transcriptional repression of many genes via chromatin remodelling and histone modification	(Awad <i>et al.</i> , 2013)
MCPH12	7q21.2	<i>CDK6</i>	Cyclin dependent kinase 6	Centrosome	Cell cycle control	(Hussain <i>et al.</i> , 2013)
MCPH13	20q13.12	<i>ZNF335/NIF-1</i>	Zinc Finger Protein 335	Centrosome	Targeting and stability of the H3K4 methyltransferase complex. Post-mitotic neuronal differentiation regulator	(Yang <i>et al.</i> , 2012)
MCPH14	1p21.2	<i>SASS6</i>	Centriolar Assembly Protein	Centrioles	Play roles in centrosome duplication and procentriole development	(Khan <i>et al.</i> , 2014); (Kleylein-Sohn <i>et al.</i> , 2007)
MCPH15	1p34.2	<i>MFSD2A</i>	Major Facilitator Superfamily Domain-Containing Protein 2a	Plasma membrane	Sodium-dependent tunicamycin transporter	(Angers <i>et al.</i> , 2008); (Reiling <i>et al.</i> , 2011)
MCPH16	12q24.33	<i>ANKLE2</i>	Ankyrin Repeat-And Lem Domain-Containing Protein 2.	Endoplasmic Reticulum membrane (ERM)	Links chromatin with the nuclear envelope.	(Asencio <i>et al.</i> , 2012); (Ishikawa <i>et al.</i> , 1998)
MCPH17	12q24.23	<i>CIT</i>	Citron Rho-Interacting Serine/Threonine Kinase.	central spindle/ Midbody	Regulator of cytokinesis.	(Basit <i>et al.</i> , 2016); (Di Cunto <i>et al.</i> , 1998)

MCPH18	4q21.23	<i>WDFY3</i>	Wd Repeat- And Fyve Domain-Containing Protein 3	Nucleus and cytoplasm	Autophagy regulator.	(Deretic, 2010); (Yamamoto Simonsen, 2011)
MCPH19	3q23	<i>COPB2</i>	Coatomer Protein Complex, Subunit Beta-2	Cytoplasm	Regulates cell proliferation/required for Golgi budding	(Distasio <i>et al.</i> , 2017); (Mi <i>et al.</i> , 2018)
MCPH20	1q32.1	<i>KIF14</i>	Kinesin Family Member 14	Nucleus /Midbody	Mitotic spindle formation and Cytokinesis	(Gruneberg <i>et al.</i> , 2006); (Smith <i>et al.</i> , 2010)
MCPH21	12p13.31	<i>NCAPD2</i>	Non-Smc Condensin I Complex Subunit D2	Nucleus/ Cytoplasm	Condensin complex regulator	(Kimura <i>et al.</i> , 2001); (Schmiesing <i>et al.</i> , 2000)
MCPH22	11q25	<i>NCAPD3</i>	Non-Smc Condensin li Complex Subunit D3	Nucleus	Condensin-2 complex	(Kittler <i>et al.</i> , 2004); (Ono <i>et al.</i> , 2003)
MCPH23	2q11.2	<i>NCAPH</i>	Non-Smc Condensin I Complex Subunit H	Nucleus/ Cytoplasm	Condensin complex regulator	(Kimura <i>et al.</i> , 2001); (Martin <i>et al.</i> , 2016)

1.2.2.1 ASPM (Abnormal Spindle Microcephaly associated) gene.

1.2.2.1.1. The ASPM gene.

Homozygous mutations in the Abnormal Spindle-like Microcephaly-associated gene (*ASPM*) gene at the *MCPH5* locus on chromosome 1q31 was identified as the most common cause of MCPH (Pattison *et al.*, 2000; Bond *et al.*, 2002; Roberts, *et al.*, 2002; Nicholas *et al.*, 2009). The human *ASPM* is the orthologue of the *Drosophila* gene, *abnormal spindles (asp)* (Ripoll, *et al.*, 1985). In terms of structure, the *ASPM* gene is composed of 28 exons with an open reading frame (ORF) consisting of a 10434bp long coding sequence (CDS) ([NCBI GenBank](#) accession number [AF509326](#)). The *ASPM* gene covers 62kb of genomic DNA at 1q31. Exon 3 covers 1486bp and exon 18 covers 4755bp, between them covering the majority of the genes coding region. (Bond *et al.*, 2003) (Figure 1.5).

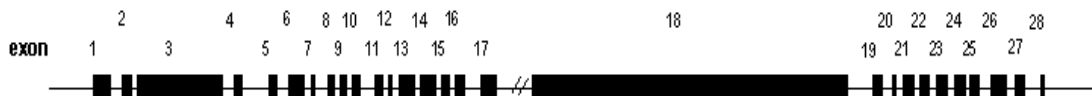


Figure 1.5: Genomic structure of ASPM. The exon intron structure is shown with size approximately equal to number of base pairs contained in the exon. Adapted from (Bond *et al.*, 2002).

The transcript of putative ASPM is identified to be alternatively spliced to produce several isoforms with different domains that expected to have potentially different functions (Kouprina, *et al.*, 2005). Further to the existing predicted full-length mRNA of 10434bp, Kouprina *et al* identified three mRNAs with ORFs of 5678, 4259 and

3189 bp using RT-PCR. Consequently, these transcript variants of ASPM encoding at least three different isoforms containing 1892, 1389 and 1062 amino acid respectively. These isoforms have different numbers of IQ motifs and are conserved in the human and mouse. However further investigation is required to study the functions of the detected ASPM isoforms.

1.2.2.1.2. Mutations in the ASPM gene

Using positional cloning of the *MCPH5* locus (Pattison *et al.*, 2000) and sequencing (Bond *et al.*, 2002) of *MCPH5*-related genes, the *ASPM* gene was identified on chromosome 1q31. To date, more than 120 different mutations have been reported in about 140 families around the world (Bond *et al.*, 2002; Bond *et al.*, 2003; Kumar *et al.*, 2004; Pichon *et al.*, 2004; Shen *et al.*, 2005; Desir *et al.*, 2006; Gul *et al.*, 2006; Nicholas *et al.*, 2009; Akbariazar *et al.*, 2013; Ariani *et al.*, 2013; Papari *et al.*, 2013; Hussain *et al.*, 2013; Hu *et al.*, 2014; Hashmi *et al.*, 2016; Bhargav, 2017). The mutations are spread throughout the gene and there does not appear to be a mutation hotspot within *ASPM*. The types of mutations include: nonsense mutations (Cherkaoui *et al.*, 2018), insertions and deletions causing frame shifts, splice site mutations (Bond *et al.*, 2003), a translocation or a recombination event (Pichon *et al.*, 2004; Verloes *et al.*, 2013) and an exception of one missense mutation altering a single IQ repeat (Gul *et al.*, 2006). Most of the identified mutations were predicted to result in protein truncation resulting in the common lack of a vital C-terminal region, instability of the truncated ASPM protein, nonsense mediated decay of *ASPM* mRNA resulting in no ASPM protein or, in

some exceptions, a low level of transcriptional read-through allowing a much-reduced production of full length ASPM protein (Bond *et al.*, 2003; Nicholas *et al.*, 2009; Higgins *et al.*, 2010). Some mutations such as c.9984+1G>T (splice site mutation) and c.3663delG (frameshift mutation) were predicted to result in protein truncation (Bond *et al.*, 2003). However, immunoblotting analysis of patient fibroblast cell lysates and sequencing of patient cDNA for both mutations identified the production of some approximately full length protein and no truncated proteins were detected (Higgins *et al.*, 2010). Homozygous mutation, IVS25+1G>T, had previously been detected in *MCPH5*-linked families of Northern Pakistani origin, was found to encode truncated ASPM protein lacking 3 amino acids from the C-terminus. The loss of these residues are sufficient to cause MCPH, suggesting a vital role for this region in normal ASPM function (Bond *et al.*, 2002; Bond *et al.*, 2003).

1.2.2.1.3. ASPM protein domain structure.

Protein domains are structural units of a given protein sequence. They may represent distinct structures that are commonly used to characterise proteins and assess their functional roles. The *ASPM* gene encodes a 3477 amino acid protein of molecular weight 410kDa. Bioinformatics analysis (Bond *et al.*, 2002) identified the most recognizable domain structures in ASPM. These domains are: a putative N-terminal microtubule (MT) binding domain, unique tandem putative calponin-homology (CH) domains, a large block of 81 Isoleucine–Glutamine (IQ) motifs, a single Armadillo-like region (ALR) and a C-terminal region (Figure 1.6) (Bond *et al.*,

2002; Bond *et al.*, 2003; Kouprina, *et al.*, 2005; Higgins *et al.*, 2010). Further investigation to ASPM structure has identified ASPM as a member of a novel family of ASH (ASPM, SPD-2, Hydin) domains, ASPM is connected to ASH family via N-terminus domain (Ponting, *et al.*, 2006; Schou *et al.*, 2014; Verdier *et al.*, 2016). The domains are present in a complex proteins together with other ciliary proteins and associated with cilia, flagella, the centrosome and the Golgi complex (Ponting, *et al.*, 2006), suggesting roles for ASPM in ciliary and flagellar function.

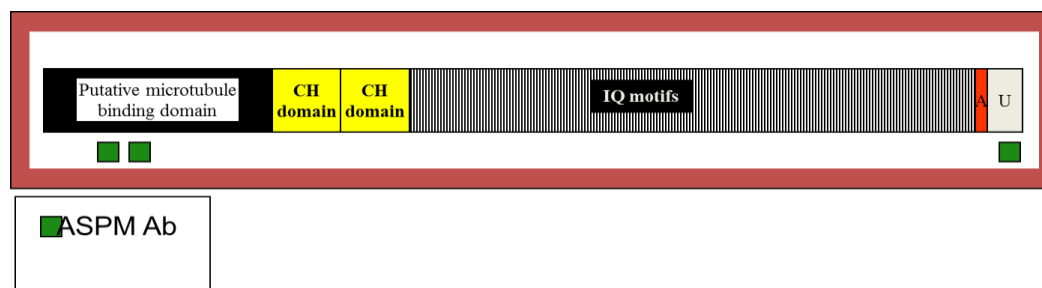


Figure 1.6: ASPM protein domain organisation Putative functional domains are shown; A is the Armadillo-like domain, U is an undefined functional region at the C-terminus of the protein. The location of the sequences to which the ASPM-specific antibodies used in this work were raised are shown in green.

A GFP-tagged fragment of the *N*-terminus of ASPM, the first 940 amino acids, expressed in rat localized to centrosomes and the spindle poles during mitosis (Paramasivam, *et al.*, 2007). The calponin homology (CH) domains are typically actin binding domains. They were detected at the *N*-terminus of a protein called calponin and consist of around 100 amino acids in 4 alpha helices (Castresana *et al.*, 1995). CH domains are commonly found in actin binding proteins (Winder *et*

al., 1993; Korenbaum et al., 2002). The 81 IQ motifs in human were identified by sequencing of *ASPM* (Bond et al., 2002; Kouprina, et al., 2005). The IQ motifs are composed of 20-25 amino acids and are anticipated to undergo a conformational change when bound to calmodulin (Saunders, et al., 1997; Craig et al., 1998; Rhoads et al., 2005). The differences in IQ motif number among different species are significant, with an increase in brain size apparently related to an increase in the number of IQ repeats (*C. elegans* 2 IQ, *Drosophila* 24 IQ, mouse 67 IQ, chimpanzee 74 IQ and in human 81 IQ motifs) (Bond et al., 2002; Kouprina, et al., 2005). However, the presence of conserved IQ motifs amongst different species suggests they play a crucial role in *ASPM* function (Kouprina, et al., 2005). The IQ motifs may mediate a protein conformational change that controls actin binding to the *N*-terminal and CH domains via an interaction between IQ motifs and the CH domains (Winder et al., 1995; Bähler et al., 2002).

1.2.2.1.4. Mitotic Distribution of *ASPM*

ASPM is a protein with a clear mitotic function and its role during neurogenesis has been investigated extensively *in vitro* and *in vivo* (Bond et al., 2002; Kouprina, et al., 2005; Zhong et al., 2005; Higgins et al., 2010; Capecchi et al., 2015). In interphase, *ASPM* is localized mainly to the nucleus and centrosome (Zhong et al., 2005). After nuclear envelope breakdown, from prometaphase to early telophase, *ASPM* redistributes to the spindle poles (Figure 1.7). During cytokinesis *ASPM* is predominantly positioned at the centre of the midbody, a localisation associated

with its C-terminal region (CTR) (Higgins *et al.*, 2010). ASPM interacts directly with several proteins through its C-terminus, including nuclear mitotic apparatus protein (NuMA) (Seldin *et al.*, 2013). NuMA interacts with the dynein/dynactin complex (motor protein) (Lechler *et al.*, 2005) which are thought to generate the force needed to enable transport of ASPM along the spindles to the midbody during cytokinesis. However, further investigations to identify involvement of this complex in ASPM transportation is necessary.

The localisation and distribution pattern of ASPM in human cells has been consistent using different cell lines including: HT1080 cells (Kouprina, *et al.*, 2005), U2OS cells (Zhong *et al.*, 2005; Higgins *et al.*, 2010) and HeLa cells (Paramasivam, *et al.*, 2007; Higgins *et al.*, 2010). The localisation pattern of ASPM is similarly conserved among other species including: *Aspm* localisation in mouse embryonic neuroepithelial (NE) cells (Fish, *et al.*, 2006) and *Asp* localisation in *Drosophila larval* neuroblasts (Saunders, *et al.*, 1997; Wakefield *et al.*, 2001; Riparbelli *et al.*, 2002). During cell division (from prometaphase to early telophase) ASPM localizes to the spindle poles and is also associated with the minus ends of spindle MT bundles where it is thought to stabilise them (Higgins *et al.*, 2010; Jiang *et al.*, 2017). This localisation pattern is in agreement with *Aspm* localisation in mouse (Xu, *et al.*, 2012), *Drosophila* (Saunders, *et al.*, 1997; Wakefield *et al.*, 2001; Morales *et al.*, 2005; Ito, *et al.*, 2015) and in *C. elegans* (Van Der Voet, *et al.*, 2009).

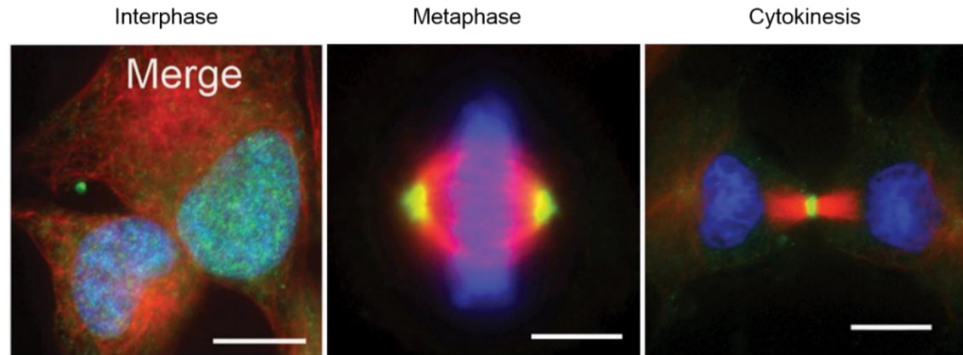


Figure 1.7: ASPM distribution and localisation. Confocal images of U2OS cells immunofluorescently labelled with DAPI (blue, DNA), ASPM (green) and α -tubulin (red, microtubules). ASPM is predominantly localised to the nucleus in interphase (Scale bar = 10 μ m), to the spindle poles and central spindle during mitosis (Scale bar = 5 μ m) and localized at the midzone of the central spindle during late telophase (Scale bar = 10 μ m). Adapted from (Higgins *et al.*, 2010).

1.2.2.1.5. *ASPM* expression in development and cancer

Aspm expression in developing mouse brain was detected through *in situ* hybridization and Northern blot analysis (Bond *et al.*, 2002; Fish, *et al.*, 2006). *Aspm* expression was noted within the neuroepithelium in the cerebral cortical ventricular zone and the ventricular zone of the dorsal diencephalon of the developing brain as mid-neurogenesis occurred (E14, E16; E=embryonic day) and illustrated to be postnatally down regulated (Bond *et al.*, 2002). In another study using *in situ* hybridization of the murine embryonic forebrain, *Aspm* mRNA was detected in most of the ventricular zone (VZ) in the cerebral cortex during early stages of neurogenesis. The expression of *Aspm* was intense when NPCs were

undergoing symmetric (proliferative) divisions. On the other hand, *Aspm* expression was greatly reduced at later stages of neurogenesis when NPCs switched to asymmetric (neurogenic) divisions (Fish, *et al.*, 2006). During fetal development, *Aspm* mRNA was detected by *in situ* hybridization in other developing organs such as the thymus, epidermis, perichondrium and metanephric tubules on day E16.5 (Luers *et al.*, 2002) and in the liver, heart, lung and kidney on day E14 (Kouprina, *et al.*, 2005). In the adult, *Aspm* mRNA was detected in mouse testis, ovary and spleen (Luers *et al.*, 2002). A similar expression pattern for human *ASPM* was obtained using RT-PCR analysis (Kouprina, *et al.*, 2005). Human *ASPM* was highly regulated in the vast majority of human embryonic tissues, however the level of expression was much lower in adult tissues and was below the detection limit in the brain (Kouprina, *et al.*, 2005).

Human *ASPM* expression was found to be upregulated in a variety of malignant tissues. Upregulation of *ASPM* was associated with an increase in tumour grade and a decrease in the survival rate of a variety of cancer types, indicating an important involvement of *ASPM* in tumourigenesis (Alsiary *et al.*, 2014). Analysis of *ASPM* expression revealed upregulation in ovarian, uterine cancers (Kouprina, *et al.*, 2005; Brüning *et al.*, 2011), malignant glioma (Horvath *et al.*, 2006; Bikeye, *et al.*, 2010), in primary and metastatic prostate cancer (PCA) (Xie *et al.*, 2017; Pai *et al.*, 2018), hepatocellular carcinoma (Lin *et al.*, 2008; Wang *et al.*, 2017) and invasive breast carcinoma (Zhong *et al.*, 2005; Shubbar *et al.*, 2013). *ASPM* is well known for its function in cell division as a mitotic protein. However, whether this also explains its oncogenic role remains under investigation.

1.2.2.1.6. ASPM functional studies.

Human ASPM is an interesting MCPH candidate to be explored since its structural and localisation pattern are conserved among other species (Saunders, *et al.*, 1997; Wakefield *et al.*, 2001; Riparbelli *et al.*, 2002; Fish, *et al.*, 2006). Fragment of the *N*-terminus of mutated *asp* in *Drosophila* embryo caused severe loss of microtubule focus at spindle poles *in vivo* during mitosis, suggesting an essential role of the *N*-terminus in spindle pole focusing (Do Carmo., *et al.*, 1999). These findings support a conserved role of the *N*-terminal region of ASPM as a microtubule binding domain. The CH domains in murine *Aspm* are required for mitotic spindle function, while a defective gene in fission yeast prevented bipolar spindle formation and disrupted the S/M checkpoint (Craig *et al.*, 1998). The CH domains and IQ motifs within ASPM may therefore act as crucial regulators of ASPM interactions during mitosis (Kouprina, *et al.*, 2005). Furthermore, the C-terminal region of ASPM (CTR) has a conserved armadillo-like repeat domain and an undefined domain. However, most common *ASPM* mutations are thought to lead to the synthesis of a truncated protein lacking the CTR, suggesting a crucial role for this region during in mitosis and neurogenesis.

Mutations in *ASPM* lead to the formation of a small but architecturally normal brain indicating that ASPM is involved in regulating cerebral cortical size via maintenance of proliferative divisions of neuroprogenitor cell (NPC) (Bond *et al.*, 2002). *Aspm* mutant mice show mild microcephaly and loss in the germline (due to

a severe reduction in testis and ovary size) as a result of a truncated form of *Aspm* protein excluding the CTR, similar to those which cause microcephaly in humans. The truncated *Aspm* fails to localize to the midbody in M-phase, supporting previous findings that ASPM is involved in regulating cerebral cortical size via defects in neural progenitor proliferation (Pulvers *et al.*, 2010) as well as confirming that ASPM is functionally similar in mice and humans. In addition to this, knockdown of *Aspm* at an early stage of brain development (E15) and a later stage of brain development (E19) in the developing mouse brain was studied. The depletion of *Aspm* resulted in a decrease in neural progenitor cell number in proliferative regions and at the cortical plate (CP), the final destination for newly born neurons. This indicated the importance of ASPM in maintaining proliferation of NPCs (Buchman *et al.*, 2011). In keeping with these roles, ASPM functions at the cellular level have been identified. Using siRNA *ASPM* knockdown, a function for ASPM in preserving symmetrical cell division through the maintenance and orientation of the cleavage furrow was found (Fish, *et al.*, 2006; Higgins *et al.*, 2010). Murine *Aspm* knockdown using siRNAs in NPCs resulted in its delocalisation from centrosomes during mitosis, a change in the vertical cleavage plane orientation of NE cells, an early switch from symmetric to asymmetric cell division and a reduction in the number of proliferative cells in the ventricular zone (Fish, *et al.*, 2006). This is consistent with an ASPM role in the maintenance of symmetric neural progenitor divisions which have a great impact on the regulation of brain size. In human, siRNA-mediated *ASPM* knockdown caused cytokinesis failure and cell death (Higgins *et al.*, 2010). In *Drosophila*, mutation in *Asp* leads to

disruption or incorrect organisation of the contractile ring that drives the cleavage process, resulting in a failure to complete cytokinesis, indicating a requirement for Asp in this process (Wakefield *et al.*, 2001; Riparbelli *et al.*, 2002). Roles for ASPM in spindle assembly, spindle organization and spindle orientation have been shown (Paramasivam, *et al.*, 2007; Van Der Voet, *et al.*, 2009; Higgins *et al.*, 2010; Xu *et al.*, 2012; Connolly *et al.*, 2014) suggesting ASPM is vitally involved in mitotic spindle function. ASPM as a microtubule minus end-associated protein is thought to autonomously regulate the minus ends of central spindle microtubules (Jiang *et al.*, 2017). Upon MT depolarisation ASPM staining is lost indicating that MTs are required for ASPM recruitment to the spindle poles (Higgins *et al.*, 2010; Tungadi *et al.*, 2017). In *Drosophila*, the microtubule minus ends at the spindle poles are focused, stabilised and cross-linked as a result of direct binding of asp to the MTs via the N-terminal region, the region corresponding to the microtubule-binding domain (Saunders, *et al.*, 1997; Ito, 2015; Schoborg *et al.*, 2015). However and upon *asp* depletion during cell division *in vivo*, spindle poles were un-focused during mitosis, confirming ASPM as a spindle pole-focusing factor. Specifically, Asp contributes to pole focusing during mitosis, a process where the microtubule minus ends at the spindle poles become focused toward the two poles, giving the typical shape of the mitotic spindle (Ripoll, *et al.*, 1985; Saunders, *et al.*, 1997; Do Carmo *et al.*, 1999; Do Carmo *et al.*, 2001). In addition to the potential role of ASPM in spindle pole focusing, experiments involving *Aspm* morpholinos have shown *Aspm* to be involved in mitotic progression beyond prometaphase (Kim *et al.*, 2011; Novorol *et al.*, 2013). Murine *Aspm* knock out studies using

immunohistochemistry and morphometry suggested *Aspm* was required for the migration and differentiation of NPCs (Fujimori *et al.*, 2014). In addition, roles for ASPM in influencing DNA double strand break repair and Wnt signalling have been suggested (Buchman *et al.*, 2011; Kato *et al.*, 2011). The loss of Wnt signaling caused by *Aspm* shRNA knockdown was rescued by expression of stabilized CTNNB1 (β -catenin), which is a core downstream component of the Wnt signalling cascade (Buchman *et al.*, 2011). Finally, the involvement of ASPM with the ASH domains in cilia, flagella, the centrosome and the Golgi complex (Ponting, *et al.*, 2006; Schou *et al.*, 2014; Verdier *et al.*, 2016), indicates that ASPM may play crucial roles in cilia-mediated neuronal migration. Thus, mutation or depletion of ASPM in cilia might be responsible for reduced head size in primary microcephaly due to disruption of neuronal migration (Mochida *et al.*, 2013).

1.2.2.1.7. Interactants of ASPM

Further studies into elucidating and understanding the function of ASPM have included identifying the potential functioning proteins that interact with ASPM CTR.

1.2.2.1.7.1. Citron kinase (CITK)

Citron kinase (CITK) directly interacts with the ASPM CTR (Figure 1.8A). Encoded by the *CIT* gene, CITK is an enzyme that functions in the later stages of cytokinesis. Using yeast two hybrid (Y2H) system and overlay assays (Madaule *et al.*, 1995) and immunoprecipitation (IP) (Di Cunto *et al.*, 1998), CITK was originally identified as a putative binder to the GTP-bound forms of rho and rac1 in mouse.

CITK in humans is a 240 kDa protein with a complex structure contains of more than 2000 amino acids long. It consists of an *N*-terminal domain, 2 long coiled-coil structures forming a Rho/Rac binding domain, a PH domain, and the *C*-terminus (D'avino, et al., 2017). CITK in humans is present in two isoforms, Citron-N lacking the kinase domain and Citron-K containing the kinase domain. Citron-N was first discovered by Madaule in 1998 for its ability to interact with GTP-bound Rho and Rac (Madaule *et al.*, 1995) and its function remains unidentified. It is shorter than Citron-K and its expression is restricted to neuronal tissues with a localisation to postsynaptic densities (Furuyashiki *et al.*, 1999). On the other hand, Citron-K, also referred to as CRIK, consists of an *N*-terminal extension containing a serine/threonine kinase domain. It is widely expressed in different tissues and proliferating cells (Di Cunto *et al.*, 1998). The expression of CITK in mice is widely recognised throughout the neuraxis during embryogenesis (Di Cunto *et al.*, 2000). CITK is expressed throughout the cell cycle; it is localised to the nucleus and distributed as aggregates in the cytoplasm in interphase cells (Eda *et al.*, 2001), and accumulates at the cleavage furrow and midbody ring during cytokinesis (Madaule, *et al.*, 1998; Kosako *et al.*, 2000). These data provide suggest that CITK and ASPM have a functional overlap.

The first ever protein that was found to correlate with the localisation pattern and function of ASPM was CITK (Di Cunto *et al.*, 2000; Paramasivam, *et al.*, 2007). Though, contrary to ASPM, CITK does not localise to the centrosomes or spindle poles during mitosis, suggesting a specific relationship between ASPM and CITK during cytokinesis (Madaule, *et al.*, 1998). CITK co-localizes with ASPM at the

cytokinesis furrow and midbody ring, is required for abscission (Paramasivam, *et al.*, 2007) and plays a role in cytokinesis furrow ingression (Madaule, *et al.*, 1998). The ASPM-CTR was co-immunoprecipitated with CITK from HeLa cell lysates confirming an association between ASPM and CITK (Paramasivam, *et al.*, 2007). Similarly, *in situ* proximity ligation assay (PLA), a method used to detect protein-protein closeness, detected an interaction between ASPM and CITK (Gai, *et al.*, 2016). CITK and ASPM have the same localisation pattern during cytokinesis and upon their mutation or deletion cause spindle orientation defects, cytokinesis failure, apoptosis and eventually microcephaly (Higgins *et al.*, 2010; Li *et al.*, 2016; Bianchi *et al.*, 2017). CITK mutation in mammals (Bianchi *et al.*, 2017) and *Drosophila* (Naim *et al.*, 2004) causes defective cytokinesis suggesting the wild-type function of CITK is required for progenitor cells to complete cytokinesis. In addition, CITK knockout in *Drosophila* caused a primary microcephaly associated with chromosomal instability, cytokinesis failure and increased apoptosis in neural progenitors (Bianchi *et al.*, 2017). Further studies of the *flathead* mutation in rats revealed the importance of CITK for neuronal progenitors to complete cytokinesis *in vivo*. A recessive mutation in the gene encoding CITK in the *flathead* rat resulted in cytokinesis failure followed by apoptosis that eventually led to a substantial growth reduction in the central nervous system, ultimately leading to severe microcephaly (Sarkisian *et al.*, 2002). Similarly, CITK knockout in mice caused defective neurogenesis *in vivo* as a result of disrupted cytokinesis and increased apoptosis (Di Cunto *et al.*, 2000). In addition, mice showed massive testicular damage and died before reaching adulthood (Di Cunto *et al.*, 2002). In mammals

and insects, CITK knockdown caused spindle orientation defects (Gai *et al.*, 2017). It has been suggested that CITK is recruited to the mitotic spindle by ASPM to be used for spindle positioning and orientation (Gai, *et al.*, 2016).

1.2.2.1.7.2. Nuclear Mitotic Apparatus (NuMA).

The second protein confirmed to functionally associate with ASPM localisation and function was the nuclear mitotic apparatus protein (NuMA), a MTs tethering protein required for mitotic spindle organisation (Noatynska *et al.*, 2012). *LIN-5* (NuMA) was identified as binding partner of ASPM-1 in *C. elegans* (Van Der Voet, , *et al.*, 2009). NuMA in humans is encoded by the *NUMA1* gene and was originally identified in a human/hamster hybrid cell in 1980 (Lydersen *et al.*, 1980). NuMA is 238-kDa coiled-coil type protein which is named as NuMA protein in vertebrates, mud in flies and LIN-5 in worms (Endo *et al.*, 2013). It has also been known as spindle pole-nucleus (SPN) or centrophilin. It localizes at spindle poles, or close the minus-ends of MTs from prometaphase to anaphase during mitosis. During interphase, NuMA is predominantly localised in the nucleus, however it re-locates to the pericentrosomal matrix of the spindle poles in early mitosis (Merdes *et al.*, 1996). Different studies have highlighted the crucial role of NuMA as a MT focusing factor at the mitotic spindle poles, playing a vital role in mitotic spindle organisation (Haren *et al.*, 2002; Kotak, *et al.*, 2012). It plays a key role in the positioning and assembly of the mitotic spindle and also in chromosome movement (Yanget al., 1992; Gaglio *et al.*, 1995; Gordon, *et al.*, 2001; Haren *et al.*, 2009). During

asymmetric cell division, NuMA plays an important role in driving spindle orientation via interaction with the dynein/dynactin complex (Seldin *et al.*, 2013). NuMA interacts with the dynein/dynactin complex to enable its transport to the spindle poles during mitosis (Lechler *et al.*, 2005). Dynein works as a motor protein and dynactin, a multiprotein complex necessary for dynein function, works as a dynein co-factor. They are thought to generate the force needed to pull the spindle poles towards the cell cortex during mitosis (Kotak, *et al.*, 2012). Upon mutation, NuMA loss causes spindle orientation defects, perturbs mitotic spindle organization and blocks mitosis in HeLa cells (Compton *et al.*, 1995). Depletion of NuMA using siRNA in HeLa cells confirmed a crucial role of NuMA in the focusing of MTs at spindle poles, a failure in which caused prometaphase arrest (Haren *et al.*, 2009). NuMA knockout in mice disrupted the tethering of spindle MTs to the spindle poles (Silk *et al.*, 2009). Studies also have suggested roles for NuMA in centrosome replication, chromosome separation, the maintenance of spindle pole integrity and cytokinesis (Noatynska *et al.*, 2012). Recently, NuMA became a subject of interest to many cancer researchers as it may play a key role in different types of cancer, such as leukaemia (Wells *et al.*, 1997) and epithelial ovarian cancer (Brüning *et al.*, 2012).

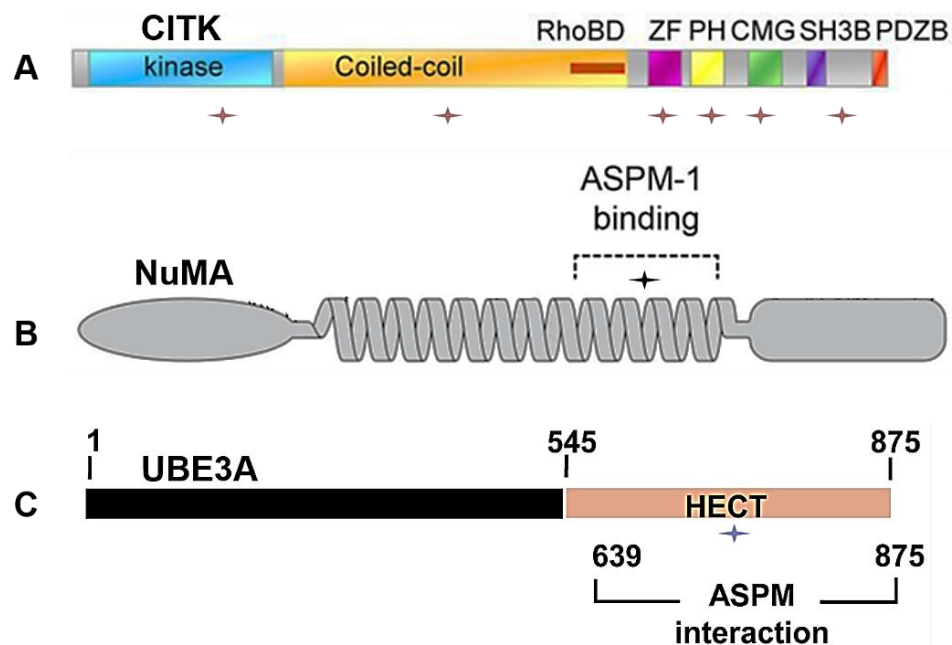
Unlike CITK, NuMA co-localizes with ASPM in the nucleus in interphase and at the spindle poles during mitosis (Gaglio *et al.*, 1995; Merdes *et al.*, 1996; Higgins *et al.*, 2010). The close similarity in localisation and function of NuMA and ASPM suggests they may share a common role in mitosis. NuMA interacts with several proteins through binding domains at its C-terminus, including ASPM (Seldin *et al.*,

2013) (Figure 1.8B). There are few studies covering the interaction between ASPM and NuMA. Previous studies of the *Drosophila* protein Asp found a key role in spindle pole focusing, suggesting a functional connection with the dynein-dynactin/NuMA complex during the focusing of MTs at spindle poles (Wakefield *et al.*, 2001). In *C. elegans*, ASPM-1 protein was confirmed to interact with the C-terminal residues 469–604 of LIN-5, a NuMA orthologue. ASPM-1 and LIN-5 co-localize at the spindle poles. There was a localization overlap between ASPM-1 and LIN-5 in the nuclear cortex during interphase, with MTs in prophase, the spindle poles in metaphase and early anaphase and at the spindle midzone in late anaphase. These observations strongly support the interesting hypothesis that ASPM and NuMA functionally interact at the spindle poles during early and mid-mitosis (Van Der Voet, *et al.*, 2009). The interaction between ASPM-1 and LIN-5 was confirmed by co-immunoprecipitation from embryonic lysates. ASPM-1 knock down resulted in a failure to detect LIN-5 at spindle poles suggesting that ASPM-1 recruits LIN-5 to the poles. However, ASPM knockout studies in HeLa cells did not affect NuMA localization to the minus ends of the mitotic spindle (Jiang *et al.*, 2017). The interaction between ASPM and NuMA is not well defined. Further investigations to identify the nature of the interaction and the involvement of this complex in cell division is necessary.

1.2.2.1.7.3. Ubiquitin-protein Ligase E3a (UBE3A).

A Yeast-two- hybrid (Y2H) screen of a foetal cDNA library using an ASPM C-terminal fragment (aa3276-3477) as a bait identified an interaction with UBE3A

(Figure 1.8C), a centrosomal protein involved in the regulation of chromosome segregation. UBE3A is the Angelman syndrome gene product which, like ASPM, localises to centrosomes during mitosis. UBE3A is a cell cycle regulated protein that when knocked down resulted in a number of different mitotic abnormalities, such as an abnormal mitotic spindle, failed cytokinesis and increased apoptosis (Singhmar et al., 2011).



- ◆ ASPM interaction with CITK regions (aa1-423), (aa458-1334), (aa741-830), (aa1378-1459), (aa1485-1607) and (aa1643-1931)
- ◆ ASPM interaction with NuMA region (aa469-604)
- ◆ ASPM interaction with UBE3A region (aa639-875)

Figure 1.8: CITK, NuMA and UBE3A regions involved in the interaction with ASPM C-terminus (CTR). **A:** Identification of interaction between ASPM and CITK by co-immunoprecipitation analysis from HeLa cell lysates. CITK regions involved in the interaction including Ser/Thr kinase domain (kinase), coiled-coil region (Coiled-coil), Rho-binding domain (RhoBD), type-2 zinc finger (ZF), pleckstrin homology domain (PH), CMG

domain (CMG), proline-rich, putative SH3 binding domain (SH3B), PDZ binding domain (PDZB), picture adapted from (Gai, *et al.*, 2016). **B:** Identification of interaction between ASPM and NuMA by co-immunoprecipitation analysis from embryonic lysates, ASPM-1 binding domain is located within coiled-coil domain, picture adapted from (Singhmar, 2011). **C:** Identification of interaction between ASPM and UBE3A using Y2H analysis. UBE3A region involved in the interaction is located within HECT (Homologous to the E6AP C terminus) domain, picture adapted from (Portegijs *et al.*, 2016).

1.2.2.1.8. The importance of the C-terminus of ASPM

The C-terminal region (CTR) structure of ASPM is highly conserved among its other species including *Drosophila*, Asp, and murine Aspm orthologues (Craig *et al.*, 1998). The CTR is a short recognisable domain in ASPM protein structure, consists of including a single armadillo-like domain (ALR), but otherwise with no similarity to any currently defined domains (Higgins *et al.*, 2010). The function of the single armadillo domain ALR in ASPM has yet not been identified with been clear functionally defined, however the armadillo repeats protein which form a large family that have diverse functions have already been characterised and identified in many eukaryotes (Wolf *et al.*, 2006; Tewari *et al.*, 2010). Although the CTR domain in ASPM has not been extensively studied, most of the known mutations that cause MCPH in humans (Bond *et al.*, 2002; Bond *et al.*, 2003) and in *Drosophila* (Saunders, *et al.*, 1997) are expected to result in the production of a truncated protein lacking the C-terminal region, indicating that this region is vital for normal ASPM function. The 3' region of *ASPM* has long been of interest to our group due to the presence of a splice site mutation (c.9984+1G>T/IVS25+1G>T),

which is predicted to result in the loss of only 3 amino acids and consequently but which still results in MCPH (Higgins *et al.*, 2010). Previous studies by our group have shown that the C-terminus of ASPM localises to the midbody and is involved in cytokinesis (Higgins *et al.* 2010). Moreover, C-terminally GFP-tagged ASPM fragments is localized to highly expressed in the midbody during cytokinesis in rat neural progenitors *in vivo* (Paramasivam, *et al.*, 2007). Human ASPM lacking C-terminal fragments caused mitotic spindle formation defects and failed to complete cytokinesis (Higgins *et al.*, 2010). Further evidence for this latter role is provided through the interaction of the ASPM C-terminus with citron kinase (CITK) (Paramasivam, *et al.*, 2007), a kinase which is required for the transition from cleavage furrow constriction to abscission during cytokinesis (Watanabe *et al.*, 2013). The ASPM C-terminus controls spindle orientation via direct interactions with different regions of CITK which in turn regulate astral MTs nucleation and stability, indicating that the CTR is an important factor in neurogenesis and cell proliferation (Gai, M. *et al.*, 2016). In addition, mutation in murine *Aspm*, which is highly conserved to the structure of *asp* in *Drosophila*, disrupts S-M checkpoint control and stops the formation of a bipolar spindle. in fission yeast (Craig *et al.*, 1998). As noted above, a Yeast two-hybrid (Y2H) screen using an ASPM C-terminal sequence as bait identified Angelman syndrome gene product UBE3A, co-localise with ASPM in the centrosome, as a putative interactant (Singhmar, *et al.*, 2011). Collectively, these findings localisation pattern of the CTR of ASPM and its role during cell division as well as initiating MCPH as a result of its loss indicate that the CTR is the most functionally important domain in ASPM that needed to

be identified. Further investigation of the C-terminus of ASPM and its interacting partners will increase our understanding of ASPM function in mitosis and particularly in cytokinesis.

1.3. Yeast 2-hybrid (Y2H) assay to identify protein interactions

Cell functions and processes are entirely dependent on protein-protein interactions (Brückner *et al.*, 2009) (Chang *et al.*, 2016). Identifying protein-protein interactions is of the utmost importance in elucidating a proteins function. A vast number of methods to identify protein-protein interactions have been utilised to detect and screen different types of protein interactions (Xing *et al.*, 2016). These methods can be carried out *in vitro*, *in vivo*, and *in silico*. The *in vitro* methods such as co-immunoprecipitation studies (co-IP) are performed outside a living organism, the *in vivo* methods such as such as Y2H are carried out inside a living organism and *in silico* methods are performed using a computer (Rao *et al.*, 2014). Protein–protein interactions are commonly identified using the Y2H system (Berggard *et al.*, 2007). Y2H was first described by Fields and Elledge in the yeast *Saccharomyces cerevisiae* (Fields *et al.*, 1989). The method has the ability to screen large numbers of gene products at the same time *in vivo*. A Y2H assay is based around the reconstitution of a functional transcription factor then the expression of a reporter gene in yeast cells (Stynen *et al.*, 2012). It uses the 2 individual domains of eukaryotic transcription activators, the DNA binding domain (DBD), which recognises a specific DNA sequence and the activation domain (AD) which allows RNA polymerase II to transcribe a reporter gene downstream of the DBD

(Pawlowski *et al.*, 2003). Accordingly, the DNA binding domain (DBD) is fused to the protein of interest X. The term “bait” is commonly used to denote the DBD–X fusion. The AD is fused to a second protein of interest – or for screening purposes sequences from a specific cDNA library, such as a foetal brain library, are fused to the AD, which is referred to as the “prey” (Figure 1.9). Only when proteins X and Y interact are the bait and prey brought together, allowing the expression of the downstream reporter gene such as GAL4. The positive clones are sequenced to identify interacting partners of the bait (Causier, *et al.*, 2004).

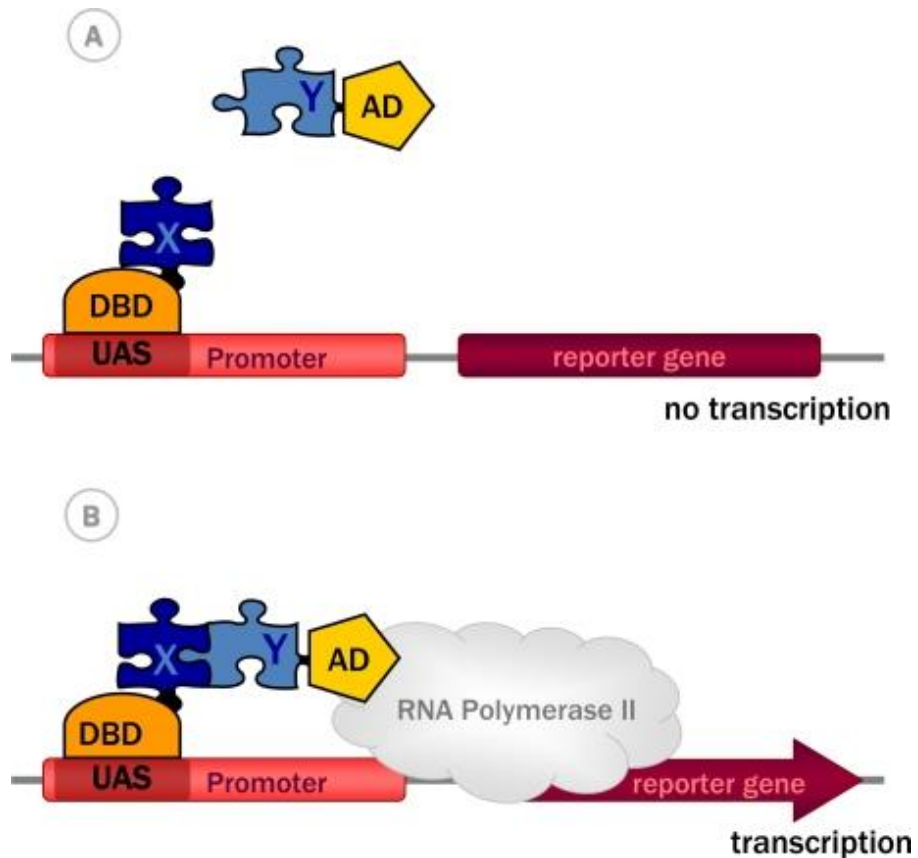


Figure 1.9: Schematic of the Yeast-two-Hybrid system. **A.** The use of Y2H assay to identify protein-protein interactions (Brückner *et al.*, 2009). Bait (X) and Prey (Y) are 2 interacting proteins, BD and AD are DNA-binding domain that binds to the upstream activator sequence (UAS) and transcription activator domain respectively. The bait protein is fused to the BD and the prey proteins are fused to the AD. **B.** The reporter gene gets activated only if both proteins interact which in turn recruits RNA polymerase II and hence activate the reporter gene. Adapted from (Brückner *et al.*, 2009).

1.4. Hypothesis and Aims

Mutation in the *ASPM* gene is the most common cause of MCPH and the C-terminus of ASPM is essential for its function. Mutations in *ASPM* are localized across the 10434 bp gene, yet they broadly cause one MCPH phenotype. It has been predicted that *ASPM* mutations result in premature protein truncation where the common region of loss is the extreme C-terminus (nt 688 to 10434) or nonsense mediated decay (Bond *et al.*, 2002; Bond *et al.*, 2003; Kumar *et al.*, 2004; Pichon *et al.*, 2004; Shen *et al.*, 2005; Desir *et al.*, 2006; Gul *et al.*, 2006; Nicholas *et al.*, 2009a; Akbariazar *et al.*, 2013; Ariani *et al.*, 2013; Papari *et al.*, 2013; Hussain *et al.*, 2013; Hu *et al.*, 2014; Abdel-Hamid *et al.*, 2016; Hashmi *et al.*, 2016; Bhargav, 2017; Letard *et al.*, 2018). At the start of this PhD project mitotic roles for ASPM have been identified, including spindle assembly, spindle organization and spindle orientation as well as maintaining of symmetric cell division and cytokinesis, however little research has been performed to determine the direct effect of individual mutations on ASPM expression and mitotic function and how this directly results in MCPH. NuMA, CITK and UBE3A protein interactions with ASPM had been identified. Given the predicted importance of the the C-terminus of ASPM this regions warrants further functional investigation including the investigation of additional protein interactions.

The hypotheses for this thesis is that *ASPM* mutations result in the loss of the C-terminal of ASPM which gives rise to a single aberrant mitotic phenotype and that ASPM interacts through its C-terminus with novel interacting proteins during mitosis to control spindle and/or cleavage furrow orientation or to orchestrate

cytokinesis. The aim of this project is to further investigate the function of ASPM to enrich our understanding of ASPM function and through its dysfunction to gain knowledge of the aberrant mitotic mechanism(s) of MCPH. This will be achieved as follows:

- Fully assess the mitotic functions of human ASPM through siRNA-mediated inhibition of ASPM in wild type U2OS cells.
- Investigate changes in mitotic phenotype in *MCPH5* patient fibroblast cells containing homozygous *ASPM* mutations compared to wildtype control fibroblasts.
- Ascertain and confirm ASPM CTR interactions from a commercial Y2H study and determine how these interaction play a role in mitosis.

Chapter 2 : Materials and methods

2.1. Cell culture.

All general chemicals, reagents, media and media supplements used in this study were commercially available and purchased from Sigma-Aldrich (Gillingham, UK) unless otherwise specified. Microcentrifuge tubes were purchased from Sarstedt (Nümbrecht, Germany) and tissue culture plasticware were obtained from Corning (Amsterdam, The Netherlands). Membrane filters, single-use filter unit, (pore size, 0.2µm) (Millipore, USA), were used to perform sterilization process. NuAire Labgard 437 ES Class II Biosafety Cabinets (NuAire, Plymouth, MN) were used to performed cell culture.

2.1.1. Cell lines.

In this study, several non-immortalised patient cell strains standard and immortalised cell lines were used. *ASPM*^{WT} are non-immortalized control neonatal human dermal fibroblasts purchased from Genlantis (San Diego, California). *ASPM*^{3663delG} and *ASPM*^{9984+1G>T} HDF cell strains were previously created from *MCH5* patient forearm skin biopsies from two individual patients of Northern Pakistani origin by the Yorkshire Cytogenetics laboratory (Higgins et al., 2010). Human bone osteosarcoma epithelial cells (U2OS) and neuronal cells (SHSY-5Y) were acquired from the ATCC Cell Biology Collection (ATCC, South London, UK). HeLa is a cervical cancer cell line which was obtained from the European Collection of Cell Cultures (ECACC, South London, UK).

2.1.2. Cell lines culture conditions.

U2OS and HeLa cells were cultured in Delbuccos Modified Eagles Media (DMEM), and SHSY-5Y cells were cultured in Dulbecco's Modified Eagle Medium: Nutrient Mixture F-12 (DMEM/F12) GlutaMAX™ (Thermo Fisher Scientific, MA, USA). The cells were cultured in 25cm² (T-25) and 75cm² (T-57) flasks as adherent monolayers in 10% (v/v) foetal calf serum (FCS) (PAA, Austria) and 100U/ml penicillin/streptavidin (P/S) (Sigma-Aldrich, Gillingham, UK) at 37 °C, 95% air and 5% CO₂ humidified atmosphere. Non-immortalised ASPM^{WT} cells were cultured in human fibroblast growth media (Genlantis, San Diego, California), while human ASPM^{8663delG} and ASPM^{9984+1G>T} patient fibroblasts were cultured in Hams F10 (Life Technologies, Paisley, U.K.) with 1mM L-glutamine, 20% (v/v) FCS and 100U/ml P/S. Contaminated fluids were decontaminated using a 2% Virkon solution, and solid waste underwent autoclaving prior to discarding. Each cell line had a negative result when assessed for mycoplasma infection.

2.1.3. Cell recovery.

Following removal of the cell vial from liquid nitrogen, 1ml cell suspension in DMEM freezing media was swiftly defrosted at 37°C. Then cell suspension was diluted in 40ml media and cells pelleted at 1200rpm. Finally, the cell pellet was re-suspended in 15ml of media in a T75 culture flask.

2.1.4. Feeding cells.

Cells were fed with fresh culture media every 3 days. The old media was removed and replaced with 5ml or 15ml (T25cm² and T75cm² flasks respectively) fresh media.

2.1.5. Passaging of cells.

When cells reached 80-90% confluence they were harvested and passaged at 1:10 split ratio for U2OS, HeLa and SHSY5Y, and 1:3 split ratio for normal human fibroblast cells and human *ASPM*^{β663delG} and *ASPM*^{9984+1G>T} patient fibroblast cells. The media was removed and cells washed with 5/15ml (T25/T75) Phosphate buffered saline (PBS). The PBS was removed and cells harvested by adding 2ml of trypsin and incubating for 5min at 37°C. Flasks were briskly tapped to dislodge the trypsinised cells then pipetted up and down to create a single cell suspension. The cell suspension was collected and added to an equal volume of FCS containing media in a falcon tube and spun at 1200rpm for 5min to pellet the cells. The media was removed and the cell pellet was agitated to create a single cell suspension and media was added depending on the split ratio required, for instance if a 1:10 split ration was needed, cell pellet was re-suspended in 10ml of media and 1ml of this cell suspension added to 14ml media in an T75 flask. The flask was placed in the incubator at 37°C, 5%CO₂.

2.1.6. Cell counting

Cell counting was carried out using a Countess Cell Counter (Thermo Fisher Scientific, MA, USA). In a 500 μ l eppendorf 10 μ l blue dye was added to 10 μ l single cell suspension in media. 10 μ l of the dye/cell suspension was added to each end of a cell counting chamber (Invitrogen, Paisley, UK) and live and dead cell populations of cells counted as per the manufacturer's instructions. Two readings were taken and the average of the two were used as the total live cell count.

2.1.7. Cell Cryopreservation.

The cells were harvested from an 80-90% confluent flask using trypsin (PAA, Austria) as above to create a single cell suspension, pelleted and re-suspended in 1ml freezing medium (90% FCS + 10% Dimethyl sulfoxide (DMSO) in a freezing vial and put at -80°C to chill from room temperature to -80°C at a rate of 1°C each min. The cells were placed in liquid nitrogen for long-term storage.

2.1.8. Treatment of U2OS cells with the mitotic inhibitor monastrol.

To synchronise cells in mitosis, U2OS cells were treated with monastrol overnight. A T75 of 60-75% confluent U2OS cells were treated with 250 μ mol/l monastrol (Sigma-Aldrich, Gillingham, UK) for 18-24hr, to create a population of cells with approximately 20% dividing cells. Prior to further processing eg cell lysis or microscopy, the prometaphase block was lifted by washing the monastrol out twice with PBS and then the cells were fed with media, allowing the cells to progress through mitosis as normal.

2.1.9. Culture of cells on glass coverslips

Cells at 80% density trypsinised and seeded on 22x22mm ethanol-sterilised glass coverslips (VWR®, Lutterworth, UK) in individual wells of a six well plate. Prior to cell seeding, coverslips were sterilized within a laminar flow hood through immersion in acetone followed by immersion in ethanol and air-drying. 2×10^5 of cells in 2ml media were added to each well of the plate and the cells incubated for 24hr until 60% - 80% confluent.

2.1.10. siRNA mediated ASPM gene knockdown

An *ASP1* short interfering RNA (siRNA) oligonucleotides targeting sequence UGCCAUGGUGCAACUUGCU (nt 691-709) (synthetic oligos UGCCAUGGUGCAACUUGCUUU and AGCAAGUUGCACCAUGGCAUU) and a commercial control siGENOME Non-Targeting siRNA Control Pools and RNAiMAX (Thermo Scientific Basingstoke, UK) were used for *ASPM* knockdown experiments in U2OS and HeLa cells. The basic reverse transfection protocol using a six-well plate consists of an experiment extending over four days, which necessitates contributions for Day1 and Day 4. Two wells were each dedicated as containing RNAiMAX only (no siRNA), non-targeting siRNA and *ASPM* siRNA of interest respectively. 80-90% confluent plate of cells were trypsinised to harvest the cells as previously described (section 2.1.5). The cell pellets obtained were re-suspended in 5 ml DMEM (antibiotic-free medium) containing FCS. In order to transfect two identical (duplicate) wells from a six-plate, 10 μ l of 20 μ M siRNA was added to 1ml Optimem in a bijot and mixed by pipetting. For the transfection of

RNAiMAX only, 1.10 ml (1ml +10 μ l) of Optimem was added into a bijot. 5 μ l of RNAiMAX was added to each diluted siRNA/Optimem or Optimem (only RNAiMAX) bijots and then mixed by pipetting the solution up and down. The solution was incubated at room temperature for a period of 15-20 minutes. 500 μ l siRNA-RNAiMAX-Optimem solution was transferred into each of the duplicate wells. 1.5ml of U2OS cell suspension containing 5x10⁵ cells was gently added to 500 μ l of previously prepared RNAi-RNAiMAX-Optimem solution (the final siRNA concentration is 50nM) and then mixed by rocking the dish back and forth. The cell suspension was incubated in 5% CO₂ for 72 hours before to be fixed on glass coverslips.

2.2. Immunofluorescence (IF) and microscopy.

2.2.1. Fixation of cells on glass coverslips

In the 6-well plates, the media was removed and cells were washed in 2ml PBS (Invitrogen, Paisley, UK). For methanol fixation the PBS was removed and 2ml of ice cold methanol (Sigma-Aldrich, Gillingham, UK) was gently introduced to the side of the well and the plate incubated for 5min at -20°C. The methanol was removed and substituted with 2ml PBS to rehydrate the cells and to wash away the methanol. Paraformaldehyde (PFA) fixation was performed in the laminar flow cabinet. 2ml of 2% PFA (Avantor, Gliwice, Poland) was gently introduced to the side of the well of the plate and the cells incubated at room temperature for 15min.

The PFA was removed and cells permeabilised in 2ml of a 0.1% [v/v] Triton X 100 (company) in PBS solution for 10min. Cells were rinsed twice using PBS.

2.2.2. Immunofluorescence staining

Fixed cells were incubated for 5min in 1% Marvel milk /PBS to block non- specific background staining. Primary antibodies (Appendix 1) were diluted in 1% milk/PBS and centrifuged in a table top centrifuge for 3min at 13,000 rpm. 200µl of antibody solution was spotted onto a strip of parafilm in a humidified chamber and the coverslip placed cell side down into the solution. The coverslips were incubated at RT for 1hr then coverslips rinsed 3x in 2ml PBS for 2min. The cells were incubated in Alexafluor highly cross-absorbed Fluorophore-conjugated secondary antibody (Molecular Probes at Invitrogen, Paisley, U.K,) (Appendix 2) in a similar manner to the primary antibody. Coverslips were incubated for 1hr in the dark at room temperature. Coverslips were rinsed four times with PBS and mounted cell side down in approximately 50µl Mowiol (Southern Biotech, USA) onto a glass slide. A summary of the specific primary and secondary antibodies (Ab), their use and their optimized dilutions is provided in Appendices 1 and 2.

2.2.3 Fluorescence Widefield Microscopy

IF immunostained and fixed cells were imaged on a Nikon TiE widefield fluorescence microscope running NIS Elements 4.20 software. Cells were focused using 60x (oil) objective lenses and motorised with wild-field epi-fluorescence filter turret containing DAPI (340-380nm excitation filter (EX) and 435-485nm emission

filter (EM)). Followed by visualizing the FITC channel using green filter (EX 465-495, EM 515-555) and the TRITC channel using a red filter (EX 540-580, EM 600-660).

2.2.3.1. Comparative analysis of ASPM spindle pole expression in ASPM^{WT} and ASPM^{3663delG} cell lines.

The ASPM integral intensity of *ASPM*^{mt} cells and *ASPM*^{3663delG} cells were measured at the spindle poles using 216-1 anti-ASPM as antibody. The integral intensity was estimated by multiplying the full pixel area with the intensities area of interest. The cells were imaged on a Nikon TiE widefield fluorescence microscope running NIS Elements 4.20 software (Nikon Instruments, Surrey, UK). Images were analysed by Fiji/ImageJ software to calculate ASPM abundance at the spindle pole and to identify phenotypic changes (National Institutes of Health) (Schneider *et al.*, 2012). The integral integrity values of ASPM at the spindle poles in *ASPM*^{mt} and *ASPM*^{3663delG} cells were compared using paired two tailed Student t-test, P-value of less than 0.05 was treated as statistically significant.

2.2.4 Time-lapse live cell imaging.

Time-lapse imaging of live cells was performed using a Nikon BioStation IM microscope (Nikon Instruments, Surrey, UK) at X20 magnification. Transfected cells were cultured in 35 mm glass-bottomed culture dishes (Barloworld Scientific, UK) and incubated at a constant 37°C temperature in CO₂ independent media with 10% (v/v) FCS, 1% (w/v) P/S, 1% (w/v) L-glutamine. Cell images were captured a

5 number of positions every 3min over a period of 18hr using NIS Elements 4.20 software and high sensitivity charge-coupled device (CCD) camera. Images at each individual position were combined to create a movie and visually analysed for mitotic activity and outcome.

2.3. Cryptic splice site investigation

2.3.1 Splice site creation analysis programme.

The Berkeley Splice site prediction program by neural network (http://www.fruitfly.org/seq_tools/splice.html) was used to assess the *ASPM* region 3444-3832nt to identify if the *ASPM* 3663delG mutation predicted the creation a cryptic splice site.

2.3.2. RNA extraction and quantification.

TRizol extraction (Invitrogen, Paisley, UK) was used as per manufacturer's instructions to Isolate RNA from *ASPM*^{WT} and *ASPM*^{3663delG} fibroblasts cells. 0.2 ml of isopropyl alcohol was used to precipitate RNA from sample and incubated for 10 min. The sample was centrifuged at 12,000g for 15min at 4°C and the supernatant was discarded from the tube leaving the pellet. The RNA pellet was washed in 70% ethanol and vortex mixed before further centrifugation at 6500g for 5min at 4°C. The pellet was air dried and 30 µl of RNase-free water was added to dissolve the pellet before being heated at 60°C for 10-15min. A Nanodrop spectrophotometer (Labtech International) was used to measure the RNA

concentration per sample in ng/μl. The ratio of absorbance 260/280 nm (ratio of 2 was used as reference of pure RNA) was used to assess purity of RNA.

2.3.3. cDNA synthesis

Superscript reverse transcriptase (Stratagene, Agilent Technologies, West Lothian, UK) was used to produce cDNA according to manufacturer's protocol with oligo dT primers (Promega). RNA solution (1mg, 5μl) tube was charged and mixed with Random hexamers (50μM, 1μl), deoxyribonucleotides, dNTPS (10mM, 1μl) and molecular biology grade water (Mol.Bio. Grade H₂O, 7μl). The mixture were heated at 65°C for 3 minutes. The tube was cooled down on ice for 2 min, and quickly centrifuged for 30sec at 1200rpm. Standard buffer (5X, 4μl), DTT (0.1M, 1μl) and superscript III Reverse Transcriptase (200U/μl, 1μl) reagents were then added to the RNA solution tube and incubated at RT for 5min. The tube was then heated in a water bath at 42°C for 50min followed by heating in a hot block at 70°C for 15min and placed on ice for 2min before being stored at -20°C.

2.3.4. Primer design for the PCR of *ASPM* Exon 14-16 .

Primers were designed to give a PCR product from cDNA of 390 bp in size and spanning sequence covering Exon 14-16. Primers were designed using primer 3 software (<http://primer3.ut.ee>) as forward (CCACCATTACCATCCTTGCT) and reverse (TCCATGTTGTTTGTATGAGTCG) primers.

2.3.5. Polymerase chain reaction (PCR).

PCR reactions were performed using 5µl of Hotshot Diamond PCR Mastermix (Clontech Life Science, UK), 0.25µL of the forward and reverse primers, and completed the volume with dH₂O up to 10µL total. The reactions were carried out in three steps: first, one cycle at 94°C for 5 min for denaturation; the second step included 40 repeat cycles of 94°C for 30sec (denaturation), 60°C for 30s (annealing) and 72°C for 30s (extension). The third step was heating up to 72°C for 10min (final extension). Tubes were then held at 4°C.

2.3.6. Purification of PCR amplified DNA

NucleoSpin® Gel and PCR clean-up Kit (Macherey Nagel, Düren, Germany) was used to purify the PCR according to the manufacturer's instructions. The DNA binding condition was first adjusted by mixing 1 volume of sample with 2 volumes of binding buffer NT1. To bind DNA, the collection Tube (2ml) was charged with NucleoSpin® Gel and PCR clean-up kit followed by addition of 700µl of sample. The content was centrifuged for 30s at 11,000 x g speed, the flow-through liquid was then discarded and the column was placed back into the collection tube. The column was then washed with 700µl Buffer NT3, centrifuged for 30s at 11,000 x g speed and the flow-through liquid was discarded. The column was then dried completely to remove remaining buffer by centrifuging for 1 min at 11,000 x g. Finally, the DNA was eluted by placing the NucleoSpin® Gel and column into a new 1.5ml microcentrifuge tube, 15–30µl Buffer NE were added and incubated at RT for 1min followed by centrifuging for 1min at 11,000 x g.

2.3.7. Agarose gel electrophoresis of DNA and sequencing.

PCR aliquots were electrophoresed in 1% (w/v) of agarose gels in TBE (90mM boric acid, 2mM EDTA) buffer and stained with 0.5 μ M ethidium bromide. Loading buffer (2.5 % Ficoll 400, 11mM EDTA, 3.3mM Tris-HCl, 0.017 % SDS, 0.015 % Bromophenol Blue, pH 8.0) was used to load DNA followed by separation at 120V for 30-60min. Agarose gel bands were detected on a Bio-Rad ChemiDoc® XRS+ imaging system. DNA sequencing were outsourced to Eurofins MWG Operon, Germany. cDNA sequences were assessed and analysed using Snap gene viewer (GSL Biotech, Chicago, IL, <https://www.snapgene.com/>) and NCBI Blast 2 sequence alignment using template identification tools in the NCBI online engine. (https://blast.ncbi.nlm.nih.gov/Blast.cgi?PAGE_TYPE=BlastSearch&BLAST_SPEC=blast2seq&LINK_LOC=align2seq).

2.4. Determination of protein expression by Immunoblotting.

2.4.1. Protein extraction.

All chemicals were obtained from Life Technologies (Paisley, UK) or Sigma-Aldrich (Gillingham, UK) unless otherwise specified. Cell lysates were made from a T75 flask of cells grown to 90% confluence. Media was removed and cells rinsed with 15ml PBS, which was then removed by pipetting. 1ml of ice cold RIPA lysis buffer (50mM Tris, 150mM NaCl, 0.5% sodium deoxycholate, 0.1% sodium dodecyl sulphate (SDS) and 1% NP40 (Tergitol)) containing a protease inhibitor cocktail

tablets (Roche Diagnostics GmbH) to protect protein from proteases, was added to the cell monolayer and the cells incubated on ice for 30min prior to being scraped from the flask and placed in a 1.5ml Eppendorf tube. The cell mixture was drawn through a syringe five times using a thin gauge needle, and centrifuged at 4°C for 20min. at 13000rpm to pellet the cell debris. The supernatant was stored as aliquots at -80°C. To make lysates for protein-protein interaction studies the same protocol was followed however an NP40 lysis buffer (BD Life Sciences) containing protease inhibitor cocktail tablets (Roche Diagnostics GmbH) was used.

2.4.2. Determination of protein concentration.

The Bradford assay (DC™ protein assay, Bio-Rad) was used to measure the concentration of protein in each sample solution using a 96- well plate according to the manufacturer's instructions (Bio-Rad). The extracted protein samples were diluted (1:10) in distilled water. Serial dilutions (0, 0.1, 0.25, 0.5, 0.8, 1, and 1.5 to 2µg/µl) of BSA dissolved in distilled water were prepared for standard curve of absorbance. 5µl per well of BSA standard solutions, protein samples and 10% RIPA buffer (assay blank) were tested in triplicate. 20µl of Bio-Rad DC™ Protein assay Reagent S and 200µl of Reagent B were added per well containing BSA, blank and samples. The plate was then mixed using a rotary shaker and allowed to stand at room temperature for 15 minutes to give enough time for the Coomassie Brilliant Blue dye to conjugate with the protein which then was loaded into the microplate reader Titertek® (Thermo Electron Corporation). The standard

concentration was obtained at a wavelength of 690nm and results were analysed by Ascent software.

2.4.3. Western blotting.

All equipment and reagents for this section were supplied from Life Technologies (Paisley, U.K.) unless otherwise stated. The setup of the Invitrogen XCellSureLock™ Mini-Cell gel tank and location of the precast NuPage 3- 8% tris acetate gel was performed in accordance with the manufacturer's directions. 50µg cell lysate containing 10µg of protein, 10µl 4x sample loading buffer (LDS) plus 4µl sample reducing agent (DTT) and RIPA buffer to make the whole sample up to 40µl was heated to 70°C for 10min. To maintain protein integrity the sample tube was placed on ice, until being heated, then it was spun for 3min and maintained on ice until loading. The samples and markers (10µl Precision Plus Protein standard (BioRad) and 10µl High Mark (Invitrogen, Paisley, UK)) were loaded onto the gel which was run in tris-acetate SD running buffer (Invitrogen, Paisley, UK) at 150V, 400 mA for 70min. A wet transfer to membrane was carried out in accordance with the manufacturer's directions in the Invitrogen Xcell II Blot Module at 30V over 2hr in the cold room. For MACF1 and ASPM the transfer was performed at 4°C over a 4hr period at 221mA in 10% methanol conversion buffer in accordance with manufacturer's directions. Membranes were blocked in 10% milk/1x PBS for 30 minutes on the rocker and incubated in primary antibody overnight in the cold room. Membranes were washed in PBS, three times for 10min. Blots were incubated in horseradish peroxidase-conjugated secondary antibodies (Dako, Ely,

UK) (Appendix 2) in 10ml 5%-milk/1x PBS at room temperature for 30min on the rocker. The membrane was rinsed 3x in PBS for 10min. and proteins were identified using SuperSignal West Pico/Femto Tracing Reagent (Thermo Fisher Scientific, MA, USA) in line with manufacturer's directions. The protein imaging was carried out using a Chemidoc XRS+ imaging system with QuantityOne® software (Bio-Rad, Hemel Hempstead, UK). For precise quantitative measurements for the protein content, a β -Actin antibody was included as a loading control. Multiple biological and replicative repeats of western blots were performed.

2.4.4. Western blot densitometry and normalisation to the B-actin control.

An equal intensity of the β -Actin band across the samples gives a clear indication of consistent protein loading, however if the band intensity varied between samples this indicated overloading or mis-loading of the protein amount. Semi-quantitative analysis was therefore conducted to quantify the relative protein intensity in each Western blot band for at least 3 independent experiments using Fiji/ImageJ software to identify phenotypic changes (National Institutes of Health) (Schneider *et al.*, 2012). The densitometric analysis of each band was calculated as the average relative density which is the ratio of the average intensity of each protein band to the average intensity signal of the β -actin (loading control) for that sample to normalize the likely errors arising from the whole process. The average relative density of 1 correlates to high protein expression, whereas the average relative density of 0 correlates to cells with no protein expression.

2.5. Protein interaction studies.

2.5.1. GST pull down Protein-Protein interaction technique

To confirm Y2H derived putative interactions between the ASPM C-terminas and GCC2/SRGAP2/MACF1, GST pull downs were performed. Stored lysate of bacterially induced ASPM-C terminal fragments fused to the 26kDa Glutathione-S-Transferase (GST) were available as a resource to use. 150µl of 50% slurry of glutathione –Sepharose 4B beads was added to 2ml of the ASPM fragment-GST lysate and mixed end-over end overnight at 4°C in order for affinity capture of the GST-ASPM fusion protein. Beads were pelleted and washed 5x at 500xg in 0.1% Triton-X100-Tris Buffered Saline (TBS) containing 150mM NaCl. The beads were incubated overnight whilst rotating end over end in pre-cleared cell lysate. The beads were spun down at 500xg and washed 5x in 0.1% Triton-X100-Tris Buffered Saline (TBS) containing 1M NaCl. The beads were spun down and resuspended in 50ml Triton-TBS, 1x sample buffer and 1x sample reducing agent, heated at 70°C for 10min and a Western blot performed as previously described.

2.5.2. Co-IP for ASPM interactions

50µl of Protein A (rabbit antibody) beads per co-IP sample and 50µl of cell lysate per 1ml were aliquoted and spun in an eppendorf for 2min. at 500g at 4°C. The storage buffer was removed and the beads washed twice in 1ml PBS and spun for 2min. at 500g. The beads were then washed in 200µl of PBS/0.01% Tween and re-suspended to twice their volume with PBS. Unsynchronized cell lysates were

defrosted and 35 μ l of each lysate kept as the input sample. Each lysate was pre-cleared with 50 μ l beads/ml lysate and rotated for 30min. at 4°C. The beads were pelleted at 500g for 2min. and 250 μ l of cleared lysate decanted into fresh eppendorf tubes. 10 μ l of pre-immune serum or 216-1P Ab was added to the correct tubes and rotated for 2hr at 4°C to bind to ASPM. To capture the complexes, 50 μ l of washed bead was added to each sample and rotated overnight at 4°C. Bead complexes were pelleted by centrifugation for 2min. at 500g and washed three times with 500 μ l wash buffer at 4°C. To elute the 216-1-ASPM-interactant complexes from the beads, 45 μ l of 2% SDS was added to each sample at room temperature for 30min, mixing the samples through inversion every few minutes before pelleting the beads by spinning for 2min. at 1000rpm. The supernatant was transferred into tubes and LDS and DTT added to each sample. The samples were heated for 10min at 70°C to denature the complex and loaded onto the gel. Finally WB analysis was performed using SRGAP2 and MACF1 Ab.

2.6. Statistical analysis

The analysis of all data presented in this study including paired two tailed student t-test was carried out using GraphPad Prism v6.0 (GraphPad Software, Inc., San Diego, CA). Data is presented as the mean \pm SE of at least 3 independent experiments. Vertical bars were used to identify the standard deviation average values for the mean. The statistical significance of the result was examined using a paired two tailed Student t-test. P-value (probability value of the observed data) of less than 0.05 was treated as statistically significant.

Chapter 3 : Investigation into the effect of siRNA mediated *ASPM* knockdown upon mitosis.

3.1 Introduction

Previous to the start of this project, the identification of a number of mitotic functions of ASPM had been achieved through *in vivo* and *in vitro* siRNA *ASPM* knockdown studies (Kim *et al.*, 2001; Fish, *et al.*, 2006; Van Der Voet, *et al.*, 2009; Bikeye, *et al.*, 2010; Higgins *et al.*, 2010; Xu, 2012; Connolly *et al.*, 2014; Capecchi *et al.*, 2015; Tungadi *et al.*, 2017). Inhibition of the expression of ASPM by *in vivo* and *in vitro* siRNA *ASPM* knockdown resulted in reduced ASPM protein expression at the spindle pole (Higgins *et al.*, 2010), altered the plane of cell division from symmetrical to asymmetrical by means of changing cleavage furrow orientation (Fish, *et al.*, 2006), and caused mitotic delay, changes in microtubule organisation and cytokinesis failure leading to multinucleated cells and apoptosis (Higgins *et al.*, 2010). Roles for ASPM in spindle assembly and spindle rotation have been shown following *ASPM* mediated knock-down (Van Der Voet, *et al.*, 2009; Xu *et al.*, 2012; Connolly *et al.*, 2014). Experiments involving *Morpholino*-mediated knock-down of *Aspm* have shown *Aspm* is involved in mitotic progression beyond prometaphase (Kim *et al.*, 2011; Novorol *et al.*, 2013). A significant loss of spindle pole focus and morphology as well as a defect in spindle organization were detected in *Drosophila* as a result of RNAi depletion of the *abnormal spindle* (*Asp*) (Morales *et al.*, 2005). During brain development, *ASPM* knockdown would effectively result in an early

switch from symmetric to asymmetric division, delays in mitosis and cell death which would reduce the NPC pool and therefore the number of neurons which could be produced from the NPC within the neurogenic window (Fish, *et al.*, 2006; Higgins *et al.*, 2010; Capecchi *et al.*, 2015), so a small brain would develop.

To date, in our lab *ASPM* knockdown has been performed using the *ASPM* siRNA (UGCCAUGGUGCAACUUGCU). To identify further roles of *ASPM* this chapter describes knockdown of the *ASPM* gene RNA in the extensively studied and characterised human bone osteosarcoma epithelial cell line (U2OS) and the resultant changes in interphase and in the mitotic apparatus during mitosis. We show in this study that *ASPM* knockdown in U2OS cells is a partial knockdown of *ASPM*. A number of interesting mitotic phenotypes were identified in *ASPM* siRNA-mediated depletion cells which suggest interesting roles for *ASPM* in chromosome segregation, actin organisation, abscission and confirm roles in mitotic spindle/cleavage furrow orientation

3.2 Hypothesis

Analysis of alterations to mitosis and the structure of the mitotic machinery after siRNA mediated *ASPM* knockdown will identify additional functions of *ASPM*.

3.3 Objectives.

The aim of the current study is to fully assess the changes in mitotic functions of human *ASPM* in U2OS and HeLa cells through inhibition of the *ASPM* protein by siRNA-mediated *ASPM* gene knockdown.

3.4 Methods

3.4.1 Cell lines

The immortal human bone osteosarcoma epithelial cell line (U2OS) and the human cervical cancer cell line (HeLa) were studied for this chapter.

3.4.2 Methods

Methodologies used in this chapter were (i) siRNA mediated *ASPM* gene knockdown (Chapter 2.1.10) to investigate the mitotic role of *ASPM*. Human bone osteosarcoma epithelial cells (U2OS) were reverse transfected with *ASPM* (Dharmacon Inc Lafayette, CO, USA.) short interfering RNA (siRNA) using RNAiMAX (Invitrogen, Paisley, U.K.) transfection reagent. The negative controls for the experiment were; RNAiMAX transfection reagent (negative control for the effect of transfection reagent on the cells) and a commercial control Non-Targeting (NT1) siRNA negative control (to control for the effect of the addition of an siRNA) (ii) Immunoblotting to determine protein expression (Chapter 2.4.3), (iii) IF staining and microscopy (Chapters 2.2 IF and Chapter 2.2.3. Image capture) for protein localisation studies and the identification of mitotic alterations, (iv) Time-lapse live cell imaging (Chapter 2.2.2.4) to identify phenotypic changes in mitosis and mitotic outcomes. Data was analysed using GraphPad Prism 6.0 (GraphPad Software, Inc., San Diego, CA). Images obtained were analysed by Fiji/ImageJ software (National Institutes of Health) (Schneider *et al.*, 2012). Vertical bars were used to

identify the standard deviation average values for the mean and data is presented as the mean of at least 3 independent experiments.

3.5 Results

3.5.1 Investigation of the effect of *ASPM* siRNA mediated KD on *ASPM* protein expression.

WB were performed using the rabbit polyclonal anti-*ASPM* 217-2 antibody to recognise *ASPM* and anti-mouse β -actin antibody as a loading control. U2OS cells were reverse transfected with RNAiMAX transfection reagent only, control non-targeting siRNA (NT siRNA) and *ASPM* siRNA for 72 hrs. *ASPM* protein levels and the occurrence of isoforms were measured in U2OS cell lysates. Levels of *ASPM* proteins in each lane were normalised to β -actin and the mean of three independent experiments was calculated using Fiji/ImageJ software. In RNAiMAX and NT1 siRNA treated cell lysates the immunoblotting assay detected full length *ASPM* protein at 410kDa and second smaller band at approximately 120kDa (Figure 3.1A). A highly significant decrease in the amount of *ASPM* protein (410kD and 120KDa bands) was observed in *ASPM* siRNA treated U2OS cell lysates in comparison to the RNAiMAX and NT1 siRNA treated cells (RNAiMAX $p=0.0004$, siNT1 $p=0.0006$) (Figure 3.1B). In comparison to the average *ASPM* expression levels in RNAiMAX and siNT1 siRNA cells, analysis of *ASPM* protein achieved 65% reduction in the relative intensity of *ASPM* 410kDa and 120kDa protein levels in *ASPM* siRNA cells. The expressions of β -actin between the three cell lysate

lanes in on the WB was consistent between each lysate which indicates accurate quantitative measurements for ASPM protein concentration and accurate loading.

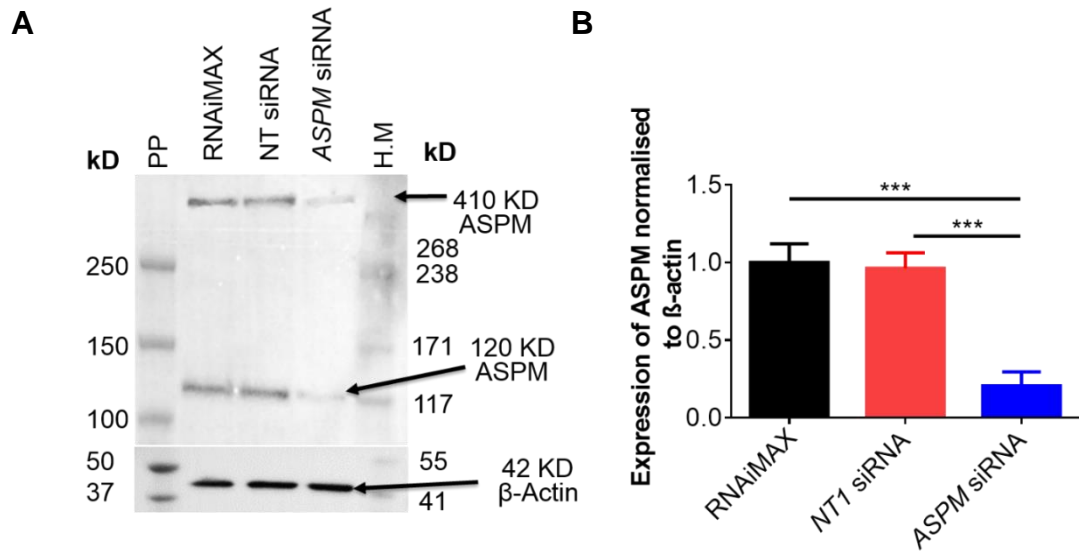


Figure 3.1: ASPM siRNA mediated KD leads to a significant reduction in ASPM protein level. A. Immunoblotting of U2OS cell lysates treated for 72hrs with RNAiMAX (lane 2), *NT1* siRNA ((lane 3) and *ASPM* siRNA (lane 4) using rabbit polyclonal anti-*ASPM* 217-2 *N*-terminal antibody to detect ASPM and an anti-mouse β-actin antibody as a loading control. Protein marker ladders were Precision Protein (PP) and HiMark (H.M.). The expression of ASPM protein was identified in the three cell lysates with a highly significant reduction in ASPM in the *ASPM* siRNA knockdown U2OS cells. **B.** The histogram shows a significant reduction of the relative intensity of ASPM protein in *ASPM* siRNA treated U2OS cells compared to RNAiMAX and *NT1* siRNA treated U2OS cells.

3.5.2. Effect of ASPM siRNA mediated ASPM knock down on U2OS cells.

3.5.2.1 ASPM localization in U2OS cells.

The normal intracellular localisation of the human ASPM protein was identified in methanol fixed U2OS cells (Higgins *et al.*, 2010). Human ASPM was predominantly localized to the nucleus and cytoplasm in interphase, to the spindle poles in mitosis and the midbody during cytokinesis (Figure 3.2).

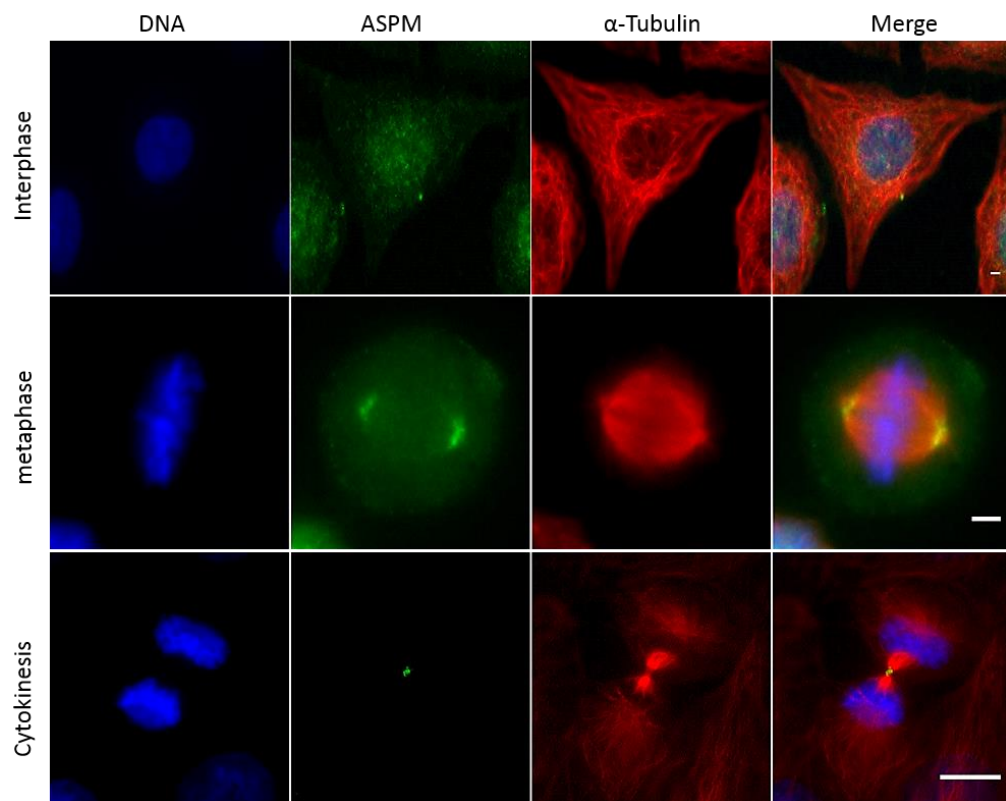


Figure 3.2: ASPM protein cellular localisation in U2OS cells during interphase, mitosis and cytokinesis. Panel shows methanol fixed U2OS cells immunostained with anti-ASPM 216-1 antibody (green), anti- α -tubulin (red) to show microtubules and with DAPI (blue) to recognise DNA. ASPM was predominantly localised to the nucleus in interphase (Scale bar = 5 μ m), at the spindle poles in metaphase (Scale bar = 5 μ m) and to the midbody during cytokinesis (Scale bar = 10 μ m).

3.5.2.2. Analysis of efficiency of *ASPM* siRNA mediated *ASPM* KD in U2OS cells.

To confirm the effect of *ASPM* siRNA mediated KD on *ASPM* protein during the cell cycle, comparative immunofluorescence microscopy was carried out. RNAiMAX, NT1 siRNA and *ASPM* siRNA transfected U2OS cells were fixed in methanol 72hrs after transfection and immunostained. In comparison to RNAiMAX and NT1 siRNA treated U2OS cells, an observable reduction of *ASPM* protein in *ASPM* siRNA transfected U2OS cells was identified in the nucleus in interphase (Figure 3.3), spindle poles during metaphase (Figure 3.4) and midbody during cytokinesis (Figure 3.5).

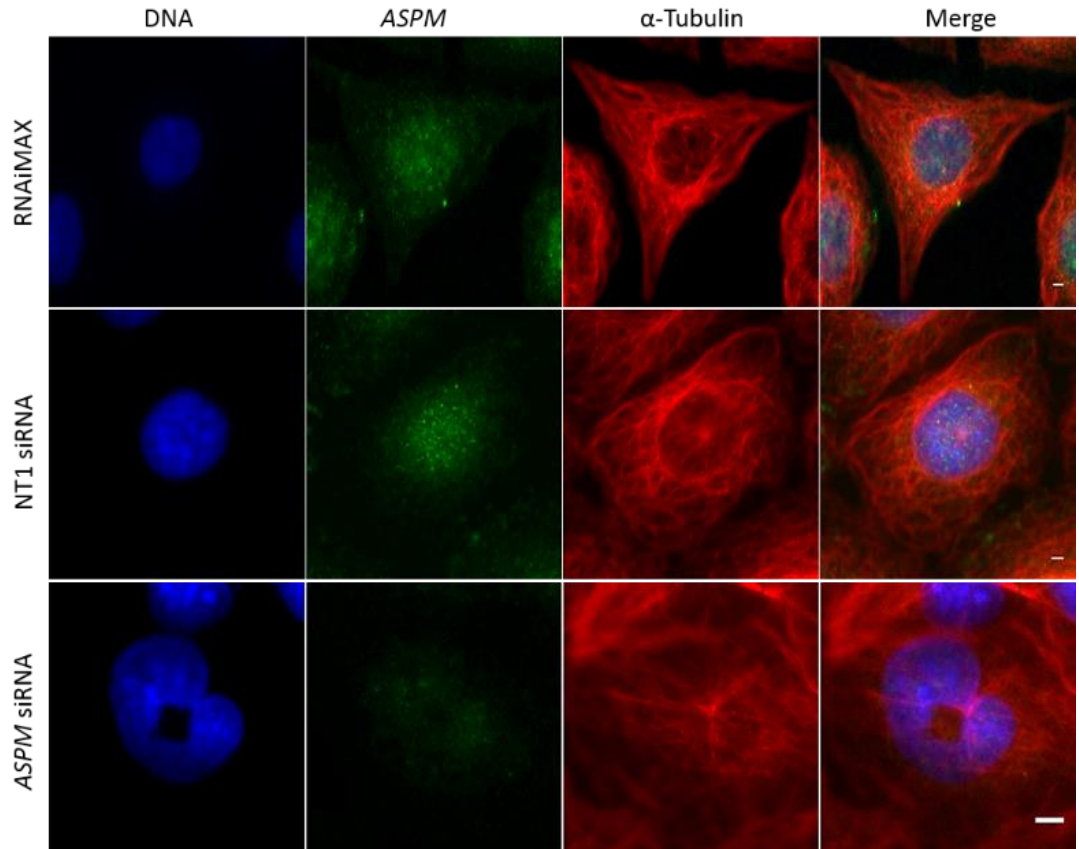


Figure 3.3: *ASPM* siRNA mediated KD causes a reduction of ASPM protein level in the nucleus and cytoplasm during interphase. Analysis of ASPM distribution following methanol fix and immunostaining with anti-ASPM-antibody 216-1 (green) to identify ASPM, anti- α -tubulin (red) to identify MT as well as with DAPI (blue) to recognise DNA. ASPM is predominantly localised to the nucleus in RNAiMAX and *NT1* siRNA treated U2OS cells. A clear reduction in ASPM expression in the nucleus was observed in *ASPM* siRNA treated U2OS cells. Scale bar = 5 μ m.

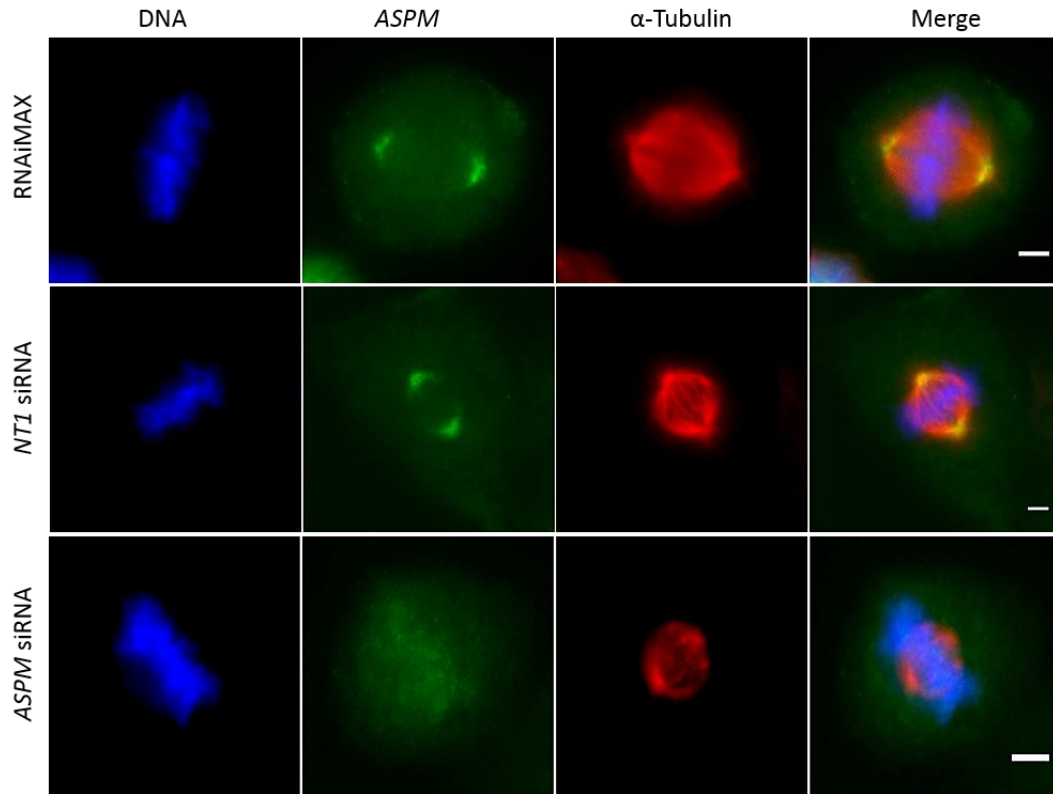


Figure 3.4: *ASPM* siRNA mediated *ASPM* KD knocks down the *ASPM* protein at the spindle pole during metaphase. Panel shows *ASPM* localisation in mitotic cells following methanol fixation and immunostaining with anti-*ASPM*-antibody 216-1 (green) to identify *ASPM*, anti- α -tubulin (red) to identify MT as well as with DAPI (blue) to recognise DNA. *ASPM* is localised to the spindle poles in RNAiMAX and *NT1* siRNA treated U2OS cells but clearly reduced from the spindle poles in *ASPM* siRNA treated U2OS cells. Scale bar = 5 μ m.

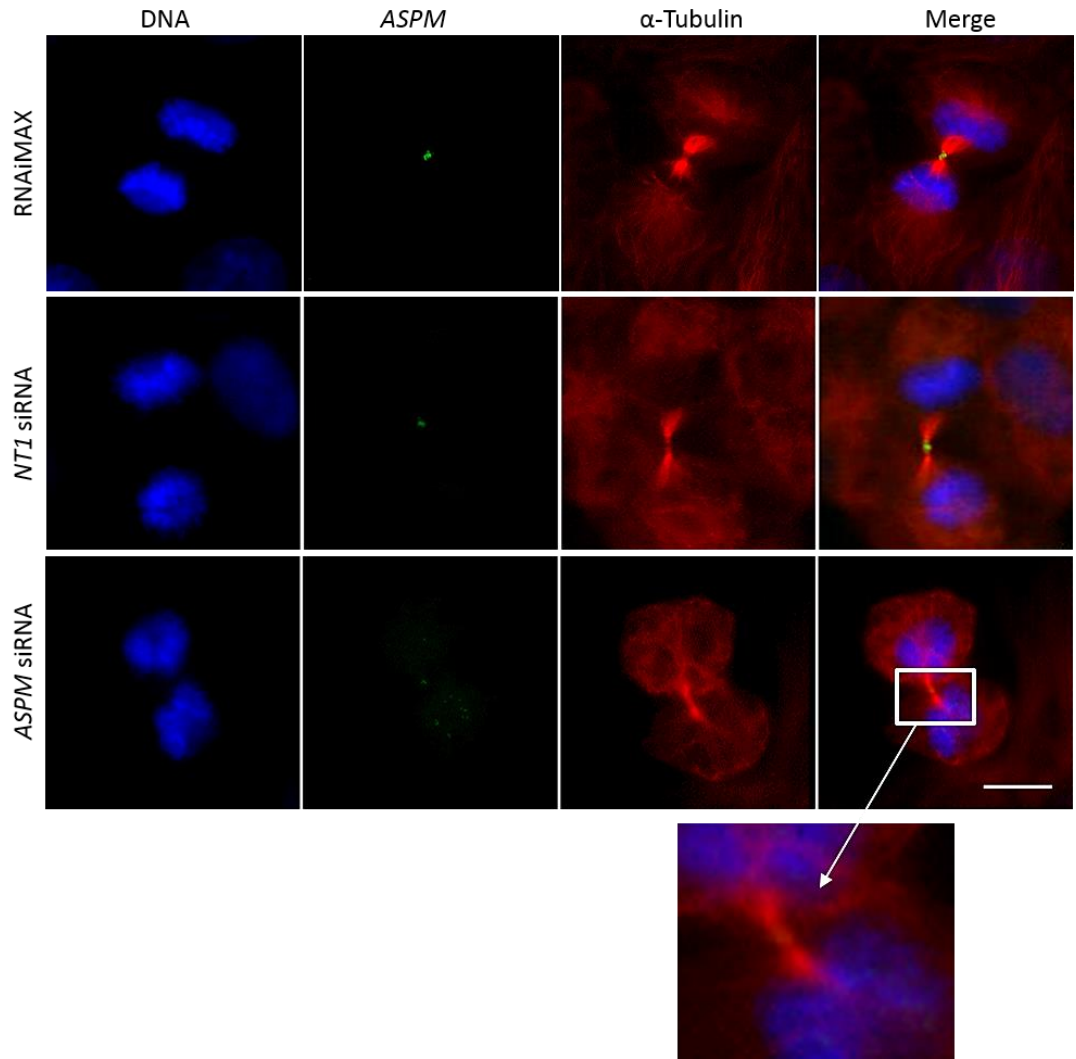


Figure 3.5: 72 hr *ASPM* siRNA treatment efficiently decreases ASPM protein at the midbody during cytokinesis. Panel shows ASPM localisation during cytokinesis following methanol fixation and immunostaining with anti-ASPM-antibody 216-1 (green) to identify ASPM, anti- α -tubulin (red) to identify MT as well as with DAPI (blue) to recognise DNA. ASPM is localised to the Flemming body/midbody in RNAiMAX and *NT1 siRNA* treated U2OS cells nonetheless ASPM is absent along with the Flemming body/midbody in *ASPM* siRNA treated U2OS cells. Scale bar = 10 μ m.

3.5.2.3 Nuclear, centrosomal, actin and microtubule changes in interphase *ASPM* siRNA treated U2OS cells.

Changes in centrosomes, microtubules and the nucleus due to *ASPM* KD were identified by comparative analysis of images of RNAiMAX, *NT1* siRNA and *ASPM* siRNA treated U2OS cells immunofluorescently labelled with anti- γ -Tubulin (green), anti- α -tubulin (red) and DAPI (blue) to identify respectively.

3.5.2.3.1 *ASPM* siRNA mediated *ASPM* KD induces nuclear alterations in interphase U2OS cells.

Abnormal nuclear phenotypes observed in *ASPM* siRNA treated U2OS cells included donut-shaped, lobular, enlarged, low density nuclei and the occurrence of micro nuclei (Figure 3.6A). In comparison to control, a significant decrease of normal interphase nuclei in *ASPM* siRNA treated U2OS cells (to 30.8% of interphase cells) was identified (Figure 3.6B). The quantitative analysis of these nuclear phenotypes revealed significant changes were observed for donut-shaped nuclei ($p < 0.0001$ and $p < 0.0001$), lobular nuclei ($p = 0.0004$ and $p = 0.0003$), enlarged nuclei ($p = 0.0003$ and $p = 0.0002$), low DNA density nuclei ($p = 0.0003$ and $p = 0.0001$) and micro nuclei ($p = 0.014$ and $p = 0.014$) in the *ASPM* siRNA treated U2OS cells compared to RNAiMAX and *NT1* siRNA transfected interphase U2OS cells respectively (Figure 3.6C).

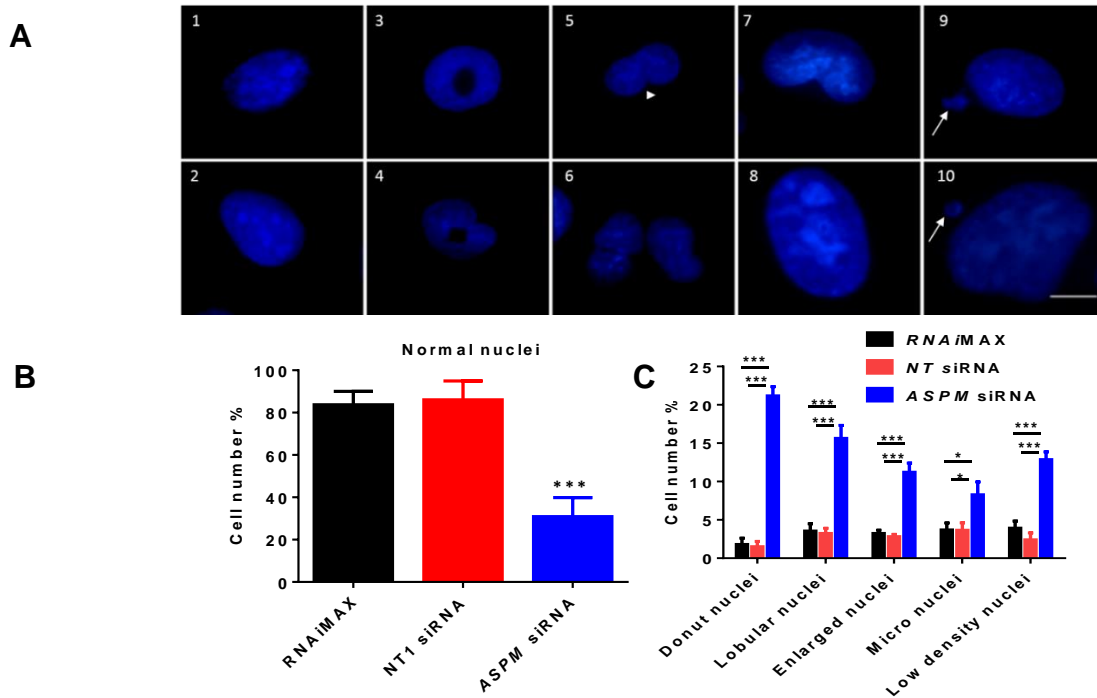
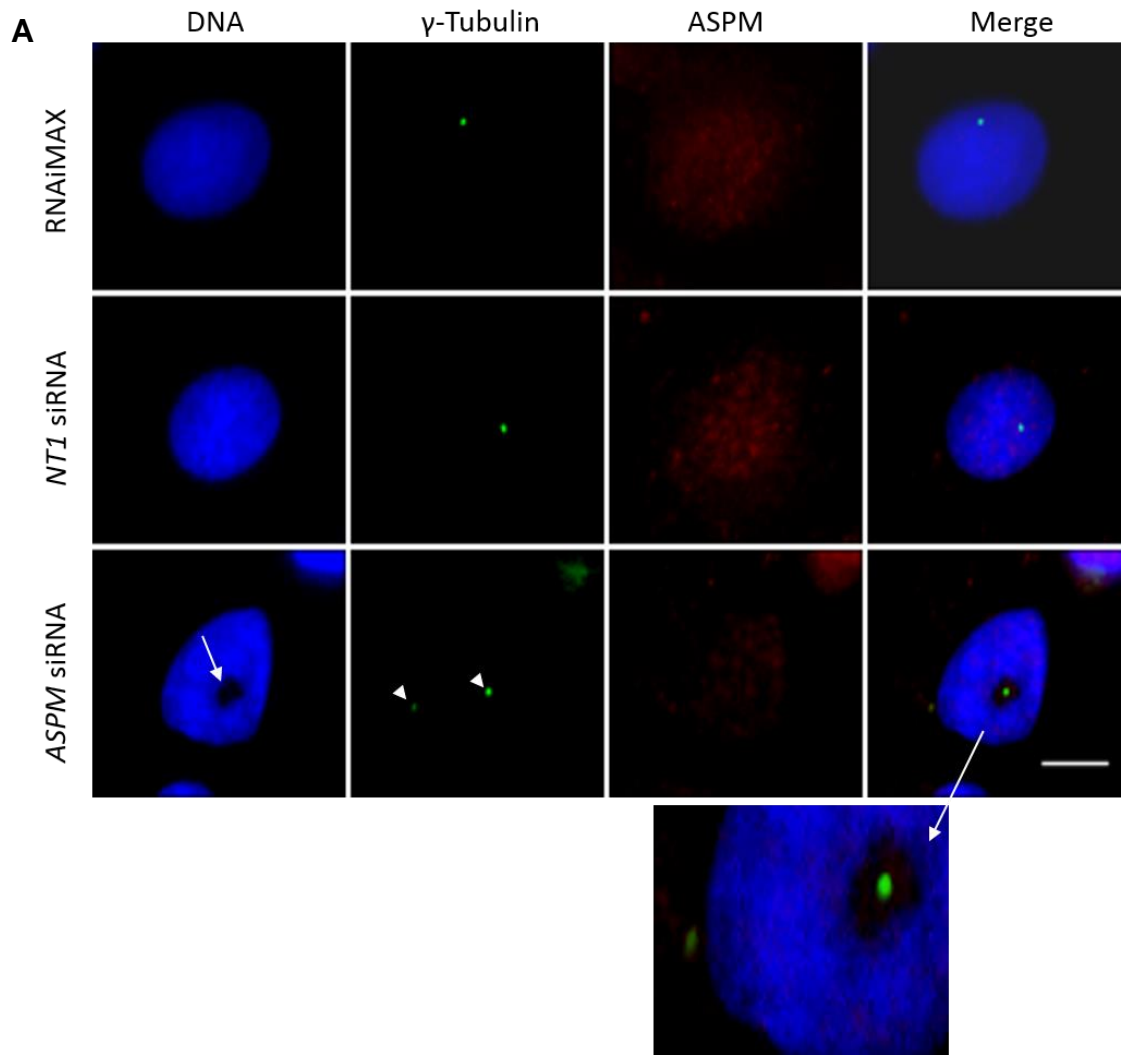


Figure 3.6: *ASPM* siRNA mediated *ASPM* KD in U2OS cells causes aberrant interphase nuclei. **A.** U2OS cells were fixed in methanol and immunostaining with DAPI (blue) to recognise DNA. Images 1 and 2; RNAiMAX and *NT1* siRNA transfected U2OS cells (control) respectively. The nuclei have normal shape and size. Images 3 and 4; *ASPM* siRNA transfected U2OS cells. These transfected cells possessed donut-shaped nuclei as a result of *ASPM* siRNA mediated KD. Images 5 and 6; *ASPM* siRNA transfected U2OS cells with lobular nuclei (arrowhead). Images 7 and 8; *ASPM* siRNA transfected U2OS cells with large nuclei. Images 9 and 10; *ASPM* siRNA transfected U2OS cells with micro nuclei (arrow). Scale bar = 10 μ m. **B.** Percentage of cells with normal smooth nuclei in RNAiMAX (n= 370 cells), *NT1* siRNA (n= 382 cells) and *ASPM* siRNA (n= 358 cells) treated U2OS cells compared. A significant decrease in cells with a normal interphase nucleus was detected in *ASPM* siRNA cells compared to control. **C.** Statistical analysis of aberrant interphase nuclear phenotypes. Unlike RNAiMAX and *NT1* siRNA transfected U2OS cells, *ASPM* siRNA transfected U2OS cells showed a significant increase in the

number of cells with nuclear defects such as donut-shaped, enlarged, lobular and micro nuclei.

3.5.2.3.2. The effect of *ASPM* siRNA mediated *ASPM* KD on centrosome number.

In comparison to RNAiMAX and NT1 siRNA transfected control U2OS cells which displayed only one regular size centrosome in interphase, *ASPM* siRNA transfected U2OS cells showed an increase in the number of centrosomes per cell and structural centrosomal defects, such as enlarged centrosomes (Figure 3.7A). *ASPM* siRNA transfected U2OS cells displayed a significant higher percentage of cells with centrosomal abnormalities (63.3%) than RNAiMAX and NT1 siRNA transfected U2OS cells, which displayed 9.3% and 8.3% of interphase cells as having centrosomal abnormalities (Figure 3.7B). The quantitative analysis of these centrosomal phenotypes revealed a significant change in the number of cells with haloed centrosomes ($p=0.001$ and $p=0.0008$) compared to RNAiMAX and NT1 siRNA transfected U2OS cells respectively, and increased centrosome number/interphase cell ($p<0.0001$ and $p<0.0001$) in *ASPM* siRNA transfected U2OS cells compared to RNAiMAX and NT1 siRNA transfected U2OS cells respectively (Figure 3.7C).



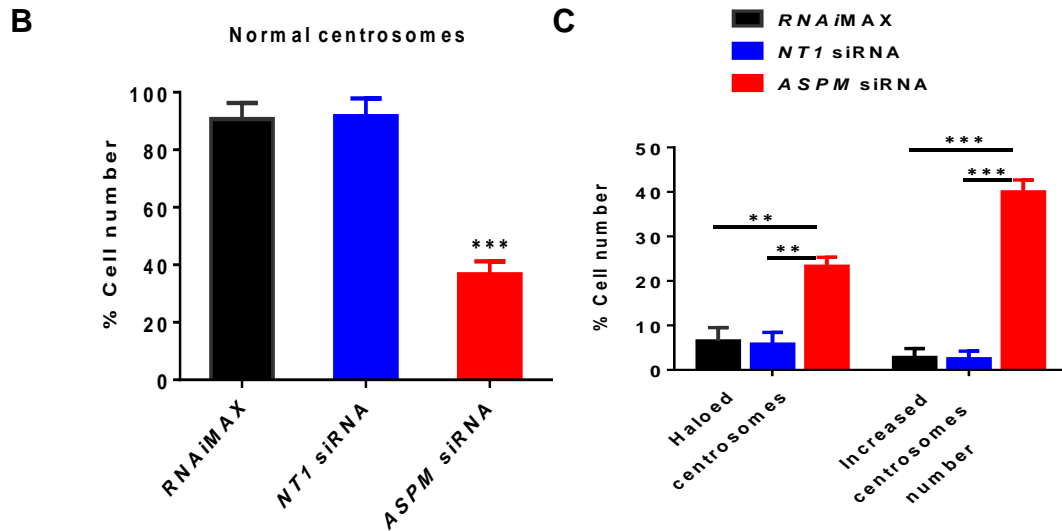
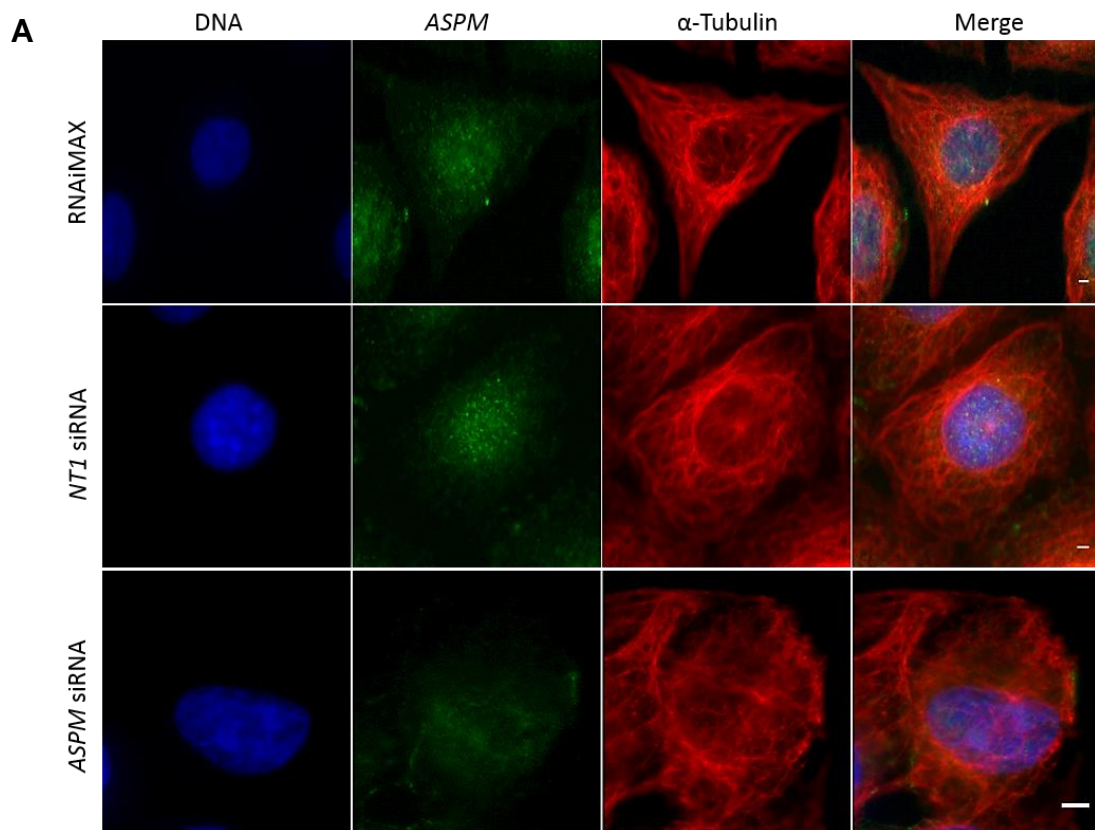


Figure 3.7: *ASPM* siRNA mediated KD results in interphase centrosomal alterations.

A. U2OS cells following methanol fixation and immunostaining with anti- γ -Tubulin (green) to identify centrosomes, anti-*ASPM*-antibody 216-1 (red) to identify *ASPM* and DAPI (blue) to recognise DNA. Panel shows RNAiMAX and NT1 siRNA transfected interphase U2OS cells with normal centrosome number and structure. *ASPM* siRNA transfected U2OS cells possessed increased number of centrosomes (Arrowhead) and haloed centrosomes (Arrow) c. Scale bar = 10 μ m. **B.** Percentage of interphase cells exhibiting normal centrosomes in *ASPM* siRNA (n= 358 cells) transfected U2OS cells compared with RNAiMAX (n= 370 cells) and NT1 siRNA (n= 382 cells) transfected U2OS cells. A significant decrease of % cells with normal centrosome phenotype was detected in *ASPM* siRNA cells compared to the controls. **C.** Statistical analysis shows a significant increase in structural centrosome defects (p=0.001 and p=0.0008) and increased number of centrosomes (p<0.0001 and p<0.0001) in *ASPM* siRNA mediated KD cells compared with RNAiMAX and NT1 siRNA transfected U2OS cells respectively.

3.5.2.3.3. Analysis of the effect of *ASPM* siRNA mediated KD on interphase microtubule organisation

ASPM siRNA transfected U2OS cells displayed abnormal MT organisation where MT phenotypes included clustered, disorganised and low density MT (Figure 3.8A). A significantly higher percentage of MT abnormalities was identified in *ASPM* siRNA transfected U2OS cells (86.6%, $p=0.0002$) than in cells transfected with the negative *NT1* siRNA (20%) or RNAiMAX alone (15.1%) (Figure 3.8B). Statistically significant changes were observed for clustered MT ($p<0.0001$, $p=0.0001$), disorganised MT ($p=0.003$ and $p=0.003$) and low density MT ($p=0.005$ and $p=0.02$) compared to MT phenotypes in RNAiMAX and *NT1* siRNA transfected U2OS cells respectively (Figure 3.8C).



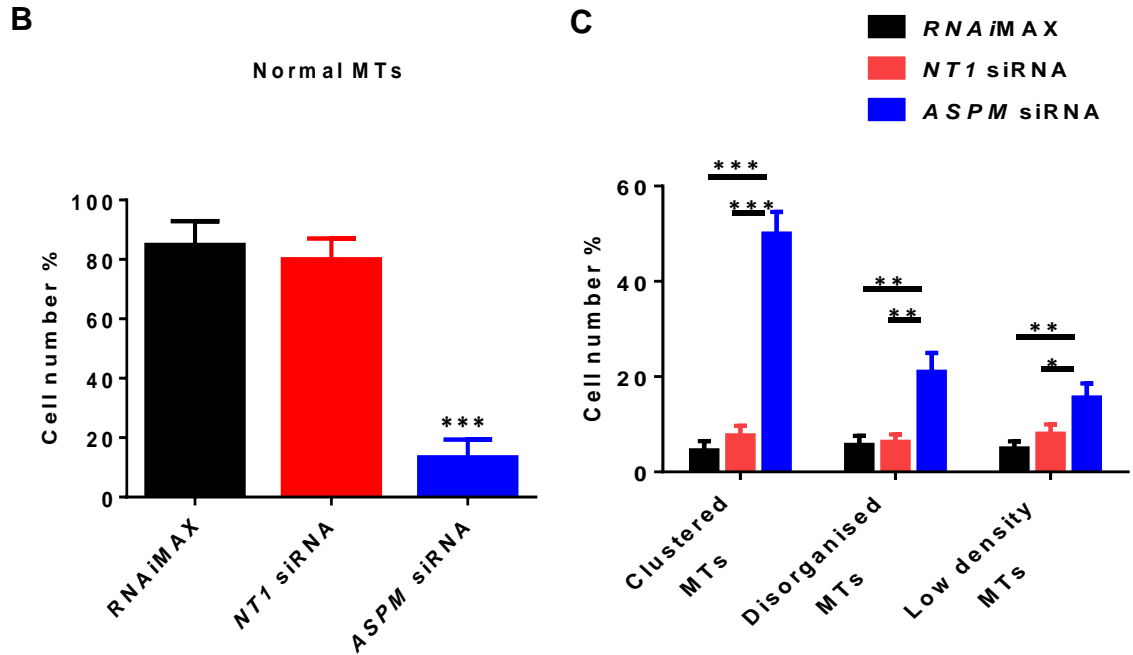
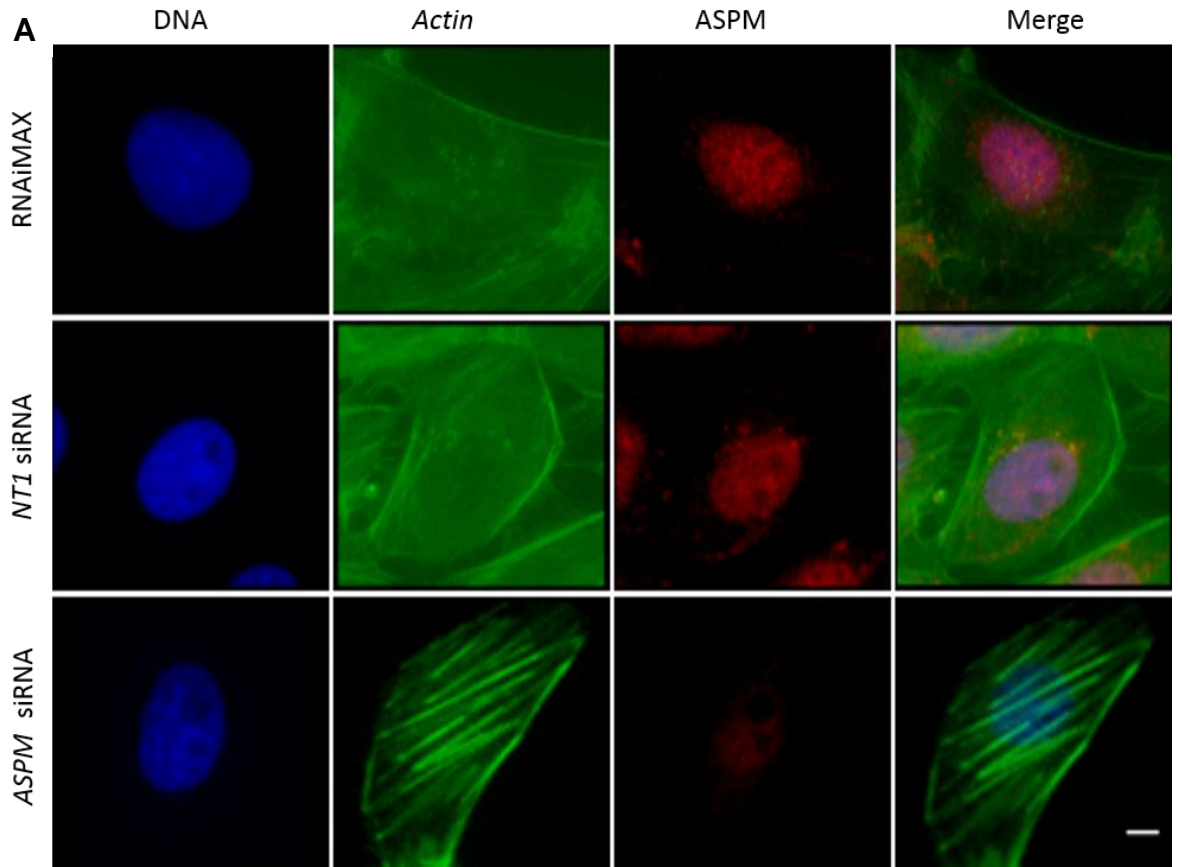


Figure 3.8: *ASPM* siRNA mediated KD induced low density, disorganised and clustered microtubules. **A.** Panel shows RNAiMAX, *NT1 siRNA* and *ASPM* siRNA transfected interphase U2OS cells. Cells were fixed in methanol and stained using the *N*-terminal anti-*ASPM* -antibody 216-1 (green), anti- α -tubulin (red) and DAPI (blue) to identify *ASPM*, MT and DNA respectively. Control transfected cells showed a well organised and distributed MT network. With *ASPM* siRNA treated cells, MT phenotypes included clustered, disorganised or low density. Scale bar = 5 μ m. **B.** Percentage of cells exhibiting normal MT network in interphase in *ASPM* siRNA (n= 358 cells) transfected U2OS cells compared with RNAiMAX (n= 370 cells) and *NT1 siRNA* (n= 382 cells) transfected U2OS cells. A significant decrease in the normal MT distribution was detected in *ASPM* siRNA cells compared to control treated cells. **C.** Statistical analysis shows MT aberrations. *ASPM* siRNAs cells showed a higher percentage of clustered ($p < 0.0001$, $p = 0.0001$), disorganised ($p = 0.003$ and $p = 0.003$) and low density ($p = 0.005$ and $p = 0.02$) MT compared to MT phenotypes in RNAiMAX and *NT1 siRNA* transfected U2OS cells respectively.

3.5.2.3.4. Analysis of the effect of *ASPM* siRNA mediated KD on actin filament phenotypes.

MT and actin filaments are functionally intertwined and physically bridged via a number of protein complexes, hence *ASPM* involvement in actin filament organisation and distribution was studied. The effect of *ASPM* siRNA mediated KD on the actin cytoskeleton was investigated in U2OS cells. The siRNA transfected U2OS cells were fixed in paraformaldehyde (PFA) to maintain the actin structures and stained with Alexa 488 phalloidin (green) to identify actin. RNAiMAX and *NT1* siRNA transfected U2OS cells displayed normal distribution and organization of actin filaments which were distributed in the cytoplasm as thin strand-like structures. However, *ASPM* siRNA transfected U2OS cells displayed clustered and actin bundling which also localised at the cell periphery (Figure 3.9A). Using quantitative analysis of the occurrence of aberrant phenotypes, RNAiMAX and *NT1* siRNA transfected U2OS cells displayed only 16.2% and 18% respectively of abnormal actin filament distribution, but a significant increase of abnormal actin filaments distribution, 80.7%, was observed in *ASPM* siRNA transfected U2OS cells (Figure 3.9B). Quantitative analysis of abnormal actin phenotypes revealed significant changes for clustered actin ($p < 0.0001$) and actin bundling ($p = 0.005$) in the *ASPM* siRNA transfected U2OS cells compared to RNAiMAX transfected U2OS cells and for clustered actin ($p < 0.0001$) and actin bundling ($p = 0.007$) in the *ASPM* siRNA transfected U2OS cells compared to *NT1* siRNA transfected U2OS cells (Figure 3.9C).



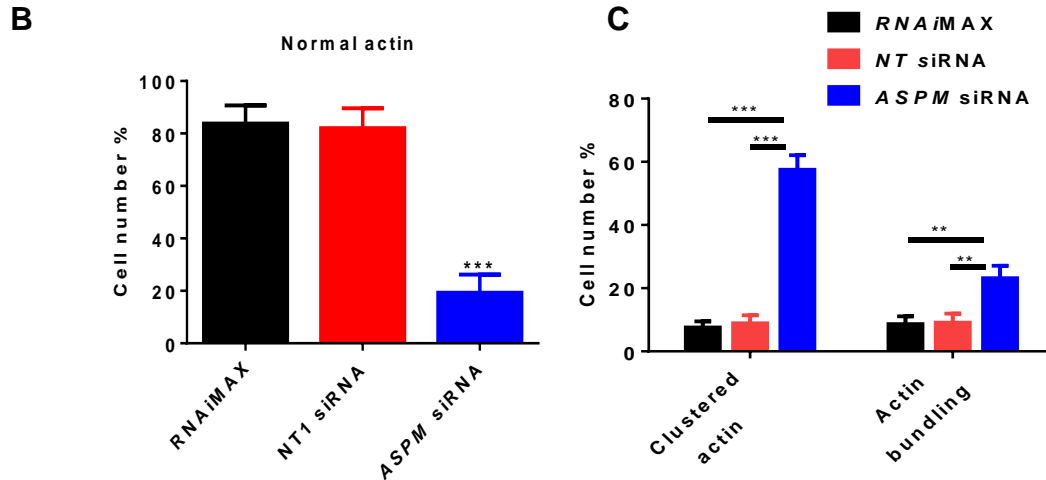


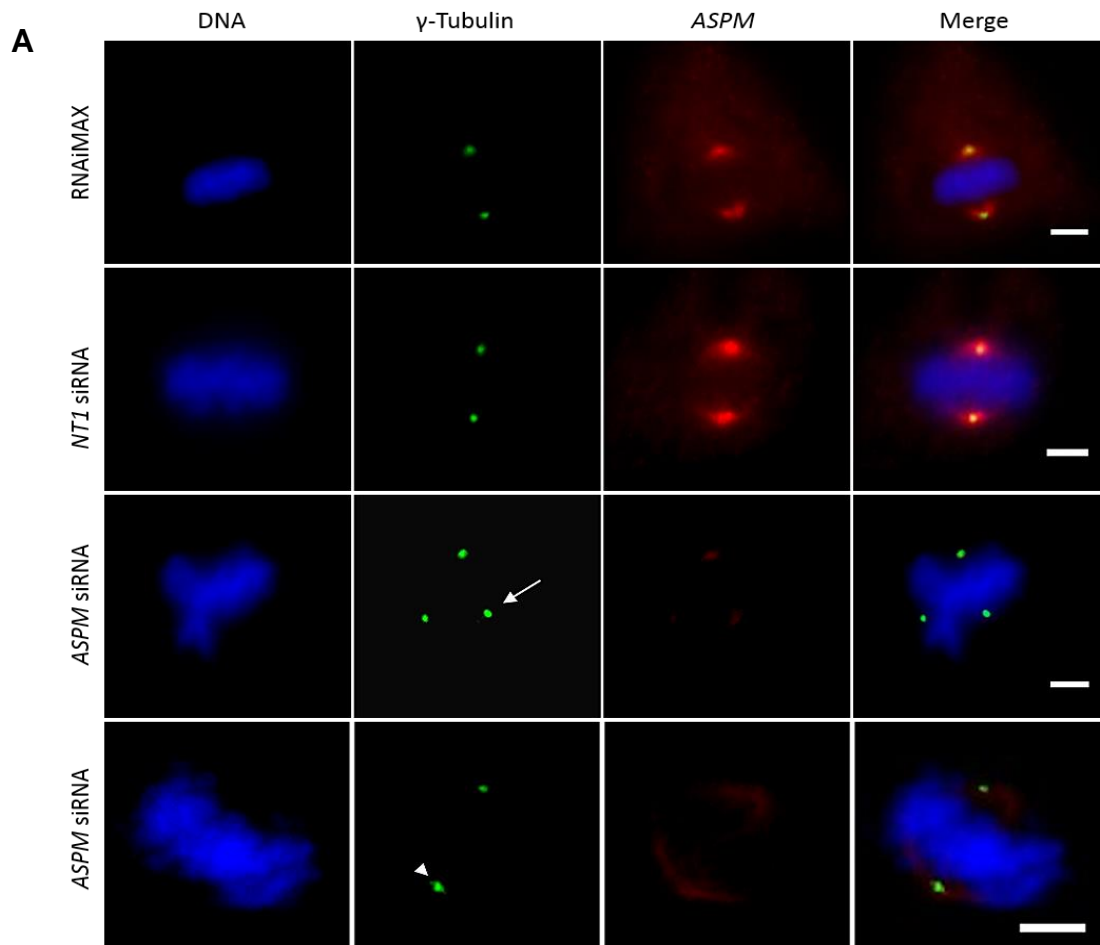
Figure 3.9: *ASPM* siRNA mediated KD induced redistribution of the actin network. A. Panel shows control and *ASPM* transfected U2OS cells during interphase. Control RNAiMAX and NT1 siRNA treated cells showed normal distribution of actin filaments around the cell periphery and through the cytoplasm. *ASPM* siRNA transfected cells showed disrupted actin filaments which were mainly clustered at the cell periphery. Cells were fixed and stained with Alexa 488 phalloidin (green) to identify actin, anti-*ASPM*-antibody 216-1 (red) to identify *ASPM* and DAPI (blue) to recognise DNA. Scale bar = 5 μ m. **B.** Percentage of interphase cells exhibiting normal actin distribution in interphase in *ASPM* siRNA (n= 330 cells) transfected U2OS cells compared with RNAiMAX (n= 342 cells) and *NT1 siRNA* (n= 350 cells) transfected U2OS cells. A significant decrease of normal actin distribution was detected in *ASPM* siRNA transfected cells compared to control transfected cells. **C.** Statistical analysis shows a higher percentage of *ASPM* siRNA treated cells exhibited clustered actin ($p < 0.0001$) and actin bundling ($p = 0.007$) than control treated cells.

3.5.2.4. Assessment of aberrations in mitosis in *ASPM* siRNA treated U2OS cells.

The mitotic phenotypes in RNAiMAX, *NT1* siRNA and *ASPM* siRNA treated U2OS cells were investigated and compared using immunofluorescence microscopy. Cells were fixed in methanol and stained with anti- γ -Tubulin (green), anti- α -tubulin (red) and DAPI (blue) to identify centrosomes, MT and DNA respectively.

3.5.2.4.1. Analysis of the effect of *ASPM* siRNA mediated KD on spindle pole number and cohesion during mitosis.

ASPM transfected U2OS cells showed abnormalities in spindle pole number and cohesion, where tripolar spindles (Figure 3.10A, arrow) and haloed spindle poles (Figure 3.10A, arrowhead) were formed upon *ASPM* siRNA mediated KD, compared to RNAiMAX and *NT1* siRNA transfected U2OS cells which displayed two cohesive spindle poles during mitosis. *ASPM* transfected cells showed a significant increase in abnormal spindle pole phenotypes (67.8%) in metaphase cells compared to RNAiMAX and *NT1* siRNA transfected U2OS cells (15.7% and 9.4% respectively) (Figure 3.10B). Using a paired two tailed t-test analysis, it was revealed that *ASPM* siRNA transfected U2OS cells were statistically significant for an increase in tripolar spindle poles ($p=0.0001$ and $p=0.0001$) and haloed spindle poles ($p=0.0003$ and $p=0.0003$) compared to RNAiMAX and *NT1* siRNA transfected U2OS cells respectively (Figure 3.10C).



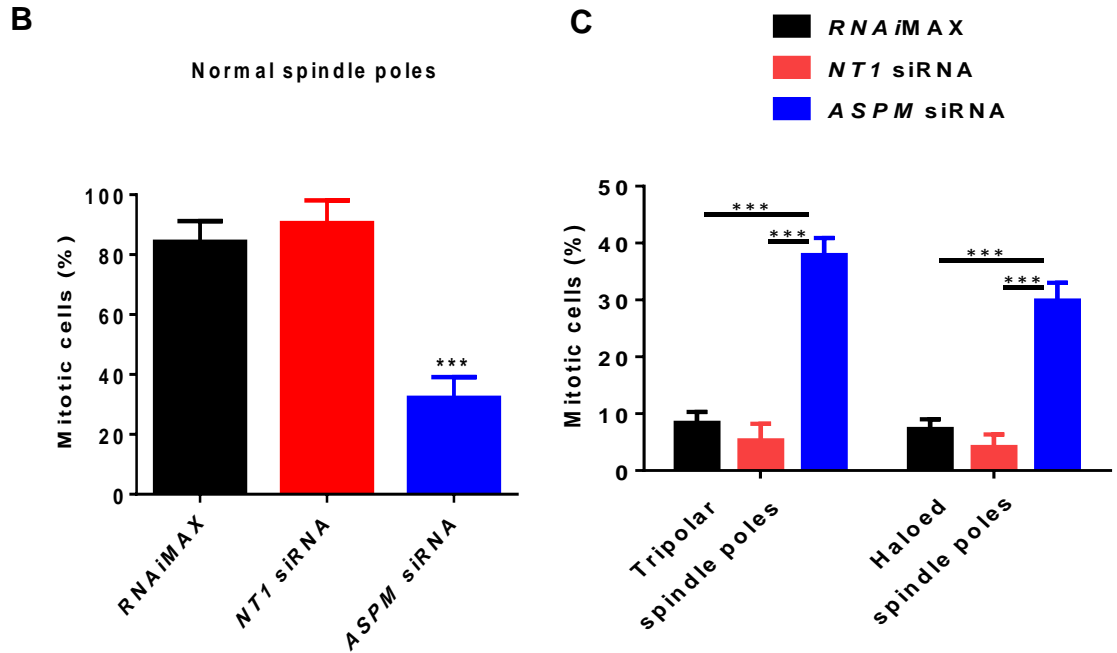


Figure 3.10: *ASPM* siRNA mediated KD induced increase in centrosomes number during mitosis and decrease in mitotic cell number. A. Panel showing RNAiMAX, *NT1* siRNA and *ASPM* siRNA transfected U2OS cells during mitosis. RNAiMAX and *NT1* siRNA cells displayed two cohesive spindle poles during mitosis with regular shape and size. *ASPM* siRNA treated cells showed tripolar spindle poles (arrow) and haloed spindle poles (arrowhead) due to *ASPM* depletion. Cells were fixed in methanol and stained with anti- γ -Tubulin (green) to identify centrosomes, anti-*ASPM*-antibody 216-1 (red) to identify *ASPM* and DAPI (blue) to recognise DNA. Scale bar = 5 μ m. **B.** Statistical analysis of % cells exhibiting a normal mitotic spindle pole phenotype in RNAiMAX (n= 130 dividing cells), *NT1* siRNA (n= 125 dividing cells) and *ASPM* siRNA (n= 110 dividing cells) treated cells which indicates that there is a decrease in the number of *ASPM* siRNA transfected U2OS cells exhibiting normal spindle poles compared to the control cells. **C.** Statistical analysis of abnormal spindle pole phenotypes which were significantly higher for an increase in tripolar spindle poles (p=0.0001 and p=0.0001) and haloed spindle poles

($p=0.0003$ and $p=0.0003$) compared to RNAiMAX and *NT1 siRNA* transfected U2OS cells respectively.

3.5.2.4.2. *ASPM* siRNA mediated KD effects on the frequency of mitosis and mitotic stage distribution.

The effect of *ASPM* siRNA mediated KD on distribution of mitotic stage was studied. *ASPM* siRNA transfected U2OS cells displayed a significant decrease in frequency of cell division (2.5%) compared to RNAiMAX and *NT1 siRNA* transfected U2OS cells (4.37% and 4.81%) respectively (Figure 3.11A). *ASPM* siRNA transfected U2OS cells displayed a change in mitotic distribution across the mitotic stages. An increase in the proportion of the mitotic cells in prometaphase ($p=0.006$ and $p=0.001$) and metaphase ($p=0.003$ and $p=0.003$) was detected in *ASPM* siRNA transfected U2OS cells compared to the RNAiMAX and *NT1 siRNA* transfected U2OS cells respectively. In addition, a significant decrease in the proportion of mitotic cells undergoing cytokinesis was detected in *ASPM* siRNA transfected U2OS cells ($p=0.001$ and $p=0.0002$) compared to the RNAiMAX and *NT1 siRNA* transfected U2OS cells respectively (Figure 3.11B). A panel of *ASPM* siRNA transfected U2OS cells in prometaphase and metaphase stage is displayed in (Figure 3.11C).

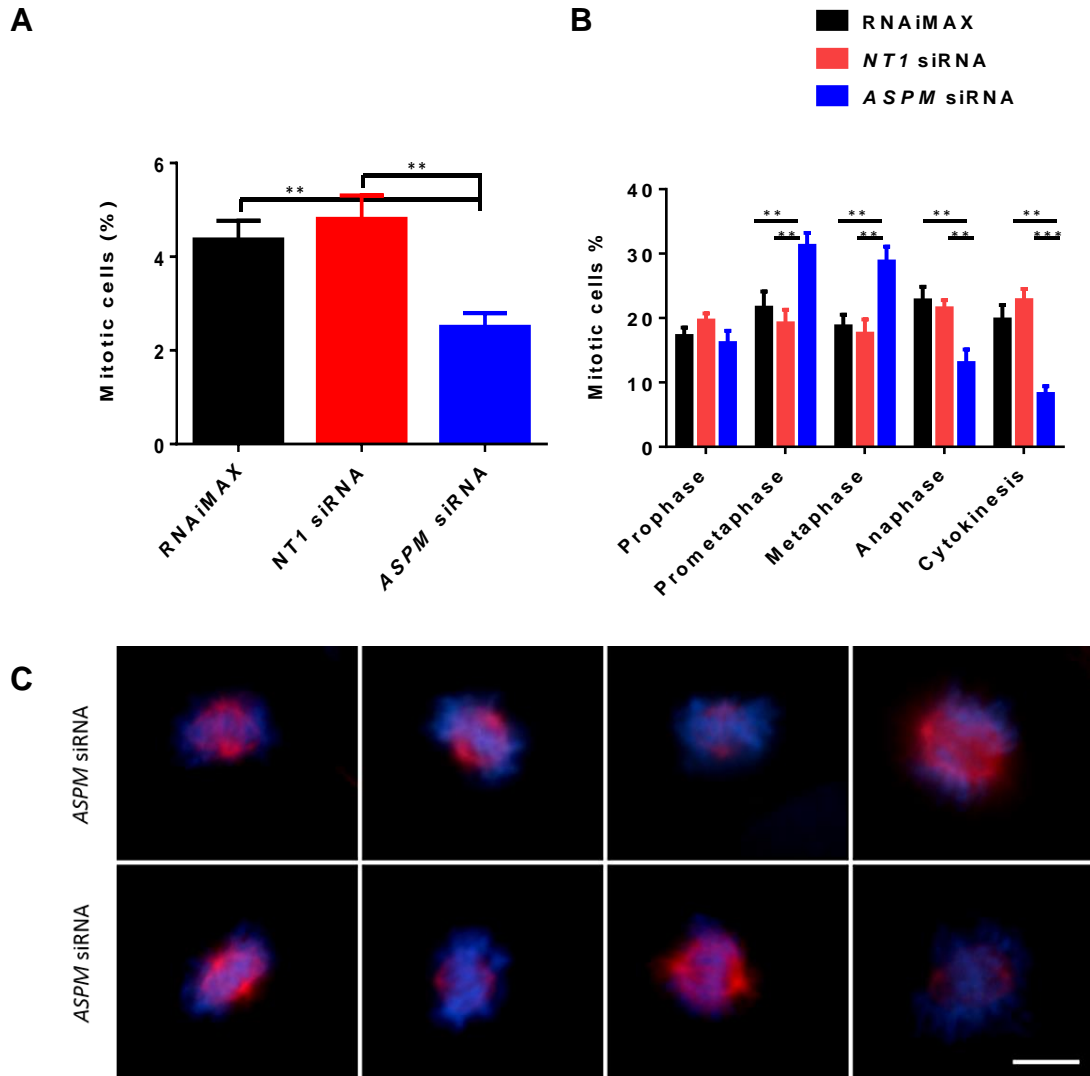


Figure 3.11: *ASPM* siRNA mediated KD results in decrease in cell division and increase in frequency of prometaphase-metaphase cells. A. Analysis of mitotic cell number which indicates that *ASPM* siRNAs (n= 110 dividing cells) cells perform less divisions compared with RNAiMAX (n= 130 dividing cells) and *NT1 siRNA* (n= 125 dividing cells) cells. **B.** Statistical analysis of RNAiMAX, *NT1 siRNA* and *ASPM* transfected U2OS cells during mitosis. The histogram shows a higher proportion of cells in prometaphase/metaphase stages and less cells undergoing cytokinesis in *ASPM* siRNAs cells than in control cells. **C.** Panel shows *ASPM* transfected U2OS cells in prometaphase

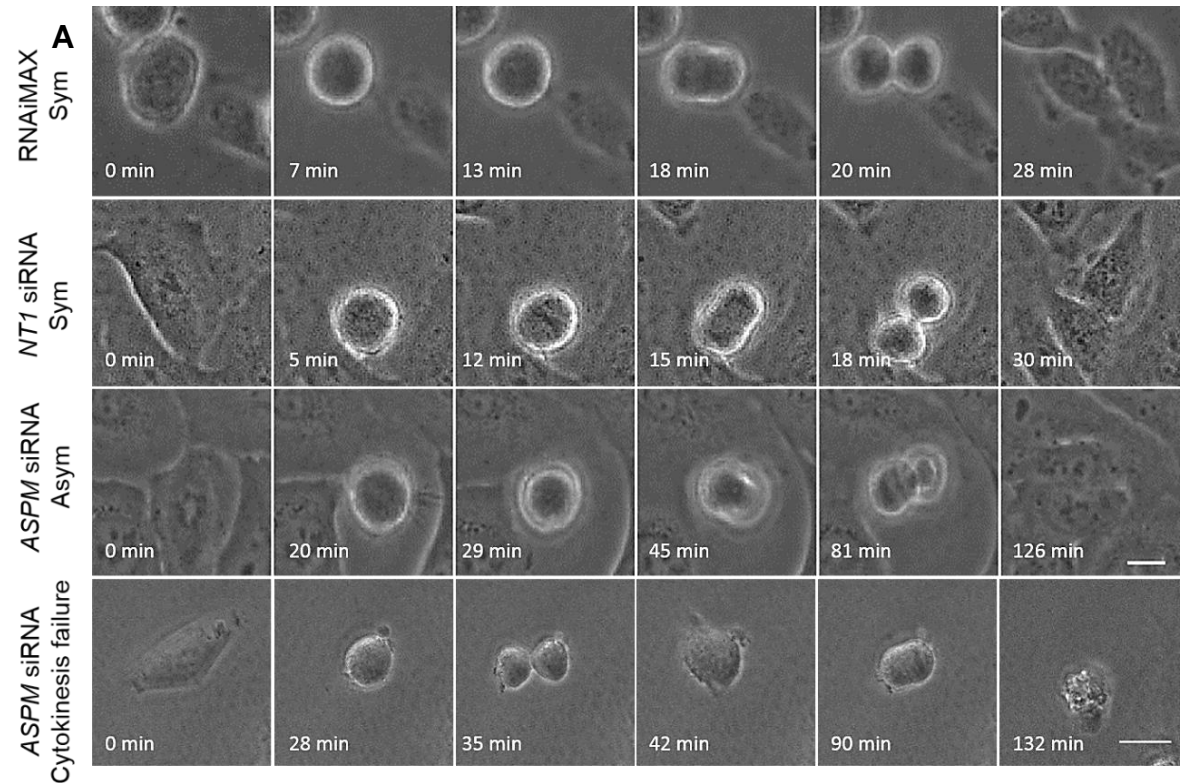
and metaphase stage. Cells were stained with anti- α -tubulin (red) to identify MT and DAPI (blue) to recognise DNA. Scale bar = 10 μ m.

3.5.2.5. Live cell imaging experiments to observe changes in mitosis in *ASPM* siRNA treated U2OS cells.

3.5.2.5.1 Live cell imaging of *ASPM* siRNA treated U2OS cells identifies changes in division type and length of time taken to complete each stage of mitosis.

To investigate the effect of *ASPM* siRNA mediated KD on interphase and mitotic processes, 72 hours time-lapse imaging of live U2OS cells post siRNA transfection with RNAiMAX, *NT1 siRNA* or *ASPM* siRNA was performed. Live cell imaging experiments were performed on a Nikon BioStation IM live cell imaging microscope and the images viewed in Fiji/ImageJ software. In contrast to control transfected cells, *ASPM* siRNA treated cells displayed an increase in asymmetric division where cleavage furrow was formed approximately parallel to the surface of the imaging dish (Figure 3.12A). *ASPM* siRNA cells displayed a significant increase in the frequency of asymmetric division (to 62.3% of dividing cells) compared to RNAiMAX and *NT1 siRNA* siRNA cells respectively (19.6% and 26.6% of dividing cells) (Figure 3.12B); a statistically significant increase in the time taken for cells to complete both symmetric division ($p=0.004$ and $p=0.004$) and asymmetric division ($p=0.001$ and $p=0.003$) was detected in *ASPM* siRNA treated cells compared with the RNAiMAX and *NT1 siRNA* siRNA transfected cells respectively (Figure 3.12C). The time stamps shown in the images denote the cumulative time cells took to

complete the stages of cell division and illustrates *ASPM* siRNA cells took longer to complete cell division than negative control (RNAiMAX and *NT1* siRNA) transfected cells.



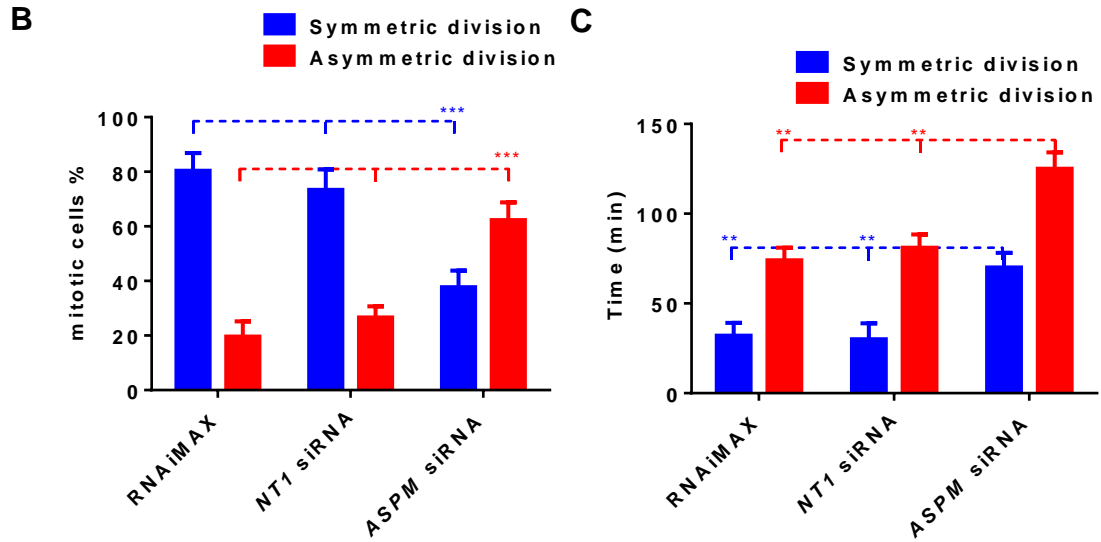


Figure 3.12: ASPM siRNA mediated KD using U2OS cells induces mitotic spindle misorientation leading to an increase in asymmetric cell division. A. Panel shows phase-contrast live cell images of RNAiMAX, *NT1 siRNA* and *ASPM* transfected U2OS cells during mitosis taken at indicated times from time-lapse movies. The first and second row show RNAiMAX and *NT1 siRNA* transfected U2OS cells undergoing symmetrical division during mitosis. The third and fourth rows show *ASPM* siRNA treated U2OS cells undergoing asymmetrical division and cytokinesis failure respectively (fourth row panel) creating a binucleated cell which then underwent apoptosis. *ASPM* transfected U2OS cells took longer time to complete mitosis than control cells (time frames are indicated). Scale bar = 10 μ m. **B.** Mean percentage of cell division for RNAiMAX (n= 125 dividing cells), *NT1 siRNA* (n= 120 dividing cells) and *ASPM* siRNA (n= 100 dividing cells) treated U2OS cells. The occurrence of asymmetrical division was higher in the *ASPM* siRNA treated with a corresponding decrease in the occurrence of symmetrical division than control cells. **C.** Graph showing the mean time taken to complete symmetrical and asymmetrical divisions for RNAiMAX, *NT1 siRNA* and *ASPM* siRNA treated U2OS cells (n=180 cells) which illustrates that asymmetrical divisions take longer than symmetric divisions to complete and that both types of divisions take longer to complete when ASPM is reduced.

Specifically in the *ASPM* siRNA cells undergoing both symmetric and asymmetric division the time taken to complete all stages of mitosis was significantly increased; Prometaphase ($p=0.001$ and $p=0.004$), metaphase ($p=0.0005$ and $p=0.0007$), anaphase ($p=0.001$ and $p=0.007$) and cytokinesis ($p=0.0003$ and $p=0.0006$) compared with the RNAiMAX and *NT1 siRNA* siRNA transfected cells respectively (Figure 3.13A).

3.5.2.5.2 Live cell imaging of *ASPM* siRNA treated U2OS cells identifies the induction of apoptosis and cytokinesis failure

An increase in cytokinesis failure in *ASPM* siRNA treated cells was observed after both symmetric and asymmetric cell divisions (Figure 3.12A), where the cell reached telophase with two discrete nuclei, but failed to abscise and reformed as a single cell. A significant visible increase in the cell death was also detected in *ASPM* siRNA cells ($p<0.0001$ and $p<0.0001$), 72 hours post transfection, compared with the RNAiMAX and *NT1 siRNA* siRNA transfected cells respectively. On average, *ASPM* siRNA cells showed approximately a 10-fold increase in the number of apoptotic cells compared to RNAiMAX and *NT1 siRNA* cells (Figure 3.13B). (The time-lapse imaging movie is included in a CD attached to this thesis).

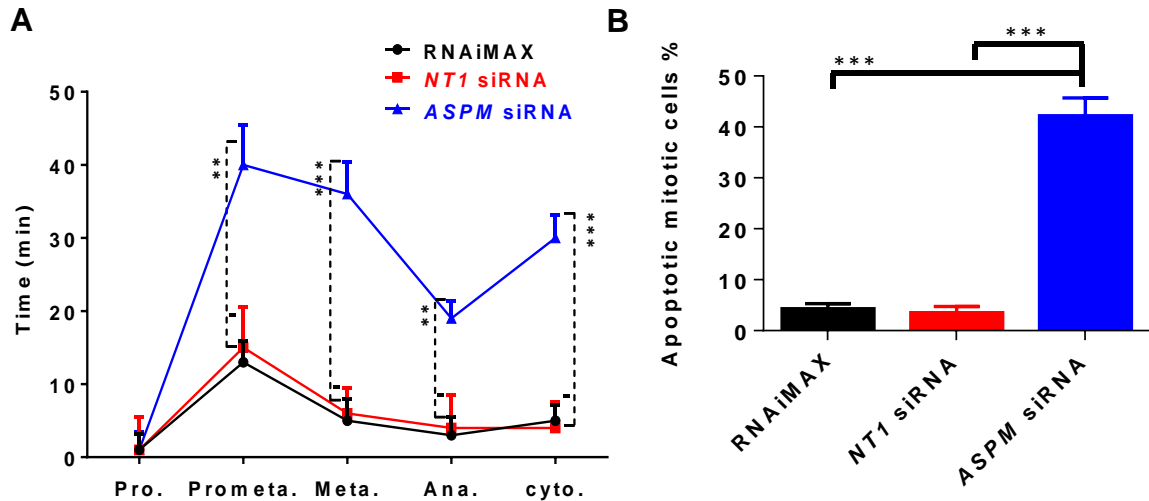


Figure 3.13: *ASPM* siRNA mediated KD in U2OS cells induces an increase in the time taken to complete each stage of mitosis and in the occurrence of apoptosis **A.** Histogram showing the length of time taken in each mitotic stage of asymmetric cell divisions for each of the cell strains, which shows *ASPM* siRNA cells took significantly longer to complete all stages of mitosis (in particularly metaphase and cytokinesis) in comparison to RNAiMAX and *NT1 siRNA* siRNA cells. **B.** Graph showing the mean percentage of apoptotic cells in RNAiMAX, *NT1 siRNA* and *ASPM* siRNA cells. A significant increase in the percentage of apoptotic cells was detected in the *ASPM* siRNA cells compared to the control cells.

Although the incidence of cytokinesis failure in *ASPM* siRNA treated cells was increased in symmetrical cell divisions, it was far more prevalent in cells undergoing asymmetric cell divisions, where 84% cells undergoing asymmetrical divisions failed to complete cytokinesis (Table 3.1).

Table 3.1: Comparison of the effect of siRNA mediated ASPM depletion on mitotic spindle position and cytokinesis in ASPM siRNA, RNAiMAX, NT1 siRNA treated U2OS cells.

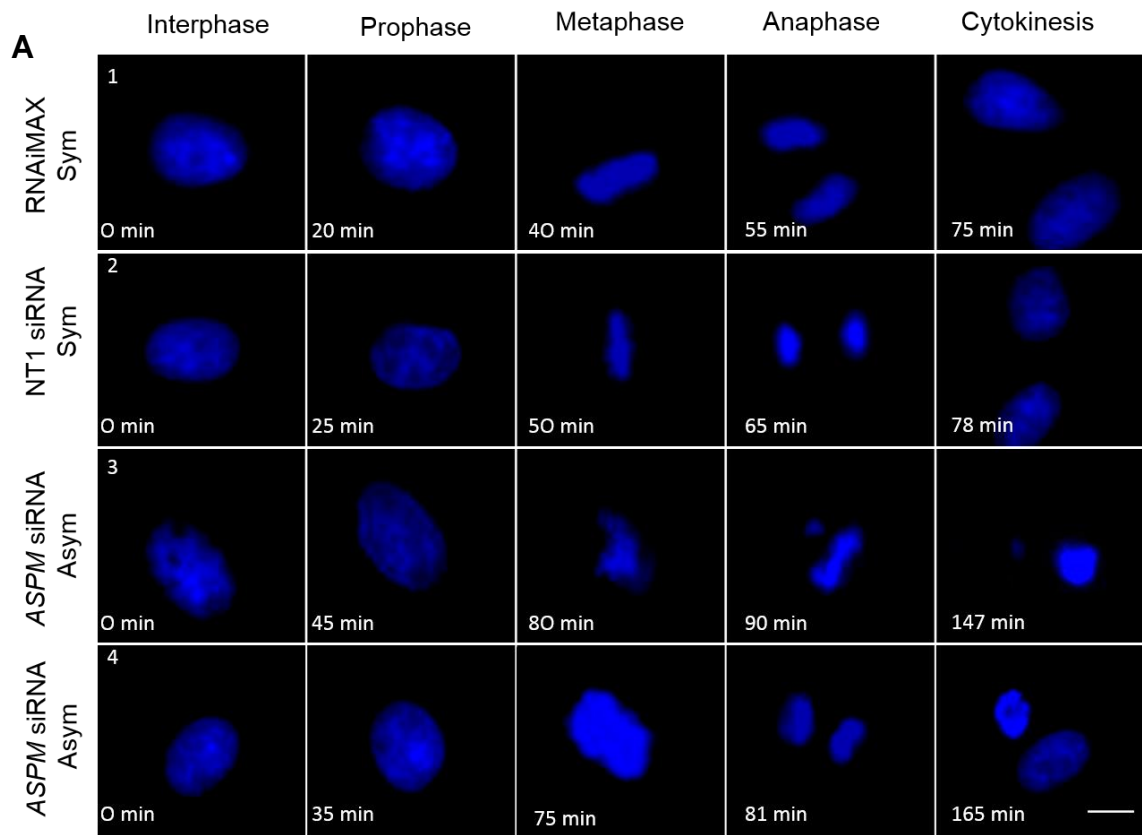
Cell types	Symmetric division with cytokinesis (%)	Symmetric division with cytokinesis failure (%)	Asymmetric division with cytokinesis (%)	Asymmetric division with cytokinesis failure (%)
RNAiMAX	(70.2%)	(10.2%)	(13.3%)	(6.3%)
Total (%)	(80.4%) Sym.		(19.6%) Asym.	
NT1 siRNA	(64.1%)	(9.3%)	(22.1%)	(4.5%)
Total (%)	(73.4%) Sym.		(26.6%) Asym.	
ASPM siRNA	(24.9%)	(12.8%)	(9.6%)	(52.7%)
Total (%)	(37.7%) Sym.		(62.3%) Asym.	

3.5.3. Live cell imaging of Histone H2B-GFP stably transfected HeLa cells to further explore the effect of ASPM siRNA mediated KD on the nucleus.

To understand if interphase nuclear abnormalities observed in ASPM KD cells resulted from changes in nuclear chromatin organisation or mitotic abnormalities, live cell imaging of HeLa cells expressing green fluorescent protein (GFP) fused to Histone H2B-GFP, which results in GFP-tagged chromosomes was performed so that changes in DNA could be observed through mitosis. The ASPM siRNA reverse transfected GFP-cells were incubated at 37°C for 48hrs after which time-lapse imaging was performed for 24hrs in CO₂ independent media containing FBS. The

experimental timing was aimed at catching images as aberrant phenotypes were created rather than when they were a feature as seen by IF. Time-lapse imaging experiments were performed using a BioStation IM live cell imaging microscope and the images obtained at 3 minute intervals were then viewed using Fiji/ImageJ software.

ASPM KD in H2B-GFP HeLa cells induced mitotic aberrations similar to those observed in U2OS upon ASPM KD (Figure 3.14A). A statistically significant increase in aberrant nuclear phenotypes (lobular nuclei, micronuclei, binucleation, uneven nuclei in daughter cells and large nuclei) were observed after *ASPM siRNA* treatment of H2B-GFP HeLa cells (Figure 3.14B and C). Quantitative analysis revealed significant increase of the lagging chromosomes ($p=0.002$ and $p=0.001$) and metaphase arrest ($p=0.0002$ and $p=0.0002$) phenotypes due to *ASPM siRNA* transfection in HeLa cells compared with RNAiMAX and *NT1 siRNA* cells respectively (Figure 3.14B). *ASPM siRNA* cells also showed statistical significance for cytokinesis failure ($p=0.002$ and $p=0.004$) and cell death ($p=0.0001$ and $p<0.0001$) when compared using a paired two tailed t-test to RNAiMAX and *NT1 siRNA* cells respectively (Figure 3.14B). As in U2OS cells quantitative analysis of aberrant nuclear phenotypes in *ASPM siRNA* cells revealed significant changes for frequency of lobular nuclei ($p=0.0001$ and $p=0.0001$), micro nuclei ($p=0.001$ and $p=0.001$), enlarged nuclei ($p<0.0001$ and $p<0.0001$) and multinucleated cells ($p=0.0004$ and $p=0.0007$) compared with RNAiMAX and *NT1 siRNA* cells respectively (Figure 3.14.C).



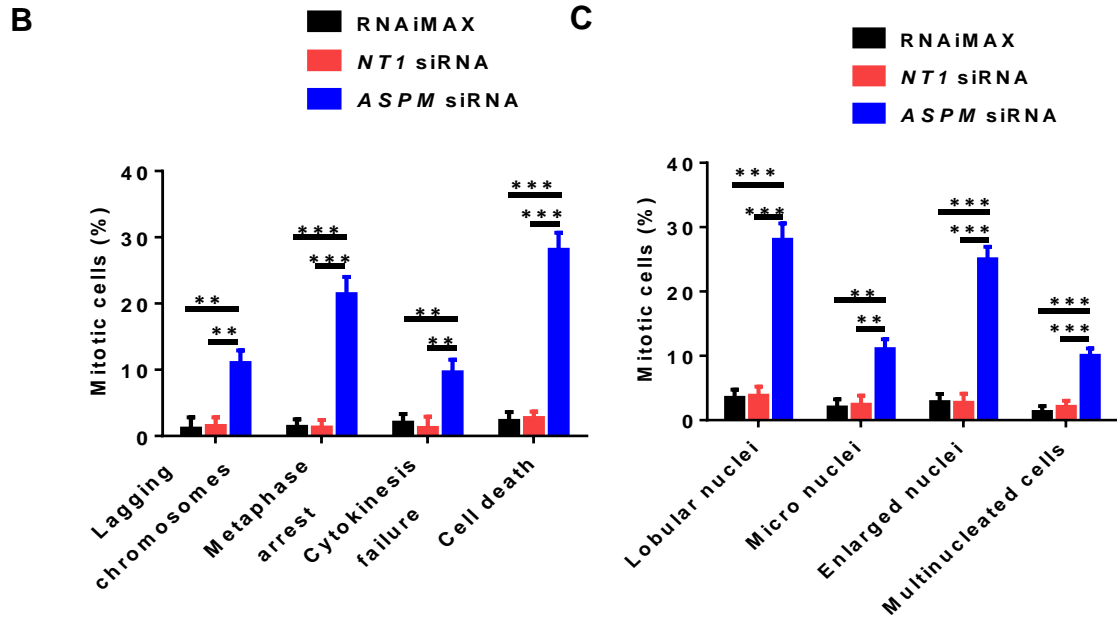


Figure 3.14: *ASPM* siRNA mediated KD Histone H2B-GFP HeLa cells results in metaphase arrest and cytokinesis failure and causes aberrant nuclear interphase phenotype. A. Panel shows phase contrast images of RNAiMAX, *NT1 siRNA* and *ASPM* siRNA transfected GFP-Histone 3 HeLa cells during mitosis taken at specified time points (cumulative timings are given in the bottom left hand corner of each image). First top two rows show RNAiMAX and *NT1 siRNA* treated cells with normal mitosis respectively. Row 3 shows *ASPM* siRNA treated cell with lagging chromosomes entrapped in micronuclei and the main nucleus remain lobular and row 4 shows cytokinesis failure leading to cell death. Scale bar = 10 μ m. **B.** Histogram showing the mean percentage of mitotic phenotypes in RNAiMAX (n= 122 dividing cells), *NT1 siRNA* (n= 118 dividing cells) and *ASPM* siRNA (n= 103 dividing cells) cells. A significant increase of the percentage of mitotic cells undergoing metaphase arrest and cytokinesis failure was identified in *ASPM* siRNA cell populations compared to control cells. **C.** Statistical analysis of nuclear interphase phenotypes in RNAiMAX (n= 350 cells), *NT1 siRNA* (n= 364 cells) and *ASPM* siRNA (n= 370 cells) cells.

ASPM siRNA treated cells showed a greater number of enlarged, lobular and multinucleated cells than in the control transfected cells.

Live cell imaging of siRNA treated H2B-GFP HeLa cells enabled the mechanisms underlying the creation of nuclear phenotypes to be explained. All of the phenotypes arose as a result of aberrant mitosis and were not an effect of specific chromatin restructuring. Three main mitotic abnormalities (lagging chromosomes, metaphase arrest and cytokinesis failure) resulted in aberrant nuclei in daughter cells (Table 3.2). The observation of lagging chromosomes during metaphase and anaphase resulted in the formation of lobular nuclei (predominant phenotype) and micronuclei. Metaphase arrest resulted in cell death (predominant phenotype) or a single cell with an enlarged nucleus, whereas cytokinesis failure in HeLa cells also gave rise to a single cell with an enlarged nucleus (predominant phenotype) or a multinucleated single cell. Specific examples of mitotic aberrations are shown in (Figure 3.14A). (Figure 3.14) row 3 shows a typical abnormal scenario exhibited by an *ASPM* siRNA transfected cell in mitosis, where the cell takes longer to reach metaphase and exhibits some problem with chromosome separation and is unable to progress through mitosis and eventually the cell undergoes apoptosis (compacted nuclei shown). Other phenotypes observed in *ASPM* siRNA transfected cells were uneven separation of chromosomes, in cells that took a long time to progressed mitosis through cytokinesis resulting in daughter cells with unevenly sized nuclei, which in some cells resulted in apoptosis (Figure 3.14A row 4). Post mitotic 'donut' shaped nuclei were not observed in HeLa cells transfected with *ASPM* siRNA.

Table 3.2: The correlation between mitotic phenotypes and nuclear outcomes in *ASPM* siRNA, RNAiMAX, *NT1* siRNA treated HeLa cells.

Mitotic Phenotypes outcomes						
Cell type	Lagging chromosomes	Outcomes	Metaphase arrest	outcomes	Cytokinesis failure	outcomes
RNAiMAX	(1.1%)	1. Lobular nuclei (53.4%) 2. Micro nuclei (46.6%)	(1.4%)	1. Cell death (52.3%) 2. Enlarged nuclei (47.7%)	(2%)	1. Enlarged nuclei (51.4%) 2. Multinucleated cells (48.6%)
NTi siRNA	(1.5%)	1. Lobular nuclei (53.8%) 2. Micro nuclei (46.2%)	(1.3%)	1. Cell death (52.7%) 2. Enlarged nuclei (47.3%)	(1.2%)	1. Enlarged nuclei (47.9%) 2. Multinucleated cells (52.1%)
ASPM siRNA	(11%)	1. Lobular nuclei (77.6%) 2. Micro nuclei (22.4%)	(21.4%)	1. Cell death (78.1%) 2. Enlarged nuclei (21.9%)	(9.6%)	1. Enlarged nuclei (67.7%) 2. Multinucleated cells (32.3%)

3.6 Discussion

At the onset of this project (2014) a number of mitotic functions of ASPM and Aspm had been identified, including maintaining spindle orientation and symmetric cell division (Fish, *et al.*, 2006), which is required to maintain proliferation of neural progenitor cells during cortical development (Fish *et al.*, 2008; Buchman *et al.*, 2011), spindle assembly (Tillement *et al.*, 2009), cytokinesis (Higgins *et al.*, 2010), metaphase arrest (Gonzalez *et al.*, 1990) and cell death (Kouprina, *et al.*, 2005; Bikeye, *et al.*, 2010; Higgins *et al.*, 2010). Further studies of ASPM function have been identified whilst this project has been ongoing and some of these bare relations to the findings identified in this chapter.

The U2OS cells used in this study expressed two ASPM bands when analysed by WB. The larger MW band corresponded to the full length 410kDa ASPM protein, whilst a lower MW band was observed at ~120kDa. The WT protein plus three isoforms for ASPM have previously been identified (Kouprina, *et al.*, 2005), however the ASPM 217-2 peptide sequence corresponds to the 3' end of exon 3 DNA sequence which is a region spliced out in the published ~125kDa Variant 3 ASPM isoform. This suggests that other unpublished cell type specific ASPM isoforms exist whose transcript contain at least part the 3' of Exon 3. This isoform was not identified in the Higgins *et al.* 2010 ASPM paper which also used U2OS cells. The WB protocol used in this study was optimised during this project, therefore the identification of the additional ASPM band in U2OS cells may be due to the more sensitive detection methods used in this study. The reduction of the

level of the ~120kDa ASPM protein upon use of the exon 3 localised *ASPM* siRNA (3' region of exon 3) indicates that the band is an ASPM specific isoform. Other previously reported ASPM isoforms (Kouprina, *et al.*, 2005) were not identified in this study. WB and IF analysis showed that ASPM was reduced in U2OS cells following 72hr incubation with *ASPM* siRNA, however ASPM was not completely removed. The level of ASPM KD in U2OS cells and the more severe phenotypes identified in this chapter vary slightly to those reported in a previous study performed within our group (Higgins *et al.*, 2010). This can be explained by the use of a different transfection reagent (RNAiMAX rather than Oligofectamine) which resulted in a more efficient *ASPM* knockdown. The partial knockdown of *ASPM* in U2OS cells reported in this chapter had a significant effect on mitosis, confirming ASPM is an essential mitotic protein in the U2OS cell line.

The experiments performed in this chapter identified that ASPM KD in U2OS cells caused aberrations in centrosomes/spindle poles (structure/integrity and number) and in MT and actin (disorganisation/reorganisation and low density). Such centrosomal and cytoskeletal malformations led to the formation of an aberrant mitotic bipolar spindle or multipolar spindle where the spindle pole was not cohesive (haloed centrosome). The integrity of the mitotic bipolar spindle is key for accurate chromosome segregation. In this study the formation of a defective spindle pole and mitotic spindle resulted in poor chromosome separation (lagging chromosomes, micronuclei and unequal separation phenotypes) and changes in spindle orientation, again indicating MT impairments. The transition of mitotic cells through mitosis was delayed with some cells exiting mitosis during prometaphase

and returning to G1 (mitotic slippage) but with double the quantity of DNA (enlarged nucleus) and increased centrosomes, or undergoing programmed cell death (apoptosis). Another MT associated aberrant phenotype observed in ASPM KD cells was a failure to complete cytokinesis, where telophase ended with DNA packaged into two nuclei, but in a single cell. Malfunctions in centrosome duplication led to multipolar spindles which coupled with cytokinesis failure resulted in the formation of multi-nucleated cells. Cells with chromosome separation defects (lagging chromosomes, micronuclei and unequal separation phenotypes) but which transited through mitosis, completed mitosis with nuclear shape defects (lobular or donut shaped nuclei) or micronuclei.

Although our N-terminal ASPM antibody did not detect an interphase centrosomal localisation pattern, a co-localisation pattern of ASPM with γ -tubulin has previously been reported (Zhong *et al.*, 2005; Singhmar, 2011; Jayaraman *et al.*, 2017) along with an essential role of ASPM in centriole biogenesis (Chavali *et al.*, 2014; Jayaraman, 2015; Jayaraman *et al.*, 2016; Jayaraman *et al.*, 2017). Centrosomal abnormalities have been observed to result from *asp* mutations in *Drosophila* (Gonzalez *et al.*, 1990). The microcephaly protein WDR62 (at the *MCPH2* loci) (Bhat *et al.*, 2011) is required for ASPM centriolar localisation and interacts physically with ASPM to control centriole duplication and hence the reduction of ASPM would influence this role (Jayaraman *et al.*, 2017). Moreover, ASPM is required for centromere associated protein J (CENPJ, *MCPH6*) localisation to the centrosome (Jayaraman *et al.*, 2016) which is required to maintain centrosome integrity and elongation (Schmidt, *et al.*, 2009; Kitagawa *et al.*, 2011; McIntyre *et*

et al., 2012). Centrosomes are microtubule-organizing centres (MTOC) which nucleate the polymerization of α - and β -tubulin dimers, the protein building blocks of microtubules (Mckean *et al.*, 2003; Moutinho *et al.*, 2009; Blas *et al.*, 2017; Sanchez *et al.*, 2017). Consequently, some centrosomal defects will be associated with MT abnormalities. The Immunofluorescence staining of microtubules revealed that the depletion of ASPM induced clustered microtubules where MT exhibited a tendency to grow in groups and disorganised microtubules where the normal distribution of MT network was misoriented and formed unstable opposing MT growth trajectories. In addition to that low-density microtubule network was observed where the MTs density was diminished (lower molecular mass) in most cells compared to control cells. In the other hand, control NT1 siRNA and RNAiMAX treated cells showed normal distribution, organisation and density of MT network. Our research group has previously identified that ASPM spindle pole localisation is dependent upon microtubules (Higgins *et al.*, 2010). ASPM is known to have roles in mitotic spindle assembly functions, including spindle pole focussing, spindle assembly, with ASPM depletion resulting in mono and tripolar spindle formation (Tillement *et al.*, 2009). The mitotic spindle uses MTs and mitotic motors to accurately segregate DNA into the daughter cells (Civelekoglu *et al.*, 2010). The assembly of the mitotic spindle relies highly on ASPM (Saunders, *et al.*, 1997; Fish, Kosodo, *et al.*, 2006; Higgins *et al.*, 2010; Ito, *et al.*, 2015), with Asp acting mainly independently of the motor protein dynein and the MT spindle regulator Mud (NuMA in humans) to maintain centrosome-spindle coupling, preventing the occurrence of supernumerary cells (Bosveld *et al.*, 2017). NuMA,

was identified as a potential interactant partner for ASPM at mitotic spindle poles in *C. elegans* (Van Der Voet, *et al.*, 2009). A reduction in ASPM would lead to a reduction in spindle pole focussing and a reduction in the forces required for accurate chromosome separation and segregation, leading to chromosome separation defects during mitosis.

In this study, ASPM depletion caused cells to take longer to complete each stage of mitosis, with an associated increase in the number of cells in prometaphase and metaphase and a decrease in the number of cells in anaphase and cytokinesis. In support of this, *Asp* (*Drosophila melanogaster*) playing a specific role in prometaphase-metaphase stage has already been reported (Ito, *et al.*, 2015). In HCT116 colorectal carcinoma cells, *ASPM* knock out along with the depletion of the pericentriolar material protein CDK5RAP2 (CEP215, *MCPH3*) caused a four-fold increase in the number of prometaphase and metaphase cells compared to that in untreated KO cells due to a significant delay in the anaphase onset (Tungadi *et al.*, 2017). However, deletion of the *ASPM* gene alone did not affect mitotic progression. In a mouse model for human microcephaly, *Aspm* controlled time spent in G1 by protecting Cyclin E from ubiquitin-mediated degradation, therefore loss of ASPM increased cell cycle lengthening (Capecchi *et al.*, 2015). ASPM is required to maintain symmetrical (proliferative cell division), with ASPM depletion resulting in reorientation of the mitotic spindle to form neurogenic divisions (Fish *et al.*, 2006; Higgins *et al.*, 2010). ASPM may regulate spindle orientation by interacting with CITK (Gai, *et al.*, 2016). ASPM is required to recruit citron kinase (CITK) to the mitotic spindle and CITK regulates nucleation and

stability of astral MT which assemble via a centrosome controlled pathway in prometaphase. Both ASPM and CITK affect the organisation of astral microtubules. It is proposed that ASPM promotes astral MT organisation by recruiting CITK to the astral MTs, thus ensuring the spindle is anchored to the cell cortex. However another interacting partner of ASPM, the MCPH2 protein, WD Repeat-Containing Protein 62 (WDR62), is required in its phosphorylated form for correct mitotic spindle orientation (Miyamoto *et al.*, 2017; Sana *et al.*, 2018). A reduction in ASPM could affect each of these pathways. A role for ASPM in cytokinesis was also confirmed in this study. The ASPM C-terminus interacts with CITK, and CITK and ASPM co-localise to the midbody during cytokinesis (Paramasivam, *et al.*, 2007). Cytokinesis failure due to a reduction in ASPM may occur through a reduction in the interaction with CITK which controls the transition from cleavage furrow constriction to abscission during cytokinesis (Watanabe *et al.*, 2013) through the maintenance of F-actin (Dema *et al.*, 2018).

ASPM is located in the nucleus in interphase, suggesting a nuclear function for ASPM. Immunofluorescence staining of *ASPM* siRNA U2OS cells detected an unexpected and significant increase in aberrant nuclear interphase phenotype when compared with control cells, which initially suggested that ASPM is playing a direct role in maintaining the nuclear shape. However, these abnormalities were found to arise as a result of mitotic defects including chromosome separation irregularities. Visible increase in donut-shaped nuclei or ring-shaped nuclei, where cells appeared to have hole in the centre as a result of defective mitosis, in the majority of U2OS cells was observed along with enlarged (double the quantity of

DNA), lobular (DNA is packaged in multiple spheres instead of one big sphere) and micro nuclei (small nucleus with fragment of DNA) in *ASPM* siRNA cells. The formation of donut-shaped nuclei has been reported to arise due to centrosome separation defects and DNA de-condensation in mitosis (Verstraeten *et al.*, 2011; Adam *et al.*, 2013) and is a phenotype associated with the induction of premature senescence. Post mitotic 'donut' shaped nuclei were not detected in HeLa cells transfected with *ASPM* siRNA compared to *ASPM* transfected U2OS cells. It is conceivable that U2OS cells are more sensitive to *ASPM* depletion and lost have lost their ability to respond to checkpoint signals, compared to HeLa cells.

MT and actin filaments are two cytoskeletal networks that are physically bridged and cross-linked via proteins or protein complexes (Applewhite *et al.*, 2013). Hence, we would expect that *ASPM* depletion due to *ASPM* KD to have an effect on actin filaments localisation and distribution. Immunofluorescence analysis confirmed that *ASPM* is involved in actin filaments organisation and distribution. Unlike control transfected U2OS cells, actin filaments disorganisation/redistribution was induced in *ASPM* siRNA treated U2OS cells. In control transfected cells, actin filaments displayed organised linear network distributed around the cell periphery and extend throughout the cytoplasm. The involvement of microtubules and actin filaments in changing nuclei shape and structure has been previously reported (Brandt *et al.*, 2006; Khatau *et al.*, 2009; Vishavkarma *et al.*, 2014; Hu *et al.*, 2015).

In summary a number of interesting mitotic phenotypes have been identified in *ASPM* siRNA knockdown U2OS cells which suggest roles for *ASPM* in actin organisation, microtubule organisation, centrosomal biogenesis symmetric division,

mitotic progression, abscission and possibly nuclear chromatin organisation. A novel ASPM role in maintaining cell shape has been indicated which may offer support for a novel ASPM role in interphase. Moreover, ASPM roles in prometaphase-metaphase stage during mitosis and cytokinesis were confirmed. Taken together, our findings indicate that ASPM is playing roles in interphase as well as to complete mitosis and cytokinesis. It is suggested that the mitotic defects arising from ASPM reduction would result a dramatic reduction in neural progenitor and neuronal cell number either by (i) an increase in the length of time taken to complete cell division which would give rise to fewer cell divisions within the defined period of neurogenesis (ii) a premature change in the orientation of division from symmetric to asymmetric divisions leading to a decrease in the number of progenitor cells and hence neurons produced (iii) an inability to complete mitosis or (iv) cell death. In comparison to the 2010 study (Higgins *et al.*, 2010) in U2OS cells, novel ASPM specific Isoform was discovered at approximately 120kDa due to more sensitive detection methods was used in this study as a result of protocol optimization. Aberrations in nuclear (lobular, enlarged and micro nuclei), centrosomes/spindle poles (structure/integrity and number) and in MT and actin (disorganisation/reorganisation and low density) were identified. In addition to that, MT associated aberrant phenotype observed in U2OS cells was an increase in the proportion of cells in prometaphase and/or metaphase stages, a corresponding decrease in the proportion of cells in anaphase and cytokinesis, and changes in division type and length of time taken to complete each stage of mitosis. Furthermore, live cell imaging of Histone H2B-GFP stably transfected

HeLa cells was used to further explore the effect of ASPM siRNA mediated KD on the nucleus. One criticism that could be made for the assignment of abnormal post mitotic phenotypes is that there could be biases in phenotype interpretation between scorers. To minimise this effect in future samples could be blinded, so researchers would not know if they were scoring negative controls or knockdown samples, or for multiple researchers to score the slides and discuss outcomes. The availability of a unique resource of MCPH5 patient fibroblast cells containing ASPM mutations offers the ideal opportunity to study which mitotic processes are affected in ASPM patients.

Chapter 4 : Comprehensive analysis of the effect of *ASPM* mutation upon cellular mitosis.

4.1 Introduction

Previous siRNA knockdown studies, including those described in the preceding chapter, have identified many mitotic roles for ASPM, including cleavage furrow orientation/spindle orientation and cytokinesis (Bond *et al.*, 2002; Kouprina, *et al.*, 2005; Zhong *et al.*, 2005; Fish, *et al.*, 2006; Higgins *et al.*, 2010; Capecchi *et al.*, 2015). In addition, roles for ASPM in spindle assembly and spindle rotation have been shown (Van Der Voet, *et al.*, 2009; Xu *et al.*, 2012; Connolly *et al.*, 2014). However, understanding the functions of ASPM disrupted by mutation in *ASPM* has been less studied. Mutations in the *ASPM* gene at the *MCPH5* locus on chromosome 1q31 are the most common cause of MCPH (Roberts, *et al.*, 2002). The types of mutation identified include nonsense, missense, translocations, splice site and frameshift mutations (Bond *et al.*, 2002; Bond *et al.*, 2003; Kumar *et al.*, 2004; Pichon *et al.*, 2004; Shen *et al.*, 2005; Desir *et al.*, 2006; Gul *et al.*, 2006; Nicholas *et al.*, 2009a; Akbariazar *et al.*, 2013; Ariani *et al.*, 2013; Papari *et al.*, 2013; Hussain *et al.*, 2013; Hu *et al.*, 2014; Hashmi *et al.*, 2016; Bhargav, 2017; Letard *et al.*, 2018). The mutations are spread throughout the *ASPM* gene and there does not appear to be a mutational hotspot within the gene. With the exception of 1 missense mutation (Gul *et al.*, 2006), splice site mutations (Bond *et al.*, 2003) and a translocation or a recombination event (Pichon *et al.*, 2004;

Verloes *et al.*, 2013) , the remaining mutations were forecast to cause protein truncation with the resultant protein predicted to varying in size from 25 amino acids (74del G) to 3,474 amino acids (Bond *et al.*, 2002; Bond *et al.*, 2003; Kumar *et al.*, 2004; Pichon *et al.*, 2004; Shen *et al.*, 2005; Desir *et al.*, 2006; Gul *et al.*, 2006; Gul *et al.*, 2007; Nicholas *et al.*, 2009; Higgins *et al.*, 2010; Pulvers *et al.*, 2010; Akbariazar *et al.*, 2013; Ariani *et al.*, 2013; Papari *et al.*, 2013; Hussain *et al.*, 2013; Hu *et al.*, 2014; Abdel-Hamid *et al.*, 2016; Hashmi *et al.*, 2016; Bhargav, 2017; Letard *et al.*, 2018), or nonsense mediated decay (Brognia *et al.*, 2009) and the predicted region of loss common to all ASPM protein truncating mutations is the extreme C-terminus of ASPM, suggesting the C-terminus has an important function in maintaining cell division (Higgins *et al.*, 2010).

Access to the unique resource of two *MCPH5* patient fibroblast cell strains (Higgins *et al.*, 2010) offers the opportunity to study how specific mutations in *ASPM* affect mitosis. In this chapter, the phenotypic outcome of the *ASPM* mutations, *ASPM*^{663delG} and *ASPM*^{9984+1G>T} was investigated to determine the effect of *ASPM* mutation on the mitotic apparatus and mitotic progression to further our understanding of the function of ASPM and the reduction in brain size resulting in MCPH. Previous investigations have identified *ASPM*^{9984+1G>T} as creating a novel cryptic splice site resulting in the loss of 3 amino acids from the C-terminal region.

4.2 Hypothesis.

It is hypothesised that the homozygous *MCPH5 ASPM* 3663delG mutation will result in truncation of the ASPM protein or nonsense mediated decay of the *ASPM*^{3663delG} protein. It is also hypothesized that both the homozygous *ASPM* 3663delG and *ASPM* 9984+1G>T mutations will lead to severe aberrations in mitosis. It is suggested that during neurogenesis aberrations may lead to an early switch from symmetric division to asymmetric division and to an increased length of time taken to complete mitosis leading to reduced mitotic potential and a reduction in cell number produced during the neurogenesis window. This will reduce neuronal cell number and therefore brain size.

4.3 Objectives.

The aim of this study is to investigate changes in mitotic phenotype in *MCPH5* patient fibroblast cells containing homozygous *ASPM* mutations (*ASPM*^{3663delG} and *ASPM*^{9984+1G>T}), compared to wildtype control fibroblasts. Observations of alterations in mitotic timing, the structure of cellular components including the mitotic machinery, type of division, outcome of division and commonalities and differences resulting from the two individual mutations will indicate further functions of ASPM and the etiology of MCPH.

4.4 Methods

4.4.1 Cell lines.

A non-immortalized control human neonatal dermal fibroblast cell strain (HDF Neo (*ASPM*^{MT})), was obtained from Genlantis (San Diego, California). Fibroblast cells from two individual patients of Northern Pakistani origin (*ASPM*^{β663delG} and *ASPM*^{9984+1G>T}) had been created from forearm skin biopsies (collected by Prof C.Geoffrey Woods) by the Yorkshire Cytogenetics laboratory and the sample collection, cell line creation and experimental use of the fibroblast cells for research purposes was approved by the Ethical Committee of Leeds (East) Research Ethics Committee (REC reference number 05/Q1206/80). The outcome of the *ASPM*^{9984+1G>T} mutation on both ASPM protein content and molecular weight had previously been investigated (Higgins et al., 2010), however further investigation of mitotic outcomes in this cell strain had not been performed.

4.4.2 General Methodologies.

Methodologies used in this study were (i) cDNA sequencing (Section 2.3.3) and PCR (Section 2.3.5) to investigate the effect of mutational change on splicing; (ii) Immunoblotting using anti-ASPM 217-2 N-terminal antibody to determine ASPM expression and anti-mouse β-actin to determine β-actin expression as a loading control (Chapter 2.4), (iii) IF microscopy using N-terminal anti-ASPM-antibody 216-1 (green) (Chapters 2.2 IF and Chapter 2.2.3. Image capture) for ASPM localisation studies and the identification of mitotic alterations and (iv) Time-lapse

live cell imaging (Chapter 2. 2.2.4) to identify phenotypic changes in mitotic timing and mitotic outcomes Fibroblast cells were cultured and imaged in 35 mm quadrant glass-bottomed culture dishes and images were taken for a period of 72 hours. Data and figures were assembled, analysed and annotated using GraphPad Prism 6.0 (GraphPad Software, Inc., San Diego, CA). All images presented in this chapter were analysed by Fiji/ImageJ software to identify phenotypic changes. Vertical bars were used to identify the standard deviation average values for the mean and data was presented as the mean of at least 3 independent experiments.

4.5 Results

4.5.1. *MCPH5* patient clinical diagnosis and predicted ASPM protein translation information.

Two *MCPH5* patient fibroblast cell lines (*ASPM*^{3663delG} and *ASPM*^{9984+1T>G}) and a normal ASPM wildtype control (*ASPM*^{WT}) cell line were available for investigation. The *ASPM*^{9984+1T>G} mutation is associated with moderate MCPH and mental retardation and is an intronic base pair substitution of the first nucleotide of intron 25 at IVS25+1G>T (c.9984+1G>T). This mutation has been shown to remove the splice donor site, resulting in the creation of an in frame cryptic splice donor site 9 base pairs upstream and causing the loss of 3 amino acids (amino acids 3326-3328), giving a predictive ASPM protein size of approximately 410KDa (Higgins et al., 2010). The *ASPM*^{9984+1T>G} mutation causes a reduction in the amount of ASPM localised to the mitotic spindle poles (Higgins *et al.*, 2010) The *ASPM*^{3663delG}

mutation is associated with severe MCPH and mental retardation and is the deletion of a single guanine at c.3663delG (exon 15) p1221Arg which lies towards the end of the second CH domain of ASPM (Bond *et al.*, 2003). Bioinformatics indicated the mutation would result in a frame shift followed by the translation of a further 12 amino acids before reaching a stop codon (P.Arg1221SerfsTer12). Therefore, this mutation was predicted to produce the translation of a truncated ASPM protein of 1,233 amino acids or to result in nonsense mediated decay (NMD) (Bond *et al.*, 2003; Mahmood *et al.*, 2011; Hug *et al.*, 2016).

4.5.2 Investigation of the effect of ASPM mutations on ASPM protein molecular weight.

The effect of the *ASPM*^{9984+1T>G} mutation had previously been shown to result in an in-frame deletion of 3 C-terminal amino acids (Higgins *et al.*, 2010). The *ASPM*^{3663delG} mutation was predicted to result in protein truncation, with the resultant protein predicted to be of molecular weight 220 KDa (Bond *et al.*, 2003). To determine the effect of the *ASPM*^{3663delG} mutation on the molecular weight of the ASPM protein, WB was performed using the previously optimized 217-2 N-terminal rabbit-anti-ASPM antibody (Higgins *et al.*, 2010) and an anti-mouse β -actin antibody, which was used as a loading control to show loading of equal amounts of protein extract for each cell sample. The intensity of ASPM protein in each of the cell lines was normalised to the corresponding β -actin intensity, measured using

Fiji/ImageJ software and the average ASPM protein level per cell lysate calculated from three independent experiments using GraphPad Prism software.

Immunoblotting analysis of cell lysates from control and patient cell lines surprisingly identified expression of a single band approximately corresponding to the molecular weight of wild type ASPM protein in all three samples (410kDa) (Figure 4.1A). Evidence for the existence of *ASPM* splice variants or truncated proteins was not observed for the samples. β -actin showed equal protein loading in each lane. Densitometry was performed on the ASPM and β -Actin bands and the ASPM band was normalised to the control β -actin band using the HDF Neo cells as the control lysate (Figure 4.1B). A highly significant decrease in the amount of ASPM protein was observed in the patient cell lysates in comparison to the $ASPM^{WT}$ ($ASPM^{3663delG}$ $p=0.0002$, $ASPM^{9984+1T>G}$ $p=0.0009$).

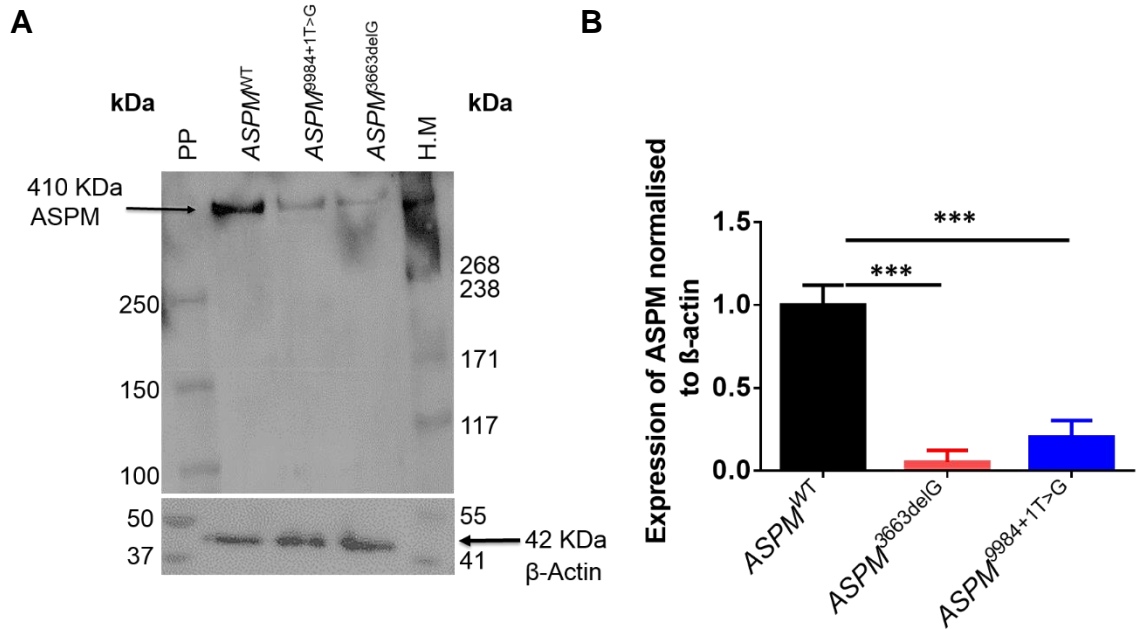


Figure 4.1: Effect of *ASPM* mutations *ASPM*^{3663delG} and *ASPM*^{9984+1T>G} on *ASPM* protein size and level of expression. **A. Immunoblotting of cell lysates of HDF Neo (*ASPM*^{WT}) cells (lane 2), TC 363-06 cells (*ASPM*^{3663delG}, lane 4) and TC 273-05 cells (*ASPM*^{9984+1T>G}, lane 3) with anti-*ASPM* 217-2 N-terminal antibody (Appendices 1 and 2 *ASPM* structure and Antibodies) and anti-mouse β-actin. Protein marker ladders were Precision Protein (PP) and HiMark (H.M.). *ASPM* mutations, *ASPM*^{3663delG} and *ASPM*^{9984+1T>G}, lead to the expression of a reduced level of approximately full length *ASPM* protein in patient cells. *ASPM* was detected as a discrete band at 410kDa in every cell lysate. A faintly visible band of slightly lower molecular weight was observed in the *ASPM*^{9984+1T>G} lane but not in the *ASPM*^{WT} and *ASPM*^{3663delG} lanes, may be corresponding to an isoform/paralogue, post-translational modification or degradation products. N=3 **B.** The histogram illustrates the expression of *ASPM* protein levels normalised to β-actin, *ASPM* expression level was significantly lower in *ASPM*^{3663delG} and *ASPM*^{9984+1T>G} than in *ASPM*^{WT}.**

4.5.3 Investigation of alternative splicing in exons 14, 15 and 16 in *ASPM*^{3663delG} patient cells

As the *ASPM* 3663delG mutation resulted in the production of some approximately full length *ASPM* protein it was theorized that the mutation may have resulted in the creation of a cryptic splice donor site in exon 15. The *ASPM*^{3663delG} sequence (Exons 14-16) was run through The Berkley Splice site prediction program and basic bioinformatics of this mutation within the *ASPM*^{WT} and *ASPM*^{3663delG} sequences predicted (assigning a high prediction score of 0.96) the 3663delG mutation could create a novel cryptic splice site donor site at *ASPM* nucleotides (nts) 3656-3659 (Figure 4.2A), which was predicted to splice out 84bp of exon15 sequence before reaching the existing exon 15 splice acceptor site. The Berkeley Splice site prediction program by neural network, can be accessed at (http://www.fruitfly.org/seq_tools/splice.html). mRNA was extracted from the *ASPM*^{WT} and *ASPM*^{3663delG} cells using Trizol and cDNA was created using Power Script. Primer3 (<http://primer3.ut.ee>) was used to design PCR primers to amplify a PCR product of 388bp (CACTTGGTTAGGTCTGCAGTT) spanning exons 14-16 (nt3444-3832) (Figure 4.2B, method section 2.3). The PCR was cleaned up and sent for sequencing using the PCR primers as sequencing primers and the sequence data annotated in SnapGene Viewer. The *ASPM*^{3663delG} cDNA produced continuous sequence data for 387bp and demonstrated the presence of the 3663delG mutation but the mutation did not create an alternative splice site within the 388nt region (Figure 4.2C).

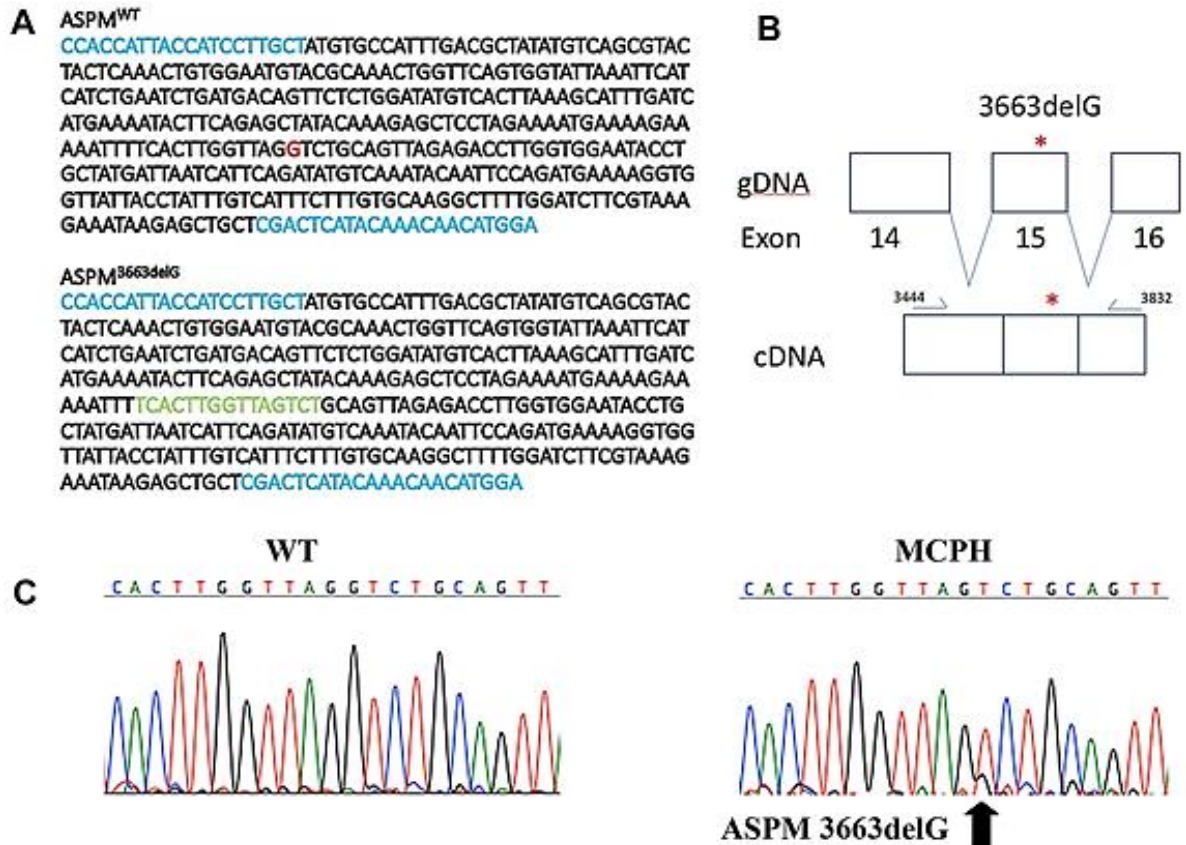


Figure 4.2: The *ASPM* 3663delG mutation does not result in the generation of a cryptic splice donor site in exon 15. A. The *ASPM* 3663delG mutation is predicted to result in the creation of a cryptic splice donor site. Blue lettering denotes cDNA PCR primers, Red G is the site of the deleted nucleotide Purple lettering denotes the exon boundaries and the sequence denoted in green is the novel predicted splice sequence with the exon boundary shown in bold. **B.** Schematic of the exons 14-16 PCR. The point of mutation caused by *ASPM*^{3663delG} is indicated by an asterisk. **C.** Sequencing data showing the 3663delG mutation but no other change in the *ASPM*^{3663delG} cDNA sequence, suggesting the 3663del G mutation does not result in the creation of an alternative splice donor site.

4.5.4. Investigation of ASPM distribution and localization in *MCPH5* patient cells

4.5.4.1 ASPM distribution and localization in *ASPM*^{WT} fibroblast cells.

To determine the normal intracellular distribution and localisation of the human ASPM protein, *ASPM*^{WT} fibroblasts were fixed in methanol (to preserve MTs structure) and immunostained with the N-terminal anti-ASPM-antibody 216-1 (green), anti- α -tubulin (red) and with DAPI (blue) to identify ASPM, MTs and DNA respectively. Human ASPM is a mitotic protein predominantly localizing to the nucleus and with a weaker signal in the cytoplasm in interphase, to the spindle poles from prometaphase to telophase and cytoplasm and Flemming body/midbody during cytokinesis (Figure 4.3).

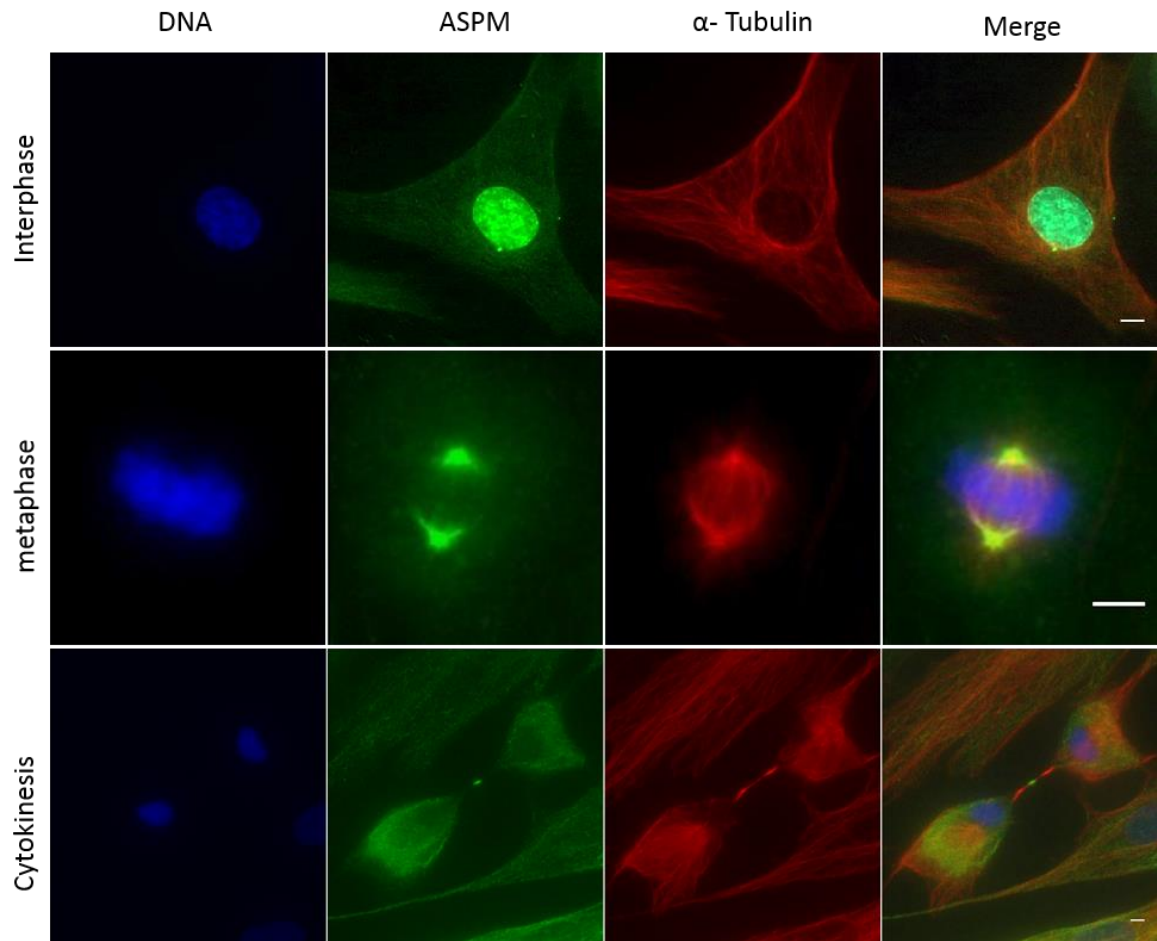


Figure 4.3: ASPM protein cellular localisation in $ASPM^{WT}$ fibroblast cells during interphase, metaphase and cytokinesis. Panel shows $ASPM^{WT}$ localization in $ASPM^{WT}$ cells in interphase (Scale bar = 5 μ m), metaphase (Scale bar = 10 μ m) and cytokinesis (Scale bar = 5 μ m). Cells were fixed in methanol and immunostaining using specific anti-ASPM antibody 216-1 (green) to identify ASPM, anti- α -tubulin (red) to identify MTs and with DAPI (blue) to recognise DNA. ASPM is localised to the nucleus and cytoplasm in interphase, spindle poles in metaphase and midbody during cytokinesis.

4.5.4.2. Analysis of ASPM localization in (*ASPM*^{3663delG} and *ASPM*^{9984+1T>G}) patient cells during interphase.

To define the effect of *ASPM* mutations on ASPM protein distribution and localisation in interphase stage, a comparative immunofluorescence microscopy experiment was carried out for the control and patient cell lines. *MCPH5* patient cells containing the *ASPM* mutations *ASPM*^{3663delG} and *ASPM*^{9984+1T>G} were fixed and stained with N-terminal anti-*ASPM*-antibody 216-1 (green for ASPM), DAPI (blue for DNA), plus α -tubulin (red for MTs). In the patient cell lines, in comparison to *ASPM*^{WT}, ASPM is localised to the nucleus and cytoplasm where the cytoplasmic expression appears stronger than in the control *ASPM*^{WT} cells where it appears to form small aggregates and puncta (Figure 4.4). The concentration of ASPM protein appears to be reduced in the nucleus in *ASPM*^{3663delG} and *ASPM*^{9984+1G>T} cells.

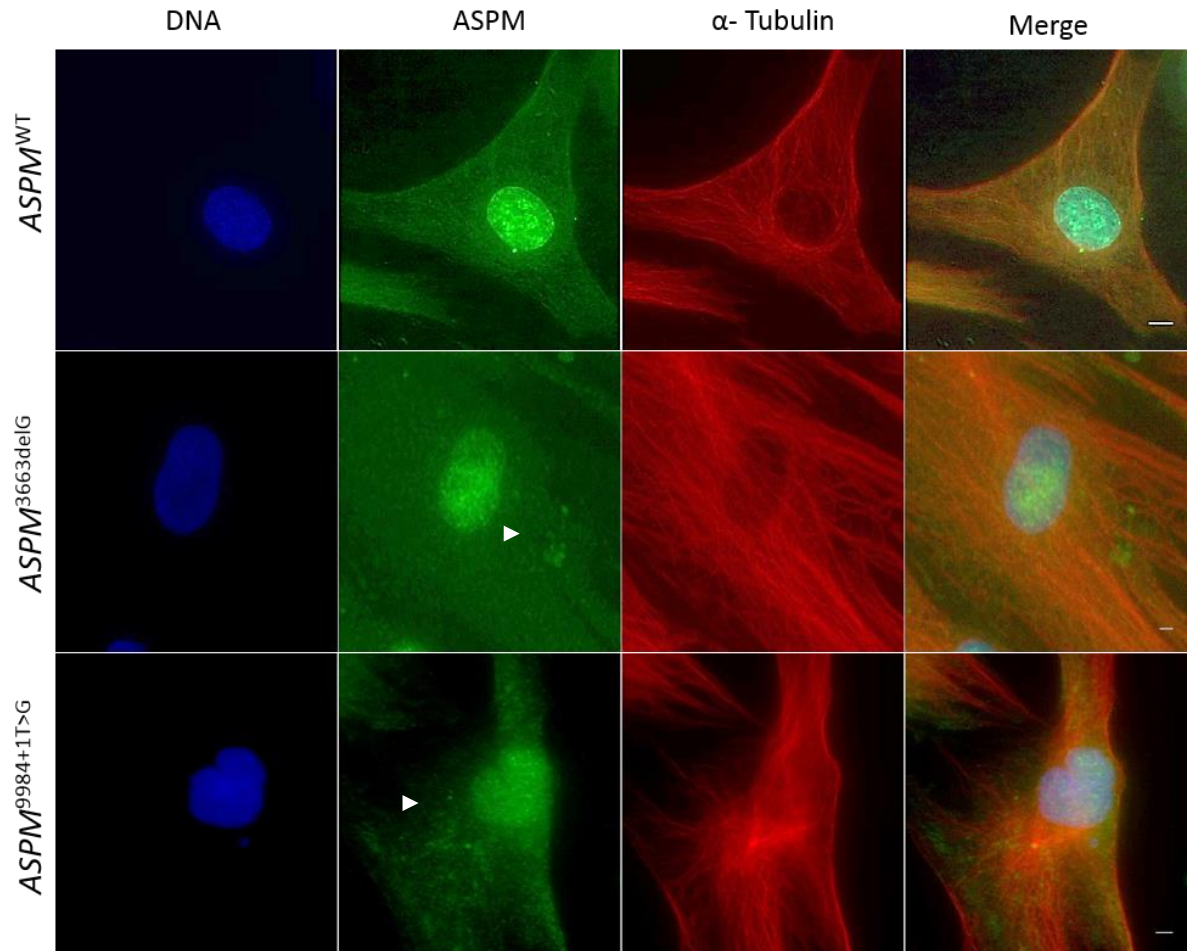


Figure 4.4: Analysis of ASPM localization in patient fibroblast cells during interphase. *ASPM*^{WT}, *ASPM*^{3663delG} and *ASPM*^{9984+1T>G} cells in interphase were methanol fixed and immunostained using the specific *N*-terminal anti-ASPM antibody 216-1 (green) to identify ASPM, anti- α -tubulin (red) to identify MT and DAPI (blue) to recognise DNA. In interphase patient fibroblasts ASPM expression is reduced and redistributed in the cytoplasm where it forms aggregates (arrowhead). Scale bar = 5 μ m

4.5.4.3 Comparison of ASPM localization in $ASPM^{WT}$, $ASPM^{3663delG}$ and $ASPM^{9984+1T>G}$ cells during metaphase.

To determine changes in ASPM localisation caused by *ASPM* mutation during the metaphase stage of mitosis, $ASPM^{WT}$, $ASPM^{3663delG}$ and $ASPM^{9984+1T>G}$ cells were methanol fixed and stained for ASPM, MT and DNA. Images of cells in metaphase were captured. Previously a decrease in ASPM staining at the spindle had been identified in the $ASPM^{9984+1T>G}$ cells (Higgins et al., 2010) in comparison to $ASPM^{WT}$ cells. A similar decrease in ASPM staining at the spindle poles was observed in $ASPM^{3663delG}$ cells compared to the ASPM level in $ASPM^{WT}$ fibroblasts (Figure 4.5). For both patient cell lines the decrease in spindle pole staining was accompanied by a redistribution of ASPM to the cytoplasm compared to the $ASPM^{WT}$ control cell lines.

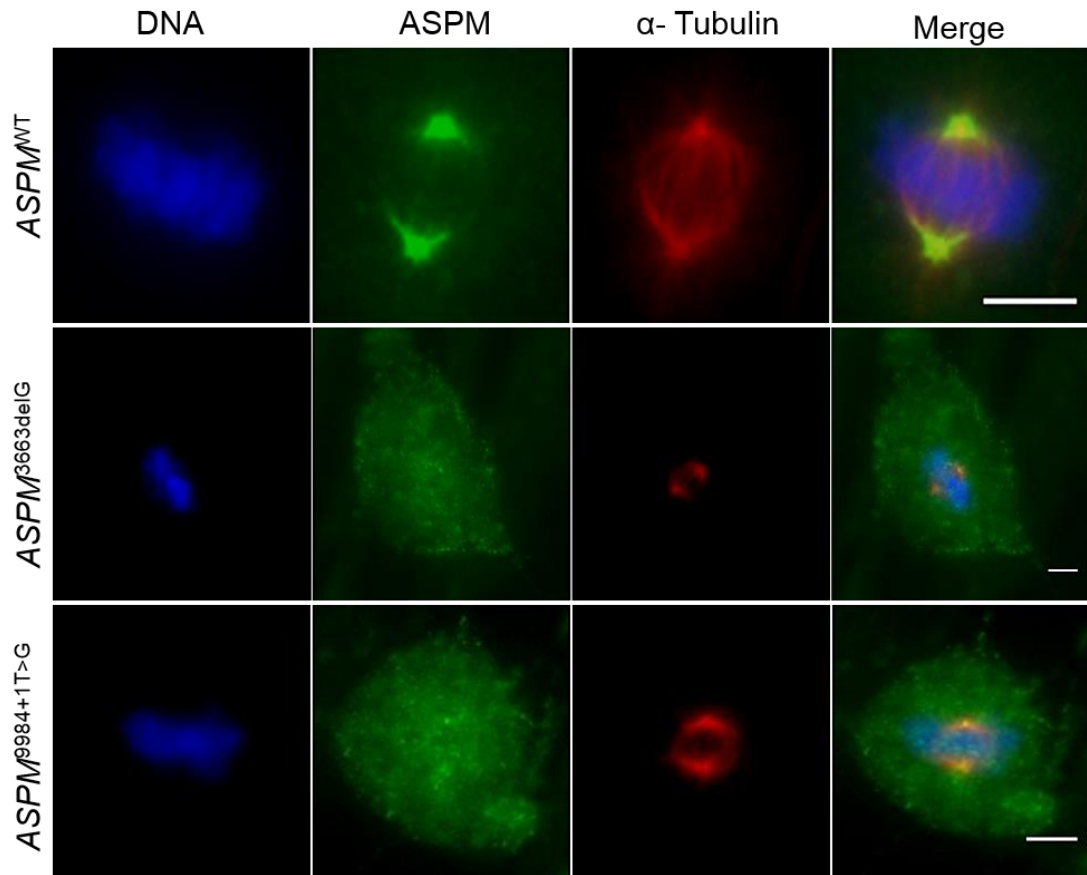


Figure 4.5: Analysis of ASPM localization in patient fibroblasts during metaphase.

Cells were fixed in methanol and stained using the specific *N*-terminal anti-ASPM antibody 216-1 (green) to identify ASPM, anti- α -tubulin (red) to identify MTs and DAPI (blue) to recognise DNA. ASPM is reduced at the spindle poles and relocalised to the cytoplasm in mitotic patient fibroblasts. Scale bar = 10 μ m.

To quantitatively determine the effect of *ASPM*^{3663delG} mutation on the ASPM mitotic spindle pole localisation, a comparison of the ASPM integral intensity (estimated by multiplying the pixel area by the fluorescent intensities of the region of interest) at the spindle poles of 50 metaphase *ASPM*^{WT} cells (100 spindle poles in total), and 50 metaphase *ASPM*^{3663delG} cells (50 spindle poles in total) was

performed (Methods section 2.2.3.1). Similar data for $ASPM^{9984+1T>G}$ has previously been published (N=80, Average integral intensity $ASPM^{WT} = 16427\mu m^2 \pm 1166 \mu m^2$ (s.e.m), average integral intensity $ASPM^{9984+1G>T} = 2351\mu m^2 \pm 260\mu m^2$ (s.e.m), $p = < 0.0001$). ((Higgins *et al.*, 2010). A t-test determined that ASPM integral intensity associated at the metaphase spindle pole in $ASPM^{3663delG}$ cells was significantly reduced in comparison to $ASPM^{WT}$ cells (Figure 4.6). (N=100, Average integral intensity $ASPM^{WT} = 11536 \mu m^2 \pm 653.3 \mu m^2$ (s.e.m), average integral intensity $ASPM^{3663delG} = 1379 \mu m^2 \pm 98.66 \mu m^2$ (s.e.m), $p = < 0.0001$).

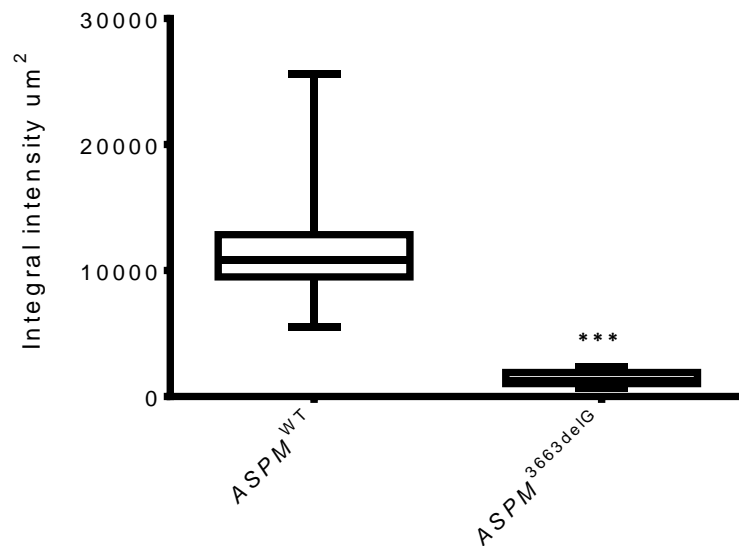


Figure 4.6: Analysis of ASPM integral intensity at the spindle poles of $ASPM^{WT}$ and $ASPM^{3663delG}$ fibroblast cells. Graph showing average ASPM integral intensity at the spindle poles of $ASPM^{WT}$ and $ASPM^{3663delG}$ fibroblast cells. The average integral intensity of the ASPM staining at the spindle poles of mitotic $ASPM^{3663delG}$ was significantly lower than the integral intensity of ASPM at the mitotic spindle poles in the $ASPM^{WT}$ cells.

4.5.4.4 Comparison of ASPM central spindle localization in *ASPM*^{WT}, *ASPM*^{3663delG} and *ASPM*^{9984+1T>G} cells during cytokinesis.

To further determine the effect of *ASPM* mutations on ASPM distribution and localisation during cytokinesis, *ASPM*^{WT}, *ASPM*^{3663delG} and *ASPM*^{9984+1T>G} cells were fixed and stained for ASPM, MTs (α -tubulin) and DNA (DAPI). Visual comparative immunofluorescence analysis revealed ASPM staining was reduced in the patient cells but was localized to the midbody and cytoplasm in all cell lines, however in the patient cells *ASPM*^{3663delG} *ASPM*^{9984+1T>G} was partially redistributed to the central spindle between the two daughter cells during cytokinesis, prior to abscission (Figure 4.7).

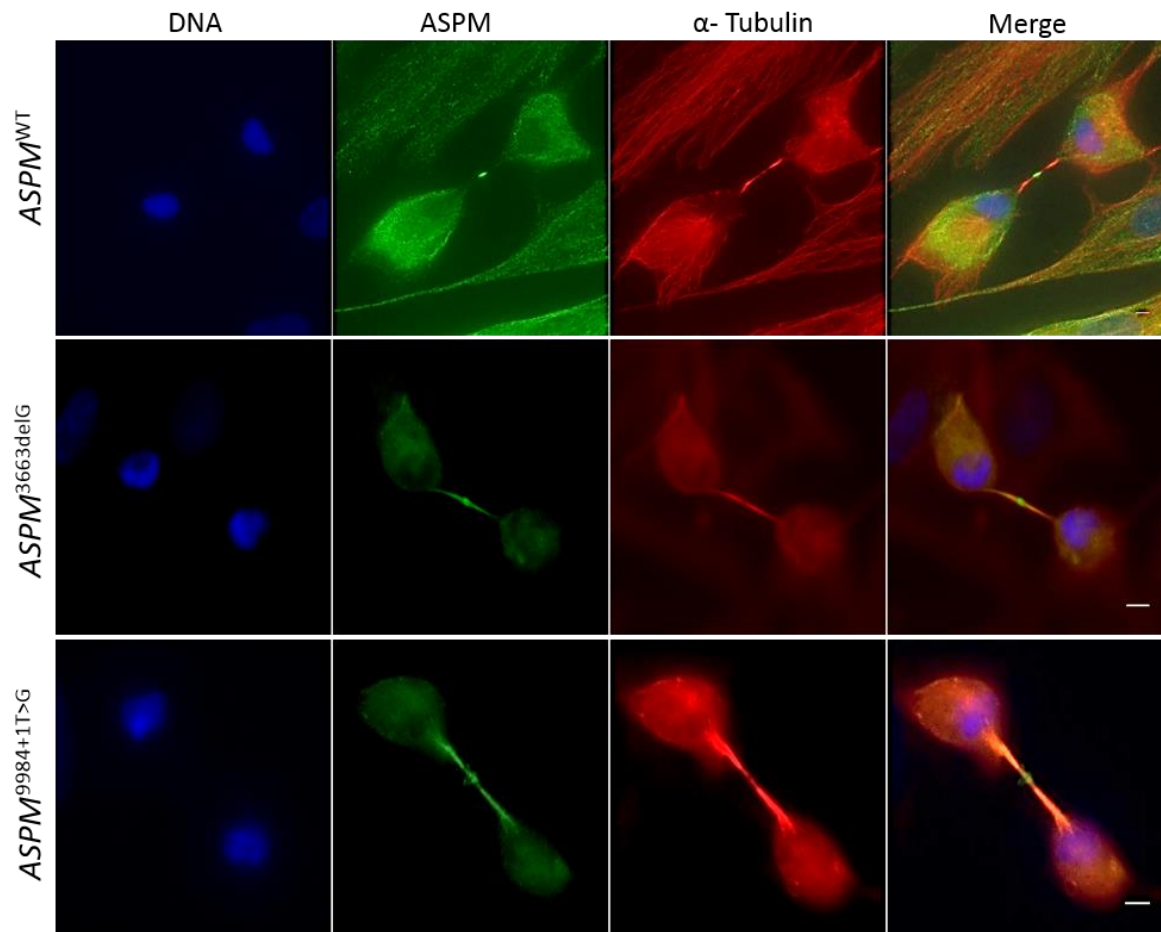


Figure 4.7: Analysis of ASPM localisation in *ASPM*^{3663delG} and *ASPM*^{9984+1T>G} cells in comparison to *ASPM*^{WT} cells during cytokinesis. The ASPM localisation to the Fleming Body was common to all three cell strains, however ASPM localisation was mis-localised to the central spindle in the patient cells. Cells were fixed in methanol and stained using the *N*-terminal anti-ASPM -antibody 216-1 (green), anti- α -tubulin (red) and DAPI (blue) to identify ASPM, MTs and DNA respectively. Scale bar = 5 μ m.

4.5.5 Comparison of interphase and mitotic nuclear, microtubule, centrosomal and spindle pole changes between *ASPM*^{WT} and *ASPM*^{3663delG} and *ASPM*^{9984+1T>G} MCPH5 patient cells.

As shown so far in this chapter, *ASPM* mutations lead to mis-localisation of the *ASPM* protein during interphase and mitosis in the MCPH5 patient cells. To investigate the effect of protein changes on *ASPM* mis-localisation leading to the interphase and mitotic phenotypes in *ASPM*^{WT}, *ASPM*^{3663delG} and *ASPM*^{9984+1T>G} fibroblast cells were investigated and compared using immunofluorescence microscopy. Cells were fixed in methanol and stained with anti- γ -Tubulin (green), anti- α -tubulin (red) and DAPI (blue) to identify centrosomes, MTs and DNA respectively.

4.5.5.1 Identification of aberrant interphase phenotypes in *ASPM*^{3663delG} and *ASPM*^{9984+1T>G} MCPH5 patient cells in comparison to *ASPM*^{WT} cells.

During interphase *ASPM*^{WT} cells were observed to have smoothly shaped nuclei, one centrosomal location and organized and evenly distributed MTs (Figure 4.8).

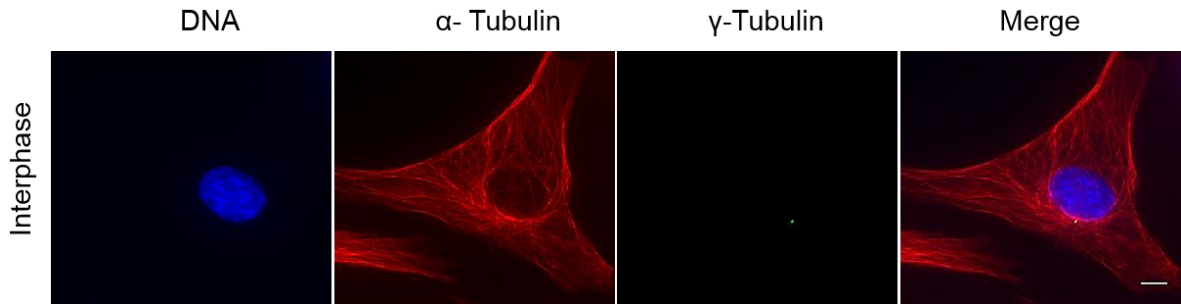
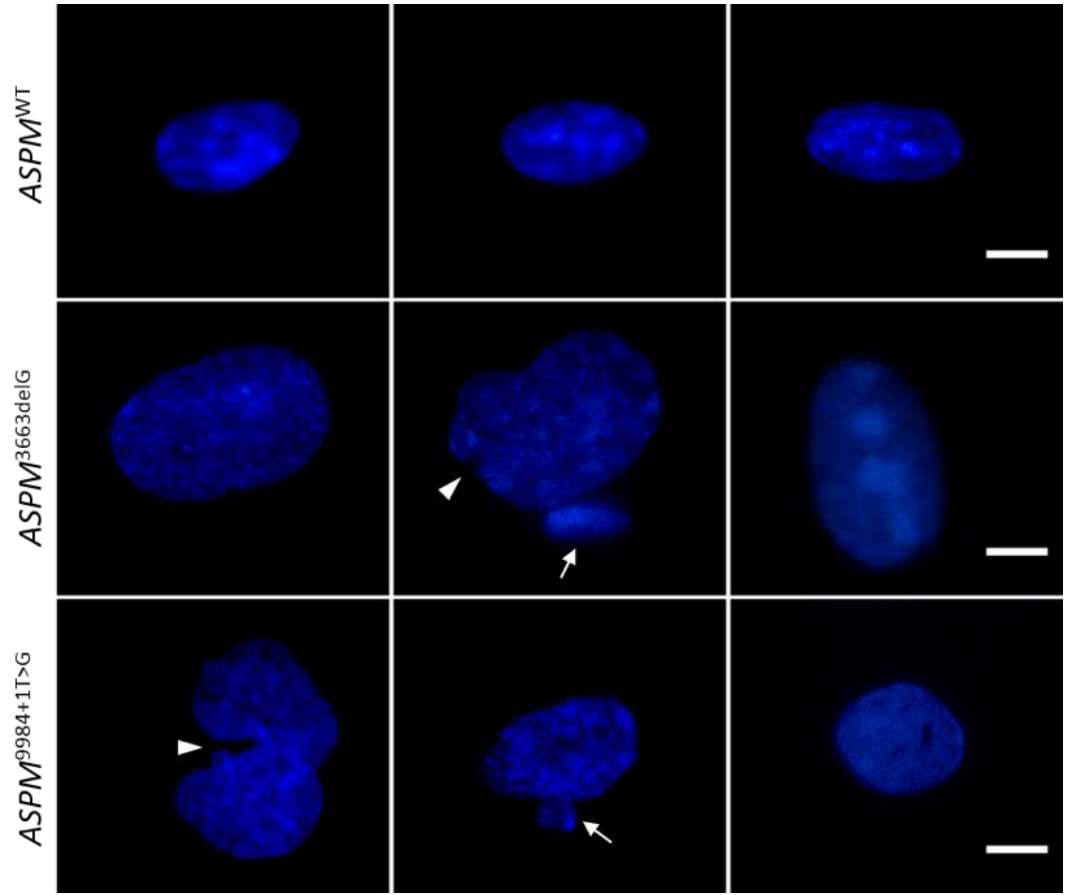


Figure 4.8: Analysis of interphase nuclear, microtubule and centrosomal phenotypes of *ASPM*^{WT} fibroblast cells. Human dermal fibroblast cells (control) showed normal interphase nuclei, evenly distributed MTs and one centrosomal location. Cells were fixed in methanol and stained with anti- γ -Tubulin (green) to identify centrosomes, anti- α -tubulin (red) to identify MTs and DAPI (blue) to recognise DNA. Scale bar = 5 μ m.

4.5.5.1.1 Analysis of the effects *ASPM* mutations on interphase nuclear phenotypes.

In comparison to *ASPM*^{WT}, the nuclear phenotypes observed in patient cells included lobular (arrowhead), enlarged nuclei and the occurrence of micro nuclei (arrow) (Figure 4.9A). In comparison to *ASPM*^{WT} nuclei a significant decrease of 68.5% and 56.4% of normal nuclear interphase phenotypes in *ASPM*^{3663delG} and *ASPM*^{9984+1T>G} cells respectively were detected (Figure 4.9B). The quantitative analysis of these nuclear phenotypes revealed significant changes were observed for cell with enlarged nuclei ($p < 0.0001$) and lobular nuclei ($p = 0.003$) in the *ASPM*^{3663delG} cells and for enlarged nuclei ($p = 0.0001$), lobular nuclei ($p < 0.0001$) and micro nuclei ($p = 0.006$) in the *ASPM*^{9984+1T>G} cells. (Figure 4.9C).

A



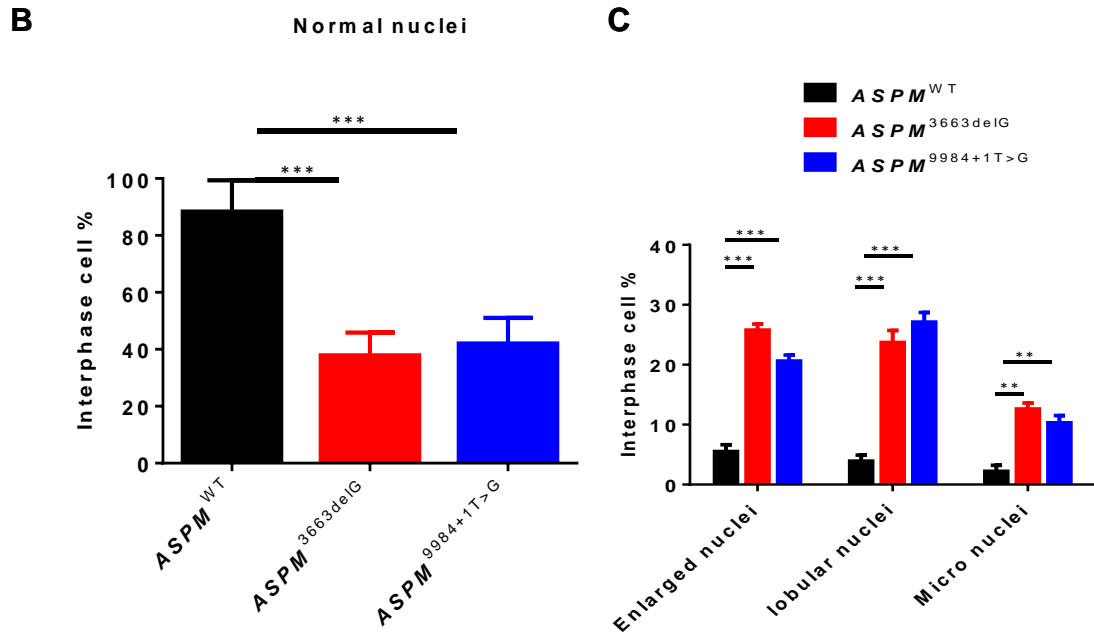


Figure 4.9: Effect of *ASPM* mutations on nuclear interphase phenotypes. A. Panel shows nuclear data for control and patient cells during interphase. *ASPM* mutations resulted in aberrant nuclear interphase phenotypes including enlarged, knobby (arrowheads) and micronuclei (arrows). Cells were fixed in methanol and stained using DAPI (blue) to recognise DNA. Scale bar = 10 μ m. **B.** Graph shows percentage of normal interphase nuclei observed in each of the fibroblast cell strains. *ASPM*^{3663delG} (n= 278 cells) and *ASPM*^{9984+1T>G} (n= 283 cells) showed significant decrease of normal nuclear interphase compared to *ASPM*^{WT} (n= 291 cells). **C.** Statistical analysis of aberrant nuclear interphase phenotypes. Nuclear interphase phenotype abnormalities were significantly higher in patient cells than in the control cells.

4.5.5.1.2 Analysis of the effect of *ASPM* mutations on interphase microtubule distribution.

ASPM^{WT} cells displayed a well-distributed MT network with an obvious microtubule organizing centre (MTOC) (Figure 4.8 and Figure 4.10A -arrowhead). Patient cells showed clustered (arrows), disorganised and a low density of MTs (Figure 4.10A and C). Quantitative visual analysis of the occurrence of aberrant MT phenotypes in patient cells showed a higher percentage of MT abnormalities than in control cells (Figure 4.10B). In comparison to *ASPM*^{WT} which displayed only 11.5% of interphase cells showing abnormal MT distribution, a significant increase to 74.2% and 33.3% of abnormal MT distribution in *ASPM*^{β663delG} and *ASPM*^{9984+1T>G} respectively was detected. The quantitative analysis of these MT phenotypes revealed significant changes were observed for clustered MTs ($p < 0.0001$), disorganised MTs ($p=0.0006$) and low density MTs ($p=0.006$) in the *ASPM*^{β663delG} cells and for clustered MTs ($p= 0.0001$), disorganised MTs ($p=0.003$) and low density MTs ($p=0.02$) in the *ASPM*^{9984+1T>G} cells (Figure 4.10C).

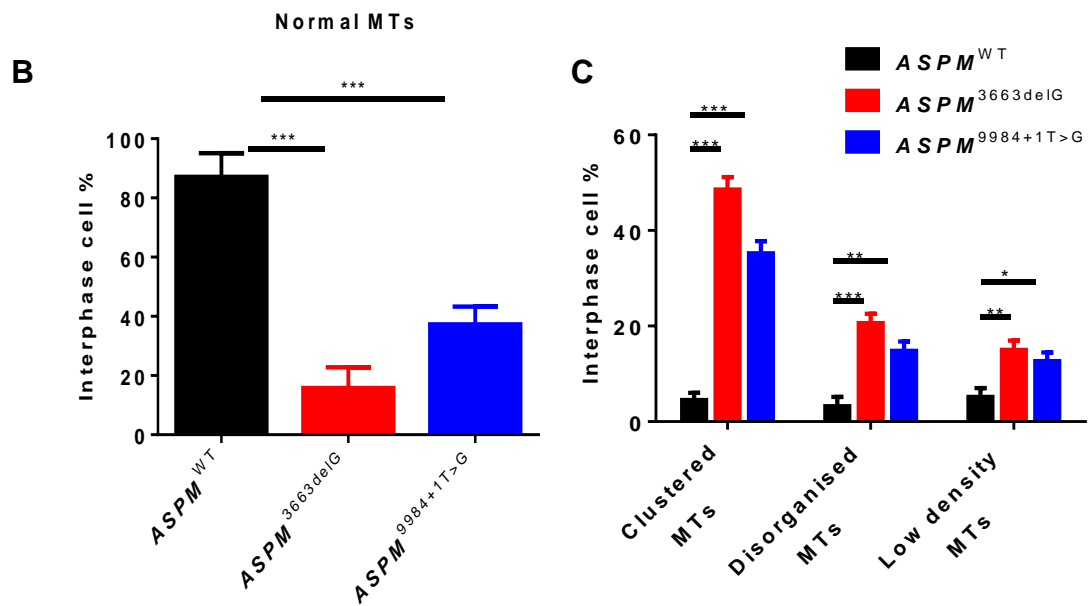
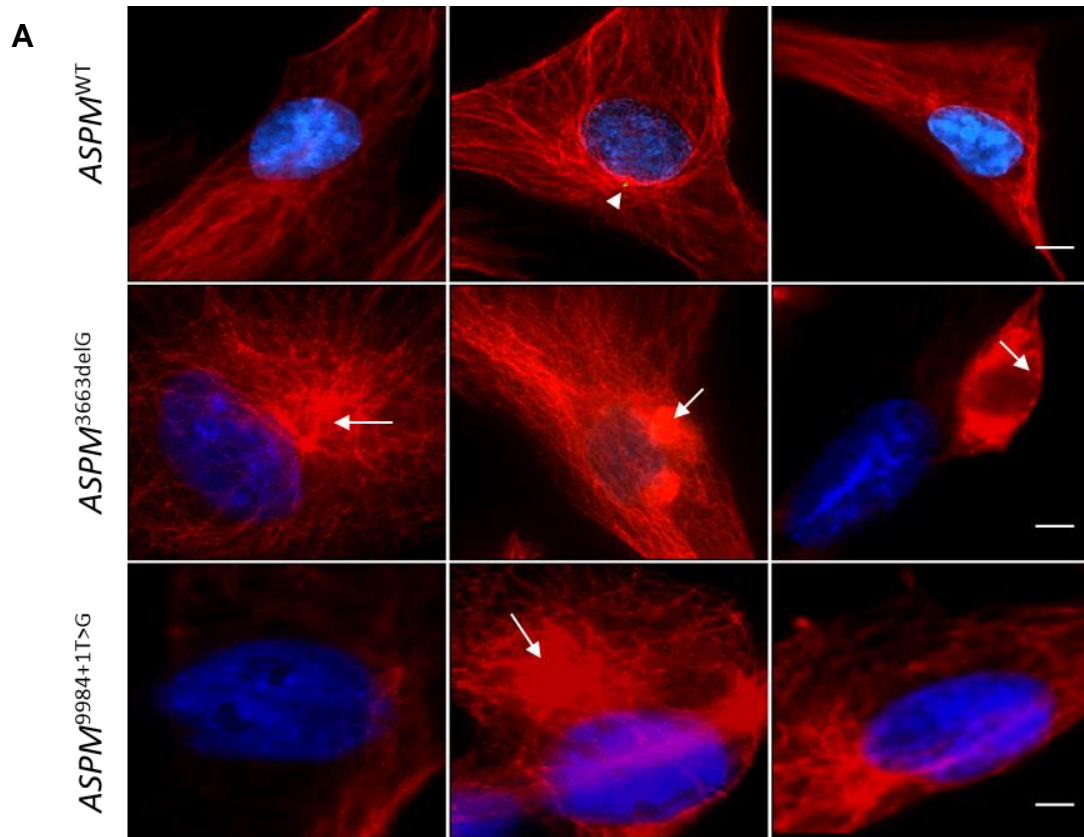


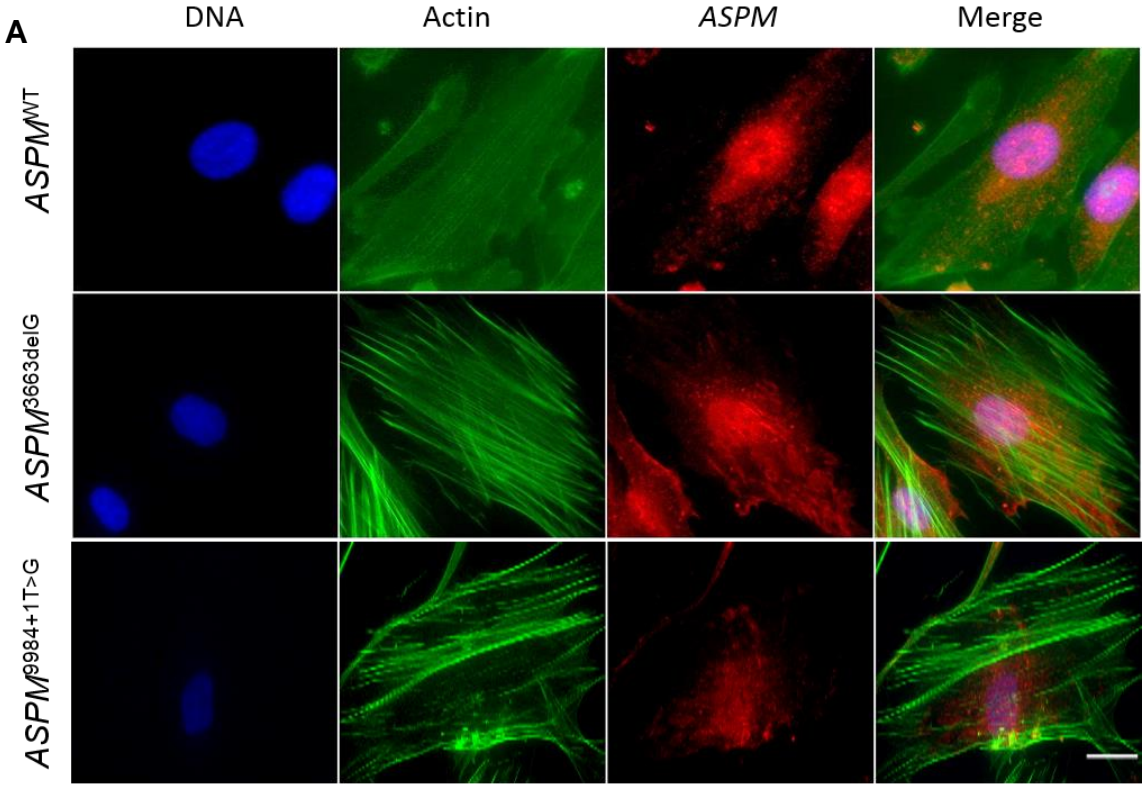
Figure 4.10: Effect of *ASPM* mutations on MT organization. A. Panel shows control cells with an obvious microtubule organizing centre (MTOC) (arrowhead) and patient cells

during interphase stage. *ASPM* mutations result in MT clusters (arrows), disorganization and low density MT. Cells were fixed in methanol and stained with anti- α -Tubulin (red) to identify MT and DAPI (blue) to recognise DNA. Scale bar = 5 μ m. **B.** Graph shows percentage of cells with normal MT configuration in interphase in *ASPM*^{WT} cells (n= 291 cells) compared with *ASPM*^{3663delG} (n= 278 cells) and *ASPM*^{9984+1T>G} (n= 283 cells) cells. *ASPM*^{3663delG} and *ASPM*^{9984+1T>G} showed a significant increase in abnormal MTs compared to *ASPM*^{WT}. **C.** Statistical analysis of MT abnormalities. The occurrence of MT abnormalities was significantly increased in patient cells compared to control cells. A microtubule organizing centre (MTOC) is indicated by an arrowhead and clustered MTs by arrows.

4.5.5.1.3 Investigation of the effect of *ASPM* mutation on interphase actin distribution.

To investigate if *ASPM* mutation had an effect on the structure of the actin cytoskeleton during interphase, fibroblast cells were fixed in paraformaldehyde (PFA) to maintain the actin structures and stained with Alexa 488 phalloidin (green) to identify actin, DAPI (blue) for DNA and anti-*ASPM*-antibody 216-1 (red) to identify *ASPM*. *ASPM*^{WT} cells displayed well organised actin filaments, they were organized at the cell periphery and passed through the cytoplasm as thin strand-like structures. *ASPM*^{3663delG} and *ASPM*^{9984+1T>G} cells displayed a tremendous change in actin filament morphology and distribution. Actin strands were thicker in *ASPM*^{3663delG} cells and formed clusters and bundling striated strands in *ASPM*^{9984+1T>G} cells. In patient cells actin was not visible all the way around the cell

periphery (Figure 4.11A). Quantitative analysis of the occurrence of aberrant actin phenotypes in patient cells showed a higher percentage of actin abnormalities than in control cells (Figure 4.11B). Quantitative analysis of actin phenotypes revealed significant changes for clustered actin ($p < 0.0001$) and actin bundling ($p < 0.0001$) in the *ASPM*^{8663delG} cells and for clustered actin ($p < 0.0001$) and actin bundling ($p = 0.0004$) in the *ASPM*^{9984+1T>G} cells (Figure 4.11C). ASPM was strongly and predominantly localised to the nucleus in the *ASPM*^{WT} cells, but weaker in the *ASPM*^{8663delG} and *ASPM*^{9984+1T>G} cells in interphase which is in agreement with previous sections (Sections 4.5.4.1).



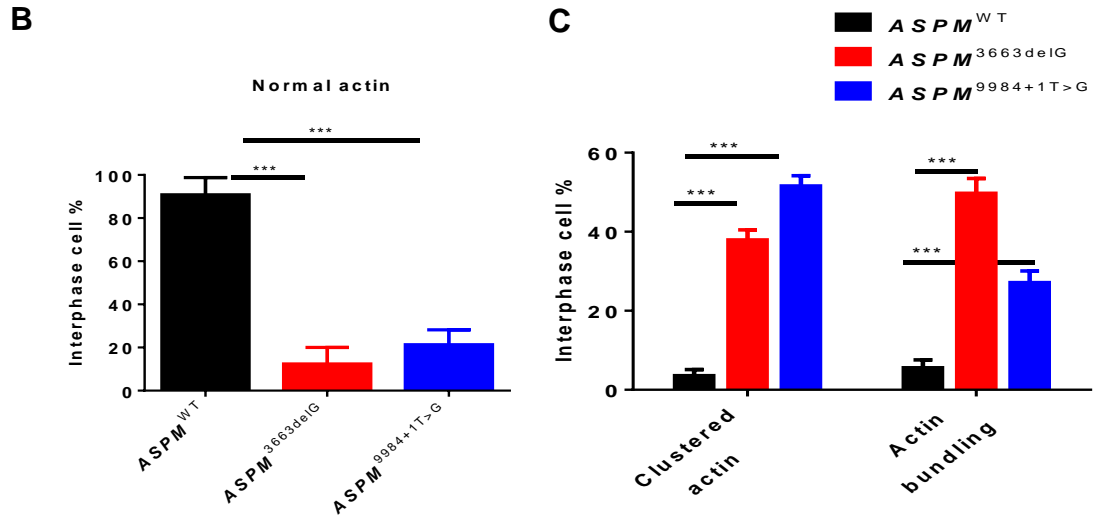
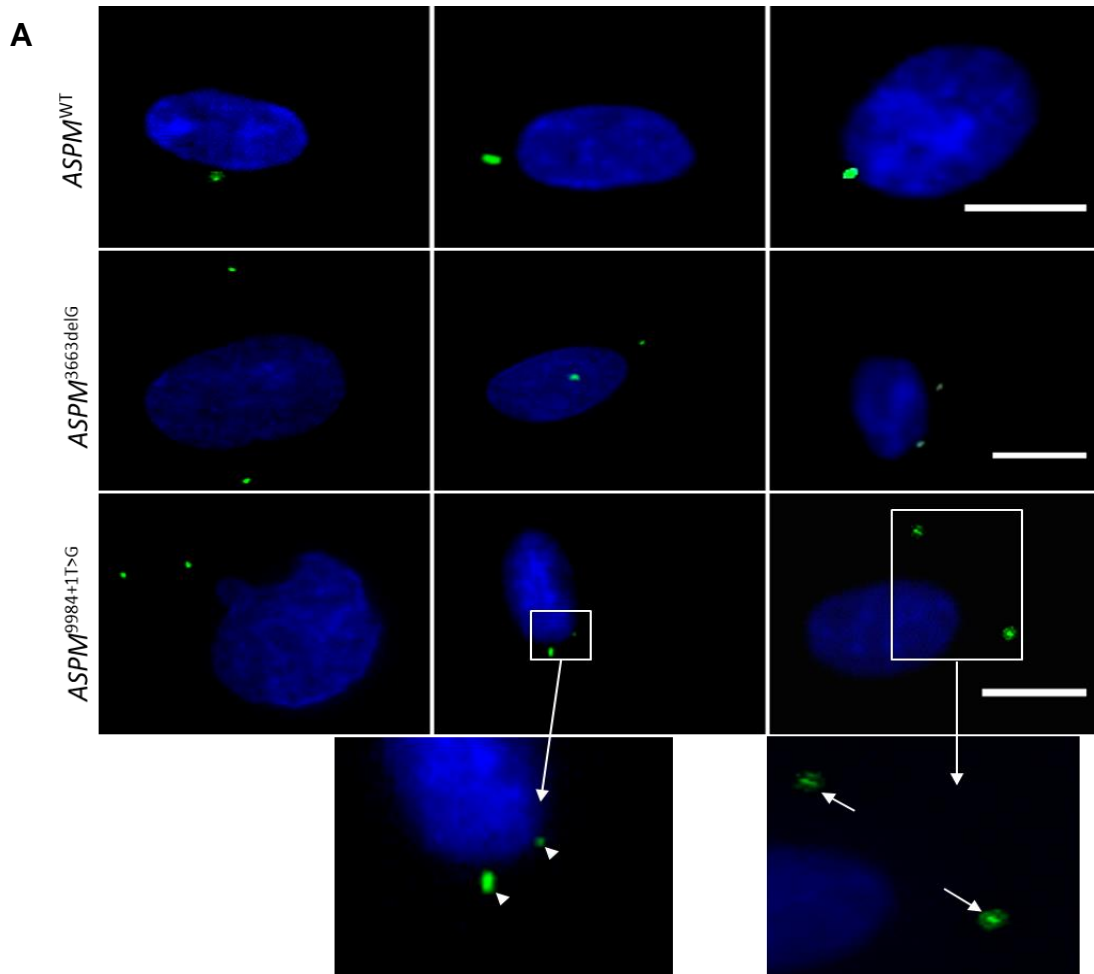


Figure 4.11: Analysis of the effect of *ASPM* mutations on actin structure and distribution. **A.** Panel shows control and patient cells during interphase. Cells were fixed and stained with Alexa 488 phalloidin (green) to identify actin, anti-*ASPM*-antibody 216-1 (red) to identify *ASPM* and DAPI (blue) to recognise DNA. *ASPM*^{WT} cells showed a well-organised actin network. *ASPM*^{3663delG} and *ASPM*^{9984+1T>G} cells displayed clustered actin and bundling actin strands. Scale bar = 10 μ m. **B.** Statistical analysis of normal actin percentage which was higher in *ASPM*^{WT} cells (n= 313 cells) than *ASPM*^{3663delG} (n= 290 cells) and *ASPM*^{9984+1T>G} (n= 295 cells) cells. **C.** Statistical analysis of actin abnormalities which were significantly higher in patient cells than in control.

4.5.5.1.4 Analysis of the effect of *ASPM* mutations on centrosome number and centrosome cohesion during interphase.

In comparison to *ASPM*^{WT} interphase cells which had one regular size centrosome, patient cells possessed increased centrosome number, uneven sized and shaped centrosomes (arrowheads) as well as haloed centrosomes (arrows) (Figure 4.12A).

ASPM^{3663delG} and *ASPM*^{9984+1T>G} interphase cells displayed a significant higher percentage of centrosomal abnormalities, 55.6% and 41.7% respectively, including increased centrosome number and structural defects than *ASPM*^{WT} cells, which displayed only 12% of centrosome abnormalities (Figure 4.12B). The quantitative analysis of these abnormal centrosome phenotypes revealed significant changes were observed for haloed centrosomes ($p=0.013$) and increased centrosome number ($p=0.0001$) in the *ASPM*^{3663delG} cells and for haloed centrosomes ($p=0.003$) and increased centrosome number ($p=0.0002$) in the *ASPM*^{9984+1T>G} cells (Figure 4.12C).



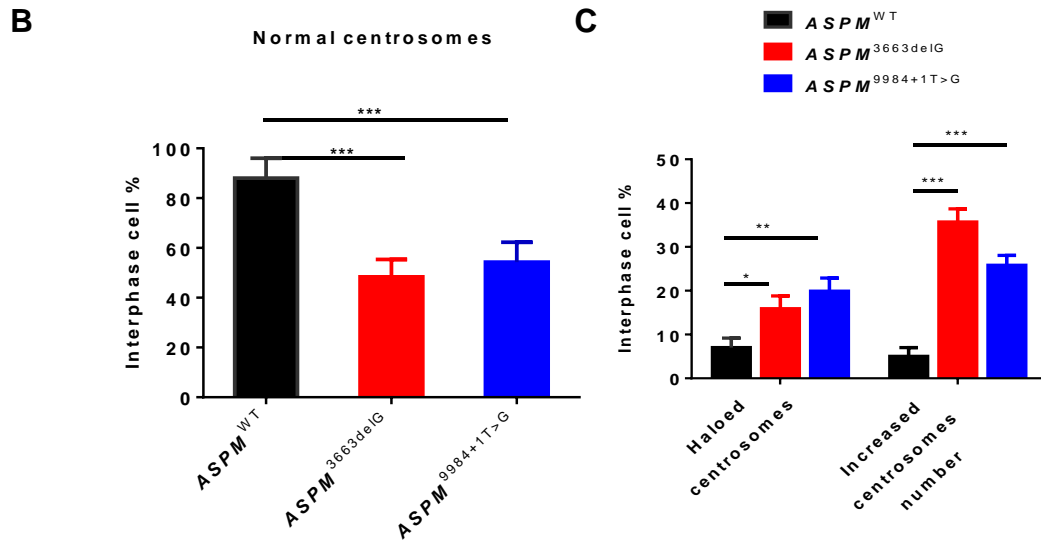


Figure 4.12: Effect of *ASPM* mutations on centrosome number and centrosome structure during interphase. **A.** Panel shows control and patient cells during interphase. *ASPM* mutations result in centrosome aberrations including centrosomal structure defect (uneven sized and shaped centrosomes (arrowheads) and haloed centrosomes (arrows)) and increased centrosome number. Cells were fixed in methanol and stained with anti- γ -Tubulin (green) to identify centrosomes and DAPI (blue) to recognise DNA. Scale bar = 10 μ m. **B.** Statistical analysis of percentage of normal centrosomes during interphase in *ASPM*^{WT} cells (n= 291 cells) compared with *ASPM*^{3663delG} (n= 278 cells) and *ASPM*^{9984+1T>G} (n= 283 cells) cells. *ASPM*^{3663delG} and *ASPM*^{9984+1T>G} showed a significant increase in abnormal centrosome structure and number compared to *ASPM*^{WT}. **C.** Statistical analysis of centrosome phenotypes. The centrosome abnormalities were significantly higher in patient cells than in control.

4.5.5.2 Analysis of the effect of *ASPM* mutations on mitotic phenotypes

In mitosis, *ASPM*^{MT} cells displayed normal DNA, centrosome duplication (two centrosomes from prophase>cytokinesis) consistent sized mitotic spindles and DNA separation (Figure 4.13).

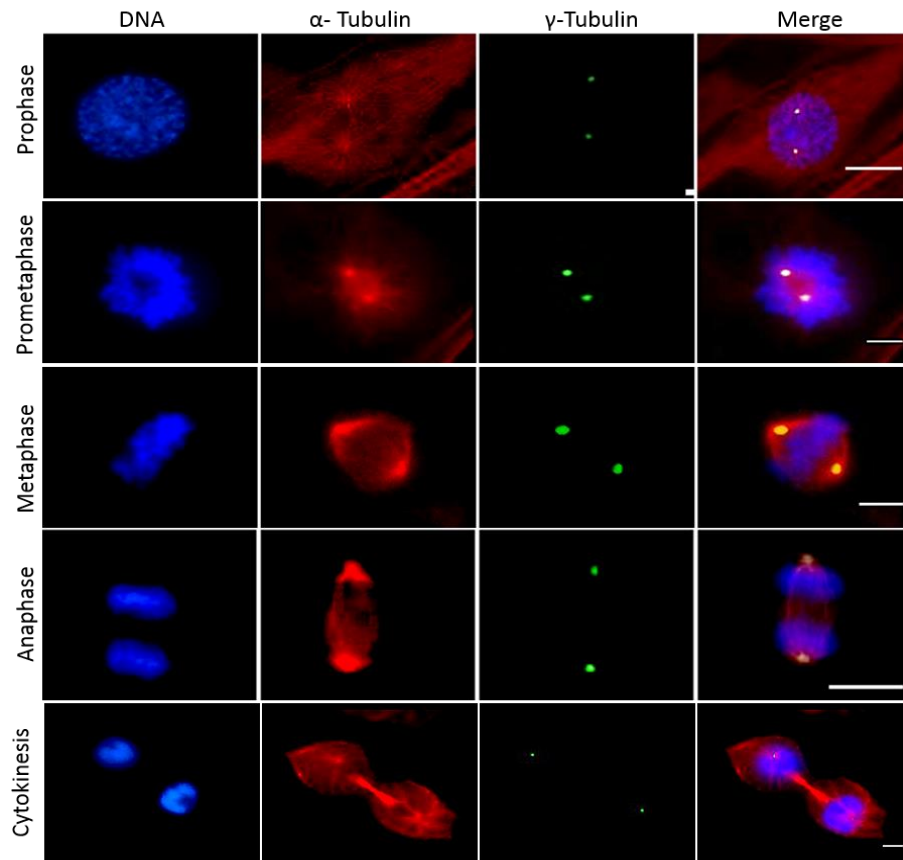
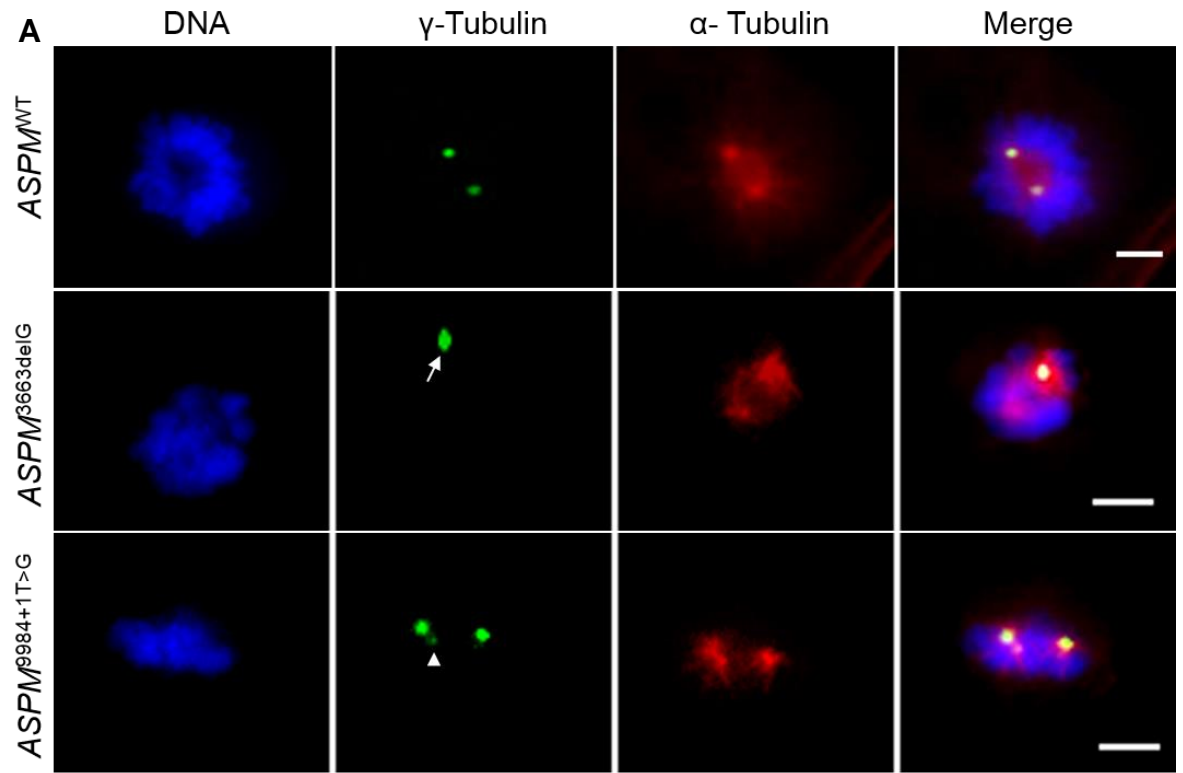


Figure 4.13: Analysis of nuclear, spindle pole, centrosome and microtubule organisation in *ASPM*^{MT} fibroblast cells during mitosis. Human dermal fibroblast cells (control *ASPM*^{MT}) have organised DNA, two spindle poles from prophase to cytokinesis and an evenly sized and distributed mitotic spindle. Cells were fixed in methanol and stained with anti- γ -Tubulin (green) to identify spindle poles, anti- α -tubulin (red) to identify MTs and DAPI (blue) to recognise DNA. Scale bar = 10 μ m.

4.5.5.2.1. Analysis of the effect of *ASPM* mutations on spindle pole number during prometaphase.

ASPM^{WT} cells displayed two spindle poles during prometaphase. *ASPM*^{3663delG} and *ASPM*^{9984+1T>G} cells exhibited monopolar or asymmetric spindle poles as illustrated in *ASPM*^{3663delG} and multipolar (>2) spindle poles along with partially decondensed-looking DNA as demonstrated in *ASPM*^{9984+1T>G} (Figure 4.14A) arrow and arrowhead respectively). The quantitative analysis of the spindle pole number during prometaphase indicated that patient cells exhibited an increase in spindle pole defects compared to control cells. *ASPM*^{3663delG} and *ASPM*^{9984+1T>G} cells displayed a significant lower percentage, 36.3% and 41.2% respectively, of bipolar spindle poles than *ASPM*^{WT} cells, which displayed 91% (Figure 4.14B). Spindle pole number was statistically significantly different in the patient cells than *ASPM*^{WT} when compared using a paired two tailed t-test for monopolar spindle poles ($p < 0.0001$) and multipolar (>2) spindle poles ($p = 0.0008$) in the *ASPM*^{3663delG} cells and for monopolar spindle poles ($p = 0.0003$) and multipolar (>2) spindle poles ($p < 0.0001$) in the *ASPM*^{9984+1T>G} cells (Figure 4.14C).



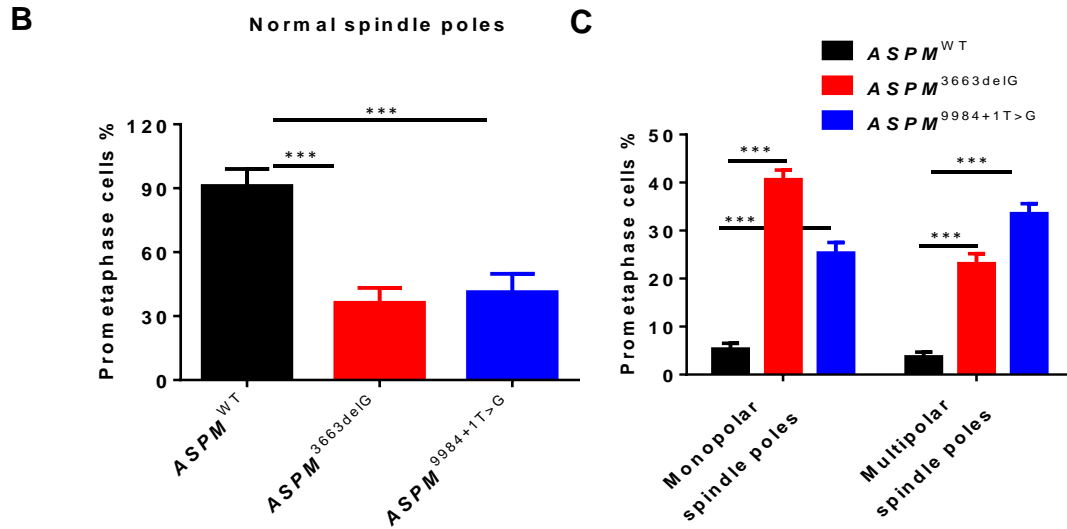
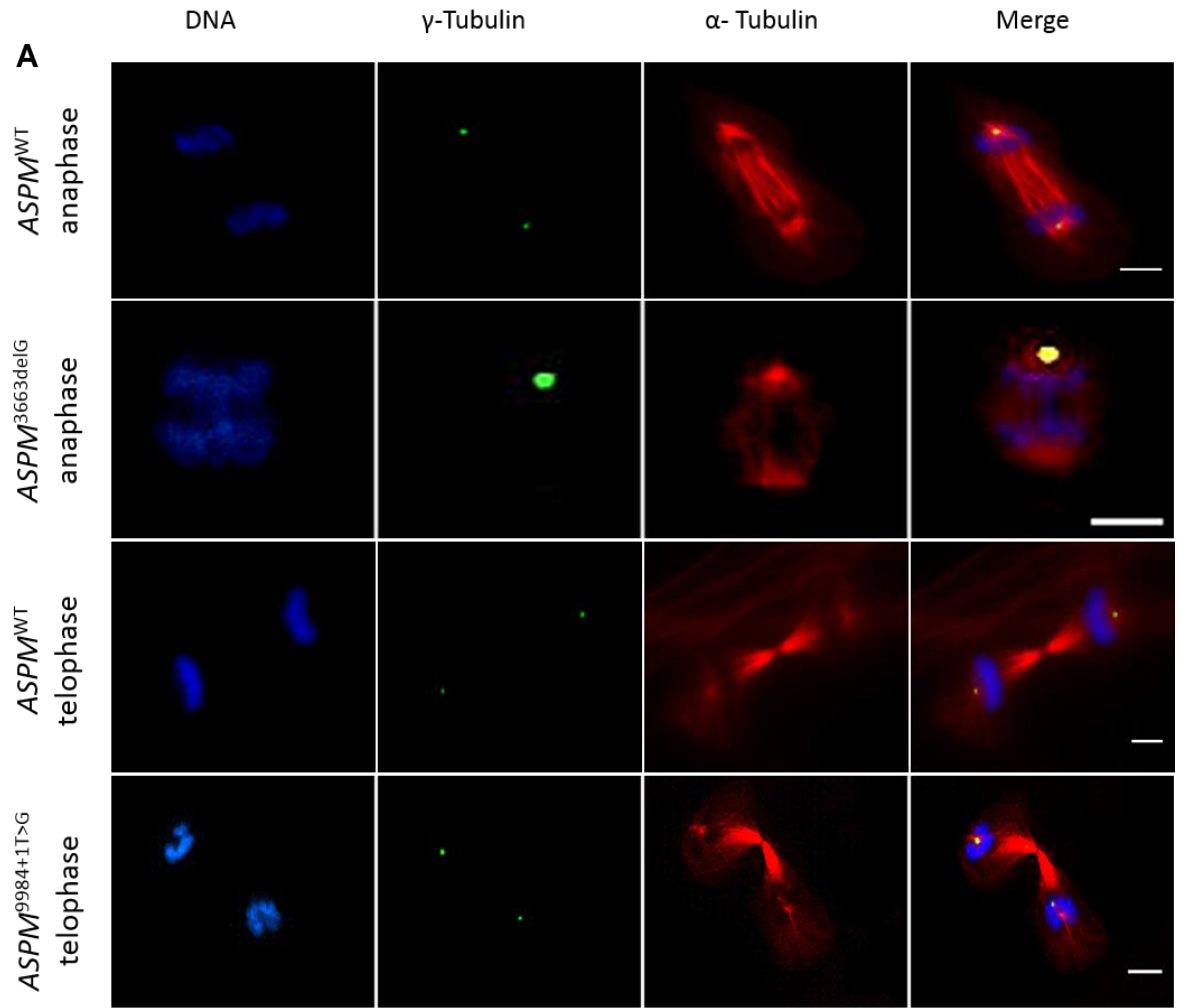


Figure 4.14: Analysis of the effect of *ASPM* mutations on spindle pole number during prometaphase. **A.** Panel shows control and patient cells during prometaphase stage of mitosis. *ASPM* mutations cause single (arrow) and multipolar (arrowhead) spindle poles during mitosis. Cells were fixed in methanol and stained with anti- γ -Tubulin (green) to identify centrosomes, anti- α -tubulin (red) to identify MTs and DAPI (blue) to recognise DNA. Scale bar = 10 μ m. **B.** statistical analysis of normal spindle poles amongst the three cell lines. *ASPM*^{3663delG} (n= 69 cells) and *ASPM*^{9984+1T>G} (n= 75 cells) showed significant decreases in the number of spindle poles compared to *ASPM*^{WT} (n= 82 cells). **C.** Statistical analysis of abnormal spindle pole phenotypes during prometaphase stage. The occurrence of spindle pole abnormalities were significantly higher in patient cells than in control cells.

4.5.5.3 Analysis of effect of *ASPM* mutations on anaphase and telophase spindle poles.

ASPM^{WT} cells showed normal spindle poles positioned at opposite ends of the spindle and cell during anaphase and telophase. However, patient cells displayed abnormal spindle pole phenotypes such as a single spindle poles (monopolar) during anaphase (illustrated in *ASPM*^{3663delG} cells), multipolar spindle poles and misplaced spindle poles during telophase as illustrated in *ASPM*^{9984+1T>G} cells (Figure 4.15A). *ASPM*^{3663delG} and *ASPM*^{9984+1T>G} cells showed a significant decrease in the occurrence of bipolar spindles during anaphase and telophase (25.8% and 33.3% respectively) than *ASPM*^{WT} cells, which were observed in 82.3% anaphase and telophase cells (Figure 4.15B). The quantitative analysis of spindle pole numbers using a paired two tailed t-test revealed a significant increase for monopolar spindle poles ($p < 0.0001$), multipolar spindles ($p = 0.001$) and misplaced spindle poles ($p = 0.016$) in the *ASPM*^{3663delG} cells and for monopolar spindle poles ($p < 0.0001$), multipolar spindles ($p = 0.004$), and misplaced spindle poles ($p = 0.002$) in the *ASPM*^{9984+1T>G} cells in comparison to *ASPM*^{WT} cells which displayed a very low occurrence of spindle pole defects (Figure 4.15C).



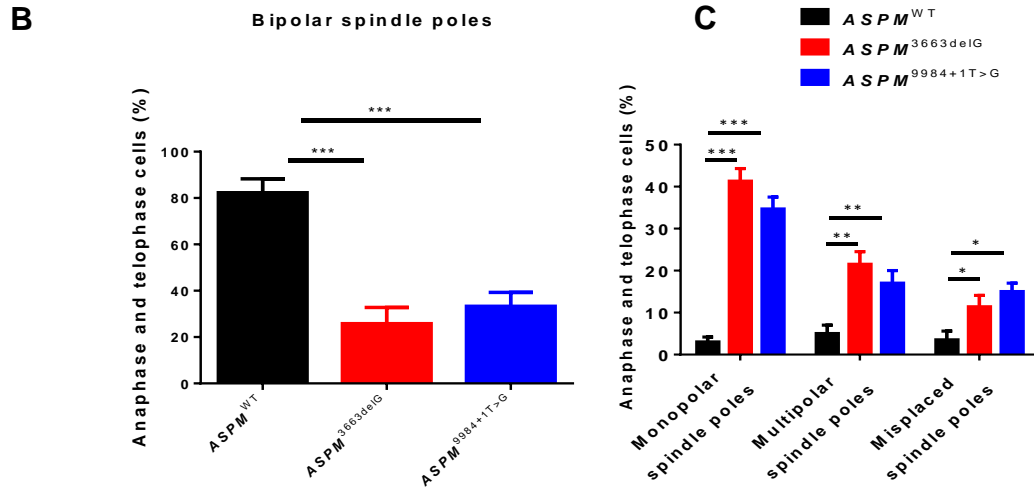
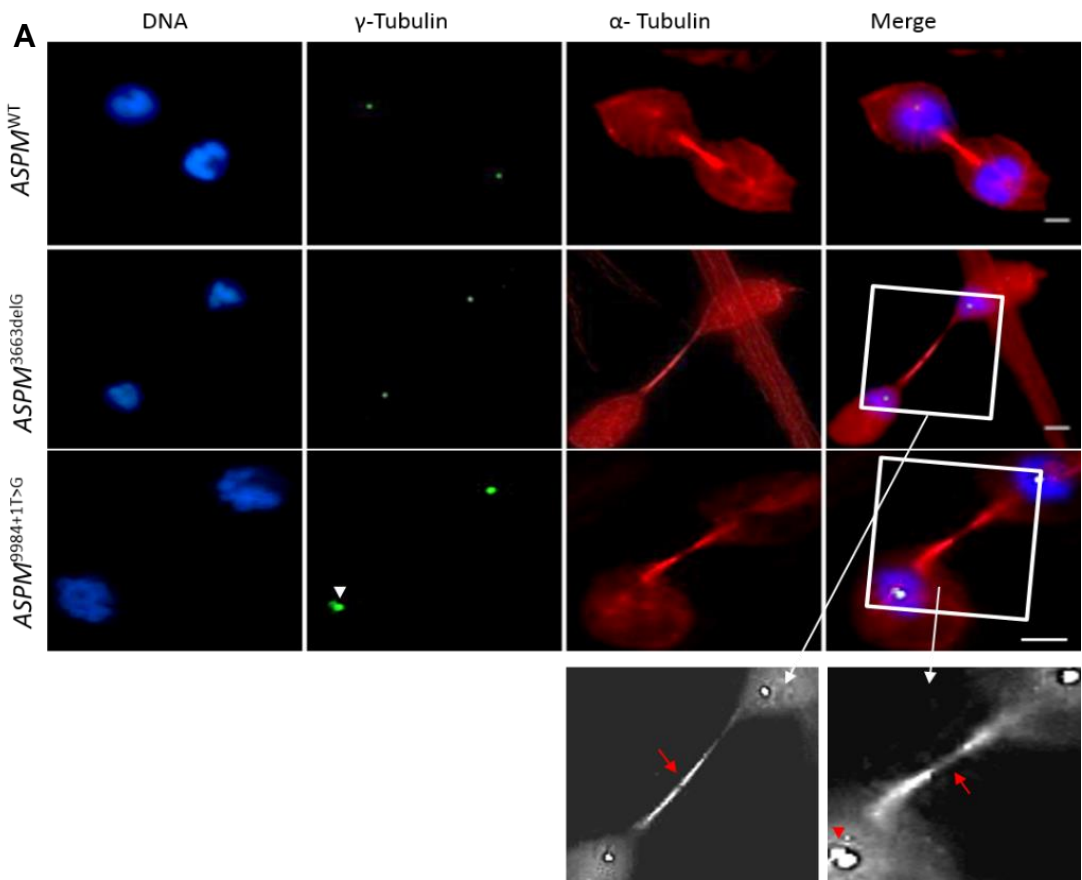


Figure 4.15: Analysis of the effect of *ASPM* mutations on spindle pole number and position during anaphase and telophase. **A.** Panel shows control and patient cells during anaphase and telophase. *ASPM* mutations cause single, multipolar and misplaced spindle poles during mitosis. Cells were stained with anti- γ -Tubulin (green) to identify centrosomes, anti- α -tubulin (red) to identify MTs and DAPI (blue) to recognise DNA. Scale bar = 10 μ m. **B.** Analysis of normal spindle poles in control and patient cell lines which was significantly lower in *ASPM*^{3663delG} (n= 80 cells) and *ASPM*^{9984+1T>G} (n= 85 cells) than in *ASPM*^{WT} (n= 90 cells) cells. **C.** Statistical analysis of spindle pole phenotypes in anaphase and telophase. The spindle pole abnormalities were significantly higher in patient cells than in control cells.

4.5.5.4 Analysis of the effect of *ASPM* mutation on the central spindle during cytokinesis.

As seen in (Section 4.5.4) *ASPM*^{WT} cells and *ASPM*^{3663delG} and *ASPM*^{9984+1T>G} have *ASPM* staining of the midbody (also termed Flemming Body) at the centre of the central spindle during cytokinesis (Figure 4.16A), where staining is reduced at

the midbody in *ASPM*^{3663delG} and *ASPM*^{9984+1T>G} cells and redistributed to the MT of the central spindle (Figure 4.16A). Patient cells exhibited an extremely long and thin central MT bridge stretching between the daughter cells (Figure 4.16A, arrow). *ASPM*^{9984+1T>G} cells displayed multiple spindle poles (Figure 4.16A, arrowhead). *ASPM*^{3663delG} and *ASPM*^{9984+1T>G} cells displayed a significantly lower percentage of late telophase cells undergoing normal cytokinesis, 49% and 54% of cells respectively, than *ASPM*^{WT} cells, where 91% of late telophase cells had a normal cytokinetic phenotype (Figure 4.16B). The analysis of the cytokinesis phenotypes in the patient cells in comparison to the *ASPM*^{WT} cells revealed significant changes were observed for multiple spindle poles (*ASPM*^{3663delG} $p=0.0001$; *ASPM*^{9984+1T>G} $p< 0.0001$) and for an elongated central spindle (*ASPM*^{3663delG} $p< 0.0001$; *ASPM*^{9984+1T>G} $p< 0.0001$) (Figure 4.16C).



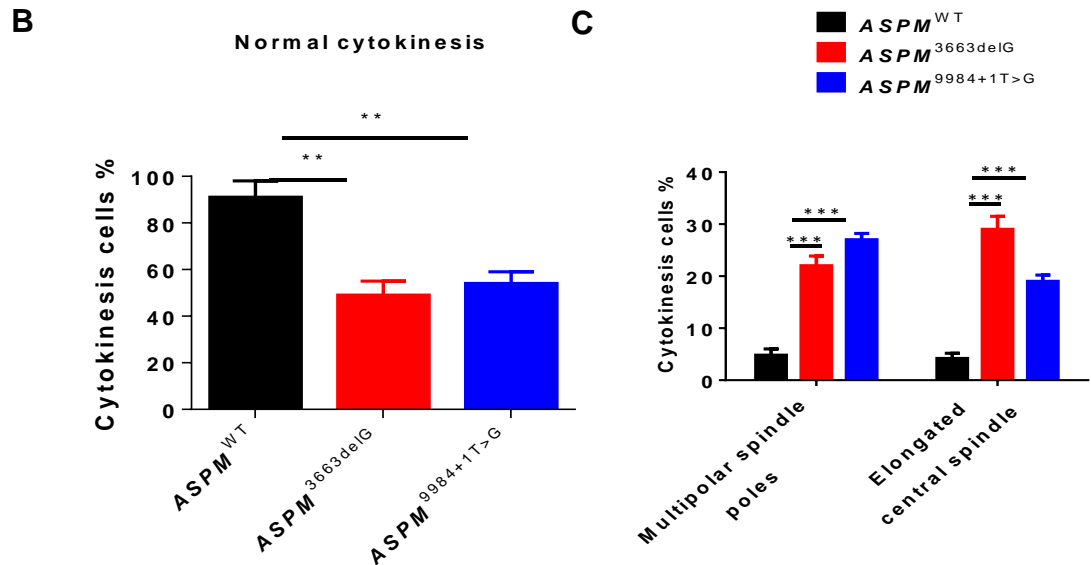
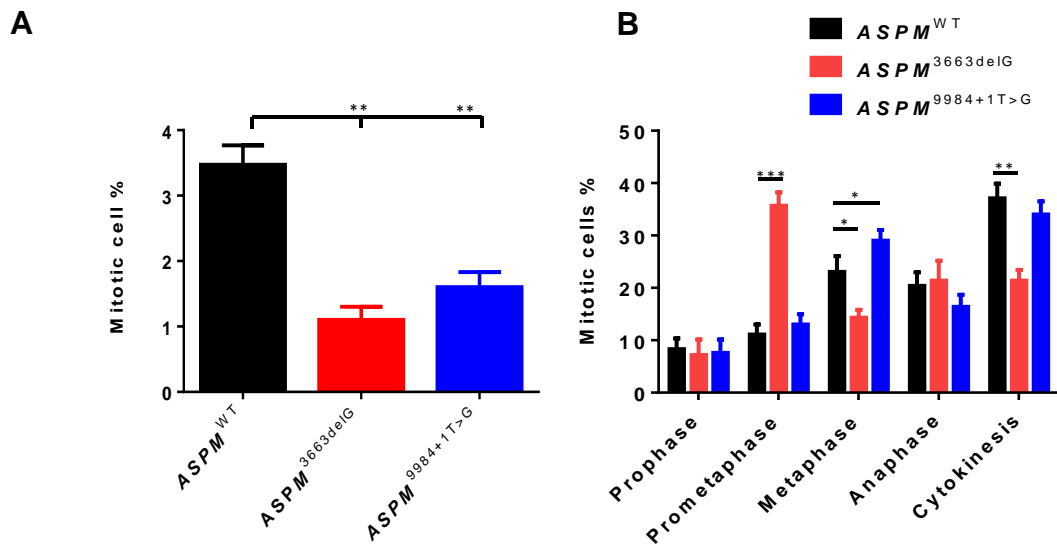


Figure 4.16: Analysis of the effect of *ASPM* mutations on cytokinesis. **A.** Panel shows control and patient cells during cytokinesis. *ASPM* mutations cause stretched central spindle (arrows) and multipolar spindle poles (arrowhead). Cells were stained with anti- γ -tubulin (green) to identify centrosomes, anti- α -tubulin (red) to identify MTs and DAPI (blue) to recognise DNA. Scale bar = 5 μ m. **B.** Statistical analysis showed normal cytokinesis was less common in *ASPM*^{3663delG} (n= 50 cells) and *ASPM*^{9984+1T>G} (n= 58 cells) cells than in *ASPM*^{WT} (n= 63 cells) cells. **C.** Statistical analysis of cytokinesis phenotypes indicates the occurrence of abnormal cytokinetic phenotypes were significantly higher in patient cells than in control telophase cells.

4.5.6 Analysis of the effect of *ASPM* mutation on distribution of mitotic stage.

The effect of *ASPM* mutations on distribution of mitotic stage was investigated using immunofluorescence microscopy. *ASPM*^{3663delG} and *ASPM*^{9984+1T>G} cells showed significant decrease in cell division (1.1% and 1.6% respectively)

compared to *ASPM*^{WT} cell populations, which displayed 3.4% (Figure 4.17A). For both of the patient cell strains, a higher proportion of the mitotic cells were observed to be in prometaphase, however only the *ASPM*^{3663delG} cells were statistically significantly increased ($p < 0.001$), with the *ASPM*^{9984+1T>G} cells having a p value of $p=0.29$. Interestingly, *ASPM*^{3663delG} cells exhibited a corresponding decrease in cells in metaphase ($p=0.01$), whereas *ASPM*^{9984+1T>G} cells showed an increase in the percentage of mitotic cells in metaphase ($p=0.03$). A decrease in cells undergoing cytokinesis was identified in both patient cell strains however again the phenotype was only significant for in the *ASPM*^{3663delG} cells ($p=0.001$, compared to *ASPM*^{9984+1T>G} cell line where $p=0.58$) (Figure 4.17B). (Figure 4.17C) displays a panel of *ASPM*^{3663delG} cells in prometaphase stage.



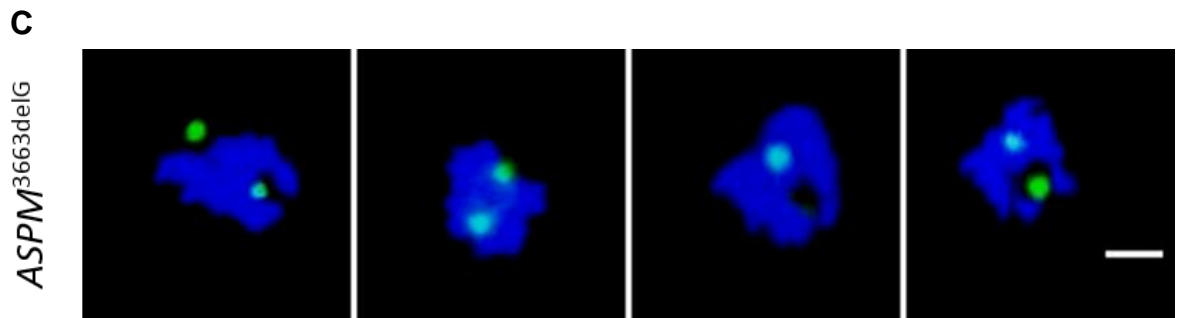


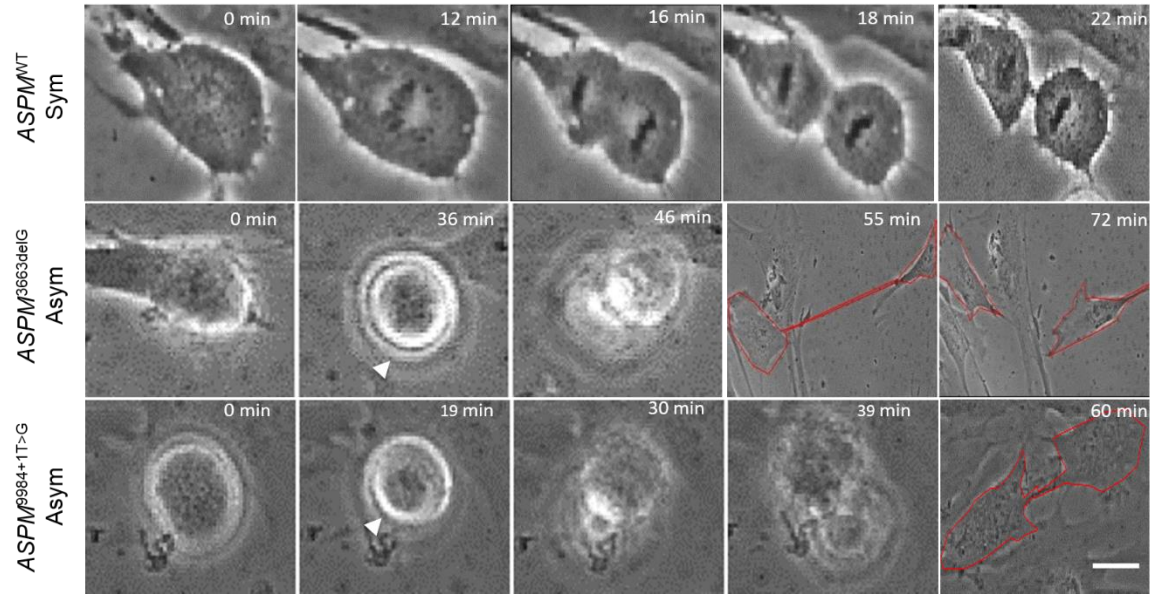
Figure 4.17: Analysis of the effect of *ASPM* mutations on frequency of mitosis and mitotic stage distribution. **A.** Analysis of mitotic cell number amongst three cell lines which indicates that *ASPM*^{3663delG} (n= 102 dividing cells) and *ASPM*^{9984+1T>G} (n= 115 dividing cells) cells undergo less divisions compared with *ASPM*^{WT} (n= 130 dividing cells). **B.** Statistical analysis of mitotic stages in cell strains which illustrates a higher proportion of cells in prometaphase and less cells in metaphase and in cytokinesis in *ASPM*^{3663delG} cells than *ASPM*^{WT} and *ASPM*^{9984+1T>G}. **C.** Panel shows *ASPM*^{3663delG} cells in prometaphase stage. Cells were stained with anti-γ-tubulin (green) to identify centrosomes and DAPI (blue) to recognise DNA. Scale bar = 10µm.

4.5.7 Investigation of the effect of *ASPM* mutation on mitotic phenotypes explored by live cell imaging.

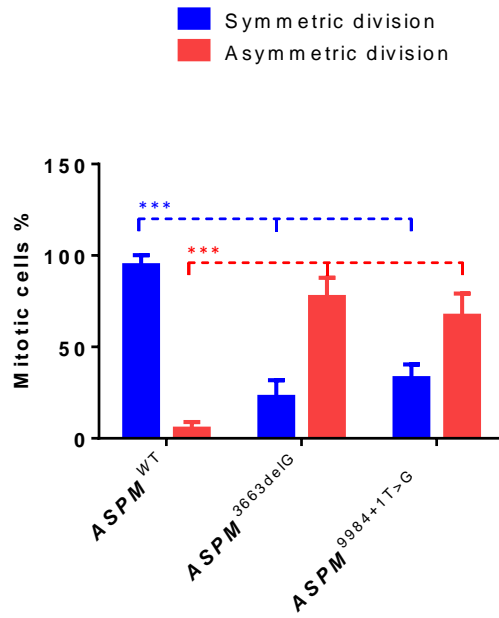
Time-lapse imaging of live *ASPM*^{WT}, *ASPM*^{3663delG} and *ASPM*^{9984+1T>G} cells was performed using a Nikon BioStation IM inverted live cell imaging microscope to study the effect of *ASPM* mutations on live cell divisions in order to determine the cause and outcome of the IF phenotypes identified in this chapter (Section 4.5.6). A number of phenotypic changes were identified for mitosis and mitotic timing in the patient cell lines in comparison to the *ASPM*^{WT} cells (Figure 4.18). These changes included a change in the orientation of the cell division from symmetrical

to asymmetrical division where one of the daughter cells was observed moving out of the focal plane towards the observer as the cleavage furrow is formed parallel to the surface of the imaging dish, (Figure 4.18A, arrowhead) and a defect in cytokinesis, particularly associated with cellular abscission (Figure 4.18A). *ASPM*^{β663delG} and *ASPM*^{9984+1T>G} cells had a higher occurrence of asymmetrical division, 77.3% and 67% respectively (p=0.0003 and p=0.001), than *ASPM*^{WT} cells (Figure 4.18B). The time points shown in the images denote the time taken from the onset of cell division, when the cell is first observed rounding up in prophase and these timings illustrate that patient cells took a longer time for completion of cell division than *ASPM*^{WT} cells (Figure 4.18C). Compared to the *ASPM*^{WT} cells a significant increase in the length of time spent in prometaphase/metaphase was observed in the *ASPM*^{β663delG} cells (p=0.001) and the *ASPM*^{9984+1T>G} cells (p=0.05). The average time taken to complete cytokinesis was increased in the patient cells (*ASPM*^{9984+1T>G} cells p=0.003, *ASPM*^{β663delG} cells p=0.01) (Figure 4.18D). From the LCI videos it was observed that one problem was with the failure of the abscission process in the patient cell lines. The central spindle MTs (cytoplasmic bridges) in the patient cells became thinner and longer than control as the cells tried to mechanically sever the MT bridge when abscission failed.

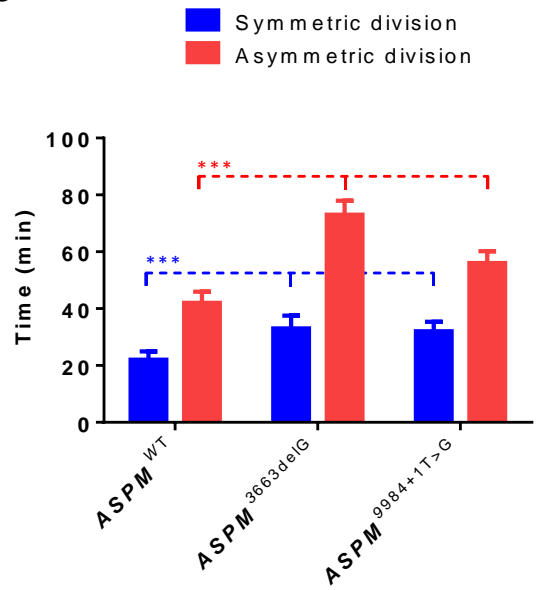
A



B



C



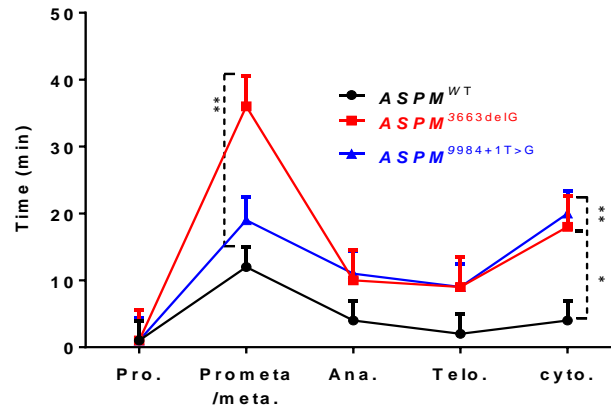
D

Figure 4.18: Analysis of the effect of *ASPM* mutations on division orientation and period of mitosis explored by live cell imaging. **A.** Panel shows phase contrast images of *ASPM*^{WT}, *ASPM*^{3663delG} and *ASPM*^{9984+1T>G} cells. Time frames are given in the top right-hand corner of each image. Top row shows normal *ASPM*^{WT} cells with symmetrical division. Middle and bottom rows show examples of *ASPM*^{3663delG} and *ASPM*^{9984+1T>G} cells respectively undergoing asymmetrical division. *ASPM* mutations induced (i) mitotic spindle division plane mis-orientation causing asymmetric cell division, (ii) aberrant cytokinesis and (iii) an overall increase in the total time of fibroblast cell division. **B.** Statistical analysis of the type and frequency of cell division amongst *ASPM*^{3663delG} (n=90 cells), *ASPM*^{9984+1T>G} (n=105 cells) and *ASPM*^{WT} (n=115 cells) cell lines showing a significant increase in the occurrence of asymmetric division in patient cells compared to control cells. **C.** Histogram comparing the mean time for cell division (n=160 cells) which showed patient cells took longer to complete cell division than control cells. **D.** Graph showing the average asymmetric division length of time taken for each mitotic stage for each of the control and patient cell strains, showing that *ASPM*^{3663delG} cells took significantly longer to complete prometaphase/metaphase stage in comparison to *ASPM*^{9984+1T>G} and *ASPM*^{WT} cells. A significant increase in the time for cells to complete cytokinesis was observed in both patient cell lines, however it was more statistically significant in *ASPM*^{9984+1T>G} cells than in *ASPM*^{3663delG} cells.

Although there was a significant increase in the occurrence of asymmetric division in patient cells (*ASPM*^{3663delG} and *ASPM*^{9984+1T>G} cells had a higher occurrence of asymmetrical division, 77.3% and 67% respectively than control cells (*ASPM*^{WT} cells had 5.3% occurrence of asymmetrical division), most of the cells managed to complete cytokinesis with significantly longer time than control cells (Table 4.3).

4.5.8 Summary tables of the effect of *ASPM* mutation on actin phenotypes.

The Table 4.1, Table 4.2 and Table 4.3 below summarize the mitotic phenotypic changes observed between *ASPM*^{WT}, *ASPM*^{3663delG} and *ASPM*^{9984+1T>G} cells in this chapter as a result of *ASPM* mutations effect on human fibroblast cells.

Table 4.1: Comparison of interphase phenotype analysis between *ASPM*^{WT}, *ASPM*^{3663delG} and *ASPM*^{9984+1T>G} cells.

Interphase phenotypes			
Nuclei	<i>ASPM</i> ^{WT}	<i>ASPM</i> ^{3663delG}	<i>ASPM</i> ^{9984+1T>G}
Normal Nuclei	• 88.4%	• 37.9%	• 42%
Enlarged nuclei	• 5.5%	• 25.8%	• 20.6%
Lobular nuclei	• 3.9%	• 23.7%	• 27.1%
Micro nuclei	• 2.2%	• 12.6%	• 10.3%
Microtubules	<i>ASPM</i> ^{WT}	<i>ASPM</i> ^{3663delG}	<i>ASPM</i> ^{9984+1T>G}
Normal MTs	• 87.1%	• 15.8%	• 37.3%
Clustered MTs	• 4.5%	• 48.6%	• 35.2%
Disorganised MTs	• 3.2%	• 20.6%	• 14.8%
Low density MTs	• 5.2%	• 15%	• 12.7%
Centrosomes	<i>ASPM</i> ^{WT}	<i>ASPM</i> ^{3663delG}	<i>ASPM</i> ^{9984+1T>G}
Normal centrosomes	• 88%	• 44.4%	• 58.3%
Haloed centrosomes	• 7%	• 15.9%	• 19.9%
Increased centrosomes number	• 5%	• 35.7%	• 25.8%
Actin	<i>ASPM</i> ^{WT}	<i>ASPM</i> ^{3663delG}	<i>ASPM</i> ^{9984+1T>G}
Normal actin	• 90.8%	• 12.4%	• 21.3%
Clustered actin	• 3.6%	• 37.9%	• 51.6%
Thick actin	• 5.6%	• 49.7%	• 27.1%

Table 4.2: Comparison of mitotic phenotype analysis between *ASPM*^{WT}, *ASPM*^{3663delG} and *ASPM*^{9984+1T>G} cells.

Mitotic Phenotypes			
Prometaphase spindle poles	<i>ASPM</i> ^{WT}	<i>ASPM</i> ^{3663delG}	<i>ASPM</i> ^{9984+1T>G}
Normal spindle poles	• 91%	• 36.3%	• 41.2%
Monopolar spindle poles	• 5.3%	• 40.6%	• 25.3%
Multipolar spindle poles	• 3.7%	• 23.1%	• 33.5%
Anaphase and Telophase spindle poles	<i>ASPM</i> ^{WT}	<i>ASPM</i> ^{3663delG}	<i>ASPM</i> ^{9984+1T>G}
Normal spindle poles	• 82.3%	• 25.8%	• 33.3%
Monopolar spindle poles	• 4.4%	• 41.3%	• 34.7%
Multipolar spindle poles	• 7.5%	• 21.5%	• 17%
Misplaced spindle poles	• 5.8%	• 11.4%	• 15%
Frequency of mitosis and mitotic stage	<i>ASPM</i> ^{WT}	<i>ASPM</i> ^{3663delG}	<i>ASPM</i> ^{9984+1T>G}
Normal cell division	3.4%	1.1%	1.6%
Prometaphase cells Proportion	11.1%	35.7%	13%
Metaphase cells Proportion	23.07%	14.3%	29%
Cytokinesis cells Proportion	37.1%	21.4%	34.0%

Table 4.3: Comparison of cytokinesis phenotype between *ASPM*^{WT}, *ASPM*^{3663delG} and *ASPM*^{9984+1T>G} cells.

Cytokinesis Phenotypes			
Telophase undergoing cytokinesis	<i>ASPM</i> ^{WT}	<i>ASPM</i> ^{3663delG}	<i>ASPM</i> ^{9984+1T>G}
Normal cytokinesis	• 91%	• 49%	• 54%
Multipolar spindle poles	• 4.8%	• 22%	• 27%
Elongated central spindle	• 4.2%	• 29%	• 19%
LCI data	<i>ASPM</i> ^{WT}	<i>ASPM</i> ^{3663delG}	<i>ASPM</i> ^{9984+1T>G}
Occurrence of symmetric division	94.7%	22.7%	32.9%
Occurrence of asymmetric division	5.3%	77.3%	67.1%
Time cells taken to complete symmetric division	22 min	33 min	32 min
Time cells taken to complete asymmetric division	42 min	73 min	56 min

4.6 Discussion

In the previous chapter, siRNA mediated *ASPM* knockdown investigations in U2OS cells determined a reduction in *ASPM* resulted in (i) centrosomal and MT aberrations in interphase and mitosis which affected spindle pole focus and caused mitotic delay, (ii) cells entered mitosis but during prometaphase/metaphase reverted to a single interphase cell with an enlarged nucleus, (iii) delay in mitotic progression from prometaphase and metaphase, (iv) spindle reorientation, (v) cell death (vi) abnormal interphase nuclei, which are most likely the outcome of chromosome separation defects during mitosis and finally (vi) cytokinesis failure, which specifically identified that *ASPM* is essential role for cellular abscission. Roles for *ASPM* have been verified as centrosome biogenesis and centrosome/spindle pole cohesion, spindle pole focusing, cytokinesis, mitotic progression and actin organisation. The aim of the experiments in this chapter was to identify the abnormal mitotic mechanisms underlying the formation of MCPH through the determination of mitotic abnormalities in dividing patient fibroblast cells. The *MCPH5* brain is reduced in size, but has the same architecture as a normal brain, where the cortical plate consists of 6 neuronal cell layers (Faheem *et al.*, 2015; Li *et al.*, 2017) suggesting that MCPH is a disease of reduced cell number.

In this chapter, interphase and mitotic cells from two patient cell strains exhibiting different homozygous *ASPM* mutations were studied. MCPH related mutations are spread throughout the *ASPM* gene, but result broadly in a single phenotype. The majority of mutations in the *ASPM* gene in *MCPH5* were predicted to result in

protein truncation or in the instruction of the nonsense-mediated decay pathway (Bond *et al.*, 2003; Nicholas *et al.*, 2009; Higgins *et al.*, 2010). Fibroblast cells from two *MCPH5* patients exhibiting mutations in *ASPM* (Bond *et al.*, 2003) were a resource available to study mitotic changes in. The *ASPM*^{3663delG} cell strain carries a homozygous *ASPM* frameshift mutation located in exon 15 and the *ASPM*^{9984+1T>G} cells carry a splice donor site mutation in intron 25 which results in the loss of 3aa from the C-terminus of *ASPM* (Bond *et al.*, 2003).

The MW of the *ASPM* protein in the three different cell strains, *ASPM*^{MT}, *ASPM*^{3663delG} and *ASPM*^{9984+1T>G} fibroblast cell lysates was evaluated by immunoblotting. As expected *ASPM*^{MT} and *ASPM*^{9984+1T>G} lanes each contained a single discrete band of size approximately 410KDa which confirmed the band was likely to equate to 3477 amino acids (aa) full length *ASPM* protein in the *ASPM*^{MT} cells (Higgins *et al.*, 2010) and to 3474aa protein in the *ASPM*^{9984+1T>G} cells. In comparison to U2OS cells (Chapter 3) isoforms of *ASPM* were not expressed in any of the fibroblast cell lines, suggesting there is tissue specificity for *ASPM* isoforms and that different functions of *ASPM* may be required by some tissues. Interestingly *ASPM*^{9984+1T>G} cell lysate contained a significantly lower concentration of *ASPM* protein than the *ASPM*^{MT} cell lysate suggesting that alterations in mitotic phenotype in these cells could result from both the low concentration of an *ASPM* protein missing 3aa from its C-terminus and from the loss of the 3aa. The lower level of altered *ASPM* protein may be explained by the cryptic splicing event in *ASPM*^{9984+1T>G} cells which spliced out nine nucleotides from the 10434bp gene within the C-terminal region of *ASPM* and hence could result in decreased stability

of the protein causing the protein to degrade more quickly (De Cristofaro *et al.*, 2006; Ode *et al.*, 2007).

It was initially anticipated that the frameshift mutation $ASPM^{3663\text{delG}}$ which causes severe mental retardation (Bond *et al.*, 2003) would initiate premature protein truncation of ASPM of 140 kDa or mRNA degradation through NMD (Mahmood *et al.*, 2011; Hug *et al.*, 2016). Unexpectedly a band at 140 kDa was not observed, however a single weak ASPM band at approximately 410kDa was visible on the WB. The possibility of the 3663delG mutation leading to the use of alternative/cryptic splice sites resulting in the loss of a small region of exon 15 was investigated. cDNA sequencing of *ASPM* exons 14-16 in the $ASPM^{3663\text{delG}}$ cells and comparison to $ASPM^{WT}$ and $ASPM^{9984+1G>T}$, cDNA did not reveal the presence of alternative splicing therefore initially this suggested that the 3663delG mutation was a hypomorphic mutation resulting in transcriptional read through (Abolhassani *et al.*, 2014; Parent *et al.*, 2015) creating a low concentration of full length ASPM protein. Consequently, the phenotypic effect arising from 3663delG mutation was initially thought to be caused due to production of an inadequate concentration of ASPM and therefore possibility of reduction of function.

Analysis of the localisation of ASPM in methanol fixed $ASPM^{WT}$ fibroblast cells was as expected (Zhong *et al.*, 2005; Higgins *et al.*, 2010). ASPM was localised and more highly expressed in the nucleus than cytosol in interphase cells and hence it was expected to be more functional in the nucleus than in the cytoplasm. Directly after nuclear envelope breakdown and mitotic spindle was formed, ASPM relocated to the mitotic spindle poles (from prometaphase to telophase) and associated with

MTs at the minus ends of mitotic spindle. From late telophase ASPM was observed at the Flemming body/midbody of the central spindle during cytokinesis. Investigations conducted by our group have shown that the fetal expression of *ASPM* mRNA using mouse brain was predominantly in the active site of neurogenesis (Bond et al., 2002). In accordance with immunoblotting results, the immunofluorescence analysis of the cellular localization of ASPM protein in *ASPM*^{3663delG} and *ASPM*^{9984+1T>G} cells showed a great reduction in the amount of ASPM protein in the nucleus in interphase cells and at the spindle poles of dividing cells. The data indicated that ASPM expression levels in *ASPM*^{3663delG} cells were significantly lower than in *ASPM*^{9984+1T>G} cells which indicated that ASPM levels at the spindle poles may correlate with the severity of the disease. In both sets of patient cells the reduction in ASPM at the spindle poles was accompanied with a redistribution of some *ASPM*^{3663delG} and *ASPM*^{9984+1T>G} to the cytoplasm. This could represent a reduced ability of *ASPM*^{3663delG} and *ASPM*^{9984+1T>G} to get to the spindle pole, possibly via MT motors or through direct interaction with the MT as ASPM has been identified as tracking growing MT minus ends (Howard et al., 2017), or to attach to the pericentrosomal matrix when it arrived at the spindle pole. Mislocalisation of the *ASPM*^{3663delG} protein identified in this chapter suggested the mutation must result in another as yet unidentified alterations in addition to the reduced level of *ASPM*^{3663delG}, such as a small cDNA loss or gain. Due to time constraints this unknown alteration was not further investigated.

The mitotic functional consequences of the mutated ASPM in mitosis was investigated in *ASPM*^{3663delG} and *ASPM*^{9984+1T>G} cells in comparison to *ASPM*^{WT}

cells. The common functional consequences of the two ASPM mutations would arise due to a decreased level of ASPM and common relocation of the respective mutated ASPM proteins. Differences would arise due to small differences in the amount of the mutated ASPM protein present in the cells and the functional effects of the domains effected by the respective mutation, which for the *ASPM*^{9984+1T>G} mutation is the specific loss of 3aa at the C-terminal, but is unknown for the *ASPM*^{3663delG} mutation. Overall, similar phenotypic changes were observed in the patient cells to those observed in Chapter 3, however subtle mutation specific differences were observed.

ASPM mutations were found to cause a significant effect on the number, morphology and size of centrosomes in interphase. The excessive numerical centrosomes with irregular structure (haloed) and size were the main phenotypes observed in *ASPM*^{3663delG} and *ASPM*^{9984+1T>G} fibroblast cells during interphase. *ASPM*^{3663delG} cells showed higher proportion of centrosome abnormalities than *ASPM*^{9984+1T>G} cells and this may contribute to the association of the 3663delG mutation with a more severe MCPH phenotype. A similar phenotype was previously identified in *Drosophila asp* mutants (Gonzalez *et al.*, 1990). ASPM is known to have a role in centrosome biogenesis (Jayaraman *et al.*, 2016) and centrosome/spindle pole cohesion in neural stem cells (Schoborg *et al.*, 2015). Similarly MTs were disorganised, low density and clustered in both patient cell strains, suggesting that this phenotype arises due to a reduction or mislocalisation of ASPM. The decrease in normal MT phenotype was larger in the *ASPM*^{3663delG} cells than the *ASPM*^{9984+1G>T} cells. A phenotypic effect upon MT has been

previously identified in U2OS cells upon reduction of ASPM (Higgins et al., 2010). Centrosomes are the major microtubule organizing centers that contain pairs of centrioles responsible for MT polarization and nucleation during interphase and spindle formation in mammalian cells (Sumiyoshi et al., 2012). It could be hypothesized that a defective centrosome, as a direct effect of homozygous *ASPM* mutation, could cause changes in MT nucleation. ASPM was also reported to be essential in focusing the MT minus ends of mitotic spindle poles (Ito, et al., 2015). In *Drosophila*, KD of *asp* causes loss of MT focus at spindle poles (Fish, et al., 2006). Additionally, mutated *asp* of *Drosophila* was found to show activity in nucleating MTs at centrosomes during interphase (Saunders, et al., 1997). A third interphase change was in the organisation of actin, where both mutations resulted in actin bundling and clusters of actin aggregates and a loss of cortical actin. More specific differences between the patient cell phenotypes were observed with actin striations being observed in the *ASPM*^{9984+1G>T} mutated cells. Loss of cortical actin could signify a role for ASPM at the cell cortex. Suggesting ASPM directly or indirectly is associated with bridging cytoskeletal structures actin and MT at the cell cortex possibly via interaction with other partners. In the patient cells actin filaments did not appear to be wavy, as may be expected if actin was not linked to the cortex, however cortical actin and filamentous actin may require different anchors at the centrosome and at the cortex. More research is required into the role of ASPM in cortical actin localisation.

A number of aberrant mitotic phenotypes were observed in the patient cells strains. Structurally, highly statistically significant alterations in spindle pole number and

spindle pole localisation were observed in prometaphase, anaphase and telophase. Mutation specific differences in the frequency of each phenotype were observed. Specifically in prometaphase a higher incidence of monopolar spindles was observed in *ASPM*^{3663delG} cells and a higher incidence of multipolar spindles in the *ASPM*^{9984+1G>T} cells, suggesting that monopolar spindles may contribute to a more severe MCPH. An increase in misplaced spindles, where the spindle poles were incorrectly positioned, was observed in both patient cell strains. Misplaced spindles tended to possess spindle poles that are placed further from the spindle pole body. These mitotic spindle pole abnormalities differed compared to mitotic *ASPM* KD U2OS cells (Chapter 3), as monopolar spindles were not observed in the U2OS *ASPM* KD cells and haloed spindle poles were not observed in the patient cells. These phenotypic differences are attributed to a number of reasons including cell type specific differences and phenotypic differences between *ASPM* depletion and *ASPM* mutation.

As in U2OS cells with reduced *ASPM*, both patient cell strains exhibited a decrease in the % cells in mitosis, suggesting the mutations caused a decrease in cell division. *ASPM*^{3663delG} cells showed the lowest % of dividing cells which is in keeping with the fact that in this patient the MCPH is more severe with a head circumference of -9 to -11SD (Bond et al., 2003). *ASPM* KD studies in U2OS cells (Chapter 3), neural stem cells (Fish, Kosodo, Enard, Pääbo, et al., 2006), glioblastoma (Horvath et al., 2006) and in malignant gliomas (Bikeye, et al., 2010) have similarly shown a decrease in proliferation. Changes in the distribution of mitotic cells across the mitotic stages was observed compared to the *ASPM*^{WT}

cells. There was also a difference in mitotic distribution between the two mutations. A modest but significant increase in % *ASPM*^{9984+1T>G} cells in metaphase was observed, suggesting ASPM is involved in progression through metaphase into anaphase and that the phenotype resulted from a reduction in ASPM, or that the ASPM C-terminus is involved in this transition or that the loss of 3aa results in misfolding of ASPM and therefore *ASPM*^{9984+1T>G} has reduced function. In support to our findings, *asp* mutations in *Drosophila* was found to increase the number of cells in metaphase leading neuroblasts to arrest in metaphase and causing a reduction in cell number resulting in reduced CNS development (Ripoll, *et al.*, 1985). Correspondingly, the mitotic cycle was blocked at metaphase in brains of homozygous *asp* larvae due to *asp* mutation (Gonzalez *et al.*, 1990). In contrast *ASPM*^{3663delG} cells showed an increase in % cells in prometaphase, with corresponding but smaller decreases in the number of mitotic cells in metaphase and cytokinesis. The time taken for the average *ASPM*^{3663delG} mitotic cell to transition through prometaphase was also significantly increased, suggesting the cells struggle to progress through prometaphase. *ASPM*^{9984+1G>T} cells did not show an increase in number of cells in prometaphase, but did show an increase in time taken to progress through prometaphase, suggesting a mutation specific effect, however the 3663delG mutation could cause a decrease in amount of 'full length' ASPM because the mutation results in reduced stability of the protein rather than a specific loss of a region. Ito and Goshima found that *asp* in *Drosophila* plays a role in the progression from early prometaphase to metaphase (Ito, *et al.*, 2015). LCI indicated that these prometaphase cells did not enter programmed cell death and

neither did they return to an interphase cell, as observed in with *ASPM* siRNA mediated KD, but eventually progressed through cell division. Unsurprisingly, given the number of aberrant mitotic phenotypes identified in both patient cell lines, a significant increase in the length of time taken for mitosis was observed. .

Neurogenesis is a tightly regulated finitely timed process (Yamaguchi et al., 2014), A simple model of brain development is that the neuronal progenitor cells undergoes two types of cell division, symmetric and asymmetric. The type of division performed is spindle and cleavage plane orientation dependent; initially symmetric divisions (vertical cleavage plane) give rise to two NPC which expands the NPC numbers (NPC pool). A switch in spindle and cleavage plane orientation then creates asymmetric divisions which give rise to daughter cells with different cell fates, one NPC (replenishing the NPC pool) and one neuron (Chenn et al., 1995). Vertical cleavages (symmetrical divisions) occur in early cortical development and as neurogenesis continues, fraction of cells undergo horizontal cleavages (Caviness *et al.*, 1995). *ASPM* mutations caused profound effect on the orientation of the mitotic spindle in fibroblast cell division. A vast increase in the proportion of asymmetric cell division was detected in *ASPM*^{8663delG} and *ASPM*^{9984+1T>G} cells compared to *ASPM*^{WT} cells. A role for *ASPM* in maintaining the plane for division for symmetric cell division has been shown in mice and humans as a result of elimination of *ASPM* (Fish, *et al.*, 2006; Godin *et al.*, 2010; Higgins *et al.*, 2010; Lizarraga *et al.*, 2010). Spindle orientation and therefore symmetric division are controlled by the (i) astral MT which reach the apical and basal cell cortex, but not by those reaching the central cell cortex (Mora *et al.*, 2014) and (ii)

pushing forces from the polymerisation of astral MT against the cell cortex (Garzon *et al.*, 2016) with pulling forces exerted by cortical dynein and MT depolymerisation creating asymmetric division (Howard *et al.*, 2017). In the developing brain an early switch for symmetric to asymmetric division would result in a vastly reduced NPC pool, which would then produce fewer neurons and a smaller brain, similarly a reduction of radial MT reaching or attaching to the apical or basal cortex could alter the division plane. The hypothesis for the role of ASPM in maintaining the symmetric division plane is that ASPM is involved in astral MT focussing at the centrosome and/or at the cortex, with a reduction or alteration in ASPM causing a reduction in astral MT attachment at the cortex and/or a reduction in the pushing force of the astral MT at the cortex. Above all other mitotic changes in patient cells a change in division orientation could arguably have the biggest reduction on neuron number and may explain the similarities in *MCPH5* phenotype. LCI data showed that in all three sets of fibroblast cells asymmetric divisions took longer than symmetric divisions, however an increase in the timing of both symmetrical and asymmetrical divisions in patient cell lines compared with control was observed. This indicated that there were additional difficulties for the patient cells to overcome in asymmetric division over and above change symmetric division.

In patient cells, ASPM midbody staining was reduced and partially localised to the central spindle, suggesting an MT associated defect such as MT dependent transport of ASPM. In agreement with our IF data, using time-lapse imaging we observed an extremely long central spindle in cytokinesis in patient cell lines, a failure of cells to complete abscission and an increase in time taken to complete

cytokinesis. Daughter cells were seen to pull in opposite directions which stretched the central spindle until the force exerted tore the cell membrane and central spindle MTs apart. The localisation pattern of ASPM at the midbody during cytokinesis suggests a crucial role in cellular abscission. Collectively, these data support our hypotheses that ASPM is crucially required to complete cytokinesis with the possible role of recruiting essential proteins to the midbody. Citron Kinase (CITK) is known to be an interactant of ASPM (Paramasivam *et al.*, 2007) and to be involved in abscission (Watanabe *et al.*, 2013). Although an elongated spindle and mechanical separation of daughter cells is common to both patient cell lines the incidence of an elongated spindle as a % of cells in cytokinesis was greater in the *ASPM*^{3663delG} cells than the *ASPM*^{9984+1G>T} cells, The commonality of phenotypes suggests the reduction in ASPM is the mechanism for this alteration rather than the specific loss of domain even though the role of ASPM in cytokinesis is linked to the C-terminus and the 9984+1G>T creates a loss of 3 aa in the C-terminus of ASPM (Higgins *et al.*, 2010). However this phenotype is different to that identified in ASPM reduction in U2OS cells (Chapter 3.5.3) where the cells failed to abscise but reformed as a single cell or died. This could reflect cell type specific differences, a reflection on the added effect of the mutations or it could be as a consequence of defective motility (more investigation needed).

In light of the previously identified effects of *ASPM* siRNA mediated KD on nuclei phenotypes in Chapter 3, whether *ASPM* mutations contribute to nuclei defects was investigated. A number of aberrant nuclear interphase phenotypes were identified in *MCPH5* patient cells. Patient cells were observed to have abnormal

lobular nuclei, enlarged nuclei and micro nuclei. Based upon the changes to ASPM localisation observed in the interphase nucleus in patient cells and the nuclear defects identified in the cells in this chapter it is possible that ASPM has some nuclear function, however this was not investigated further as part of this thesis. Based on IF data and live cell imaging results from ASPM reduction phenotypes (Chapter 3) an alternative and more likely explanation for the abnormal nuclear phenotypes is that the phenotypes arise as a result of abnormal cell division, specifically from a reduction in MT forces which are required for separating chromosomes (Civelekoglu et al., 2010), which would result in lagging chromosome phenotypes and upon reformation of the nucleus would result in micronuclei and lobular nuclei. *ASPM* mutations could also potentially impact chromatin organization such as failure to correctly separate chromatin as a result of defective mitosis, consequently resulting in changes in nuclear size and shape. The *ASPM* mutations *3663delG* and *9984+1G>T* cause centrosomal and MT defects in interphase. The abnormal mitotic phenotypes can be attributed to the effect of these defective phenotypes as centrosome and MTs modulate spindle assembly, spindle orientation, chromosomal separation and cytokinesis. This Chapter identifies that multiple mitotic aberrations contribute to the reduction in cell number leading to the MCPH phenotype. *ASPM* mutations lead to aberrations in spindle poles, MTs, mitotic progression, cytokinesis and cell fate which ultimately resulted in an increase in time to complete mitosis and a decrease in mitosis and changes in cell fate, which if extrapolated to the developing brain would cause a reduction in NPC number and the production of a small brain. Arguably the change

in division orientation would be expected to result in the biggest decrease in NPC number. Unexpectedly the two mutations caused production of a low level of ASPM at approximately the MW of full length ASPM. This suggested that not only could the aberrant phenotype arise due to physical changes in ASPM such as the loss of the 3aa in the C-terminus of ASPM, but also from a decreased expression of ASPM, with the 3663delG mutation resulting in the lowest level of ASPM. Differences in the occurrence of aberrant phenotypes between the two patient cell strains were observed, however whether this is because of losses of different in the level of ASPM in each cell strain or whether it is because of the physical effect of each mutation has not been determined in this chapter. This 3663delG mutation generally resulted in a lower level of ASPM and a higher incidence of the abnormal mitotic phenotypes and was a more severe MCPH disorder. Differences in the spectrum of abnormal phenotypes in ASPM KD cells (chapter 3) and from mutation in ASPM could be the result of the physical effect of the mutation rather than the level of ASPM in each set of cells. Interestingly, an increase in cell death was not observed in patient fibroblast cells. This suggests, but does not prove that cell death is not an outcome of ASPM mutation in NPC.

Chapter 5 : Investigation of Novel ASPM-C-terminal interacting partners.

5.1 Introduction

The investigation into the effect of *ASPM* siRNA treatments in the U2OS cell line and in *MCPH5* patient cells with mutations in *ASPM* identified roles for ASPM in microtubule organisation, centrosomal cohesion, actin filament organisation, mitotic progression, spindle orientation and cytokinesis (Chapters 3 and 4). The C-terminal region (CTR) is essential for ASPM function (Higgins et al., 2010), and is the most conserved part of ASPM structure among other species including *Drosophila* and mouse (Craig et al., 1998; Roberts, et al., 2002; Higgins et al., 2010). A number of studies have shown that the C-terminus of ASPM is localized to the midbody and plays an important role in cytokinesis in human (Higgins et al., 2010) and rat (Paramasivam, et al., 2007). ASPM C-terminus is required to recruit CITK to the mitotic spindle to control thmitotic spindle orientation (Gai, et al., 2016) and to complete abscission during cytokinesis (Paramasivam, et al., 2007). ASPM protein lacking the C-terminus caused severe spindle assembly defects and cytokinesis failure (Higgins et al., 2010). Additionally, sequencing patient cDNA from fibroblasts containing the *ASPM* mutation 9984+1G>T showed that a loss of 3aa from the C-terminus and a decreased amount of ASPM was sufficient to induce mitotic defects causing MCPH (Higgins et al., 2010 and Chapter 4).

A commercial yeast-two-hybrid (Y2H) screen of the ASPM C-terminus (bait) against a foetal brain cDNA library (prey) was performed prior to the start of this

project. (Figure 5.1). The ASPM C-terminus bait (designed and created by Miss Ruth Binns from our research group) was designed to include the region corresponding to that previously assigned to cytokinesis in the rat (Paramasivam et al., 2005).

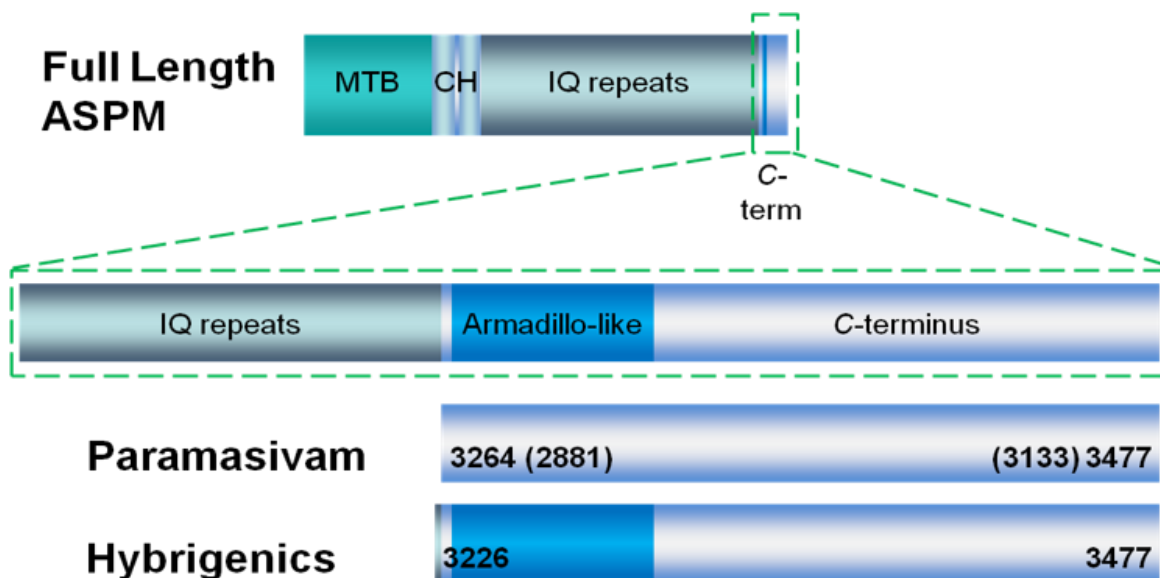


Figure 5.1 ASPM C-terminal Y2H bait design. Based on published data of a rat Aspm C-terminus interaction with CITK (Paramasivam), a Y2H bait of the ASPM C-terminus was designed to include the putative armadillo-like domain and the extreme C-terminus of ASPM. The bait was named ‘Hybrigenics’ as this was the company who performed the screen. Bait and image created by Miss Ruth Binns.

The top three candidate protein interaction hits identified by the ASPM C-terminal screen were SLIT-ROBO Rho GTPase-activating protein 2 (SRGAP2), GRIP and coiled-coil domain-containing protein (GCC2) and Microtubule-Actin Cross-linking Factor (MACF1). Further investigation is needed to investigate these hits in order to increase our ability to understand ASPM C-terminal function in mitosis and

cytokinesis. The investigation of the novel ASPM interactions with SRGAP2, GCC2 and MACF1 may offer evidence to explain some of the mitotic functions of ASPM. To date, the mitotic interactions between ASPM and these proteins have not been confirmed.

This chapter identified and confirmed novel interacting partners of the ASPM C-terminus and investigated their protein level, mitotic localisation and determines if the interaction was affected by ASPM knockdown. A number of reagents had been previously created within the Bond research group that were utilised to confirm and investigate the interactions. These included ASPM C-terminus GST fusion proteins (Miss Ruth Binns), which were used to pull down ASPM interacting proteins from cell lysates. Due to time constraints, further investigations into the function of ASPM C-terminal interactions and the effect of ASPM mutations on the function and regulation of these interactants was not performed.

5.1.1 Pilot Y2H screening data

5.1.1.1 Identification of ASPM C-terminal interacting partners by Y2H screening.

The commercial ASPM C-terminal Y2H screen against a human foetal brain *cDNA* library was commissioned by our group and performed by Hybrigenics SA (Paris, France). 183 clones were obtained, sequenced, and found to represent 130 genes/*cDNA* matches (termed hits, Appendix 4). Of these, 83 hits were discounted as they contained at least one in-frame STOP codon and 6 were discounted as their sequence was fully contained in the 5' Untranslated Region (UTR) or 3'UTR

sequence. The remaining 17 hits were ranked according to the highest predicted binding affinity (confidence rating) (Table 5.1). Four hits were represented by more than one clone. The top three putative hits with the highest predicted binding affinity represented novel ASPM interactants. They were identified SRGAP2 (5 clones which represent 3 independent sequences), GCC2 (4 clones representing 3 independent sequences) and MACF (7 clones, representing 4 independent clones).

Table 5.1: ASPM C-terminal interactant list using Y2H screen ranked by confidence rating.

Gene	Confidence rating	Number of clones (independent clones)	In Frame	Gene sequence	Function
SLIT-ROBO Rho GTPase-activating protein 2 (SRGAP2)	A	5 (3)	✓	534-1021	Control neuronal migration, differentiation and maturation (Guerrier et al., 2009).
GRIP and coiled-coil domain-containing protein 2 (GCC2)	B	4 (3)	✓	558-2352	Required to maintain Golgi structure and intracellular vesicle transport (Yoshino et al., 2003, Lin et al., 2011).
Microtubule-Actin Crosslinking Factor 1 (MACF1)	D	7 (4)	✓	9972-14276	Participate in neuronal migration (Kakinuma et al., 2004)
Spectrin Alpha, Non-Erythrocytic 1 (SPTAN1)	D	2 (2)	✓	486-4562	Calcium-dependent movement of the cytoskeleton at the membrane (Baines, 2010)
Transcription regulator protein (BACH2)	D	1	✓	1716-2161	Transcriptional regulator protein and involved in forming heterologous protein-protein interactions. (Liu <i>et al.</i> , 2009)
chromosome 7 open reading frame 60 (C7ORF60)	D	1	✓	-10-688	S-adenosyl-L-methionine-dependent methyltransferase (Gu <i>et al.</i> , 2017)
CAP-Gly domain-containing linker protein 2 is (CLIP2)	D	1	✓	1098-1601	Link microtubules to dendritic lamellar body (DLB). (Galjart, 2005)
Dystonin (DST)	D	1	✓	8157-10147	Cytoskeletal linker protein. (Dalpé <i>et al.</i> , 1998)
Cytoplasmic dynein 1 heavy chain1 (DYNC1H1)	D	1	✓	10053-10467	Acts as microtubule-based motor. (Karki e Holzbaur, 1999)
End-binding Protein1 (EB-1)	D	1	✓	219-1076	Involved in the regulation of microtubule polymerization. (Stypula-Cyrus <i>et al.</i> , 2014)
CAMSAP1L1 (KIAA1078)	D	1	✓	12 - 593	Microtubule-organizing protein. (Tanaka <i>et al.</i> , 2012)
kinesin family member 5C (KIF5C)	D	1	✓	1860- 2465	Involved in intracellular transport along microtubules. (Poirier <i>et al.</i> , 2013)
Programmed cell death 6-interacting protein (PDCD6IP)	D	1	✓	1053-2036	Involved in endocytosis, body biogenesis, membrane repair and cytokinesis. (Kanai <i>et al.</i> , 2000).
SUN domain-containing protein 1 (SUN1)	D	1	✓	1020-1526	Involved in nuclear-cytoplasmic bridging. (Haque <i>et al.</i> , 2010)
Synaptic nuclear envelope protein 2 (SYNE2)	D	1	✓	15501-16057	Involved in tethering the nucleus to the cytoskeleton
TRIO and F-actin-binding protein (TRIOBP)	D	1	✓	6381-6924	Actin cytoskeletal organization regulator. (Seipel et al., 2001)
FRY microtubule binding protein (FRY)	D	1	✓	5169-6128	maintains structural integrity of mitotic centrosomes and spindle bipolarity. (Ikeda et al., 2012)

The results of a commercial Y2H screen of ASPM C-terminus against a human foetal brain *cDNA* library identified 17 different putative interactants. The first three putative interacting proteins were selected to follow up on based on their confidence rating and the number of independent clones produced in the screen. Confidence rating A is very high confidence in the interaction, B is high confidence in the interaction and D is moderate confidence in the interaction.

5.1.1.1.1 SLIT-ROBO Rho GTPase-Activating Protein 2 (SRGAP2).

Slit-robo GTPase activating protein 2 (SRGAP2), also known as formin-binding protein 2 (*FNBP2*) on chromosome 1q32.1 is a 22 exon gene encoding a 1071 amino acid protein of molecular weight (MW) 123kDa (Kato et al, 2004). SRGAP2 is one of three SRGAP proteins (SRGAP1, 2 and 3), which contain an F-BAR domain which is generally involved in membrane curvature bending. The SRGAP2 protein also comprises an FNBP2-FNBP1 homologous (FBH) domain, Fes-CIP4 homology (FCH) domain, a Rho GTPase-activating protein domain (RhoGAP, involved in hydrolysis of GTP bound to Rho, Rac and/or Cdc42 causing inactivation of the protein), and a SRC homology 3 (SH3) domain, domains which are often identified in proteins involved in regulation of the actin cytoskeleton (Coutinho-Budd *et al.*, 2012) (Figure 5.2). SRGAP2 binds and deforms membranes (Coutinho *et al.*, 2012) and regulates actin dynamics to induce filopodia formation in order to control neuronal migration, differentiation and maturation (Guerrier *et al.*, 2009). There are two known paralogs of SRGAP2 (B and C), formed by gene duplication (Charrier *et al.*, 2012). SRGAP2C dimerises with the ancestral SRGAP2 to inhibit its function.

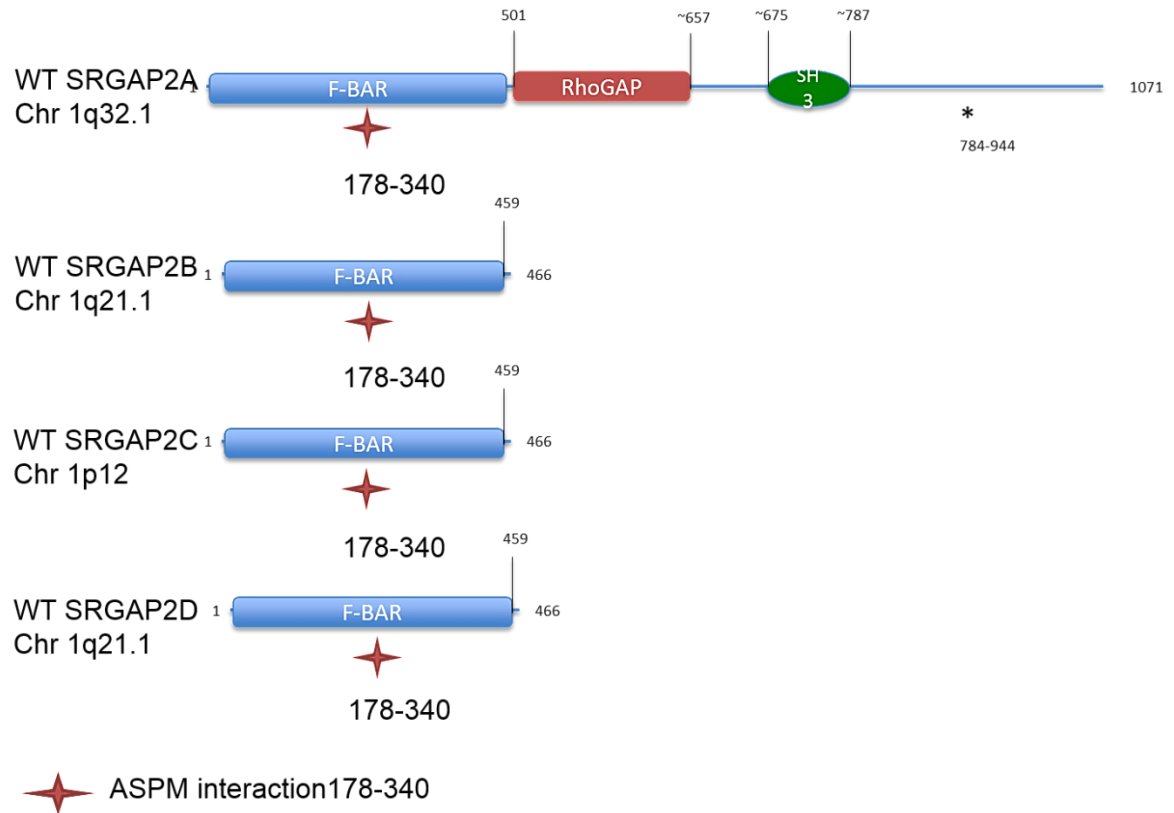


Figure 5.2. A schematic representation of the full-length SRGAP2 protein and paralogs showing the active domains. The SRGAP2 protein structure contains: the FNBP2-FNBP1 homologous (FBH) domain, FCH (MT binding) domain, a Rho GTPase-activating protein domain, the SRC homology 3 (SH3) domain and C-terminal domain. The diagram highlights the ASPM-SRGAP2 interaction site between 158–290aa.

5.1.1.1.2 GRIP and Coiled-Coil Domain-Containing Protein 2 (GCC2).

The GRIP and Coiled-Coil Domain-Containing Protein 2 is also known as GCC185 referring to its molecular weight. GCC2 has a role in MT nucleation and receptor recycling (Cheung e Pfeffer, 2016). The *GCC2* gene is localized on chromosome 2q12.3 (OMIM, 2014) and translation of the gene produces a 185kDa Golgi coiled-

coil protein localised to the membrane of the trans-Golgi network (TGN) (Figure 5.3). The C-terminus Golgi-targeting region is referred to as the GRIP domain (Munro et al., 1999). GCC2 is required to maintain Golgi structure and intracellular vesicle transport (Yoshino *et al.*, 2003; Lin *et al.*, 2011). Additionally GCC2 has been shown to interact with CLASP (CLASP 1 and 2) proteins (MT binding proteins), which GCC2 recruits to the Golgi where an MT-Golgi interaction resulting in nucleation of non-centrosomal MT and control of Golgi organisation occurs (Efimov, *et al.*, 2007).

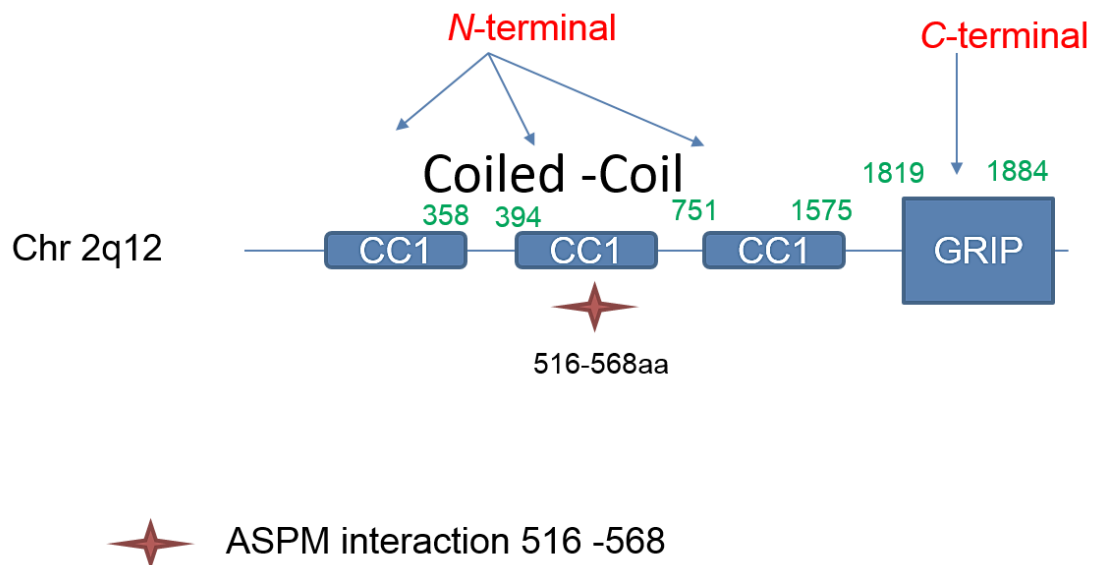


Figure 5.3. A schematic representations of full-length GCC2 protein with binding domains. The N-terminal of GCC2 protein contains, a coiled-coil domain and the C-terminal region contains the GRIP domain. The diagram highlights the ASPM-GCC2 interaction site between 516–568aa.

5.1.1.1.3 Microtubule-Actin Cross-Linking Factor 1 (MACF1).

MACF1 (also known as actin cross linking factor 7, ACF7) is a hybrid of dystonin and dystrophin and is the mammalian homologue of *Drosophila* protein, Kakapo (Bernier *et al.*, 1996). The MACF1 on Chromosome 1p32 has a minimum of 102 exons and spans over 270 kb of genomic DNA (Gong *et al.*, 2001). MACF1 is a member of the plakin family of proteins, which are giant proteins that form bridges between cytoskeletal filaments and the cell periphery (Roper *et al.*, 2002). The molecular size of MACF1 is approximately 620 KDa and structurally MACF1 has an actin-binding domain (ABD), a plakin domain (thought to have intermediate filament binding properties) and a region of spectrin repeats creating a rod domain (Figure 5.4) (Leung, *et al.*, 1999). The C-terminal of MACF1 interacts with and stabilizes microtubules (Glu-tubulins) (Moffat *et al.*, 2017). At least five isoforms of MACF1 have been described with sizes ranging from 880kDa to 135kDa; three have been partially characterized in mice; two of them contain putative ABDs (Bernier *et al.*, 1996). Isoforms 1-4 vary at their *N*-terminus and at the 5'UTR (Bernier *et al.*, 1996; Gong *et al.*, 2001) and the fifth (MACF1b) contains an additional Plakin repeat domain (Lin *et al.*, 2005). MACF1 has been shown to influence neuronal migration (Kakinuma *et al.*, 2004) by regulating microtubule dynamics and mediating GSK3Beta signalling in the developing brain (Goryunov *et al.*, 2010). Finally, MACF1 may play a role in the transportation of vesicles containing glycosyl phosphatidyl inositol-linked proteins from the trans-Golgi network to the cell periphery (Ka *et al.*, 2014).

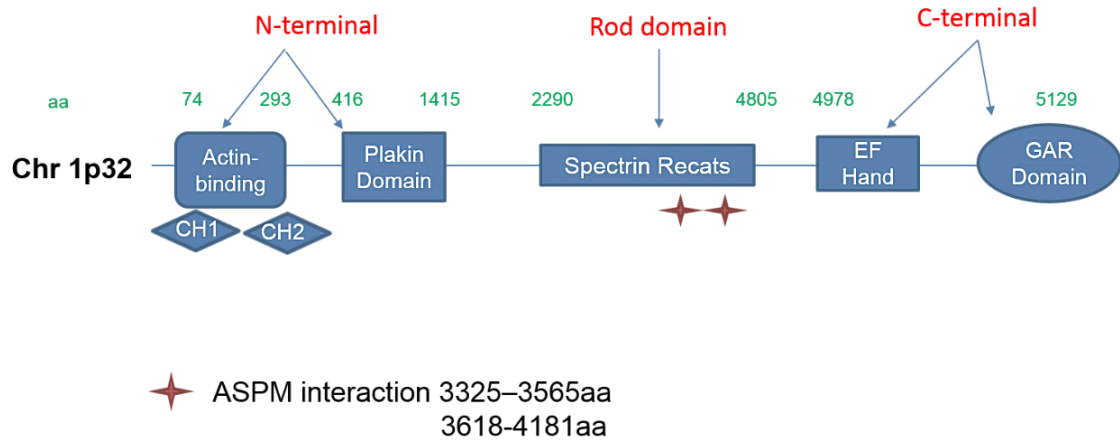


Figure 5.4. A schematic diagram of full-length MACF1 Wild-type protein with binding domains. MACF1 protein contains well-defined domains including; an actin-binding domain (ABD) with two calponin homology domains, CH1 and CH2 fragments, a plakin domain (a plakin repeats domain (PRD) between the plakin domain and the spectrin repeats for MACF1b), a rod domain of 23 α -helical spectrin repeats, an EF hand domain (EF), and a GAR domain. The diagram highlights the two interaction sites of ASPM with MACF1 at 3325–3565 and 3618–4181 amino acids respectively.

5.2 Hypothesis.

The hypothesis for this chapter was ASPM C-terminus interacts with sRGAP2, GCC2 and MACF1 during mitosis to link MT and or actin to the Golgi and/or cell cortex and/or to orchestrate cytokinesis and other mitotic processes.

5.3 Objectives.

The aim of this study to identify and confirm novel protein interactions with the ASPM C-terminus identified through a yeast-2-hybrid screen by employing a variety of techniques including Western Blotting, Protein complex co-immunoprecipitation (Co-IP) and immunofluorescence staining. To confirm co-localisation of ASPM and novel interactants and to identify the effect of *ASPM* knockdown on the localisation of these interactants.

5.4 Methods

5.4.1 Cell lines.

Human bone osteosarcoma epithelial cells (U2OS) and SHSY-5Y neuroblastoma cells were acquired from the ATCC Cell Biology Collection (ATCC-LGC Promochem Partnership, South London, UK). Cervical cancer HeLa cells were supplied by the European Collection of Cell Cultures (ECACC, South London, UK). Control human dermal fibroblast cells (*ASPM*^{WT}) were obtained from Genlantis (San Diego, California). Fibroblast cells (TC 363-06 (*ASPM*^{β663delG}) and TC 273-05

(*ASPM*^{9984+1T>G}) were previously created from two individual patients of Northern Pakistani origin (see Chapter 4, Higgins et al., 2010). Each cell line was maintained in optimum conditions (Material and Methods Section 2.1.2) and treated in accordance with the manufacturer's directions.

5.4.2 General Methodologies.

Methodologies used in this study were (i) Immunoblotting to determine interactant expression in a panel of human cell lines and fibroblasts from control and *MCPH5* patients (Chapters 2.4) (ii) GST fusion protein pull down techniques to confirm putative interactions between the *ASPM* C-terminus and novel interactants. (iii) Protein complex co-immunoprecipitation (Co-IP) to confirm putative associations between the *ASPM* C-terminus and interactants. (iv) siRNA mediated *ASPM* gene knockdown to investigate effects upon interactant localisation and function. (v) Immunofluorescence (IF) microscopy for interactant localisation studies and the identification of mitotic alterations (Chapters 2.2 IF). Antibodies for each gel are shown in Appendices 1 and 2.

5.5 Results

5.5.1 Characterization of the expression of *ASPM* and *ASPM*-interacting proteins in a panel of human cell lines, using western blotting

Protein levels and isoform expression for *ASPM*, *SRGAP2*, *GCC2* and *MACF1* were measured in lysates from three human cell lines (U2OS, HeLa and SHSY-5Y

cells) to determine the best cell model in which to investigate ASPM C-terminal interactions. All WB experiments were repeated at least three times to confirm expression levels. Protein levels were normalised against β -actin protein levels in each cell lysate using Fiji/ImageJ software.

5.5.1.1 Expression of ASPM in a panel of cell lines.

ASPM^{WT} is a 410kDa protein and WB of proteins of this size is technically demanding. ASPM WB was performed using the ASPM N-terminal 217-2 Ab (Appendix 1). Initial experiments showed multiple ASPM bands, ranging in size from 410kDa (corresponding to the predicted MW of wild type ASPM) to under 200kDa, in the lanes from all of the cell lysates (Figure 5.5A) The number of bands exceeded the reported number of isoforms and band sizes did not all correspond to the isoform sizes of 220kDa, 165kDa and 125kDa (Kouprina et al., 2005). Therefore it was decided that some bands may be degradation products and the WB protocol was optimised. The effects of long term freezing of lysates (-80°C) on the ASPM protein levels were also investigated using U2OS early passage cells (Passage 18) and after a number of further passages, using freshly created lysates (Passage 31). ASPM protein levels were not significantly different in U2OS new passage (Passage 18) compared to U2OS old passage (Passage 31) (Figure 5.5B).

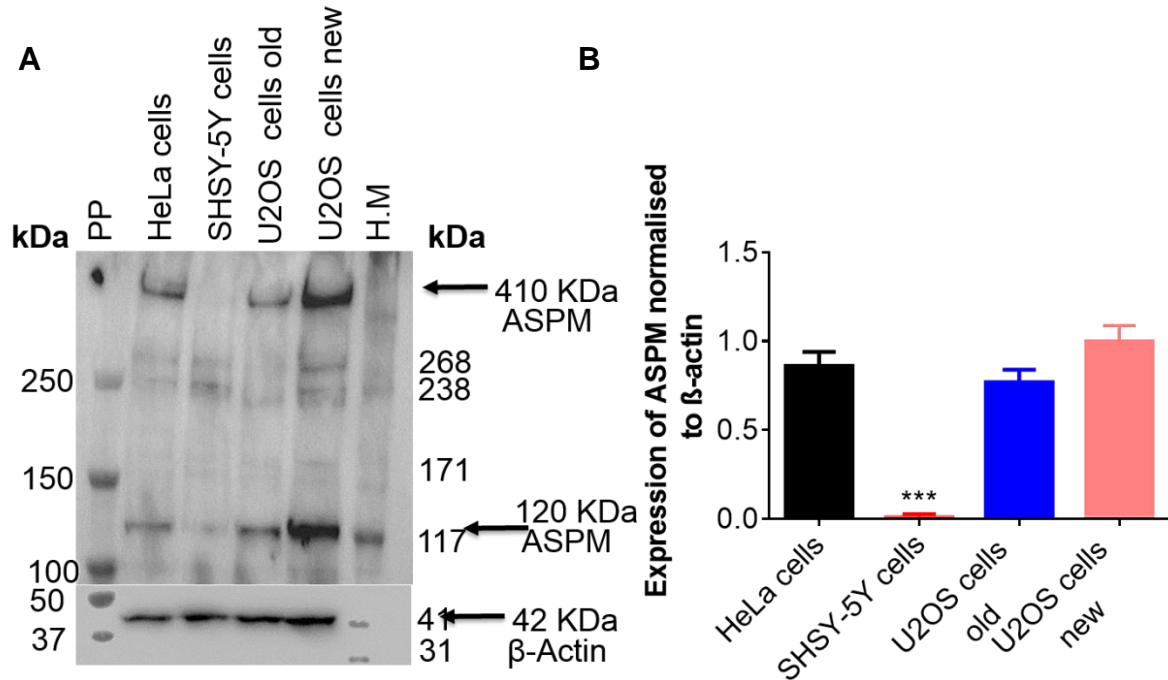


Figure 5.5: Expression of ASPM in a panel of human cell lines by western blot. A. Immunoblotting of cell lysates of HeLa cells, SHSY-5Y cells, U2OS cells (Old passage) and U2OS cells (New passage) with rabbit anti-ASPM 217-2 and mouse anti-β-actin antibodies. ASPM expression appeared in multiple bands. Protein marker ladders were Precision Protein (PP) and HiMark H.M. **B.** The histogram illustrates the level of 410KDa ASPM protein in a panel of cell lines normalised to β-actin in the same lane. ASPM protein levels were significantly lower in SHSY-5Y cells ($p < 0.0001$) than in HeLa and U2OS cells.

To optimise to ASPM WB, the standard WB transfer protocol (Section 2.4.3) was updated by increasing the time of transfer from 1.30 to 4 hours, performing the transfer at 4°C and increasing the time of each post transfer wash from 10min to 15min. Using this method, the majority of the spurious bands were removed, indicating that these were nonspecific bands (Figure 5.6A). Bands of 410kDa and 120kDa persisted and this indicated the ASPM 217-2 antibody identified two

isoforms of the ASPM protein in the U2OS cell line and a single approximately 410kDa band in the HeLa cells. Comparing ASPM protein levels to the levels of the β -actin protein band from the same lysate, it was observed that the ASPM protein level was significantly lower in the SHSY-5Y cell lysate, compared to the HeLa and U2OS cell lysates (Figure 5.6B).

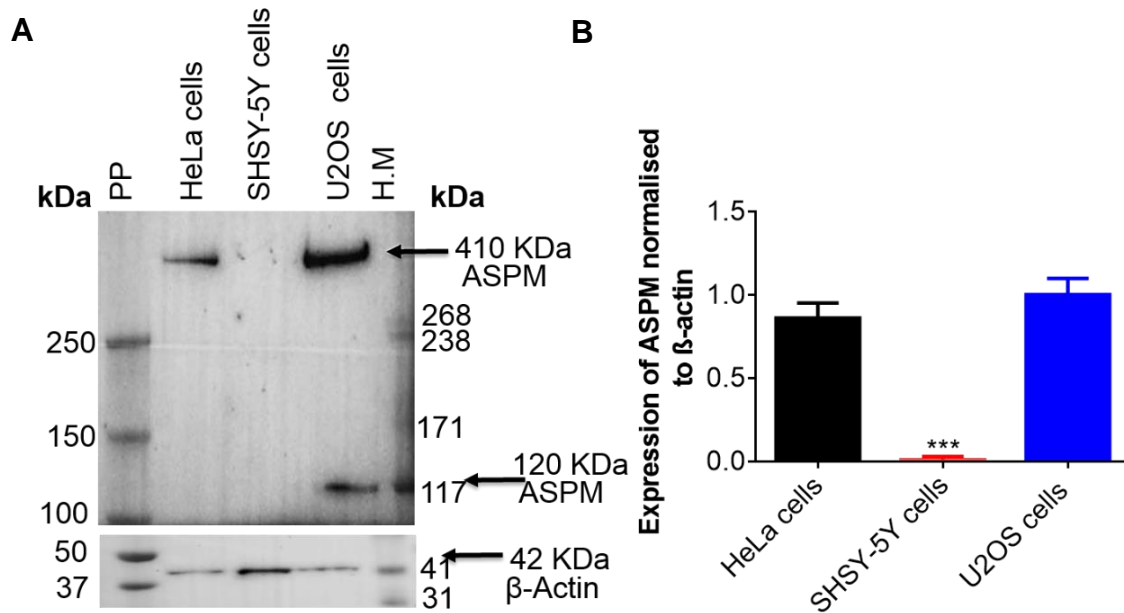


Figure 5.6: Protein levels of ASPM in a panel of human cell lines by optimised ASPM western blot. **A.** Immunoblotting of cell lysates from HeLa cells, SHSY-5Y cells and U2OS cells with rabbit anti-ASPM 217-2 and mouse anti- β -actin antibodies. ASPM nonspecific bands were removed. Protein marker ladders were Precision Protein (PP) and HiMark (H.M.). **B.** The histogram illustrates the expression of the 410kDa ASPM isoform level in a panel of cell lines normalised to β -actin, ASPM levels were similar in U2OS and HeLa, but significantly lower in SHSY-5Y cells ($p < 0.0001$).

5.5.1.2 Expression of SRGAP2 in a panel of cell lines.

The SRGAP2 WB showed a single band of the expected size of 123kDa was observed in HeLa and SHSY-5Y cell lines, but that an additional lower band of size ~121kDa, was observed in the U2OS and SHSY-5Y cells. (Figure 5.7A). The SRGAP2 levels observed were highest in the U2OS cell line lysate (Figure 5.7B).

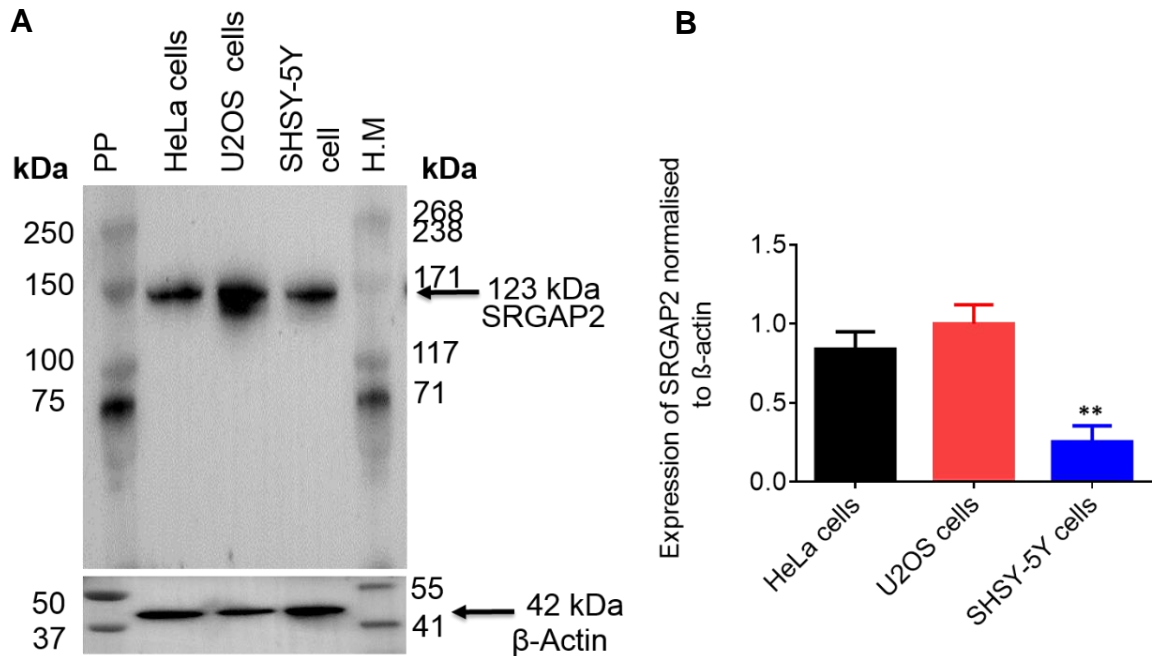


Figure 5.7: Protein levels of SRGAP2 in a panel of human cell lines determined by western blotting. **A.** Immunoblotting of cell lysates of HeLa cells, U2OS cells and SHSY-5Y cells using rabbit anti-SRGAP2 and mouse anti- β -actin antibodies. SRGAP2 was detected as a single band at 123kDa in every cell lysate. Protein marker ladders were Precision Protein (PP) and HiMark H.M. **B.** The histogram illustrates SRGAP2 (123kDa isoform protein) levels in a panel of cell lines normalised to β -actin. SRGAP2 level was significantly lower in SHSY-5Y cells ($p=0.0006$) than in U2OS cells and HeLa cells. $N=3$.

5.5.1.3 GCC2 protein level in lysates from a panel of three cell lines.

The GCC2 WB identified a single band in HeLa and U2OS cell lysates at the expected size of 185KDa. A similar band was not observed in the SHSY-5Y cell lysate (Figure 5.8A). The β -actin control band was observed for all lysates, suggesting that GCC2 was either not expressed in SHSY-5Y cells or that protein levels in these cells was below the current level of detection by WB. The level of GCC2 protein was significantly higher in HeLa cells than in U2OS and SHSY-5Y cells (Figure 5.8B).

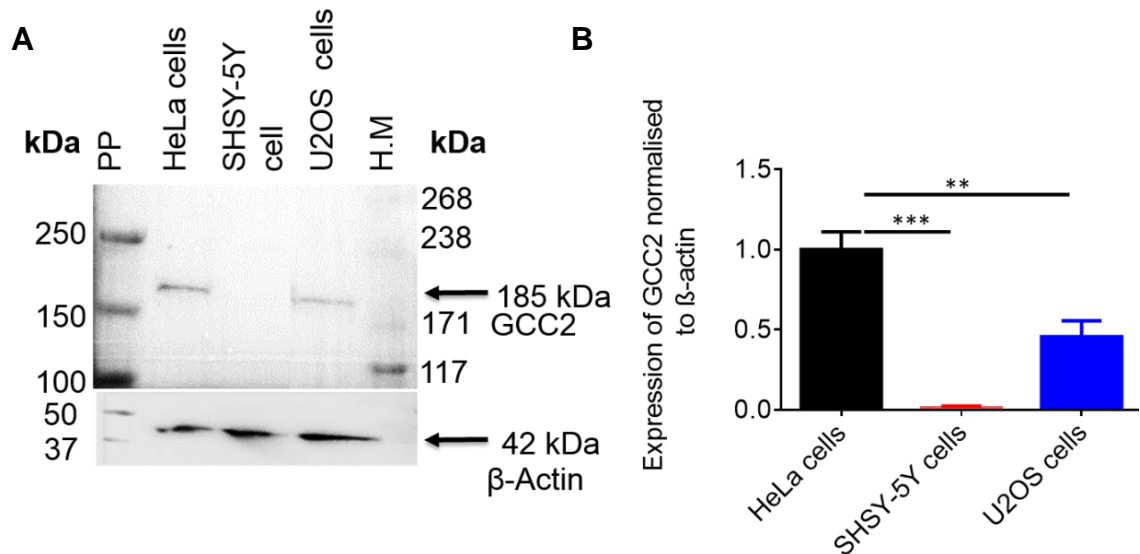


Figure 5.8 Protein levels of GCC2 in a panel of human cell lines by Western blot. A. Immunoblotting of cell lysates of HeLa cells, SHSY-5Y cells and U2OS cells with goat anti-GCC2 and mouse anti- β -actin antibodies. GCC2 was detected as a single band at 185kDa in HeLa cells and U2OS cells but not in SHSY-5Y cells. Protein marker ladders were Precision Protein (PP) and HiMark (H.M.). **B.** The histogram illustrates GCC2 protein levels in a panel of cell lines normalised to β -actin. GCC2 protein level was significantly higher in HeLa cells than in U2OS ($p= 0.003$) and SHSY-5Y ($p= 0.0001$) cells. $N=3$.

5.5.1.4 Expression of MACF1 in a panel of cell lines.

The predicted size of WT MACF1 protein is 620 KDa, which is much larger than the other predicted ASPM interactants. In addition to the WT MACF1 protein four isoforms have been identified (Bernier *et al.*, 2000; Gong *et al.*, 2001; Lin *et al.*, 2005) of sizes 880kDa, 620kDa, 400kDa and 260kD. To ensure the transfer of these large MACF1 protein isoforms from the gel to the PVDF membrane, the WB transfer protocol was set at a 4 hour transfer time and performed at 4°C. Using this modified protocol, MACF1 protein was successfully detected for each of the three cell lines by WB (Figure 5.9A). The levels of MACF1 (620kDa) protein in U2OS cell lysate was significantly higher than in SHSY-5Y and HeLa cell lysate (Figure 5.9B). The HeLa and U2OS cell lysates showed multiple bands, at approximate sizes of 800kDa, 620kDa 275kDa, 175kDa and 135kDa, indicating the expression of multiple MACF1 isoforms. The SHSY-5Y and HeLa cell lysates only contained the approximate sizes of 800kDa MACF1 protein but not the 620kDa band size.

Looking at the collective data for ASPM, GCC2, SRGAP2 and MACF1 protein levels and isoforms in the three cell lines, U2OS cells were generally of a strong level and expressed multiple isoforms of ASPM, SRGAP2 and MACF1. U2OS cells were determined as the best cells to use to confirm and study the putative ASPM C-terminal protein interactions (Table 5.2).

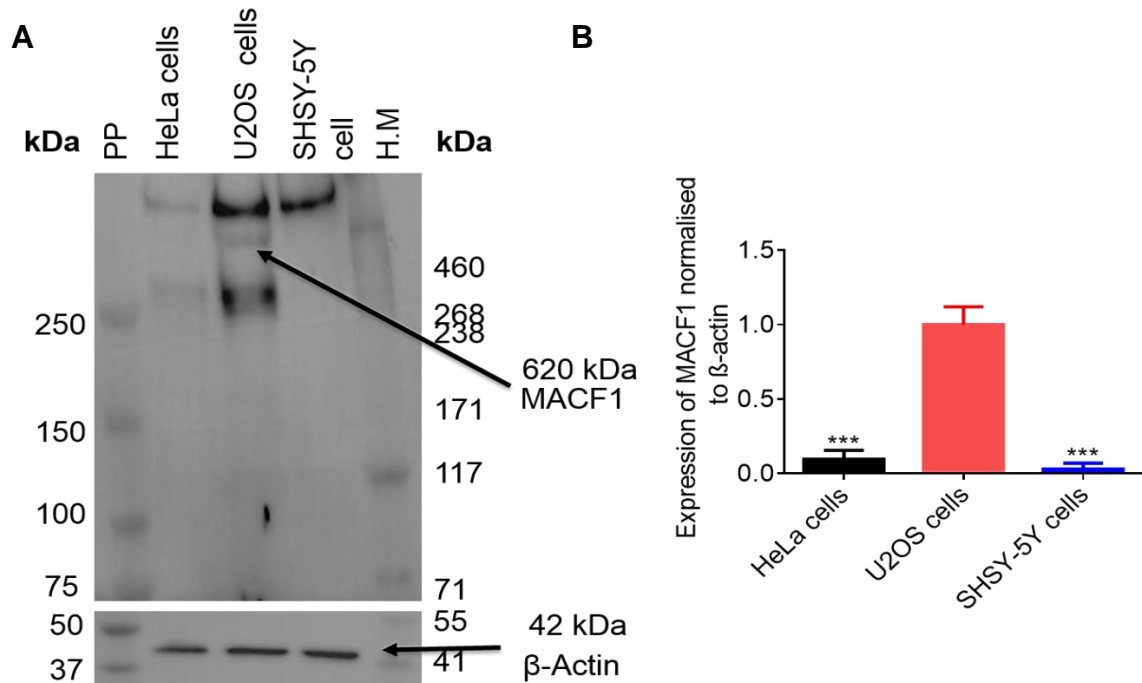


Figure 5.9: Identification by WB of MACF1 protein level in a panel of human cell lines. A. Immunoblotting of cell lysates of HeLa cells, U2OS cells and SHSY-5Y cells with mouse anti-MACF1 and mouse anti- β -actin antibodies. The MACF1 was detected as a multiple bands in HeLa cells and U2OS cells but as a single band of 800kDa size in SHSY-5Y cells. N=3. Protein marker ladders were Precision Protein (PP) and HiMark (H.M.) B. The histogram illustrates MACF1 620kDa isoform protein levels in a panel of cell lines normalised to β -actin. MACF1 protein levels were significantly lower in HeLa ($p=0.0003$) and SHSY-5Y ($p=0.0001$) cells than in U2OS.

Table 5.2. The relative intensity (RI) of protein bands in arbitrary units (AU) after normalization to the density of β -actin (loading control).

Interactants	U2OS	HeLa	SHSY-5Y
ASPM (RI)	(1.0)	(0.8)	(0.01)
SRGAP2 (RI)	(1.0)	(0.9)	(0.8)
GCC2 (RI)	(0.4)	(1.0)	(0.01)
MACF1 (RI)	(1.0)	(0.09)	(0.03)

5.5.2 Determination of ASPM C-terminal interacting protein levels in *MCPH5* patient cell lysates using western blotting.

Cell lysates from wild type fibroblast control cell line (*ASPM*^{WT}) and the two *MCPH5* patient fibroblast cell lines (*ASPM*^{3663delG} and *ASPM*^{9984+1T>G}) were tested for the protein level of each of the putative ASPM interactants. As previously shown the *ASPM*^{WT} and patient cells all express a single ASPM band of 410kDa, but varied in the level of protein.

5.5.2.1 Expression of SRGAP2 in *MCPH5* patient cell lysates.

Using WB, SRGAP2 was successfully detected at 123KDa (Figure 5.10A) with higher concentration in the control fibroblasts than the two patient derived fibroblast cell lines (Figure 5.7B). An additional lower MW band was also identified in the *ASPM*^{WT} and *ASPM*^{3663delG} cell lysates. The extra band was already identified in U2OS and SHSY-5Y cells and could be an isoform or degradation product.

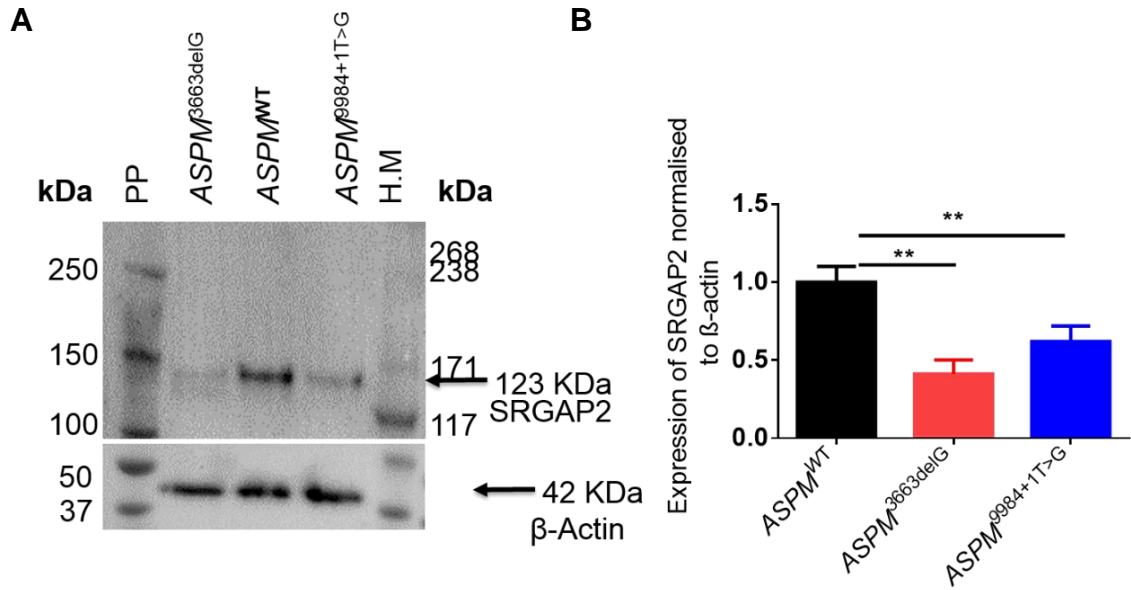


Figure 5.10: Total protein levels of SRGAP2 in *MCPH5* patient cell lines measured by WB are significantly lower in lysates from *MCPH5* patient cell lines than in control cell lines. A. Immunoblotting of cell lysates of TC 363-06 cells (*ASPM*^{3663delG}), HDF Neo (*ASPM*^{WT}) cells and TC 273-05 cells (*ASPM*^{9984+1T>G}) with rabbit anti-SRGAP2 and mouse anti-β-actin antibodies. SRGAP2 was detected as multiple bands in *ASPM*^{WT} cells and *ASPM*^{3663delG} cells but as a single band in *ASPM*^{9984+1T>G} cells. Protein marker ladders were Precision Protein (PP) and HiMark (H.M.). **B.** The histogram illustrates SRGAP2 levels in HDF Neo and patient cell lines normalised to β-actin. SRGAP2 protein level was significantly higher in *ASPM*^{WT} cells than in lysates from *ASPM*^{3663delG} ($p = 0.001$) and *ASPM*^{9984+1T>G} ($p = 0.009$) cells. N=3.

5.5.2.2 Expression of GCC2 in *MCPH5* patient cell lysates.

The expression of GCC2 failed to be detected in control and *MCPH5* patient cell lysates using Western blotting. This could be due to protein levels in these cells being below the level of detection (data not shown).

5.5.2.3 Expression of MACF1 in *MCPH5* patient cell lysates.

MACF1 WB successfully identified MACF1 WT protein at 620kDa in control and patient cell lines (Figure 5.11A). MACF1 levels were significantly higher in the *ASPM*^{WT} cell lysate than in the *ASPM*^{β663delG} and *ASPM*^{9984+1T>G} cell lysates (Figure 5.11B). Multiple additional MACF1 bands at approximate sizes of 880kDa, 275kDa, 175kDa and 135kDa, were detected in the control cell lines and many of the same isoforms were detected in the patient cell lines, The patient cell lines contained less MACF1 protein, therefore some of the bands may correspond in size to the isoforms, but may have been below the level of detection by a WB rather than not expressed.

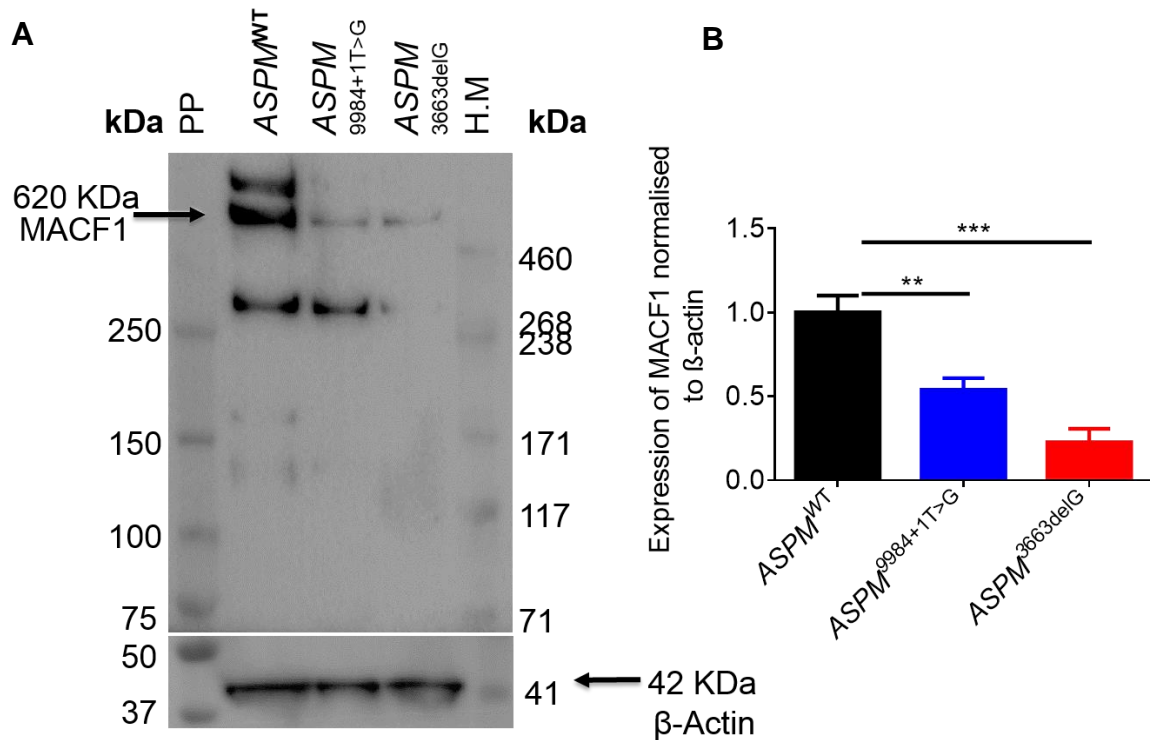


Figure 5.11: Expression of MACF1 in HDF Neo and *MCPH5* patient cell lines detected by western blot. **A.** Immunoblotting of cell lysates from HDF Neo (*ASPM*^{WT}) cells, TC 363-06 cells (*ASPM*^{3663delG}) and TC 273-05 cells (*ASPM*^{9984+1T>G}) with mouse anti-MACF1 and mouse anti-β-actin antibodies. MACF1 protein isoforms were detected as multiple bands in *ASPM*^{wt} cells, *ASPM*^{3663delG} cells and *ASPM*^{9984+1T>G} cells. Protein marker ladders were Precision Protein (PP) and HiMark (H.M.). **B.** The histogram illustrates MACF1 levels for the 620kDa band in HDF Neo and patient cell lines normalised to β-actin. MACF1 levels were significantly higher in *ASPM*^{WT} cells than in *ASPM*^{9984+1T>G} (p= 0.002) and *ASPM*^{3663delG} (p= 0.0004) cells. N=3.

5.5.3 Confirmation of ASPM C-terminal interactions

5.5.3.1 Validation of ASPM C-terminal interactions using a GST-ASPM fusion protein pull-down assay.

In order to confirm the interaction between ASPM and the putative interactants, pull down assays using a set of 2 ASPM C-terminal fragments (D1 and Lg) fused to GST at the *N*-terminal of the ASPM fragment) and a GST-only control were performed. These vectors should express fusion protein sizes of GST- ASPM D1 at 58kDa, GST-ASPM Lg at 49kDa and GST only at 26kDa. The GST-ASPM and control vectors were created by Ruth Binns and were available for expression and use in this.

The ASPM D1 region of the ASPM protein includes 'the ARM-like domain and the C-terminus of ASPM and has been used in previous experiments by our group members to determine ASPM C-terminal function in spindle assembly, mitotic progression and cytokinesis (Higgins *et al.*, 2010). The ASPM-Lg fragment is smaller than the ASPM-D1 region and it encompasses the ARM-like domain and the C-terminal region (Figure 5.12). GST-fusion proteins of these regions had been made by Ruth Binns to investigate other putative ASPM interactions and the resources were available to try to validate the ASPM C-terminal interactions with SRGAP2, GCC2 and MACF1 (Figure 5.12).

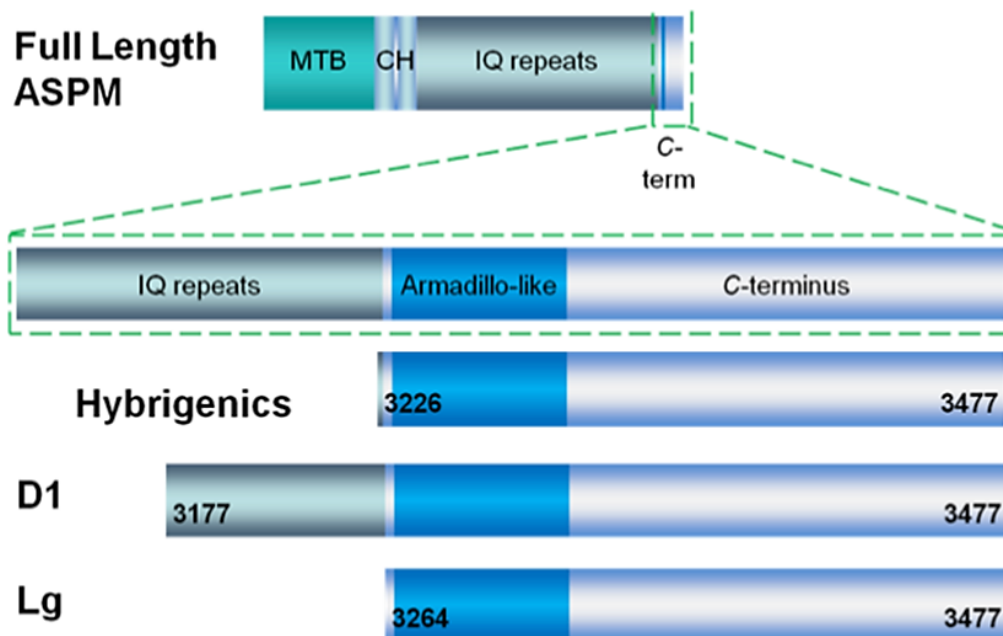


Figure 5.12: ASPM C-terminal fragments for GST pull downs design. A diagram comparing the C-terminal fragment of ASPM fused to GST to the fragments used for the Hybrigenics Y2H screen and the GST-ASPM fusion proteins used in the GST pull down experiments. D1 contained the complete Hybrigenics Y2H C-terminal fragment and Lg contained most of the Y2H fragment. Adapted from an image by Ruth Binns.

5.5.3.1.1 Confirmation of GST-ASPM fusion proteins stability in cell lysates.

Initial experiments used bacterial cell lysates containing the expressed GST-ASPM fusion proteins or the GST protein alone which had resided at -20°C for a number of years and the stability of the fusion proteins in the lysate was unknown. Therefore the ASPM fusion proteins were first tested by WB to check that they had not become degraded. Three individual aliquots of bacterial lysates expressing either the C-terminal ASPM D1-GST fusion protein (labelled D1 on gels), C-

terminal GST-ASPM Lg fusion protein (Lg) or GST only (control) were western blotted using a GST antibody to determine the protein level and the stability of the protein in the samples. For each aliquot a band corresponding approximately to the correct size for each fusion protein was observed. An additional band was observed in the GST lane on the GST WB at >50kDa. GST has a molecular weight of 26kDa and the larger band could represent dimerization of GST protein (Figure 5.13). Additional bands visible in the D1, Lg and GST lanes probably represented protein aggregates from the bacterial lysates that we couldn't avoid in more than 3 repeat gels. A WB for GST showed the GST-fusion proteins were not degraded and were hence used for initial pull down assays.

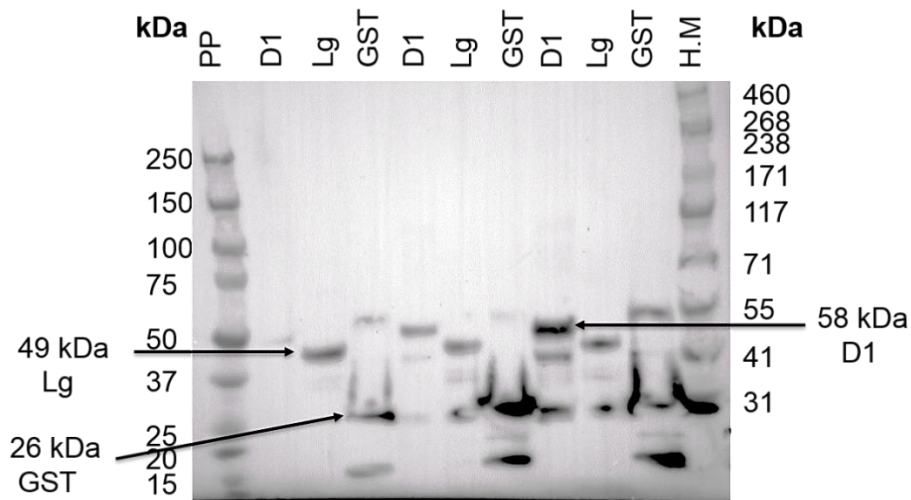


Figure 5.13: GST Western blot of GST-ASPM C-terminal fragment fusion protein expression. Three aliquots of lysates containing the three fusion proteins GST-ASPM-D1-GST-ASPM-Lg and GST were blotted with mouse anti-GST to assess fusion protein stability and protein level. Fusion proteins were intact and WB identified bands correspond to the fusion proteins estimated size. Protein marker ladders were Precision Protein (PP) and HiMark (H.M.).

5.5.3.1.2 Investigating ASPM C-terminal-GST pull-downs of SRGAP2, GCC2 and MACF1.

To confirm the existence of an interaction between the ASPM-C terminus and SRGAP2, a GST pull-down assay was performed. GST-only lysate, glutathione beads-only and lysate-only controls were included in the experiment. A 25 μ L of U2OS lysate was loaded into the input lane to indicate the expected size of the interactant. In order to enrich for the number of mitotic cells, monastrol, a cell-permeable inhibitor of the kinesin Eg5 (Duan *et al.*, 2015) was used to synchronise cells in mitosis (prometaphase) (Section 2.1.8). The block was lifted and cells allowed to progress towards cytokinesis for 30 minutes before lysate production (Figure 5.14A). To ensure a non-mitotic interaction would not be missed, experiments were also performed with non-synchronised cell lysates (Figure 5.14B).

A band corresponding to the size of SRGAP2 was faintly visible in the monastrol synchronized lysate upon WB with the SRGAP2 antibody, with a corresponding band visible in the ASPM D1-GST pull down lane (Figure 5.14A). Other bands were visible in this lane, both larger and smaller than the expected band size and in the other GST containing lanes and these could therefore represent GST-protein aggregates from the bacterial lysates. Weak bands corresponding to the size of SRGAP2 were visible in the pulldowns from unsynchronized cell lysate for both the D1 and Lg fragments fused to GST but not in any of the control lanes (Figure 5.14B). Further optimization was performed including increasing the three washes of the membrane in PBS to 15min in an attempt to remove the background

nonspecific bands. However, this did not result in cleaner results for SRGAP2. In addition to this, similar GST pull-down assay for GCC2 and MACF1 were carried out. Unfortunately this method did not validate the interactions between ASPM C-terminus and GCC2 or MACF1. It was decided to utilize the co-immunoprecipitation (co-IP) technique as an alternative method to confirm protein interactions for GCC2 and MACF1.

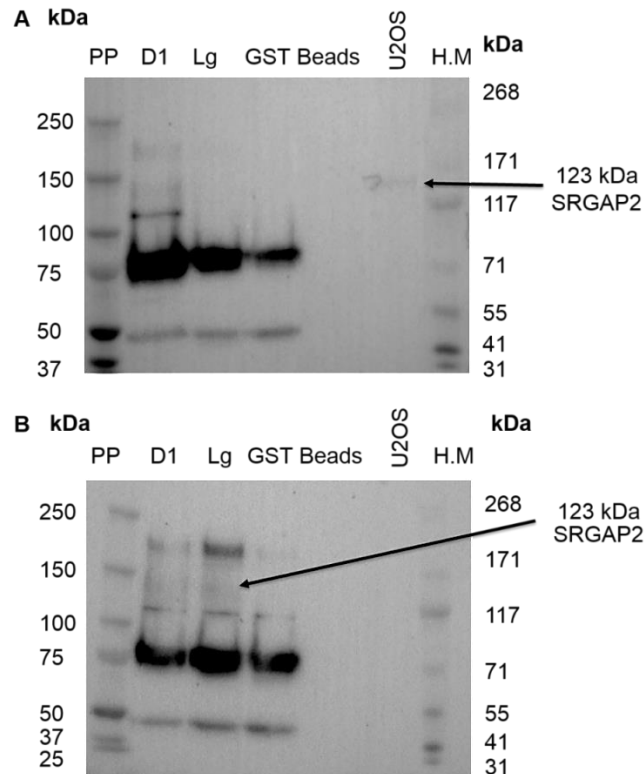


Figure 5.14: GST-ASPM pull down for SRGAP2 in synchronized (A) and unsynchronized (B) U2OS cell lysate. A. Immunoblotting of cell lysates of U2OS cell lysate with rabbit anti-SRGAP2 antibodies. Faint bands were observed in the D1 and Lg lanes, but not in the control lanes, corresponding to the MW of SRGAP2 (123KDa). B. stronger bands were observed in the D1 and Lg lanes, corresponding to the MW of SRGAP2, but not in the control lanes. Protein marker ladders were Precision Protein (PP) and HiMark (H.M.).

5.5.3.2 Investigation of *ASPM* C-terminal interactions using Co-immunoprecipitation (co-IP) assay.

An alternative method to show an association between proteins is co-immunoprecipitation (co-IP).

5.5.3.2.1. Investigating the *ASPM-GCC2* and *SRGAP2* interactions by co-IP.

Two negative controls were included for the co-IP experiments. These were a beads only input and PI (Preimmune serum control) and a nonspecific antibody which in this case was the mitochondrial protein MICU1. A U2OS lysate only sample was included to detect the interactant protein itself and the final sample was the co-IP sample. The SRGAP2 antibody used for WB was raised in rabbit as were the ASPM antibodies, therefore we were unable to use these antibodies together for the ASPM-SRGAP2 co-IP. A second SRGAP2 antibody raised in goat was purchased, however this antibody did not work for WB and failed to co-IP ASPM in U2OS lysates (data not shown). Co-IP of ASPM and subsequently blotting for GCC2 failed to show evidence of an ASPM-GCC2 interaction in either synchronized or unsynchronized using the rabbit anti-ASPM 217-2 antibody.

5.5.3.2.2 Investigating the *ASPM-MACF1* interaction by co-IP.

The interaction between ASPM and WT MACF1 was successfully detected and validated by coimmunoprecipitation (co-IP) assay in the U2OS cell lysates (Figure 5.15 A). As expected a number of bands including the 620kDa WT MACF1 band

were detected in the input lysate. A 620kDa band only was observed in the ASPM co-IP lane only. Corresponding bands were not observed in the negative control lanes. To test whether *ASPM* mutation impacted on the association between ASPM and MACF1, an IP using an ASPM-specific antibody was performed in cell lysates from the control *ASPM*^{WT} cells (HDFneo) and the two patient cell lines followed by WB for MACF1 (Figure 5.15 B). U2OS cell lysate was used as the input, to show the sizes of the MACF1 isoforms. A weak 880kDa band and a stronger 620kDa band for WT MACF1 were identified in the HDFneo *ASPM*^{WT} co-IP lane. However, MACF1 was not detected in the ASPM co-IPs from the *ASPM*^{8663delG} and *ASPM*^{9984+1T>G} cell lysates. Interactions between the smaller MACF1 isoforms and ASPM were not detected.

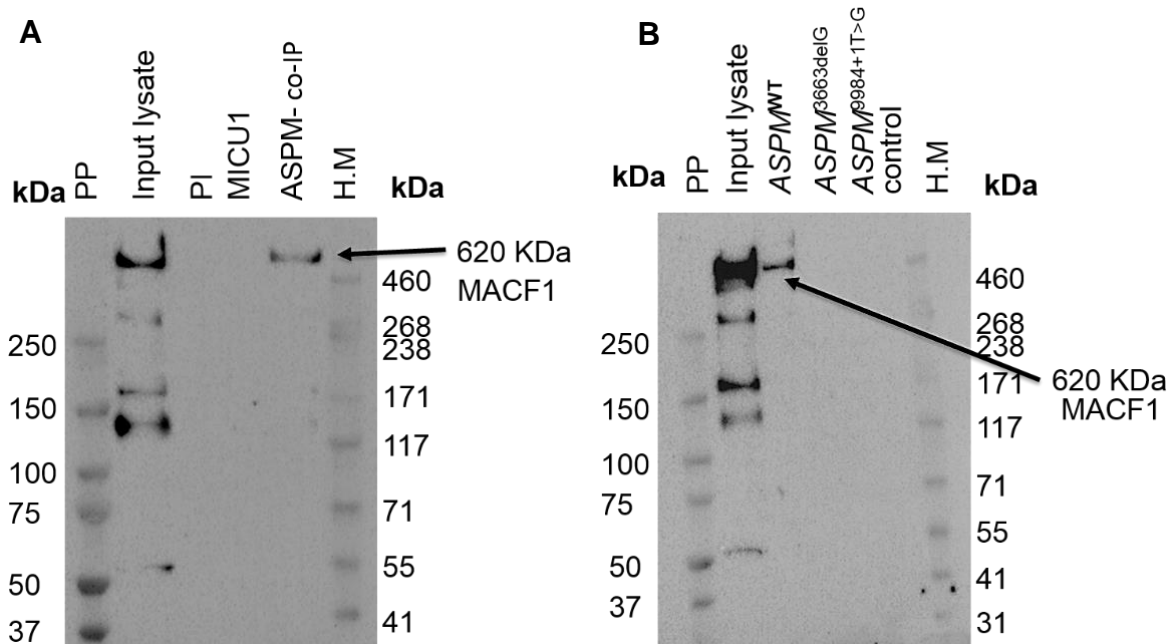


Figure 5.15: Co-IP of ASPM and MACF1 in U2OS cells and HDF Neo cell and patient cell line lysates. A. A co-IP of ASPM detected a single MACF1 band at 620kDa, but no band was observed in the negative control cell lysate lanes, indicating ASPM is associated with MACF1^{wt} in U2OS cells. **B.** A co-IP of ASPM and MACF1 detected interactions between ASPM and MACF1 for both the 620kDa and 880kDa isoforms in the ASPM^{WT} cell lysate lane, but no bands were observed in the patient cell lysate lanes. Protein marker ladders were Precision Protein (PP) and HiMark (H.M.).

5.5.4. Investigating the ASPM-MACF1 interaction after ASPM siRNA-mediated knockdown.

To further validate the interaction between ASPM and MACF1 by co-IP an ASPM siRNA knockdown experiment was performed (Chapter 2.1.10). Preimmune serum co-IPs were also performed using a negative control and ASPM-specific 216-1 N-

terminal rabbit antibody followed by WB analysis using the mouse MACF1-specific antibody. The MACF1 blot showed a band corresponding in size to the 620KDa MACF1^{wt} protein in the input U2OS cell lysate lane, the RNAiMAX control lane and the Non-Targeting siRNA lane. However, a band was not observed in the IP lane and only a very weak band observed in the *ASPM* siRNA lane (Figure 5.16). This indicates that the association seen between ASPM and MACF1 in ASPM 216-1 antibody co-IPs is specific since it requires the presence of ASPM in cell lysates.

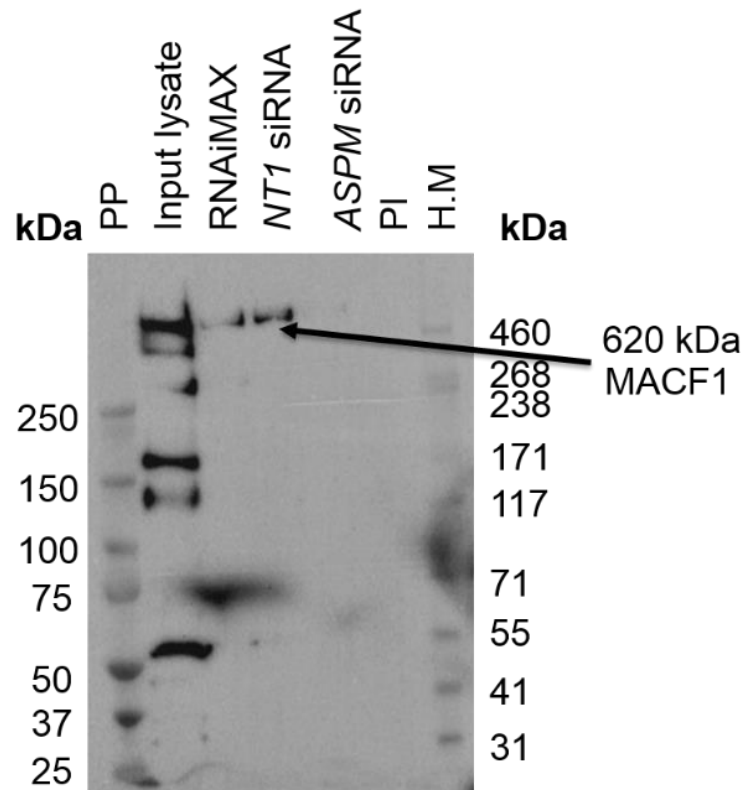


Figure 5.16: Co-IP of ASPM and MACF1 in *ASPM* siRNA mediated KD U2OS cell lysates. The successful co-IP of ASPM and the 620kDa WT MACF1 was identified in untreated U2OS cells and U2OS cells treated with RNAiMAX only and *NT1* siRNA. No interaction was detected between *ASPM* and MACF1 in the *ASPM* siRNA and PI cell lysate lanes. Protein marker ladders were Precision Protein (PP) and HiMark (H.M.).

5.5.5. Protein interactant distribution in U2OS cells visualised by IF

5.5.5.1 SRGAP2 and GCC2 distribution in U2OS cells visualised by IF.

The expected distribution of SRGAP2 is to the plasma membrane, cytoplasm and cytoskeleton (Guo et al., 2010), whilst GCC2 is reported to be distributed to the Golgi apparatus and cytoskeleton/plasma membrane (Yoshino *et al.*, 2003; Lin *et al.*, 2011). Optimisation of the staining for each protein was performed in both methanol and PFA fixed cells. However, unfortunately only strong nonspecific cytoplasmic staining was observed for both proteins using both fixations (Data not shown). For this reason and given time constraints it was decided not take SRGAP2 and GCC2 forward for further analysis but to concentrate on investigating the ASPM-MACF1 interaction.

5.5.5.2 MACF1 distribution in U2OS cells visualised by IF.

U2OS cells were fixed and permeabilised with methanol or PFA/Triton-X100 and stained using a mouse anti-MACF1 antibody (Appendices 1 and 2) (used at a concentration of 1/1000), DAPI (1/1500), and either α -tubulin (1/1000) in the methanol fixed cells or phalloidin (to detect filamentous actin) for PFA/Triton-X100 fixed cells. The mitotic distribution of MACF1 has not previously been reported. In the PFA fixed cells the MACF1 staining was non-specific. However, in the methanol fixed cells the MACF1 staining was clearly defined (Figure 5.17). In interphase cells, MACF1 was decorating microtubules as small dots but was not localized to the nucleus. In metaphase, MACF1 was localised to the spindle poles

and was associated with the ends of the microtubules. The mitotic localisation of MACF1 has not been previously published. Like ASPM, MACF1 spindle pole staining appeared to be pericentrosomal (Figure 5.18). This mitotic MACF1 localisation resembles the ASPM mitotic localization. In cytokinesis MACF1 relocated to the Flemming body and the central spindle. This localisation encompasses (midbody), but also exceeds (central spindle) the region of ASPM localisation in U2OS cells (Figure 4.3).

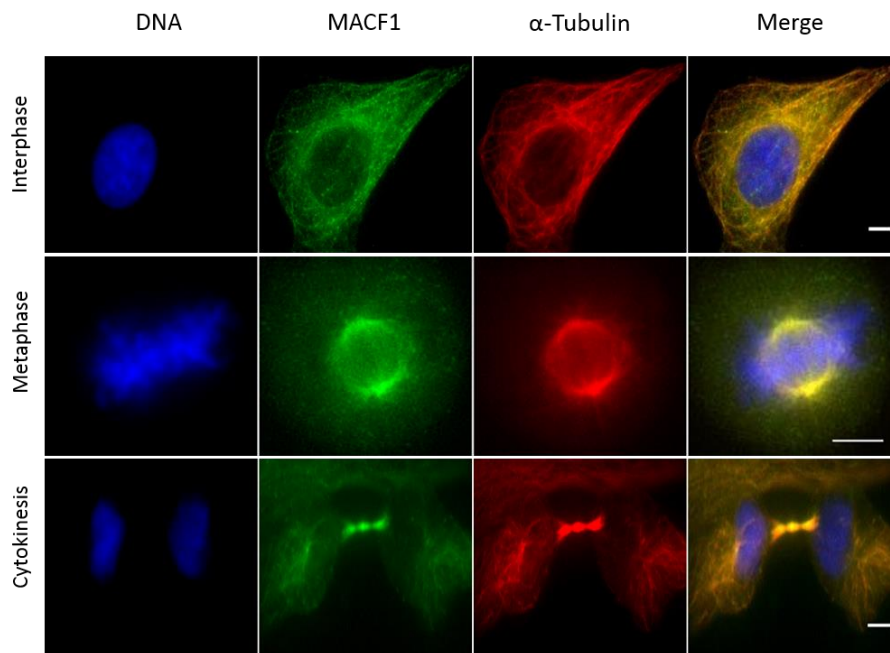


Figure 5.17: Mitotic localisation of MACF1 in untreated U2OS cells. Panel shows MACF1 localization in U2OS cells in interphase (Scale bar = 5 μm), metaphase (Scale bar = 10 μm) and cytokinesis (Scale bar = 5 μm). In interphase, MACF1 distribution showed co-localisation with microtubules. MACF1 was localized to the spindle poles and minus ends of the MT in metaphase cells and to the midbody and central spindle during late elophase/cytokinesis. U2OS cells were immunostained with anti-MACF1 (green), anti- α -tubulin to identify the MT (red) and with DAPI (blue) to recognise DNA.

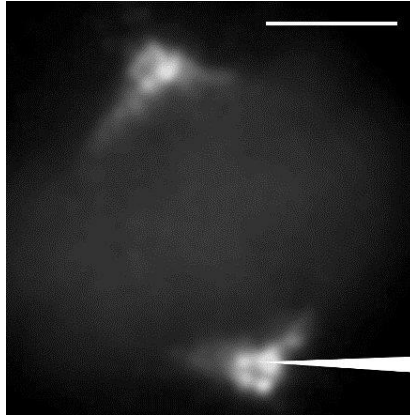


Figure 5.18: MACF1 localises to the pericentrosomal matrix of the metaphase spindle pole. Digitally magnified image of metaphase MACF1 localisation showing staining around the spindle poles (white arrow) corresponding to the pericentrosomal matrix around the centrosome and to the minus ends of the spindle MTs. MACF1 antibody staining is shown in white. (Scale bar = 5 μ m).

5.5.7 Analysis of MACF1 distribution in *ASPM* siRNA mediated KD in U2OS cells.

The effects of *ASPM* siRNA-mediated KD on MACF1 distribution and was investigated using immunofluorescence microscopy. U2OS cells were transfected with RNAiMAX, *NT1* siRNA or *ASPM* siRNA and fixed in methanol. Cells were immunostained using a mouse anti-MACF1 antibody, DAPI to stain DNA and rat anti- α -tubulin to identify microtubules. In interphase, RNAiMAX and *NT1* siRNA treated U2OS cells showed MACF1 was distributed as dots along a well-organized, defined MT network (Figure 5.19). However, the normal distribution of both MACF1 and MTs (Figure 5.19) were disrupted in *ASPM* siRNA-transfected U2OS cells.

MACF1 was dissociated from the MT and redistributed to the nuclear periphery (Figure 5.19).

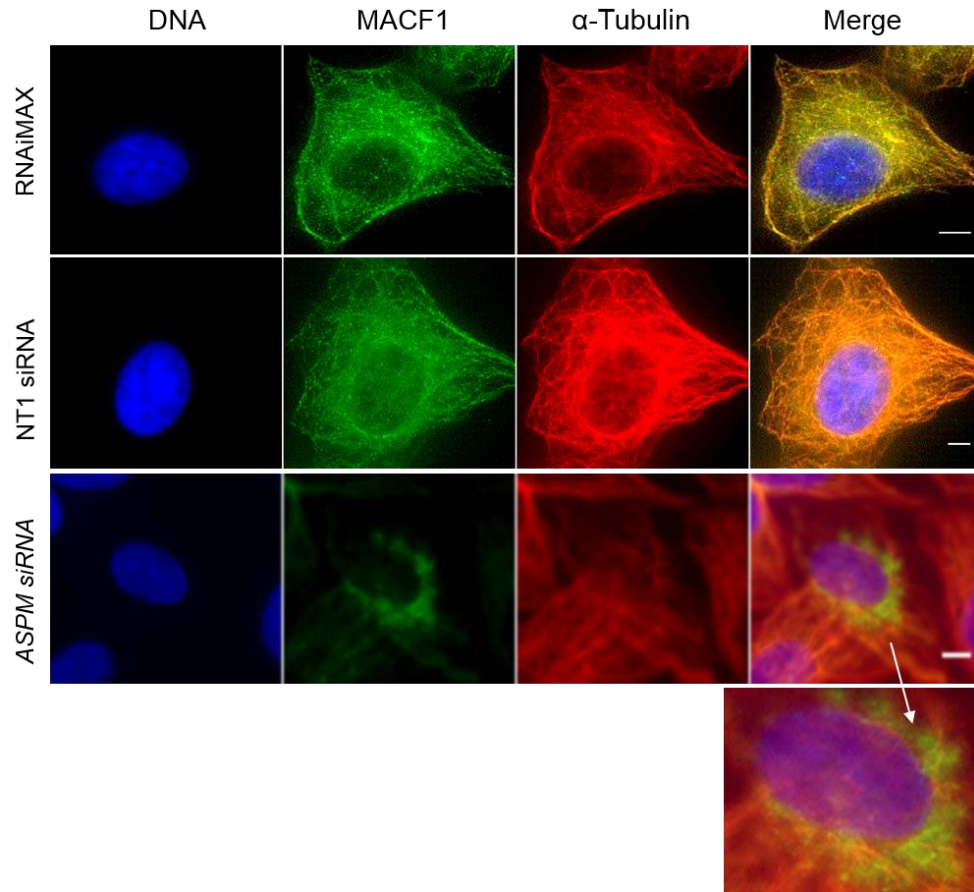


Figure 5.19: MACF is decreased and redistributed in *ASPM* siRNA treated interphase U2OS cells. U2OS cells were immunostained with mouse anti-MACF1 (green) to identify MACF1, rat anti- α -tubulin (red) to identify MTs and with DAPI (blue) to recognise DNA. MACF1 accumulates at the periphery of the nucleus in *ASPM* siRNA treated U2OS cells during interphase. Scale bar = 5 μ m

In metaphase, RNAiMAX and *NT1* siRNA treated U2OS cells (Figure 5.20) showed MACF1 was localized to the spindle poles and associated with the MT of the mitotic spindles. In *ASPM* siRNA treated U2OS cells, the spindle was less

developed and, in line with WB data, there was less MACF1 associated with the MT. α -tubulin and MACF1 and immunofluorescence were absent from the mitotic spindle pole, however a bipolar spindle was still created (Figure 5.20).

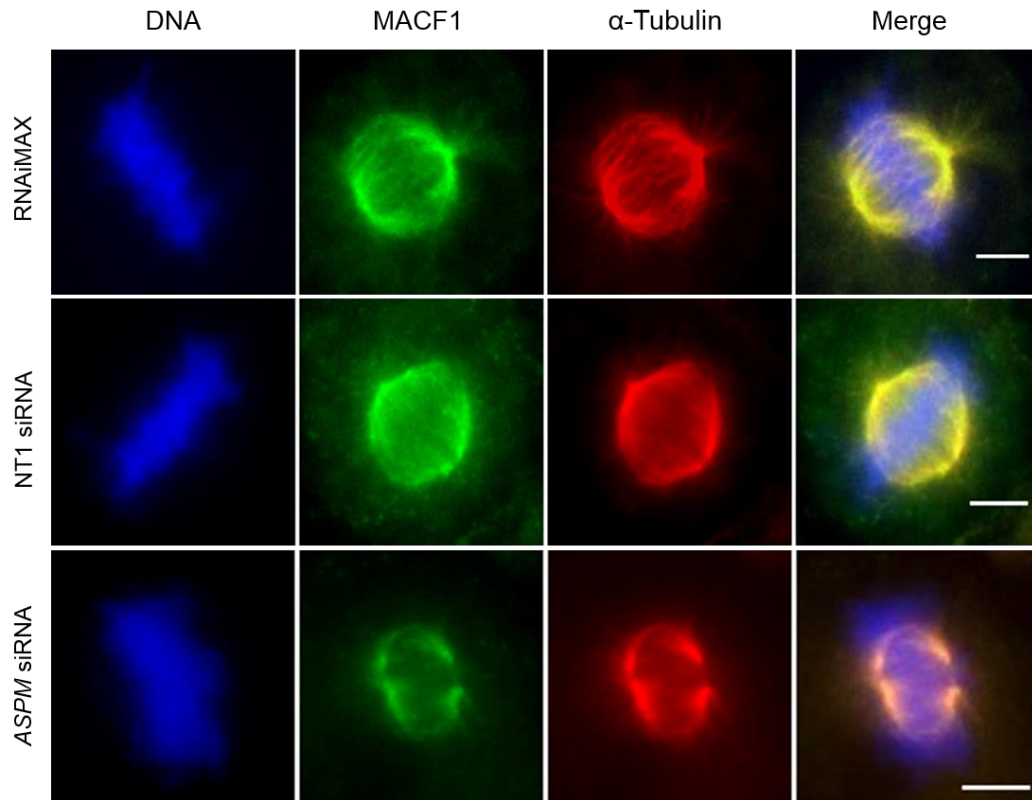


Figure 5.20 MACF1 is associated with the MTs but is reduced in *ASPM* siRNA U2OS cells. U2OS cells were immunostained with mouse anti-MACF1 (green) to identify MACF1, rat anti- α -tubulin (red) to identify MTs and with DAPI (blue) to recognise DNA. In *ASPM* siRNA treated U2OS cells, MACF1 is associated with the α -tubulin staining, but the amount of MACF1 is reduced. Scale bar = 10 μ m

In agreement with MACF1 localisation in untreated U2OS cells MACF1 was associated with the MT immunostaining during late telophase/cytokinesis in RNAiMAX and *NT1* siRNA treated U2OS cells (Figure 5.21). In *ASPM* siRNA

treated U2OS cells, the MT bundle at the central spindle was not visible. MACF1 remained associated with the central spindle (cytoplasmic bridges) between the dividing cells in late telophase/cytokinesis, but the level of MACF1 in the ASPM siRNA cells compared to the level in untreated or NT1 siRNA treated cells was reduced (Figure 5.21).

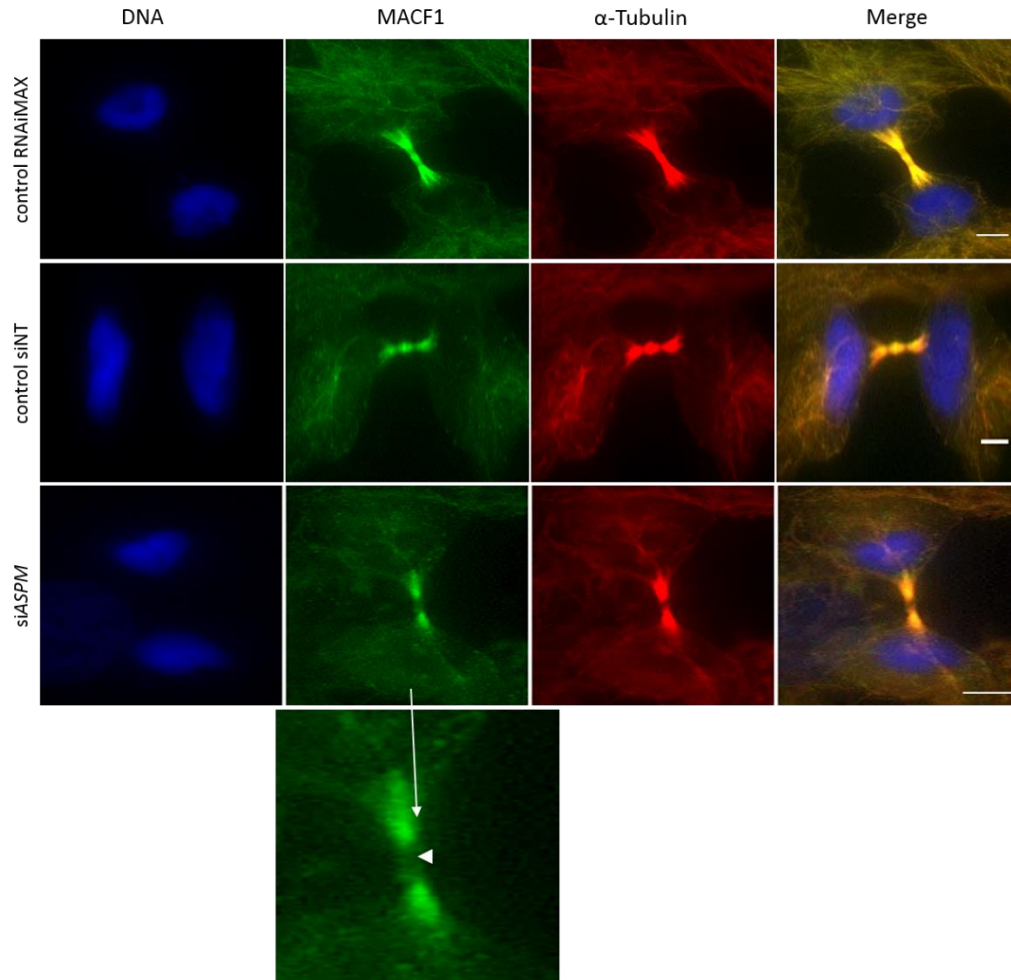


Figure 5.21: MACF1 and α -tubulin were absent from the Flemming body but remained in the central spindle of *ASPM* siRNA treated U2OS cells during cytokinesis. U2OS cells were immunostained with mouse anti-MACF1 (green), rat anti- α -tubulin (red) to identify MTs and with DAPI (blue) to recognise DNA. MACF1 is associated with MTs Scale bar = 10 μ m.

5.5.8 MACF1 distribution in control and patient fibroblast cells.

To determine the normal intracellular distribution of the MACF1 protein in fibroblasts, *ASPM*^{WT} fibroblasts were fixed and permeabilised with methanol (to preserve MT structure) and immunostained with mouse anti-MACF1 (green), rat anti- α -tubulin (red) and with DAPI (blue) to identify MACF1, MTs and DNA respectively. Methanol fixed cells displayed a clearly defined MACF1 staining pattern. Similar to the U2OS cells, *ASPM*^{WT} fibroblasts MACF1 was associated with MTs but not localised to the nucleus in interphase, localised at the spindle poles and minus ends of the spindle MTs during metaphase and distributed along the central spindle and midbody in late telophase and cytokinesis (Figure 5.22). The intensity of MACF1 approximately corresponds to the MT density. To investigate the effect of *ASPM* mutation on MACF1 distribution *ASPM*^{3663delG} and *ASPM*^{9984+1T>G} cells were fixed in methanol and stained to identify MACF1 (green), MTs (red) and DNA (blue). In comparison to *ASPM*^{WT} fibroblasts in interphase, in interphase *ASPM*^{3663delG} and *ASPM*^{9984+1T>G} fibroblasts the MT network was less clearly defined. A subset of MACF1 was dissociated from the MT and redistributed as localized clusters within the cytoplasm (arrows, Figure 5.22). Throughout the cell MACF1 intensity was reduced compared to the WT fibroblast cells.

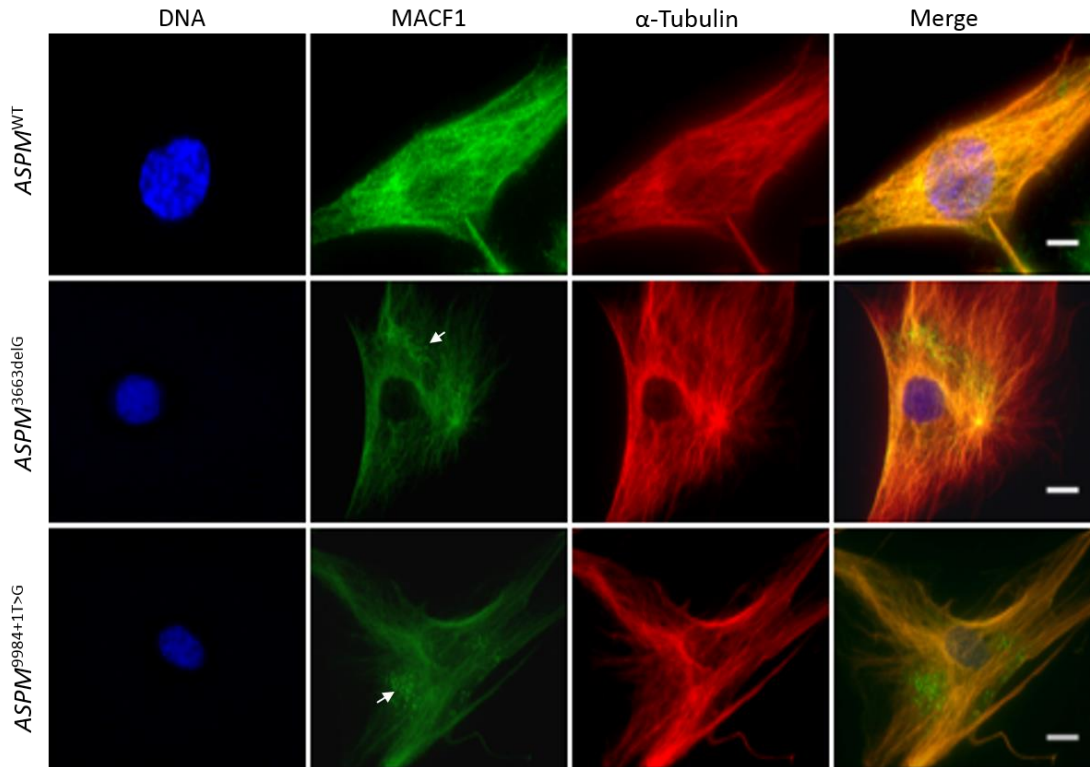


Figure 5.22: Comparison of MACF1 localization and intensity WT and patient fibroblast cells in interphase. *ASPM*^{WT}, *ASPM*^{3663delG} and *ASPM*^{9984+1T>G} cells were fixed in methanol and immunostained with mouse anti-MACF1 (green), rat anti- α -tubulin (red) to identify MTs and with DAPI (blue) to recognise DNA. In *ASPM*^{WT} cells MACF1 is associated with MTs, however in *ASPM*^{3663delG} and *ASPM*^{9984+1T>G} interphase cells MACF1 expression was only partially associated with the MT. A subset of MACF1 was observed as small aggregates in the cytoplasm. Scale bar = 5 μ m

In metaphase, patient fibroblasts exhibited striking alterations in the density and focus of the MT within the spindle. This coincided with a decrease in the intensity of MACF1 distributed along the MT (Figure 5.23). In *ASPM*^{3663delG} metaphase fibroblasts, the decrease in MTs and MT-associated MACF1 was associated with a

slight increase in cytoplasmic MACF1. Interestingly, in the *ASPM*^{9984+1T>G} metaphase fibroblasts the decrease in MT-associated and spindle pole MACF1 localisation was not associated with MACF1 partial redistribution to the cytoplasm. DNA distribution in both of the patient cell lines appeared to be abnormal.

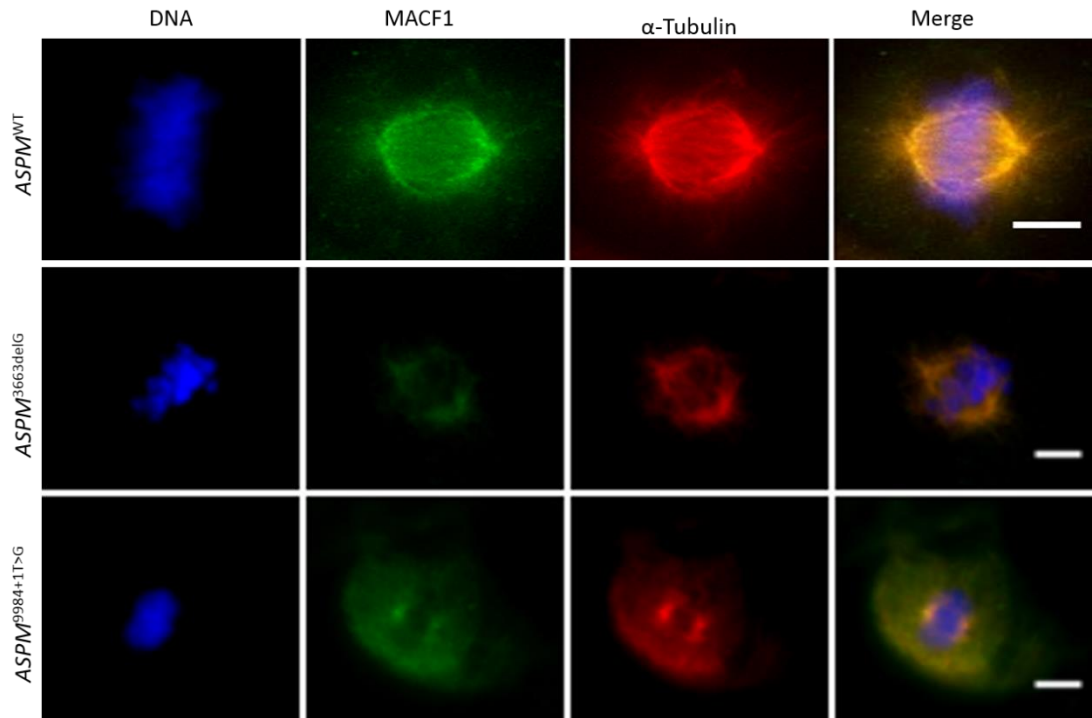


Figure 5.23: MACF1 localization in *ASPM*^{WT}, *ASPM*^{9984+1T>G} and *ASPM*^{3663delG} cells during metaphase is mostly associated with the MT. *ASPM*^{WT}, *ASPM*^{3663delG} and *ASPM*^{9984+1T>G} cells were fixed in methanol and immunostained with anti-MACF1 (green), anti- α -tubulin (red) to identify MTs and with DAPI (blue) to recognise DNA. MACF1 levels were reduced on the mitotic spindle and re-localised to the cytoplasm in patient fibroblasts. Scale bar = 10 μ m

During late telophase and cytokinesis MACF1 was localized to the midbody and associated with MTs in *ASPM*^{WT} cells. However, in *ASPM*^{3663delG} and

ASPM^{9984+1T>G} cells, MT and MACF1 were not localised to the middle portion of the central spindle (Figure 5.24). MACF1 and α -tubulin immunostaining to the other regions of the central spindle remained. The central spindle was longer in cytokinesis in *ASPM* patient fibroblasts.

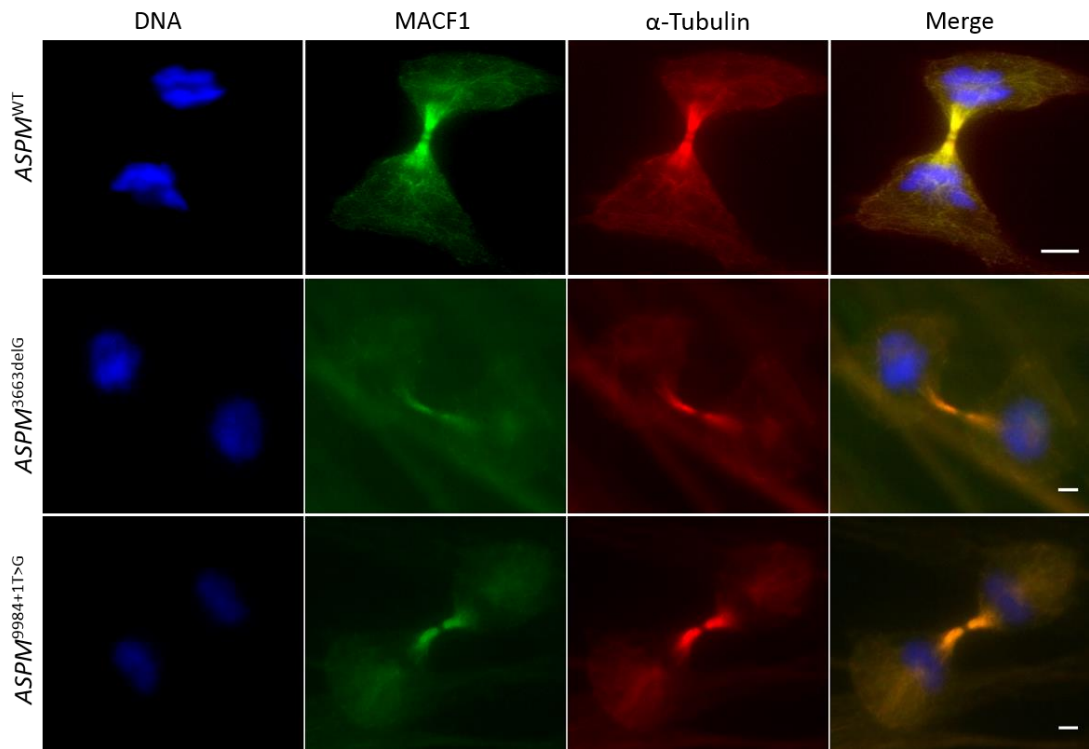


Figure 5.24: MACF1 and α -tubulin were absent from the midbody in *ASPM*^{3663delG} and *ASPM*^{9984+1T>G} cells during late telophase and cytokinesis. *ASPM*^{WT}, *ASPM*^{3663delG} and *ASPM*^{9984+1T>G} cells were fixed in methanol and immunostained with anti-MACF1 (green), anti- α -tubulin (red) to identify MTs and with DAPI (blue) to recognise DNA. MACF1 expression tracked MT but was not associated with the midbody. Scale bar = 5 μ m

5.6 Discussion

The ASPM C-terminus has been previously studied. Dominant negative expression of the C-terminal region resulted in microtubule spindle assembly defects, mitotic arrest and cytokinesis failure, showing that the C-terminus of ASPM has a number of specific functions. Known ASPM C-terminus interactants include: Nuclear Mitotic Apparatus (NuMA) (Seldin *et al.*, 2013), which has a role in nuclear stability and MT organization and tethering at the mitotic spindle pole (Sun *et al.*, 2006; Van Der *et al.*, 2009; Jiang *et al.*, 2017); Citron kinase (CITK), a protein involved in midbody formation in cytokinesis (Madaule, *et al.*, 1998; Di Cunto *et al.*, 2000; Bassi *et al.*, 2013) and Ubiquitin-Protein Ligase E3a (UBE3A) (Singhmar *et al.*, 2011) which is involved in chromosome segregation (Singhmar, *et al.*, 2011). A recent commercial Y2H screen of a brain cDNA library by our group using the ASPM C-terminus identified the 17 putative hits, of which the top three SRGAP2, GCC2 and MACF1 were novel and were taken forwards. The Y2H screen hit with the highest confidence was SRGAP2, although each of the proteins had multiple independent clones. SRGAP2 binds and deforms membranes (Coutinho *et al.*, 2012) and regulates actin dynamics (Guerrier *et al.*, 2009). GCC2 is required for Golgi structure, vesicle transport (Yoshino *et al.*, 2003; Lin *et al.*, 2011) and nucleation of non-centrosomal MTs, the latter occurring through recruitment of CLASP1 and CLASP2 proteins (Efimov, *et al.*, 2007). Finally MACF1 forms bridges between cytoskeletal filaments and the cell periphery (Roper *et al.*, 2002). The mitotic localisations of SRGAP2, GCC2 and MACF1 have not been previously published. The key proteins (CITK, NuMA and UBE3A) which are known to interact with the

C-terminal of ASPM were not identified using Y2H screen, possibly due to the interactants being below the level of detection for a Y2H screen (low representation of the mRNA in the library, prey folding, prey toxicity in yeast).

Western blotting was utilized to determine the levels of ASPM, SRGAP2, GCC2 and MACF1 proteins in HeLa, U2OS and SHSY-5Y cell line lysates. Although SHSY-5Y cells are neuronal in origin and MCPH is a brain disorder and therefore utilising SHSY-5Y cells would have been our first choice for future ASPM studies, it was decided that SHSY-5Y would not be the best cell line to use for ASPM interaction studies due to the low SRGAP2 and MACF1 protein levels and the inability to detect ASPM and GCC2 in SHSY-5Y cell lysates. U2OS cells were chosen in which to perform the interaction studies because all of the interactants and ASPM were expressed to a detectable level in this cell line. Additionally morphologically U2OS cells are good for IF microscopy studies of nuclei and MT because they are flat cells in interphase with a large amount of cytoplasm and they show a clear spindle in mitosis. WB for the extremely large 410kDa ASPM protein required additional protocol optimization resulting in the observation of the full-size ASPM wt protein 410kDa band and a 125kDa band in the U2OS cells, which corresponds to the ASPM isoform 3 protein (Kouprina, *et al.*, 2005). SRGAP2 protein was identified as a single band at 123kDa using an antibody directed against SRGAP2 which is consistent with previously reported data (Sporny *et al.*, 2017). GCC2 was detected at the estimated size of 185kDa, confirming the previously reported data (Brown *et al.*, 2011). In U2OS cells multiple isoforms of MACF1 were observed with bands at approximately 800kDa, 620kDa 400kDa and

250kDa (Leung, et al., 1999), Bernier et al., (Chen, et al., 2006). The isoforms vary in transcript size from 14kb to 18kb (kilobases) (Bernier et al., 1996) with the lower isoform possibly representing the 400kDa band. Recently it has been suggested that 3'splicing of MACF1 may occur (Poliakova et al., 2014) which may represent the lower bands on the MACF1 WB. The WB identified the MACF1b Golgi localising isoform, which is predicted to be of MW 800kDa (Bernier et al., 2000; Gong et al., 2001; Lin et al., 2005). In ASPM siRNA treated U2OS cells a reduction in SRGAP2 and MACF1 was observed adding weight to the suggestion of an association between ASPM:SRGAP2 and ASPM:MACF1. To explain this proportional decrease in expression it is possible, yet unlikely that ASPM is a transcription factor for the interactant or that a reduction of ASPM causes instability in the interacting proteins causing a more rapid turnover. It is more likely that ASPM is in one or more (signalling) pathways with these proteins where ASPM is either upstream in the cascade or acts via a feedback loop to control expression (Manning et al., 2007; Manning et al., 2017).

MCPH5 patient cell lysates containing the *ASPM* mutations *ASPM*^{8663delG} (TC 363-06) and *ASPM*^{9984+1T>G} (TC 273-05) along with normal *ASPM*^{wt} (HDF Neo) cell lysate were similarly utilized to study ASPM, SRGAP2, GCC2 and MACF1 expression. SRGAP2 expression was significantly stronger in *ASPM*^{wt} cell lysate than the *ASPM*^{8663delG} and *ASPM*^{9984+1T>G} cell lysates suggesting that mutations in *ASPM* effect the endogenous levels of SRGAP2 protein and offering supportive evidence of an association between ASPM and SRGAP2. A fibroblast specific expression of a second isoform was identified in the *ASPM*^{wt} and *ASPM*^{8663delG} cell lysate, but

weaker in the *ASPM*^{9984+1T>G} cells suggesting the 9984+1 G>T mutation affects the expression or stability of this isoform. Even though the experiment was repeated more than three times, it is not clear as to whether this band is an isoform of SRGAP2 or is one of the duplicated copies of SRGAP2 pseudogenes in the human genome, some of which are functional (Charrier *et al.*, 2012), or is the result of a post translational modification. A negative result was obtained after WB was performed with *MCPH5* patient cell lysates to characterize GCC2 expression. The examination of GCC2 expression in fibroblast cells and *MCPH5* patient cell lines was not successful. MACF1 expression was significantly stronger in *ASPM*^{wt} cell lysate than the *ASPM*^{8663delG} and *ASPM*^{9984+1T>G} cell lysates, confirming a potential role of ASPM as an interacting partner with MACF1. Moreover, the immunofluorescent staining data confirmed a lower level of endogenous ASPM, SRGAP2 and MACF1 in *MCPH5* patient fibroblasts in comparison to *ASPM*^{WT} fibroblasts strains suggesting that ASPM mutations are an important cause of down regulation expression or increasing instability of SRGAP2 and MACF1.

Using GST pull downs experiments on mitotically synchronised and unsynchronised cells lysates a tentative ASPM C-terminus:SRGAP2 interaction was observed. GST pull down and WB for the 123KDa MW SRGAP2 produced multiple bands in all lanes relating to samples expressed in bacterial lysates. The lower MW bands probably corresponded to non-specific proteins/cell debris, which was caught in the hollow glutathione beads and pulled down as 'non-interacting passengers' in the experiment. Faint bands corresponding in size to SRGAP2 were observed in the ASPM-D1-GST lane and the input lane from monastrol

synchronised cell lysates. In the unsynchronised U2OS cell lysate pull down, a similar size band was faintly seen, in the ASPM-D1 and ASPM-Lg lanes but not in the input lanes. The ASPM-Lg C-terminal sequence does not fully cover the screen bait, however the interaction between SRGAP2 and ASPM may not require the full 3226-3477aa ASPM C-terminal sequence. Although the WB for these GST pull down experiments were not fully convincing, they were suggestive of an interaction or that the interaction was weak or fleeting. The fact that ASPM reduction by siRNA and due to ASPM mutation cause alteration in the amount of SRGAP2 protein observed in these cells adds weight to the suggested association between ASPM and SRGAP2. The observation that the weak interaction between ASPM and SRGAP2 was visible at equal intensities in synchronised and unsynchronised cells U2OS cell lysates, may suggest this interaction is functional in interphase as well as in mitosis. SRGAP2 is involved in membrane deformation (Coutinho *et al.*, 2012) and actin dynamics (Guerrier *et al.*, 2009) and therefore we can suggest that the ASPM:SRGAP2 interaction may be required for cellular ingression, cell shape maintenance and cytokinesis. The GST fusion proteins used here were previously used within our group to confirm an interaction between the ASPM C-terminus and CITK (Personal communication with R Binns), suggesting that they fold correctly, although this maybe a more robust interaction. Further ASPM C-terminal-GST fusion protein must first be expressed and purified in order to continue these studies. Pull down assays were performed to confirm the ASPM interaction with GCC2 and MACF1, however unfortunately this method did not provide successful outcomes. The interactions with ASPM may occur earlier than cytokinesis, so the

correct mitotic timing for interaction studies may not be being addressed with our current synchronised cell lysates. It was therefore decided to use an alternative method to detect any interaction and co-IP was chosen.

Using U2OS cell lysate, lysates from control and *MCPH5* patient fibroblasts, co-IP and WB, it was not possible to validate an interaction of ASPM with SRGAP2 and GCC2 due to problems with antibodies. Only the ASPM-MACF1 interaction was successfully validated by co-IP and WB in U2OS cell lysates and *ASPM*^{mt} fibroblast cells. The ASPM-MACF1 interaction band could not be detected in the *ASPM*^{8663delG} and *ASPM*^{9984+1T>G} cell lysates. At this stage we cannot tell if this is due to the low levels of ASPM protein in both *MCPH5* patient cell lysates, co-immunoprecipitating a level of MACF1 that is below the detection level of the WB and/or in *ASPM*^{9984+1T>G} cells the interaction is abolished due to the 3aa loss at the C-terminal. To further validate the ASPM-MACF1 interaction, siRNA mediated *ASPM* knockdown study using co-IP and WB confirmed specific association between ASPM and MACF1.

To determine the normal intracellular distribution and localisation of human SRGAP2, GCC2 and MACF1 in U2OS and *MCPH5* patient cells, cells were fixed in methanol to preserve MT structure and in paraformaldehyde to maintain actin. Initial IF experiments for SRGAP2 and GCC2 were unsuccessful and either further optimisation is required or new antibodies sourced. Unfortunately none of the available commercial antibodies for these proteins has been validated for IF. Therefore to date we have not been able to confirm whether similar localisation patterns of ASPM and these two putative interactants occur. Correspondingly, it

was decided not to take SRGAP2 and GCC2 forward and focus on MACF1 for more investigation. The interphase localization of MACF1 in methanol fixed U2OS cells and *ASPM*^{WT} cells consisted of MT-associated puncta. This staining pattern has been previously identified (Bernier *et al.*, 2000; Gong *et al.*, 2001; Lin, C. M. *et al.*, 2005) and is not surprising as MACF1 contains a C-terminal MT binding domain, which binds to and stabilises MTs (Leung, 1999). MACF1 also contains an actin-binding domain (Leung, *et al.*, 1999), however we could not show this association as MACF1 staining in PFA fixed cells was not successful with our antibody. During interphase, MACF1 localisation was MT associated. *MACF1* siRNA mediated KD causes disruption of the MTs network (Hu *et al.*, 2015), this is not unexpected as MACF1 contains a C-terminal microtubule binding domain. MACF1 staining was not observed in the nuclei, indicating that MACF1 would not be involved in any possible nuclear *ASPM* function. MACF1 cortical staining was not expected to be observed in methanol fixed cells as the cell membrane is not preserved by this fixation method. From our staining it was not possible to determine if there was centrosome specific staining. In interphase *ASPM* does not show a specific microtubule association, however a proportion of *ASPM* is cytoplasmic, so an interphase interaction between MACF1 and *ASPM* could occur. In both *ASPM* siRNA treated cells and patient fibroblasts containing *ASPM* mutations the concentration and distribution of MACF1 was affected. MACF1 was no longer specifically associated with MT and MTs arrays were disorganised. This suggests that *ASPM* is required both for MT organisation and to maintain an association of MACF1 with the MT. It is hypothesised that the severe MT

phenotypes observed in ASPM KD studies and *MCPH5* patient cells in this thesis are caused both by the decrease in ASPM and the subsequent decrease in MACF1.

The mitotic localisation of MACF1 has not previously been reported. MACF1 distribution in U2OS cells and *ASPM*^{WT} cells was minus end of the spindle MT and surrounding the spindle poles in the pericentrosomal matrix (PCM, the area anchoring MTs at the spindle poles). At the poles, the MT and actin networks overlap (Woolner, *et al.*, 2008) suggesting that MACF1 concentrated at this site could link spindle MTs or the spindle poles to the mitotic actin network. In both *ASPM* siRNA treated cells and patient fibroblasts containing *ASPM* mutations the concentration and distribution of both MT and MACF1 were again affected. MACF1 concentration to the PCM and MT distribution was decreased in *ASPM* siRNA treated cells and a dramatic decrease in MACF1 expression, minimal association to the minus ends of the MT and PCM observed in both of the patient fibroblast cells. In the *ASPM*^{3663delG} cells cytoplasmic staining was observed. Loss of MT and PCM association and an increase in cytoplasmic MACF1 distribution suggest that *ASPM* is required for MACF1 localisation to the PCM. Together *ASPM* and MACF1 could therefore be involved in anchoring the MT to the PCM and actin network (Roper *et al.*, 2002), anchoring and stabilising the mitotic spindle and thus maintaining the mitotic spindle positioning in mitosis. Disruption of MTs by MACF1 has been already described to cause MTs-actin dissociation (Kodama *et al.*, 2003). It is suggested that impaired spindle anchorage and the pulling forces on the MTs (Coles, *et al.*, 2015) could result in and mis-orientation of the mitotic spindle

causing an early switch from symmetric to asymmetric cell division resulting in a small progenitor cell pool and a small brain. Another hypothesis is that the disruption of normal MT dynamics would form unstable opposing MT growth trajectories (Matov *et al.*, 2010), which could also result in a failure to correctly separate chromatin during mitosis which would lead in some cases to the formation of micronuclei, knobby nuclei or metaphase arrest (Hayashi, *et al.*, , 2013) as seen in Chapters 3 and 4. During late telophase and cytokinesis, MACF1 localised to the midbody and to the central spindle, whereas ASPM localisation is to the midbody alone (Chapters 3 and 4). MACF1 and ASPM localisations in cytokinesis therefore overlapped but were not identical, but were consistent with the hypothesis that ASPM and MACF1 could interact to orchestrate during cytokinesis however the underlying mechanism has not been explained by our current investigations. The central spindle is involved in midbody formation (Doxsey, *et al.*, 2005) and abscission requires midbody breakage before abscission can occur. Midbody breakage and abscission involve MT-severing proteins and the endosomal sorting complex (ESCRT) (Gromley *et al.*, 2005; Morita *et al.*, 2007; Lee *et al.*, 2008; Elia *et al.*, 2011; Guizetti *et al.*, 2011). In patient cells ASPM was found to be partially mislocalised to the central spindle, suggesting this may be the cause of the failure to abscise in *MCPH5* patient cells, however further work is required to validate and further understand this involvement.

The experiments in this chapter show that hits from an ASPM C-terminal Y2H screen are novel ASPM interacting proteins. MACF1 is a downstream interacting partner of ASPM and we tentatively suggest that the level of MACF1 expression

may be controlled by a signally cascade. ASPM is required for MACF1 MT localisation and the data supports a hypothesised requirement for both ASPM and MACF1 for MT organisation, mitotic spindle orientation and chromosome separation. Initial co-localisation of ASPM and MACF1 in cytokinesis supports our preliminary hypothesis that the ASPM-MACF1 interaction is required for this last stage of abscission. A tentative validation of the interaction of ASPM and SRGAP2 was achieved showing ASPM decrease resulted in proportional SRGAP2 protein level and ASPM C-terminal GST pulldown showed a level of SRGAP2 association but inroads into validation of the GCC2-ASPM interaction have not been made. Of the remaining candidate ASPM interacting hits identified in the Y2H screen, many have an actin association and further investigation may elucidate the role of ASPM in actin dynamics identified in Chapters 3 and 4.

Chapter 6 : Final conclusion and future work

Mutations in the *ASPM* gene are the most common cause of MCPH and *ASPM* is a key determinant of cerebral cortical size in humans (Bond *et al.*, 2002). Roles for *ASPM* in spindle assembly, spindle organization, spindle orientation and cytokinesis have already been identified (Paramasivam, *et al.*, 2007; Van Der Voet, *et al.*, 2009; Higgins *et al.*, 2010; Xu *et al.*, 2012; Connolly *et al.*, 2014). However investigations into additional roles of *ASPM*, how *ASPM* mutation affects mitotic function and results in MCPH and further *ASPM* C-terminus interactions are required. In this research study, the aim was to (i) identify novel functions of *ASPM* using *ASPM* siRNA KD studies, (ii) to understand which functions of *ASPM* were affected by *ASPM* mutations and to therefore further our understanding of how mutations in *ASPM* result in MCPH and (iii) to investigate interacting partners of *ASPM* in order to understand *ASPM* function in mitosis.

The expression of the *ASPM* protein was characterized in three different cell lines. *ASPM* was expressed as a 410KDa band by western blotting, U2OS cells gave the best overall *ASPM* expression and were used to study the effect of *ASPM* knockdown on mitosis. *ASPM* was localized mainly to the nucleus in interphase, to the spindle poles in mitosis (prometaphase to anaphase) and to the midbody during cytokinesis. *ASPM* siRNA mediated KD in U2OS cells reduced the amount of *ASPM* at the spindle poles during mitosis and the midbody during cytokinesis. The major mitotic phenotypic anomalies identified during mitosis using *ASPM* siRNA KD studies were spindle pole defects and cytokinesis failure which confirmed previously identified roles for *ASPM* in spindle pole focusing,

spindle/cleavage furrow orientation, spindle assembly and cytokinesis (Kim *et al.*, 2001; Fish, *et al.*, 2006; Van Der Voet, *et al.*, 2009; Bikeye, *et al.*, 2010; Higgins *et al.*, 2010; Xu, 2012; Connolly *et al.*, 2014; Capecchi *et al.*, 2015; Tungadi *et al.*, 2017). Reduction in ASPM identified a number of abnormalities in interphase which suggested roles for ASPM in centrosome biogenesis, actin and microtubule organisation and nuclear shape/chromatin organisation. Nuclear shape changes were found to result from poor chromosome separation due to MT abnormalities (reduced MT force) during anaphase, rather than chromatin organisation. Reduction in ASPM also caused an increase in the number of cells in prometaphase and metaphase and a corresponding decrease in the number of cells in anaphase and cytokinesis showing ASPM is required for passage through prometaphase and metaphase stages. During cytokinesis an increase in time taken for abscission to be completed was identified. It is suggested that this defect may arise due to problems anchoring MTs to the PCM, cell cortex and actin network and to complete abscission during cytokinesis possibly through interacting with other partners.

MCPH is characterised by a small brain which results from a decrease in neuronal cell number (Aicardi, *et al.*, 1998). To investigate the mechanisms underlying the formation of MCPH we studied *MCPH5* patient fibroblast cells containing homozygous *ASPM* mutations. Immunoblotting data identified that *ASPM* expression levels using HDF Neo cell line were significantly lower in the *ASPM*^{β663delG} and *ASPM*^{9984+1T>G} cell lysates than in *ASPM*^{wt} cell lysates possibly due to increased in protein degradation or reduced protein stability. This is different

from the Higgins et al (Higgins *et al.*, 2010) which showed a similar level of expression of *ASPM*^{9984+1T>G} cell lysates to the wild type using U2OS cell line. Correspondingly using immunofluorescence imaging of ASPM protein in *ASPM*^{3663delG} and *ASPM*^{9984+1T>G} cells showed a great reduction in the amount of ASPM protein in the nucleus in interphase cells, at the spindle poles in mitosis and changed the localisation of the ASPM to the cytoplasm in mitosis and to the central spindle in cytokinesis with a reduction at the midbody. This thesis shows that homozygous or bi-allelic mutations in *ASPM* do not result in NMD nor in a truncated ASPM protein as expected, but in the *ASPM*^{3663delG} cells expression of full length ASPM is consistent with transcriptional read-through and in *ASPM*^{9984+1T>G} cells would represent ASPM missing only 3aa. Changes in localisation indicate functional changes have also occurred as a result of the *ASPM*^{3663delG} alteration. Similarly to the changes in mitotic functions observed in *ASPM* siRNA mediated reduction, a number of different abnormal MT associated mitotic phenotypes were identified in *MCPH5* patient fibroblast cells. The *ASPM* gene encodes a protein that is localised mainly at the spindle poles (Higgins *et al.*, 2010) and plays crucial roles in cell mitosis (Bond *et al.*, 2002; Kouprina, *et al.*, 2005; Zhong *et al.*, 2005; Higgins *et al.*, 2010; Capecchi *et al.*, 2015), hence ASPM reduction caused mitotic defects. The major phenotypic anomalies identified during mitosis were spindle pole defects indicating important roles of ASPM in centrosome biogenesis and cohesion during mitosis. These mitotic phenotypes may have arisen due to microtubule assembly defects indicating involvement of ASPM in the regulation of spindle assembly during mitosis. *ASPM* reduction

caused poor MT focus at the spindle poles which could lead to a loss of tension in the MT from the spindle poles resulting in the inaccurate segregation of DNA into the daughter cells and changes in spindle orientation. ASPM and NuMA co-localize at the spindle poles (Gaglio *et al.*, 1995; Merdes *et al.*, 1996; Higgins *et al.*, 2010) and at the minus-ends of MTs during mitosis (Merdes *et al.*, 1996) and have been confirmed to interact to control mitotic spindle assembly (Seldin *et al.*, 2013). The mitotic spindle uses mitotic motors such as dynein and dynactin to correctly separate chromatin during mitosis (Civelekoglu *et al.*, 2010). NuMA is a MTs tethering protein interacts with dynein/dynactin complex to generate the force required to pull the spindle poles towards the cell cortex (Sun *et al.*, 2006; Van Der Voet, *et al.*, 2009; Jiang *et al.*, 2017) and a reduction in ASPM concentration has possibly led to a reduction in the ASPM:NuMA interaction and hence caused microtubule assembly defects and problems in cell separation of the two daughter cells (Noatynska *et al.*, 2012) or mitosis arrest (Compton *et al.*, 1995). In addition to that NuMA also plays an important role in driving spindle orientation via interaction with this complex suggesting role for ASPM in cleavage furrow orientation/spindle orientation. In brain development division orientation in NPC changes from symmetrical to asymmetrical (cleavage furrow orientation from vertical to parallel to the apical surface) to create one NPC and a neuron instead of doubling the NPC output. An early switch from symmetric to asymmetric cell division would ultimately lead to a comparative reduction in the number of neurons in the developing brain within the neurogenic window. Therefore, it is suggested that a reduction in ASPM in the patient cells and *ASPM* siRNA mediated KD cells has affected the

NuMA/dynein/dynactin complex and caused a reduction in spindle pole focusing leading to spindle orientation defects.

Another MT associated aberrant phenotype observed in *MCPH5* patient fibroblast cells was an increase in the proportion of cells in prometaphase and/or metaphase stages and a corresponding decrease in the proportion of cells in anaphase and cytokinesis. ASPM is confirmed to interact with and recruit citron kinase (CITK) to the mitotic spindle in prometaphase (Di Cunto *et al.*, 2000; Paramasivam, *et al.*, 2007) to function in the nucleation and stability of astral MT (Gai, *et al.*, 2016) ensuring the spindle is anchored to the cell cortex. A reduction in ASPM could affect this process leading to a delay in mitosis or metaphase arrest. Using LCI, the increase in prometaphase and metaphase cells was found to cause a significant delay in the anaphase onset that led to an increase in the duration of mitosis and/or metaphase arrest that led to cells failing to proceed to cytokinesis. Neurogenesis is a tightly regulated finitely timed process and therefore if mitosis is slower, less NPC divisions can be performed within the specific time frame (termed neurogenic window) resulting in a lower cell number and consequentially causing microcephaly.

Another MT associated aberrant phenotype observed was cytokinesis failure. In this thesis it is proposed that ASPM plays a vital role during cytokinesis via interaction with downstream interacting partners such as MACF1 (Chapter 5) and recruiting essential proteins to the midbody such as CITK. MACF1 is required to form bridges between cytoskeletal filaments and the cell periphery during mitosis (Roper *et al.*, 2002) and CITK is essential to complete abscission during

cytokinesis (Paramasivam, *et al.*, 2007). MACF1 and CITK both co-localise to the midbody during cytokinesis (Madaule, *et al.*, 1998; Kosako *et al.*, 2000). *ASPM* KD and mutations disturbed the concentration and localisation of MACF1 (Chapter 5) and CITK (Di Cunto *et al.*, 2000; Paramasivam, *et al.*, 2007). MACF1 was disassociated from MTs upon *ASPM* KD and *ASPM* mutation which indicated a role for *ASPM* in maintaining an association of MACF1 with the MT during interphase, mitosis and cytokinesis. Further to this, MACF1 and CITK are individually confirmed to potentially interact with *ASPM* C-terminus (Paramasivam, *et al.*, 2007), indicating a vital role of the *ASPM* C-terminal region in neurogenesis during cytokinesis possibly to orchestrate cytokinesis and complete abscission respectively. Therefore, it is possible that a reduction in *ASPM* concentration and a reduction in the efficacy of the interaction with MACF1 and CITK in *ASPM*^{3663delG} and *ASPM*^{9984+1G>T} proteins caused cytokinesis failure and contributed to the MCPH phenotype.

A number of aberrant nuclear interphase phenotypes including lobular nuclei, enlarged nuclei and micro nuclei were identified. A nuclear role for *ASPM* has not been reported, however this current investigation of the abnormal nuclear phenotypes in *ASPM* siRNA cells revealed that they were MT associated phenotypes arising as a result of abnormal cell division, where some phenotypes arose from poor chromosome separation most likely due to MT abnormalities such as a loss of MT associated tension (Van Der Voet, Berends, *et al.*, 2009; Xu *et al.*, 2012; Connolly *et al.*, 2014). The main mitotic abnormalities identified using LCI were lagging chromosomes, metaphase arrest and cytokinesis failure which

resulted in the formation of lobular nuclei or micronuclei, cell death or a single cell with an enlarged nucleus and multinucleated single cell respectively. These nuclear changes in *MCPH5* cells were not previously reported, but knobby nuclei and micronuclei probably resulted from the direct effect of *ASPM* mutations on spindle pole focusing followed by a reduction in the forces required for accurate chromosome separation (Noatynska *et al.*, 2012), leading to chromosome separation defects during mitosis.

Aberrations in the structure and number of centrosomes and organization of MTs and actin were also identified. Centrosomes are microtubule-organizing centres (MTOC) which nucleate the polymerization of microtubules (Mckean *et al.*, 2003; Moutinho *et al.*, 2009; Blas-Rus *et al.*, 2017; Sanchez *et al.*, 2017) and hence centrosomal defects will be associated with MT abnormalities. *ASPM* reduction caused abnormal disorganized, clustered and low density MTs, as well as areas of dense MTs arising from MTOC. *ASPM* is required for focusing MTs minus ends to the mitotic spindle poles (Ito, *et al.*, 2015) and consequently, a possible explanation for disruption of MT dynamics is *ASPM* is involved in MTs polymerization via interaction with an interacting partner and depletion has led to formation of MTs abnormalities. *ASPM* reduction and mutations resulted not only in MT abnormalities but also in changes in actin organisation and the *ASPM* interacting protein MACF was identified as a C-terminal interactant, suggesting *ASPM* is playing a central role in orchestrating the bridging of cytoskeletal structures actin and MT. *ASPM* reduction showed an effect on cellular actin filament distribution and organisation which may also indicate a role for *ASPM* at the cell cortex. *ASPM*

localisation at the interphase cell cortex was identified, but not verified as part of this current research (Appendix 3), which may involve the ASPM interaction with MACF1 (Chapter 5), however, more investigation needed in future work to confirm an involvement of ASPM in anchoring the MT to the PCM and actin network via MACF1.

The ASPM C-terminus is involved in cytokinesis (Higgins *et al.*, 2010), so to understand other components involved in this function a Yeast-2-Hybrid screen was performed and analysed. Three cytoskeletal associated proteins were identified (SRGAP2, GCC2 and MACF1) as putative ASPM C-terminal interactants. The hypothesis was that ASPM interacted with these proteins to link microtubules to the Golgi apparatus and the cell cortex as part of its role in orchestrating cytokinesis. In *ASPM* siRNA treated U2OS cells and *MCPH5* patient cell lysates, the expressions of SRGAP2 and MACF1 were significantly reduced suggested an interaction between ASPM and these proteins did exist and that they were part of a signalling cascade. An interaction between ASPM:SRGAP2 and ASPM:MACF1 was validated which suggest roles for ASPM in linking astral MT to the cell cortex during mitosis (Gai, *et al.*, 2016) and in MT requirement to complete abscission during cytokinesis (Paramasivam, *et al.*, 2007).

The typical MACF1 localisation in interphase cells was altered and disrupted in *ASPM* KD cells and *MCPH5* patient cells. *ASPM* KD cells and *MCPH5* patient cells displayed reduced levels of MACF1 and impaired MACF1 association with MTs. The MT network was clearly disrupted due to reduced ASPM and MACF1 MACF1 contains a C-terminal microtubule binding domains (Leung, *et al.*, 1999). MACF1

was delocalised from the minus ends of MTs and from the spindle poles during mitosis in *ASPM* KD cells and *MCPH5* patient cells. Moreover, an analysis of the mitotic spindle poles revealed fragmented poles. Further investigation is required to determine if MACF1 at spindle poles is involved in stabilizing MT and therefore if a decrease in ASPM:MACF1 drives poor chromosome separation. When the normal dynamics of MTs are disrupted they form unstable opposing growth trajectories, which can result in failure to correctly separate chromatin during mitosis which can lead in some cases to form micronuclei or metaphase arrest (Hayashi, et al., 2013). Disruption of MTs by MACF1 has been already described to cause MTs-actin dissociation (Kodama *et al.*, 2003). Disruption of actin resulted in impaired spindle anchorage and mis-orientation of the mitotic spindle (Woolner, *et al.*, 2008) suggesting *ASPM* is involved in tethering MT and actin to the cell cortex, possibly via MACF1 interaction. A similar phenotype was observed with *ASPM* mutations and knockdown using live cell imaging in Chapters 3 and 4. It is therefore proposed that the putative *ASPM* interaction with MACF1 is involved in maintaining the actin-MT-spindle link, which maintains spindle positioning in mitosis. Loss or reduction of of the association with MACF1 at the spindle pole and/or cell cortex may lead to mis-orientation of the mitotic spindle and an early switch from symmetric to asymmetric cell division resulting in a small progenitor cell pool and a small brain.

During cytokinesis, MACF1 was only visible at the central spindle. One of our initial hypotheses was that MACF1 may interact with *ASPM* to orchestrate cytokinesis. This was supported in control cells when MACF1 and *ASPM* localisation in cytokinesis were found to overlap. Consequently, in *ASPM* KD and *MCPH5* cells,

MACF1 failed to interact with ASPM and therefore to complete cytokinesis, eventually leading to cytokinesis failure. Consistent with this finding, ASPM KD was already reported to cause cytokinesis failure (Higgins *et al.*, 2010), however the underlying mechanism had not been explained. The data demonstrated in this study, along with previously published evidence indicate that ASPM is essentially required in U2OS and HDF Neo cells for the successful completion of cytokinesis.

In summary, multiple generally similar errors were observed during mitosis and cytokinesis in *ASPM* siRNA mediated KD and *ASPM* mutations. The common factor of most *ASPM* mediated KD and mutations are the low concentration of full length or near full length ASPM protein. Therefore, similarity in MCPH phenotypes may arise due to a reduction to properly complete the multiple ASPM functions possibly due to the decrease in ASPM protein level. ASPM has essential roles in spindle pole focusing, spindle/cleavage furrow orientation, spindle assembly, frequency of mitosis, mitotic stage and cytokinesis and hence reduction of these functions has eventually led to decrease in the number of neurons resulting in a lower NPCs and consequentially causing microcephaly.

Future work

Table 6.1 below reviews all the cell lines and proteins used in this thesis for each assay, so that future work will cover all the gaps necessary for a complete picture of the study. In addition to that, future investigations and directions for this research will include,

1. Reciprocal KD between two genes, ASPM and MACF1, to see the effect on cell cycle, using live cell imaging experiments to observe mitotic phenotypes.
2. For further investigation into donut-shaped nuclei, U2OS Histone H2B-GFP stable cell lines could be made and *ASPM* siRNA mediated reduction performed instead using of HeLa cells because U2OS may be more sensitive to cell cycle checkpoints than HeLa cells. This would enable further investigate of the roles of ASPM in interphase stage or how these nuclear defect arise from aberrant mitosis
3. For further investigation into the effect of the *ASPM 3663delG* mutation on the ASPM protein is required (approximately full length ASPM protein was identified instead of the predicted protein truncation or NMD). We need to further investigate the protein sequence to determining the amino acid sequence by Mass spectrometry methods
4. U2OS cells stably expressing m-cherry- α -tubulin are available within our group. These cells will be used for *MACF1* KD and *MACF1-ASPM* double KD to see the effect on the microtubules using live cell imaging.
5. ASPM localisation and interactions at the cell cortex requires further investigation specifically in order to understand ASPMs role in spindle orientation and cytokinesis.
6. Confirm protein interaction between ASPM and other Y2H hits that weren't confirmed using co-IP and GST pull downs experiments. Other protein-

protein interactions detection methods could be used such as Far-western blot analysis which is based on tagged proteins instead of antibodies.

7. Further study the effect of protein KD on MT during mitosis.
8. Other splice prediction tools such as GeneSplicer and Human Splicing Finder will be considered so that better understanding of intronic and exonic mutations can be achieved.
9. ASPM KD may result in the upregulation of P53 (tumor suppressor protein). Therefore, it would be useful to measure p53 expression level to see if the p53 is altered when ASPM expression is altered or not as this could be a reason for cells to commit apoptosis and hence reduce neuronal cell number.

Table 6.1: summary table of all cell lines and proteins used for each assay in this investigation.

Cell Lines	WB	IF	cDNA sequencing and PCR	siRNA	GST pull-downs	Co.IP	LCI
U2OS	✓	✓		✓	✓	✓	✓
SHSY-5Y	✓						
HeLa	✓			✓			
<i>ASPM</i> ^{WT}	✓	✓	✓				✓
<i>ASPM</i> ^{3663delG}	✓	✓	✓				✓
<i>ASPM</i> ^{9984+1G>T}	✓	✓					✓
Proteins	WB	IF	cDNA sequencing and PCR	siRNA	GST pull-downs	Co.IP	LCI
ASPM	✓	✓	✓	✓		✓	✓
MACF1	✓	✓				✓	
SRGAP2	✓				✓		
GCC2	✓						
NuMa							
CTRK							

Chapter 7 : References

- ABOLHASSANI, H., WANG, N., AGHAMOHAMMADI, A., REZAEI, N., LEE, Y. N., FRUGONI, F., NOTARANGELO, L. D., PAN-HAMMARSTRÖM, Q. & HAMMARSTRÖM, L. 2014. A hypomorphic recombination-activating gene 1 (RAG1) mutation resulting in a phenotype resembling common variable immunodeficiency. *J Allergy Clin Immunol*, 134, 1375-1380.
- AKBARIAZAR, E., EBRAHIMPOUR, M., AKBARI, S., ARZHANGHI, S., ABEDINI, S. S., NAJMABADI, H. & KAHRIZI, K. 2013. A Novel Deletion Mutation in ASPM Gene in an Iranian Family with Autosomal Recessive Primary Microcephaly. *Iran J Child Neurol*, 7, 23-30.
- ABDEL-HAMID MS, ISMAIL MF, DARWISH HA, EFFAT LK, ZAKI MS, ABDEL-SALAM GM. 2016. Molecular and phenotypic spectrum of ASPM-related Primary microcephaly: Identification of eight novel mutations. *Am J Med Genet A*.170(8):2133-40
- ALSIARY R, BRUNING-RICHARDSON, BOND J, MORRISON EE, WILKINSON N, BELL SM.2014. Deregulation of microcephalin and ASPM expression are Correlated with epithelial ovarian cancer progression. *PLoS One*. 15;9(5):e97059
- Applewhite DA1, Grode KD, Duncan MC, Rogers SL. 2013.The actin-microtubule cross-linking activity of Drosophila Short stop is regulated by intramolecular inhibition. *Mol Biol Cell*. 24(18):2885-93
- ADAM SA, BUTIN-ISRAELI V, CLEAND MM, SHIMI T, GOLDMAN RD,2013, Disruption of lamin B1 and lamin B2 processing and localization by farnesyltransferase inhibitors. *Nucleus*. 4(2):142-50
- ANGERS, M., ULDRY, M., KONG, D., GIMBLE, J. M. & JETTEN, A. M. 2008. Mfsd2a encodes a novel major facilitator superfamily domain-containing protein highly induced in brown adipose tissue during fasting and adaptive thermogenesis. *Biochem J*, 416, 347-55.
- ARAI, Y. & TAVERNA, E. 2017. Neural Progenitor Cell Polarity and Cortical Development. *Front Cell Neurosci*, 11.
- ARIANI, F., MARI, F., AMITRANO, S., DI MARCO, C., ARTUSO, R., SCALA, E., MELONI, I., DELLA VOLPE, R., ROSSI, A., VAN BOKHOVEN, H. & RENIERI, A. 2013. Exome sequencing overrides formal genetics: ASPM mutations in a case study of apparent X-linked microcephalic intellectual deficit. *Clin Genet*, 83, 288-90.
- ASENCIO, C., DAVIDSON, I. F., SANTARELLA-MELLWIG, R., LY-HARTIG, T. B., MALL, M., WALLENFANG, M. R., MATTAJ, I. W. & GORJANACZ, M. 2012. Coordination of kinase and phosphatase activities by Lem4 enables nuclear envelope reassembly during mitosis. *Cell*, 150, 122-35.
- AWAD, S., AL-DOSARI, M. S., AL-YACOUB, N., COLAK, D., SALIH, M. A., ALKURAYA, F. S. & POIZAT, C. 2013. Mutation in PHC1 implicates

- chromatin remodeling in primary microcephaly pathogenesis. *Hum Mol Genet*, 22, 2200-13.
- ABDEL-HAMID MS, ISMAIL MF, DARWISH HA, EFFAT LK, ZAKI MS, ABDEL-SALAM GM. 2016. Molecular and phenotypic spectrum of ASPM-related primary microcephaly: Identification of eight novel mutations. *Am J Med Genet A*. 170(8):2133-40
- BARBELANNE, M. & TSANG, W. Y. 2014. Molecular and cellular basis of autosomal recessive primary microcephaly. *BioMed research international*, 2014.
- BASIT, S., AL-HARBI, K. M., ALHIJJI, S. A., ALBALAWI, A. M., ALHARBY, E., EL-DARDEAR, A. & SAMMAN, M. I. 2016. CIT, a gene involved in neurogenic cytokinesis, is mutated in human primary microcephaly. *Hum Genet*, 135, 1199-207.
- BASSI, Z. I., AUDUSSEAU, M., RIPARBELLI, M. G., CALLAINI, G. & D'AVINO, P. P. 2013. Citron kinase controls a molecular network required for midbody formation in cytokinesis. *Proc Natl Acad Sci U S A*, 110, 9782-7.
- BERGGARD, T., LINSE, S. & JAMES, P. 2007. Methods for the detection and analysis of protein-protein interactions. *Proteomics*, 7, 2833-42.
- BERGSTRÖM, T. & FORSBERG-NILSSON, K. 2012. Neural stem cells: Brain building blocks and beyond. *Ups J Med Sci*.
- BERIKA M, ELQAYYAR ME, EL-HASHASH AH. 2014. Asymmetric cell division of stem cells in the lung and other systems. *Front Cell Dev Biol*
- BERNIER, G., MATHIEU, M., DE REPENTIGNY, Y., VIDAL, S. M. & KOTHARY, R. 1996. Cloning and characterization of mouse ACF7, a novel member of the dystonin subfamily of actin binding proteins. *Genomics*, 38, 19-29.
- BERNIER, G., POOL, M., KILCUP, M., ALFOLDI, J., DE REPENTIGNY, Y. & KOTHARY, R. 2000. Acf7 (MACF) is an actin and microtubule linker protein whose expression predominates in neural, muscle, and lung development. *Dev Dyn*, 219, 216-25.
- BETSCHINGER, J., MECHTLER, K. & KNOBLICH, J. A. 2003. The Par complex directs asymmetric cell division by phosphorylating the cytoskeletal protein Lgl. *Nature*, 422, 326-30.
- BHARGAV, D. S. 2017. Whole exome sequencing identifies a novel homozygous frameshift mutation in the ASPM gene, which causes microcephaly 5, primary, autosomal recessive. 6.
- BHAT V, GIRIMAJI SC, MOHAN G, ARVINDA HR, SINGHMAR P, DUVVARI, KUMAR A. 2011. Mutations in WDR62, encoding a centrosomal and nuclear protein, in Indian primary Microcephaly families with cortical malformations. *Clin Genet*. 80(6):532-40

- BIANCHI, F. T., TOCCO, C., PALLAVICINI, G., LIU, Y., VERNI, F., MERIGLIANO, C., BONACCORSI, S., EL-ASSAWY, N., PRIANO, L., GAI, M., BERTO, G. E., CHIOTTO, A. M., SGRO, F., CARAMELLO, A., TASCA, L., ALA, U., NERI, F., OLIVIERO, S., MAURO, A., GELEY, S., GATTI, M. & DI CUNTO, F. 2017. Citron Kinase Deficiency Leads to Chromosomal Instability and TP53-Sensitive Microcephaly. *Cell Rep*, 18, 1674-1686.
- BIKEYE, S. N. N., COLIN, C., MARIE, Y., VAMPOUILLE, R., RAVASSARD, P., ROUSSEAU, A., BOISSELIER, B., IDBAIH, A., CALVO, C. F., LEURAUD, P., LASSALLE, M., EL HALLANI, S., DELATTRE, J. Y. & SANSON, M. 2010. ASPM-associated stem cell proliferation is involved in malignant progression of gliomas and constitutes an attractive therapeutic target. *Cancer Cell Int*.
- BILGUVAR, K., OZTURK, A. K., LOUVI, A., KWAN, K. Y., CHOI, M., TATLI, B., YALNIZOGLU, D., TUYSUZ, B., CAGLAYAN, A. O., GOKBEN, S., KAYMAKCALAN, H., BARAK, T., BAKIRCIOGLU, M., YASUNO, K., HO, W., SANDERS, S., ZHU, Y., YILMAZ, S., DINCER, A., JOHNSON, M. H., BRONEN, R. A., KOCER, N., PER, H., MANE, S., PAMIR, M. N., YALCINKAYA, C., KUMANDAS, S., TOPCU, M., OZMEN, M., SESTAN, N., LIFTON, R. P., STATE, M. W. & GUNEL, M. 2010. Whole-exome sequencing identifies recessive WDR62 mutations in severe brain malformations. *Nature*, 467, 207-10.
- BLAS-RUS N, BUSTOS-MORAN E, SANCHEZ F, MARTIN-CORES NB.2017. Analysis of Microtubules and Microtubule-Organizing Center at the Immune Synapse. *Methods Mol Biol*.1584:31-49
- Brückner A, Polge C, Lentze N, Auerbach D, Schlattner U.2009. Yeast two-hybrid, a powerful tool for systems biology. *Int J Mol Sci*. 2763-88
- BOND, A. M., MING, G. & SONG, H. 2015. Adult Mammalian Neural Stem Cells and Neurogenesis: Five Decades Later. *Cell Stem Cell*, 17, 385-95.
- BOND, J., ROBERTS, E., MOCHIDA, G. H., HAMPSHIRE, D. J., SCOTT, S., ASKHAM, J. M., SPRINGELL, K., MAHADEVAN, M., CROW, Y. J., MARKHAM, A. F., WALSH, C. A. & WOODS, C. G. 2002a. ASPM is a major determinant of cerebral cortical size. *Nature Genetics*, 32, 316-320.
- BOND, J., ROBERTS, E., SPRINGELL, K., LIZARRAGA, S. B., SCOTT, S., HIGGINS, J., HAMPSHIRE, D. J., MORRISON, E. E., LEAL, G. F., SILVA, E. O., COSTA, S. M., BARALLE, D., RAPONI, M., KARBANI, G., RASHID, Y., JAFRI, H., BENNETT, C., CORRY, P., WALSH, C. A. & WOODS, C. G. 2005. A centrosomal mechanism involving CDK5RAP2 and CENPJ controls brain size. *Nat Genet*, 37, 353-5.
- BOND, J., SCOTT, S., HAMPSHIRE, D. J., SPRINGELL, K., CORRY, P., ABRAMOWICZ, M. J., MOCHIDA, G. H., HENNEKAM, R. C., MAHER, E. R., FRYNS, J. P., ALSWAID, A., JAFRI, H., RASHID, Y., MUBAIDIN, A., WALSH, C. A., ROBERTS, E. & WOODS, C. G. 2003a. Protein-truncating mutations in ASPM cause variable reduction in brain size. *Am J Hum Genet*, 73, 1170-7.

- BOSVELD, F.; AINSLIE, A.; BELLAÏCHE, Y. 2017. Sequential activities of Dynein, Mud and Asp in centrosome–spindle coupling maintain centrosome number upon mitosis. *J Cell Sci*.
- BROWN, F. C., SCHINDELHAIM, C. H. & PFEFFER, S. R. 2011. GCC185 plays independent roles in Golgi structure maintenance and AP-1–mediated vesicle tethering. *The Journal of Cell Biology*, 194, 779-787.
- BROWN, N. J., MARJANOVIC, M., LUDERS, J., STRACKER, T. H. & COSTANZO, V. 2013. Cep63 and cep152 cooperate to ensure centriole duplication. *PLoS One*, 8, e69986.
- BRUNELLI, S., FAIELLA, A., CAPRA, V., NIGRO, V., SIMEONE, A., CAMA, A. & BONCINELLI, E. 1996. Germline mutations in the homeobox gene EMX2 in patients with severe schizencephaly. *Nat Genet*, 12, 94-6.
- BRÜCKNER, A., POLGE, C., LENTZE, N., AUERBACH, D. & SCHLATTNER, U. 2009. Yeast Two-Hybrid, a Powerful Tool for Systems Biology. *Int J Mol Sci*.
- BRÜNING-RICHARDSON, A., BOND, J., ALSIARY, R., RICHARDSON, J., CAIRNS, D. A., MCCORMAC, L., HUTSON, R., BURNS, P. A., WILKINSON, N., HALL, G. D., MORRISON, E. E. & BELL, S. M. 2012. NuMA overexpression in epithelial ovarian cancer. *PLoS One*, 7, e38945.
- BRÜNING-RICHARDSON, A., BOND, J., ALSIARY, R., RICHARDSON, J., CAIRNS, D. A., MCCORMACK, L., HUTSON, R., BURNS, P., WILKINSON, N., HALL, G. D., MORRISON, E. E. & BELL, S. M. 2011. ASPM and microcephalin expression in epithelial ovarian cancer correlates with tumour grade and survival. *British Journal Of Cancer*, 104, 1602.
- BRANDT, A., PAPAGIANNOULI, F., WAGNER, N., WILSCH-BRAUNINGER, M., BRAUN, M., FURLONG, E. E., LOSERTH, S., WENZL, C., PILOT, F., VOGT, N., LECUIT, T., KROHNE, G. & GROSSHANS, J. 2006. Developmental control of nuclear size and shape by Kugelkern and Kurzkern. *Curr Biol*, 16, 543-52.
- BROGNA, S. & WEN, J. 2009. Nonsense-mediated mRNA decay (NMD) mechanisms. *Nat Struct Mol Biol*, 16, 107-13.
- BUCHMAN, J. J., DURAK, O. & TSAI, L. H. 2011. ASPM regulates Wnt signaling pathway activity in the developing brain. *Genes Dev*, 25, 1909-14.
- BUENO, D. & GARCIA-FERNANDEZ, J. 2016. Evolutionary development of embryonic cerebrospinal fluid composition and regulation: an open research field with implications for brain development and function. *Fluids and barriers of the CNS*, 13, 5.
- BÄHLER, M. & RHOADS, A. 2002. Calmodulin signaling via the IQ motif. *FEBS letters*, 513, 107-113.
- CAPECCHI, M. R. & POZNER, A. 2015. ASPM regulates symmetric stem cell division by tuning Cyclin E ubiquitination. *Nat Commun*, 6, 8763.

- CASTRESANA, J. & SARASTE, M. 1995. Does Vav bind to F-actin through a CH domain? *FEBS letters*, 374, 149-151.
- CAUSIER, B. 2004. Studying the interactome with the yeast two-hybrid system and mass spectrometry. *Mass spectrometry reviews*, 23, 350-367.
- CAVINESS, V. S., JR., TAKAHASHI, T. & NOWAKOWSKI, R. S. 1995. Numbers, time and neocortical neuronogenesis: a general developmental and evolutionary model. *Trends Neurosci*, 18, 379-83.
- CHAVALI, P. L.; PÜTZ, M.; GERGELY, F. 2014. Small organelle, big responsibility: the role of Centrosomes in development and disease. Philosophical Transactions of the Royal Society B: Biological Sciences.
- CHANG, J. W., ZHOU, Y. Q., UL QAMAR, M. T., CHEN, L. L. & DING, Y. D. 2016. Prediction of Protein-Protein Interactions by Evidence Combining Methods. *In: KARABENCHEVA-CHRISTOVA, T. & CHRISTOV, C. Z. (eds.) Int J Mol Sci*.
- CHARRIER, C., JOSHI, K., COUTINHO-BUDD, J., KIM, J.-E., LAMBERT, N., DE MARCHENA, J., JIN, W.-L., VANDERHAEGHEN, P., GHOSH, A., SASSA, T. & POLLEUX, F. 2012. Inhibition of SRGAP2 function by its human-specific paralogs induces neoteny during spine maturation. *Cell*, 149, 923-935.
- CHÉDOTAL, A.; RICHARDS, L. J. 2010. Wiring the Brain: The Biology of Neuronal Guidance. *Cold Spring Harb Perspect Biol*. 2(6): a001917
- CHENN, A. & MCCONNELL, S. K. 1995. Cleavage orientation and the asymmetric inheritance of Notch1 immunoreactivity in mammalian neurogenesis. *Cell*, 82, 631-41.
- CHEN, C. Y., OLAYIOYE, M. A., LINDEMAN, G. J. & TANG, T. K. 2006. CPAP interacts with 14-3-3 in a cell cycle-dependent manner. *Biochem Biophys Res Commun*, 342, 1203-10.
- CHEN, J. F., ZHANG, Y., WILDE, J., HANSEN, K. C., LAI, F. & NISWANDER, L. 2014. Microcephaly disease gene *Wdr62* regulates mitotic progression of embryonic neural stem cells and brain size. *Nat Commun*, 5, 3885.
- CHEN, H. J., LIN, C. M., LIN, C. S., PEREZ-OLLE, R., LEUNG, C. L. & LIEM, R. K. 2006. The role of microtubule actin cross-linking factor 1 (MACF1) in the Wnt signaling pathway. *Genes Dev*, 20, 1933-45.
- CHERKAOUI JAOUAD, I., ZRHIDRI, A., JDIOUI, W., LYAHYAI, J., RAYMOND, L., EGÉA, G., TAOUDI, M., EL MOUATASSIM, S. & SEFIANI, A. 2018. A novel non sense mutation in *WDR62* causes autosomal recessive primary microcephaly: a case report. *BMC Medical Genetics*, 19, 118.
- CHEUNG, P.-Y. P. & PFEFFER, S. R. 2016. Transport vesicle tethering at the trans Golgi network: coiled coil proteins in action. *Frontiers in cell and developmental biology*, 4, 18.

- CIVELEKOGLU-SCHOLEY, G.; SCHOLEY, J. M. 2010. Mitotic force generators and chromosome segregation. *Cell Mol Life Sci*
- CLEVERS, H. 2013. The intestinal crypt, a prototype stem cell compartment. *Cell*, 154, 274-84.
- COLES, C. H.; BRADKE, F. 2015. Coordinating neuronal actin–microtubule dynamics. *Current Biology*, ISSN 0960-9822
- COLLINS, A. L., LUNT, P. W., GARRETT, C. & DENNIS, N. R. 1993. Holoprosencephaly - a family showing dominant inheritance and variable expression. *Journal of Medical Genetics*, 30, 36-40.
- COMPTON, D. A. & LUO, C. 1995. Mutation of the predicted p34cdc2 phosphorylation sites in NuMA impair the assembly of the mitotic spindle and block mitosis. *Journal of Cell Science*, 108, 621.
- CONNOLLY, A. A., OSTERBERG, V., CHRISTENSEN, S., PRICE, M., LU, C., CHICAS-CRUZ, K., LOCKERY, S., MAINS, P. E. & BOWERMAN, B. 2014. *Caenorhabditis elegans* oocyte meiotic spindle pole assembly requires microtubule severing and the calponin homology domain protein ASPM-1. *Mol Biol Cell*, 25, 1298-311.
- COUTINHO-BUDD, J., GHUKASYAN, V., ZYLKA, M. J. & POLLEUX, F. 2012. The F-BAR domains from srGAP1, srGAP2 and srGAP3 regulate membrane deformation differently. *J Cell Sci*, 125, 3390-401.
- CRAIG, R. & NORBURY, C. 1998. The novel murine calmodulin-binding protein Sha1 disrupts mitotic spindle and replication checkpoint functions in fission yeast. *Journal of Cell Science*, 111, 3609-3619.
- D'AVINO, P. P. 2017. Citron kinase - renaissance of a neglected mitotic kinase. *J Cell Sci*, 130, 1701-1708.
- DERETIC, V. 2010. A master conductor for aggregate clearance by autophagy. *Dev Cell*, 18, 694-6.
- DESIR, J., ABRAMOWICZ, M. & TUNCA, Y. 2006. Novel mutations in prenatal diagnosis of primary microcephaly. *Prenat Diagn*, 26, 989.
- DEMA A, MACALUSO F, SQRO F, BERTO GE, BIANCHI FT, CHIOTTO AA, PALLAVICINI G, PALLAVICINI G, DI CUNTO F, GAIL M. 2010. Citron kinase-Dependent F-actin maintenance at secondary ingression sites mediates abscission. *J Cell Sci*.jcs209080
- DEVAKUMAR, D., BAMFORD, A., FERREIRA, M. U., BROAD, J., ROSCH, R. E., GROCE, N., BREUER, J., CARDOSO, M. A., COPP, A. J., ALEXANDRE, P., RODRIGUES, L. C. & ABUBAKAR, I. 2018. Infectious causes of microcephaly: epidemiology, pathogenesis, diagnosis, and management. *Lancet Infect Dis*, 18, e1-e13.
- DI CUNTO, F., CALAUTTI, E., HSIAO, J., ONG, L., TOPLEY, G., TURCO, E. & DOTTO, G. P. 1998. Citron rho-interacting kinase, a novel tissue-specific

- ser/thr kinase encompassing the Rho-Rac-binding protein Citron. *J Biol Chem*, 273, 29706-11.
- DI CUNTO, F., IMARISIO, S., CAMERA, P., BOITANI, C., ALTRUDA, F. & SILENGO, L. 2002. Essential role of citron kinase in cytokinesis of spermatogenic precursors. *Journal of Cell Science*, 115, 4819-4826.
- DI CUNTO, F., IMARISIO, S., HIRSCH, E., BROCCOLI, V., BULFONE, A., MIGHELI, A., ATZORI, C., TURCO, E., TRIOLO, R., DOTTO, G. P., SILENGO, L. & ALTRUDA, F. 2000. Defective neurogenesis in citron kinase knockout mice by altered cytokinesis and massive apoptosis. *Neuron*, 28, 115-127.
- DISTASIO, A., DRIVER, A., SUND, K., DONLIN, M., MURALEEDHARAN, R. M., POOYA, S., KLINE-FATH, B., KAUFMAN, K. M., PROWS, C. A., SCHORRY, E., DASGUPTA, B. & STOTTMANN, R. W. 2017. Copb2 is essential for embryogenesis and hypomorphic mutations cause human microcephaly. *Hum Mol Genet*, 26, 4836-4848.
- DO CARMO AVIDES, M. & GLOVER, D. M. 1999a. Abnormal spindle protein, Asp, and the integrity of mitotic centrosomal microtubule organizing centers. *Science*, 283, 1733-5.
- DO CARMO AVIDES, M., TAVARES, A. & GLOVER, D. M. 2001. Polo kinase and Asp are needed to promote the mitotic organizing activity of centrosomes. *Nat Cell Biol*, 3, 421-4.
- DE CRISTOFARO, R., CAROTTI, A., AKHAVAN, S., PALLA, R., PEYVANDI, F., ALTOMARE, C. & MANNUCCI, P. M. 2006. The natural mutation by deletion of Lys9 in the thrombin A-chain affects the pKa value of catalytic residues, the overall enzyme's stability and conformational transitions linked to Na⁺ binding. *Febs j*, 273, 159-69.
- DOE, C. Q. 2008. Neural stem cells: balancing self-renewal with differentiation. *Development*, 135, 1575.
- DOXSEY SJ. 2005. Molecular links between centrosome and midbody. *Mol Cell*. 2005.(2):170-2.
- DUAN, L., WANG, T. Q., BIAN, W., LIU, W., SUN, Y. & YANG, B. S. 2015. Centrin: another target of monastrol, an inhibitor of mitotic spindle. *Spectrochim Acta A Mol Biomol Spectrosc*, 137, 1086-91.
- DUDOK, J. J.; LEONARDS, P. E. G.; WIJNHOLDS, J. 2017. Genetic and Molecular Approaches to Study Neuronal Migration in the Developing Cerebral Cortex. *Brain Sci*, ISSN 2076-3425
- EDA, M., YONEMURA, S., KATO, T., WATANABE, N., ISHIZAKI, T., MADAULE, P. & NARUMIYA, S. 2001. Rho-dependent transfer of Citron-kinase to the cleavage furrow of dividing cells. *Journal of cell science*, 114, 3273-3284.
- EFIMOV, A., KHARITONOV, A., EFIMOVA, N., LONCAREK, J., MILLER, P. M., ANDREYEVA, N., GLEESON, P., GALJART, N., MAIA, A. R., MCLEOD, I. X., YATES, J. R., 3RD, MAIATO, H., KHODJAKOV, A., AKHMANOVA, A. &

- KAVERINA, I. 2007. Asymmetric CLASP-dependent nucleation of noncentrosomal microtubules at the trans-Golgi network. *Dev Cell*, 12, 917-30.
- EGGER, B.; GOLD, K. S.; BRAND, A. H. 2010. Notch regulates the switch from symmetric to asymmetric neural stem cell division in the Drosophila optic lobe. *Development*, ISSN 0950-1991
- ELIA N, SOUGRAT R, SPURLIN TA, HURLEY JH, LIPPINCOTT-SCHWARTZ J . 2011. Dynamics of endosomal sorting complex required for transport (ESCRT) machinery during cytokinesis and its role in abscission.
- ENDO, A., MOYORI, A., KOBAYASHI, A. & WONG, R. W. 2013. Nuclear mitotic apparatus protein, NuMA, modulates p53-mediated transcription in cancer cells. *Cell Death Dis*, 4, e713.
- EVANS, P. D., ANDERSON, J. R., VALLENDER, E. J., GILBERT, S. L., MALCOM, C. M., DORUS, S. & LAHN, B. T. 2004. Adaptive evolution of ASPM, a major determinant of cerebral cortical size in humans. *Hum Mol Genet*, 13, 489-94.
- EVANS, P. D., GILBERT, S. L., MEKEL-BOBROV, N., VALLENDER, E. J., ANDERSON, J. R., VAEZ-AZIZI, L. M., TISHKOFF, S. A., HUDSON, R. R. & LAHN, B. T. 2005. Microcephalin, a gene regulating brain size, continues to evolve adaptively in humans. *science*, 309, 1717-1720.
- FAHEEM, M., NASEER, M. I., RASOOL, M., CHAUDHARY, A. G., KUMOSANI, T. A., ILYAS, A. M., PUSHPARAJ, P. N., AHMED, F., ALGAHTANI, H. A., AL-QAHTANI, M. H. & SALEH JAMAL, H. 2015. Molecular genetics of human primary microcephaly: an overview. *BMC Med Genomics*.
- FERLINI, A., ANSALONI, L., NOBILE, C. & FORABOSCO, A. 1990. Molecular analysis of the Rett syndrome using cDNA synapsin I as a probe. *Brain Dev*, 12, 136-9.
- FIELDS, S. & SONG, O. 1989. A novel genetic system to detect protein-protein interactions. *Nature*, 340, 245-6.
- FISH, J. L., KOSODO, Y., ENARD, W., PAABO, S. & HUTTNER, W. B. 2006a. Aspm specifically maintains symmetric proliferative divisions of neuroepithelial cells. *Proceedings of the National Academy of Sciences of the United States of America*, 103, 10438-10443.
- FISH, J. L., KOSODO, Y., ENARD, W., PAABO, S. & HUTTNER, W. B. 2006b. Aspm specifically maintains symmetric proliferative divisions of neuroepithelial cells. *Proc Natl Acad Sci U S A*, 103, 10438-43.
- FISH, J. L., KOSODO, Y., ENARD, W., PÄÄBO, S. & HUTTNER, W. B. 2006c. Aspm specifically maintains symmetric proliferative divisions of neuroepithelial cells. *Proc Natl Acad Sci U S A*, 103, 10438-43.
- FLETCHER, D. A. 2010. Cell mechanics and the cytoskeleton. 463, 485-92.

- FONG, K. W., CHOI, Y. K., RATTNER, J. B. & QI, R. Z. 2008. CDK5RAP2 is a pericentriolar protein that functions in centrosomal attachment of the gamma-tubulin ring complex. *Mol Biol Cell*, 19, 115-25.
- FONG, K. W., HAU, S. Y., KHO, Y. S., JIA, Y., HE, L. & QI, R. Z. 2009. Interaction of CDK5RAP2 with EB1 to track growing microtubule tips and to regulate microtubule dynamics. *Mol Biol Cell*, 20, 3660-70.
- FUCHS E, CHEN T. 2013. A matter of life and death: self-renewal in stem cells. *EMBO* 14(1):39-48
- FUJIMORI, A., ITOH, K., GOTO, S., HIRAKAWA, H., WANG, B., KOKUBO, T., KITO, S., TSUKAMOTO, S. & FUSHIKI, S. 2014. Disruption of *Aspm* causes microcephaly with abnormal neuronal differentiation. *Brain Dev*, 36, 661-9.
- FURUYASHIKI, T., FUJISAWA, K., FUJITA, A., MADAULE, P., UCHINO, S., MISHINA, M., BITO, H. & NARUMIYA, S. 1999. Citron, a Rho-target, interacts with PSD-95/SAP-90 at glutamatergic synapses in the thalamus. *Journal of Neuroscience*, 19, 109-118.
- GAGLIO, T.; SAREDI, A.; COMPTON, D. A. 1995. NuMA is required for the organization of microtubules into aster-like mitotic arrays. *J Cell Biol*, ISSN 0021-9525
- GAI, M., BIANCHI, F. T., VAGNONI, C., VERNÌ, F., BONACCORSI, S., PASQUERO, S., BERTO, G. E., SGRÒ, F., CHIOTTO, A. M. A., ANNARATONE, L., SAPINO, A., BERGO, A., LANDSBERGER, N., BOND, J., HUTTNER, W. B. & DI CUNTO, F. 2016. *EMBO Rep*. Hoboken.
- GARZON-CORAL, C.; FANTANA, H. A.; HOWARD, J. 2016. A force-generating machinery maintains the spindle at the cell center during mitosis. *Science*, ISSN 0036-8075.
- GENIN, A., DESIR, J., LAMBERT, N., BIERVLIET, M., VAN DER AA, N., PIERQUIN, G., KILLIAN, A., TOSI, M., URBINA, M., LEFORT, A., LIBERT, F., PIRSON, I. & ABRAMOWICZ, M. 2012. Kinetochore KMN network gene *CASC5* mutated in primary microcephaly. *Hum Mol Genet*, 21, 5306-17.
- GESCHWIND, D. H., LOGINOV, M. & STERN, J. M. 1999. Identification of a locus on chromosome 14q for idiopathic basal ganglia calcification (Fahr disease). *Am J Hum Genet*, 65, 764-72.
- GHONGANE, P., KAPANIDOU, M., ASGHAR, A., ELOWE, S. & BOLANOS-GARCIA, V. M. 2014. The dynamic protein Knl1 - a kinetochore rendezvous. *J Cell Sci*, 127, 3415-23.
- GODIN, J. D., COLOMBO, K., MOLINA-CALAVITA, M., KERYER, G., ZALA, D., CHARRIN, B. C., DIETRICH, P., VOLVERT, M.-L., GUILLEMOT, F. & DRAGATIS, I. 2010. Huntingtin is required for mitotic spindle orientation and mammalian neurogenesis. *Neuron*, 67, 392-406.
- GONG, T. W., BESIRLI, C. G. & LOMAX, M. I. 2001. MACF1 gene structure: a hybrid of plectin and dystrophin. *Mamm Genome*, 12, 852-61.

- GORDON, M. B. 2001. Chromosome Movement in Mitosis Requires Microtubule Anchorage at Spindle Poles.
- GORYUNOV, D., HE, C.-Z., LIN, C.-S., LEUNG, C. L. & LIEM, R. K. H. 2010. Nervous-tissue-specific elimination of microtubule-actin crosslinking factor 1a results in multiple developmental defects in the mouse brain. *Molecular and Cellular Neuroscience*, 44, 1-14.
- GOULAS, S., CONDER, R. & KNOBLICH, J. A. 2012. The Par complex and integrins direct asymmetric cell division in adult intestinal stem cells. *Cell Stem Cell*, 11, 529-40.
- GRASER, S., STIERHOF, Y. D. & NIGG, E. A. 2007. Cep68 and Cep215 (Cdk5rap2) are required for centrosome cohesion. *J Cell Sci*, 120, 4321-31.
- GRUNEBERG, U., NEEF, R., LI, X., CHAN, E. H., CHALAMALASETTY, R. B., NIGG, E. A. & BARR, F. A. 2006. KIF14 and citron kinase act together to promote efficient cytokinesis. *J Cell Biol*, 172, 363-72.
- GUERNSEY, D. L., JIANG, H., HUSSIN, J., ARNOLD, M., BOUYAKDAN, K., PERRY, S., BABINEAU-STURK, T., BEIS, J., DUMAS, N., EVANS, S. C., FERGUSON, M., MATSUOKA, M., MACGILLIVRAY, C., NIGHTINGALE, M., PATRY, L., RIDEOUT, A. L., THOMAS, A., ORR, A., HOFFMANN, I., MICHAUD, J. L., AWADALLA, P., MEEK, D. C., LUDMAN, M. & SAMUELS, M. E. 2010. Mutations in centrosomal protein CEP152 in primary microcephaly families linked to MCPH4. *Am J Hum Genet*, 87, 40-51.
- GUERRIER, S., COUTINHO-BUDD, J., SASSA, T., GRESSET, A., JORDAN, N. V., CHEN, K., JIN, W. L., FROST, A. & POLLEUX, F. 2009. The F-BAR domain of srGAP2 induces membrane protrusions required for neuronal migration and morphogenesis. *Cell*, 138, 990-1004.
- GUL, A., HASSAN, M. J., MAHMOOD, S., CHEN, W., RAHMANI, S., NASEER, M. I., DELLEFAVE, L., MUHAMMAD, N., RAFIQ, M. A., ANSAR, M., CHISHTI, M. S., ALI, G., SIDDIQUE, T. & AHMAD, W. 2006. Genetic studies of autosomal recessive primary microcephaly in 33 Pakistani families: Novel sequence variants in ASPM gene. *Neurogenetics*, 7, 105-10.
- GUO, S. & BAO, S. 2010. srGAP2 Arginine Methylation Regulates Cell Migration and Cell Spreading through Promoting Dimerization. *The Journal of Biological Chemistry*, 285, 35133-35141.
- GUO, Z. & OHLSTEIN, B. 2015. Bidirectional Notch signaling regulates Drosophila intestinal stem cell multipotency. *Science*, 350, aab0988.
- GÓMEZ-LÓPEZ, S.; LERNER, R. G.; PETRITSCH, C. 2014. Asymmetric cell division of stem and progenitor cells during homeostasis and cancer. *Cell Mol Life Sci*, ISSN 1420-682X
- GÖTZ, M., SIRKO, S., BECKERS, J. & IRMLER, M. 2015. Reactive astrocytes as neural stem or progenitor cells: In vivo lineage, In vitro potential, and

- Genome-wide expression analysis. *In: GÖTZ, M. & GALLO, V. (eds.) Glia*. Hoboken.
- GORYUNOV, D., HE, C.-Z., LIN, C.-S., LEUNG, C. L. & LIEM, R. K. H. 2010. Nervous-tissue-specific elimination of microtubule-actin crosslinking factor 1a results in multiple developmental defects in the mouse brain. *Molecular and Cellular Neuroscience*, 44, 1-14.
- GONZALEZ, C., SAUNDERS, R. D., CASAL, J., MOLINA, I., CARMENA, M., RIPOLL, P. & GLOVER, D. M. 1990. Mutations at the asp locus of *Drosophila* lead to multiple free centrosomes in syncytial embryos, but restrict centrosome duplication in larval neuroblasts. *J Cell Sci*, 96 (Pt 4), 605-16.
- HALLERVORDEN, I. 1950. Ueber diffuse symmetrische Kalkablagerungen bei einem Krankheitsbild mit Mikrocephalie und Meningoencephalitis. *Arch. Psychiat.*, 184, 579-600.
- HANZLIK, E. & GIGANTE, J. 2017. Microcephaly. *In: LEONARD, H. (ed.) Children (Basel)*.
- HARDWICK, L. J. A., ALI, F. R., AZZARELLI, R. & PHILPOTT, A. 2015. Cell cycle regulation of proliferation versus differentiation in the central nervous system. *Cell Tissue Res*. Berlin/Heidelberg.
- HAREN, L., GNADT, N., WRIGHT, M. & MERDES, A. 2009. NuMA is required for proper spindle assembly and chromosome alignment in prometaphase. *BMC Research Notes*, 2, 64.
- HAREN, L. & MERDES, A. 2002. Direct binding of NuMA to tubulin is mediated by a novel sequence motif in the tail domain that bundles and stabilizes microtubules. *J Cell Sci*, 115, 1815-24.
- HARRIS, S. R. 2015. Measuring head circumference: Update on infant microcephaly. *Can Fam Physician*.
- HASHMI, J. A., AL-HARBI, K. M., RAMZAN, K., ALBALAWI, A. M., MEHMOOD, A., SAMMAN, M. I. & BASIT, S. 2016. A novel splice-site mutation in the ASPM gene underlies autosomal recessive primary microcephaly. *Ann Saudi Med*, 36, 391-396.
- HAYASHI, M. T.; KARLSEDER, J. 2013. DNA damage associated with mitosis and Cytokinesis failure. ISSN 0950-9232
- HIGGINS, J., MIDGLEY, C., BERGH, A. M., BELL, S. M., ASKHAM, J. M., ROBERTS, E., BINNS, R. K., SHARIF, S. M., BENNETT, C., GLOVER, D. M., WOODS, C. G., MORRISON, E. E. & BOND, J. 2010. Human ASPM participates in spindle organisation, spindle orientation and cytokinesis. *Bmc Cell Biology*, 11.
- HOFMAN, M. A. 2014. Evolution of the human brain: when bigger is better. *Front Neuroanat*, ISSN 1662-5129

- HORVATH, S., ZHANG, B., CARLSON, M., LU, K. V., ZHU, S., FELCIANO, R. M., LAURANCE, M. F., ZHAO, W., QI, S., CHEN, Z., LEE, Y., SCHECK, A. C., LIAU, L. M., WU, H., GESCHWIND, D. H., FEBBO, P. G., KORNBLUM, H. I., CLOUGHESY, T. F., NELSON, S. F. & MISCHEL, P. S. 2006. Analysis of oncogenic signaling networks in glioblastoma identifies ASPM as a molecular target. *Proceedings of the National Academy of Sciences*, 103, 17402.
- HOMEM, C. C., REPIC, M. & KNOBLICH, J. A. 2015. Proliferation control in neural stem and progenitor cells. *Nat Rev Neurosci*, 16, 647-59.
- HOWARD, J.; GARZON-CORAL, C. 2017, Physical Limits on the Precision of Mitotic Spindle Positioning by Microtubule Pushing forces: Mechanics of mitotic spindle positioning. *Bioessays*, ISSN 0265-9247.
- HUG, N., LONGMAN, D. & CACERES, J. F. 2016. Mechanism and regulation of the nonsense-mediated decay pathway. *Nucleic Acids Res*, 44, 1483-95.
- HU, L., SU, P., LI, R., YAN, K., CHEN, Z., SHANG, P. & QIAN, A. 2015. Knockdown of microtubule actin crosslinking factor 1 inhibits cell proliferation in MC3T3-E1 osteoblastic cells. *BMB Rep*.
- HU, H., SUCKOW, V., MUSANTE, L., ROGGENKAMP, V., KRAEMER, N., ROPERS, H. H., HUBNER, C., WIENKER, T. F. & KAINDL, A. M. 2014. Previously reported new type of autosomal recessive primary microcephaly is caused by compound heterozygous ASPM gene mutations. *Cell Cycle*, 13, 1650-1.
- HUNG, L. Y., CHEN, H. L., CHANG, C. W., LI, B. R. & TANG, T. K. 2004. Identification of a novel microtubule-destabilizing motif in CPAP that binds to tubulin heterodimers and inhibits microtubule assembly. *Mol Biol Cell*, 15, 2697-706.
- HUSSAIN, M. S., BAIG, S. M., NEUMANN, S., NURNBERG, G., FAROOQ, M., AHMAD, I., ALEF, T., HENNIES, H. C., TECHNAU, M., ALTMULLER, J., FROMMOLT, P., THIELE, H., NOEGEL, A. A. & NURNBERG, P. 2012. A truncating mutation of CEP135 causes primary microcephaly and disturbed centrosomal function. *Am J Hum Genet*, 90, 871-8.
- HUSSAIN, M. S., BAIG, S. M., NEUMANN, S., PECHE, V. S., SZCZEPANSKI, S., NURNBERG, G., TARIQ, M., JAMEEL, M., KHAN, T. N., FATIMA, A., MALIK, N. A., AHMAD, I., ALTMULLER, J., FROMMOLT, P., THIELE, H., HOHNE, W., YIGIT, G., WOLLNIK, B., NEUBAUER, B. A., NURNBERG, P. & NOEGEL, A. A. 2013. CDK6 associates with the centrosome during mitosis and is mutated in a large Pakistani family with primary microcephaly. *Hum Mol Genet*, 22, 5199-214.
- ISHIKAWA, K., NAGASE, T., SUYAMA, M., MIYAJIMA, N., TANAKA, A., KOTANI, H., NOMURA, N. & OHARA, O. 1998. Prediction of the coding sequences of unidentified human genes. X. The complete sequences of 100 new cDNA clones from brain which can code for large proteins in vitro. *DNA Res*, 5, 169-76.

- ITO, A. & GOSHIMA, G. 2015. Microcephaly protein Asp focuses the minus ends of spindle microtubules at the pole and within the spindle. *J Cell Biol*.
- JACKSON, A. P., EASTWOOD, H., BELL, S. M., ADU, J., TOOMES, C., CARR, I. M., ROBERTS, E., HAMPSHIRE, D. J., CROW, Y. J., MIGHELL, A. J., KARBANI, G., JAFRI, H., RASHID, Y., MUELLER, R. F., MARKHAM, A. F. & WOODS, C. G. 2002. Identification of microcephalin, a protein implicated in determining the size of the human brain. *Am J Hum Genet*, 71, 136-42.
- JACKSON, A. P., MCHALE, D. P., CAMPBELL, D. A., JAFRI, H., RASHID, Y., MANNAN, J., KARBANI, G., CORRY, P., LEVENE, M. I., MUELLER, R. F., MARKHAM, A. F., LENCH, N. J. & WOODS, C. G. 1998. Primary autosomal recessive microcephaly (MCPH1) maps to chromosome 8p22-pter. *Am J Hum Genet*, 63, 541-6.
- JAMIESON, C. R., FRYNS, J. P., JACOBS, J., MATTHIJS, G. & ABRAMOWICZ, M. J. 2000. Primary Autosomal Recessive Microcephaly: MCPH5 Maps to 1q25-q32. *Am J Hum Genet*.
- JAMIESON, C. R., GOVAERTS, C. & ABRAMOWICZ, M. J. 1999. Primary Autosomal Recessive Microcephaly: Homozygosity Mapping of MCPH4 to Chromosome 15. *Am J Hum Genet*.
- JAYARAMAN, D., BAE, B.-I. & WALSH, C. A. 2018. The Genetics of Primary Microcephaly. *Annual Review of Genomics and Human Genetics*, 19, 177-200.
- JAYARAMAN, D., KODANI, A., GONZALEZ, D. M., MANCIAS, J. D., MOCHIDA, G. H., VAGNONI, C., JOHNSON, J., KROGAN, N., HARPER, J. W., REITER, J. F., YU, T. W., BAE, B.-I. & WALSH, C. A. 2016. Microcephaly proteins Wdr62 and Aspm define a mother centriole complex regulating centriole biogenesis, apical complex and cell fate. *Neuron*, 92, 813-828.
- JIANG, K., REZABKOVA, L., HUA, S., LIU, Q., CAPITANI, G., ALTELAAR, A. F. M., HECK, A. J. R., KAMMERER, R. A., STEINMETZ, M. O. & AKHMANOVA, A. 2017. Microtubule minus-end regulation at spindle poles by an ASPM-katanin. *Nat Cell Biol*, 19, 480-92.
- KA, M., JUNG, E.-M., MUELLER, U. & KIM, W.-Y. 2014. MACF1 regulates the migration of pyramidal neurons via microtubule dynamics and GSK-3 signaling. *Developmental Biology*, 395, 4-18.
- KAINDL, A. M. 2014. Autosomal recessive primary microcephalies (MCPH). *Eur J Paediatr Neurol*, 18, 547-8.
- KAKINUMA, T., ICHIKAWA, H., TSUKADA, Y., NAKAMURA, T. & TOH, B.-H. 2004. Interaction between p230 and MACF1 is associated with transport of a glycosyl phosphatidyl inositol-anchored protein from the Golgi to the cell periphery. *Experimental cell research*, 298, 388-398.
- KANDEL, E. R., SCHWARTZ, J. H., JESSELL, T. M., DEPARTMENT OF BIOCHEMISTRY AND MOLECULAR BIOPHYSICS THOMAS, J.,

- SIEGELBAUM, S. & HUDSPETH, A. J. 2000. *Principles of neural science*, McGraw-hill New York.
- KATO, M. & DOBYNS, W. B. 2003. Lissencephaly and the molecular basis of neuronal migration. *Human Molecular Genetics*, 12, R89-R96.
- KATO, T. A., OKAYASU, R., JEGGO, P. A. & FUJIMORI, A. 2011. ASPM influences DNA double-strand break repair and represents a potential target for radiotherapy. *Int J Radiat Biol*, 87, 1189-95.
- KATOH, M. & KATOH, M. 2004. Identification and characterization of human FCHSD1 and FCHSD2 genes in silico. *International journal of molecular medicine*, 13, 749-754.
- KELLEY, R. I., ROBINSON, D., PUFFENBERGER, E. G., STRAUSS, K. A. & MORTON, D. H. 2002. Amish lethal microcephaly: A new metabolic disorder with severe congenital microcephaly and 2-ketoglutaric aciduria. *American Journal of Medical Genetics*, 112, 318-326.
- KHAN, M. A., RUPP, V. M., ORPINELL, M., HUSSAIN, M. S., ALTMULLER, J., STEINMETZ, M. O., ENZINGER, C., THIELE, H., HOHNE, W., NURNBERG, G., BAIG, S. M., ANSAR, M., NURNBERG, P., VINCENT, J. B., SPEICHER, M. R., GONCZY, P. & WINDPASSINGER, C. 2014. A missense mutation in the PISA domain of HsSAS-6 causes autosomal recessive primary microcephaly in a large consanguineous Pakistani family. *Hum Mol Genet*, 23, 5940-9.
- KIM BT, KITAQWAH, TAMURA J, SAITO T, KUSCHE-GULLBERG M, LINDAHI U, SUQA HARAK .2001. Human tumor suppressor EXT gene family members EXTL1 and EXTL3 encode α 1, 4-N- acetylglucosaminyltransferases that likely are involved in heparan sulfate/heparin biosynthesis. ISSN 0027-8424.
- KIM, H. T., LEE, M. S., CHOI, J. H., JUNG, J. Y., AHN, D. G., YEO, S. Y., CHOI, D. K. & KIM, C. H. 2011. The microcephaly gene *aspm* is involved in brain development in zebrafish. *Biochem Biophys Res Commun*, 409, 640-4.
- KIMURA, K., CUVIER, O. & HIRANO, T. 2001. Chromosome condensation by a human condensin complex in *Xenopus* egg extracts. *J Biol Chem*, 276, 5417-20.
- KITAGAWA, D., KOHLMAIER, G., KELLER, D., STRNAD, P., BALESTRA, F. R., FLUCKIGER, I. & GONCZY, P. 2011. Spindle positioning in human cells relies on proper centriole formation and on the microcephaly proteins CPAP and STIL. *J Cell Sci*, 124, 3884-93.
- KITTLER, R., PUTZ, G., PELLETIER, L., POSER, I., HENINGER, A. K., DRECHSEL, D., FISCHER, S., KONSTANTINOVA, I., HABERMANN, B., GRABNER, H., YASPO, M. L., HIMMELBAUER, H., KORN, B., NEUGEBAUER, K., PISABARRO, M. T. & BUCHHOLZ, F. 2004. An endoribonuclease-prepared siRNA screen in human cells identifies genes essential for cell division. *Nature*, 432, 1036-40.

- KLEYLEIN-SOHN, J., WESTENDORF, J., LE CLECH, M., HABEDANCK, R., STIERHOF, Y. D. & NIGG, E. A. 2007. Plk4-induced centriole biogenesis in human cells. *Dev Cell*, 13, 190-202.
- KLOEPFER, H. W., PLATOU, R. V. & HANSCH, W. J. 1964. MANIFESTATIONS OF A RECESSIVE GENE FOR MICROCEPHALY IN A POPULATION ISOLATE. *J Genet Hum*, 13, 52-9.
- KNUST, E. & HUTTNER, W. B. 2007. Cell polarity from cell division. *Developmental cell*, 12, 664-666.
- KODAMA, A., KARAKESISOGLOU, I., WONG, E., VAEZI, A. & FUCHS, E. 2003. ACF7: An essential integrator of microtubule dynamics. *Cell*, 115, 343-354.
- KORENBAUM, E. & RIVERO, F. 2002. Calponin homology domains at a glance. *Journal of Cell Science*, 115, 3543-3545.
- KOSAKO, H., YOSHIDA, T., MATSUMURA, F., ISHIZAKI, T., NARUMIYA, S. & INAGAKI, M. 2000. Rho-kinase/ROCK is involved in cytokinesis through the phosphorylation of myosin light chain and not ezrin/radixin/moesin proteins at the cleavage furrow. *Oncogene*, 19, 6059.
- KOTAK, S., BUSSO, C. & GONCZY, P. 2012. Cortical dynein is critical for proper spindle positioning in human cells. *J Cell Biol*, 199, 97-110.
- KOUPRINA, N., PAVLICEK, A., COLLINS, N. K., NAKANO, M., NOSKOV, V. N., OHZEKI, J. I., MOCHIDA, G. H., RISINGER, J. I., GOLDSMITH, P., GUNSIOR, M., SOLOMON, G., GERSCH, W., KIM, J. H., BARRETT, J. C., WALSH, C. A., JURKA, J., MASUMOTO, H. & LARIONOV, V. 2005. The microcephaly ASPM gene is expressed in proliferating tissues and encodes for a mitotic spindle protein. *Human Molecular Genetics*, 14, 2155-2165.
- KOUPRINA, N., PAVLICEK, A., MOCHIDA, G. H., SOLOMON, G., GERSCH, W., YOON, Y. H., COLLURA, R., RUVOLO, M., BARRETT, J. C., WOODS, C. G., WALSH, C. A., JURKA, J. & LARIONOV, V. 2004. Accelerated evolution of the ASPM gene controlling brain size begins prior to human brain expansion. *Plos Biology*, 2, 653-663.
- KOUSAR, R., HASSAN, M. J., KHAN, B., BASIT, S., MAHMOOD, S., MIR, A., AHMAD, W. & ANSAR, M. 2011. Mutations in WDR62 gene in Pakistani families with autosomal recessive primary microcephaly. *BMC Neurol*, 11, 119.
- KUMAR, A., BLANTON, S. H., BABU, M., MARKANDAYA, M. & GIRIMAJI, S. C. 2004. Genetic analysis of primary microcephaly in Indian families: novel ASPM mutations. *Clin Genet*, 66, 341-8.
- KUMAR, A., GIRIMAJI, S. C., DUVVARI, M. R. & BLANTON, S. H. 2009. Mutations in STIL, encoding a pericentriolar and centrosomal protein, cause primary microcephaly. *Am J Hum Genet*, 84, 286-90.
- LA TORRE, NIQRO G, MAZZOCCOM, BEST AM, ADLER SP. 2006. Placental enlargement in women with primary maternal cytomegalovirus infection is

associated with fetal and neonatal disease. *Clinical Infectious Diseases*,
ISSN 1537-6591

- LEAL, G. F., ROBERTS, E., SILVA, E. O., COSTA, S. M., HAMPSHIRE, D. J. & WOODS, C. G. 2003. A novel locus for autosomal recessive primary microcephaly (MCPH6) maps to 13q12.2. *J Med Genet*, 40, 540-2.
- LECHLER, T. & FUCHS, E. 2005. Asymmetric cell divisions promote stratification and differentiation of mammalian skin. *Nature*, 437, 275-80.
- LEE, M., CHANG, J., CHANG, S., LEE, K. S. & RHEE, K. 2014. Asymmetric spindle pole formation in CPAP-depleted mitotic cells. *Biochem Biophys Res Commun*, 444, 644-50.
- LEIBOVITZ, Z., DANIEL-SPIEGEL, E., MALINGER, G., HARATZ, K., TAMARKIN, M., GINDES, L., SCHREIBER, L., BEN-SIRA, L., LEV, D. & SHAPIRO, I. 2016. Prediction of microcephaly at birth using three reference ranges for fetal head circumference: can we improve prenatal diagnosis? *Ultrasound in Obstetrics & Gynecology*, 47, 586-592.
- LETARD, P., DRUNAT, S., VIAL, Y., DUERINCKX, S., ERNAULT, A., AMRAM, D., ARPIN, S., BERTOLI, M., BUSA, T., CEULEMANS, B., DESIR, J., DOCOFENZY, M., ELALAOU, S. C., DEVRIENDT, K., FAIVRE, L., FRANCANNET, C., GENEVIEVE, D., GERARD, M., GITIAUX, C., JULIA, S., LEBON, S., LUBALA, T., MATHIEU-DRAMARD, M., MAUREY, H., METREAU, J., NASSEREREDDINE, S., NIZON, M., PIERQUIN, G., POUVREAU, N., RIVIER-RINGENBACH, C., ROSSI, M., SCHAEFER, E., SEFIANI, A., SIGAUDY, S., SZNAJER, Y., TUNCA, Y., GUILMIN CREPON, S., ALBERTI, C., ELMALEH-BERGES, M., BENZACKEN, B., WOLLNICK, B., WOODS, C. G., RAUCH, A., ABRAMOWICZ, M., EL GHOZZI, V., GRESSENS, P., VERLOES, A. & PASSEMARD, S. 2018. Autosomal recessive primary microcephaly due to ASPM mutations: An update. *Hum Mutat*, 39, 319-332.
- LEUNG, C. L. 1999. Microtubule Actin Cross-Linking Factor (Macf): A Hybrid of Dystonin and Dystrophin That Can Interact with the Actin and Microtubule Cytoskeletons.
- Li H, Bielas SL, Zaki MS, Ismail S, Farfara D, Um K, Rosti RO, Scott EC, Tu S, Chi NC, Gabriel S, Erson-Omay EZ, Ercan-Sencicek AG, Yasuno K, Çağlayan AO, Kaymakçalan H, Ekici B, Bilguvar K6, Gunel M, Gleeson JG. 2016', Biallelic Mutations in Citron Kinase Link Mitotic Cytokinesis to Human Primary Microcephaly. *Am J Hum Genet*. (2):501-10
- LI, L.; XIE, T. Li L, Xie T..2005.Stem cell niche: structure and function. *Annu Rev. Cell Dev Biol* 21: 605-631.
- LI R, SUN L, FANG A, LI P, WU Q, WANGX. 2017. Recapitulating cortical development with organoid culture in vitro and modeling abnormal spindle-like (ASPM related primary) microcephaly disease. *Protein Cell*. 823-833

- LIN, C. M., CHEN, H. J., LEUNG, C. L., PARRY, D. A. & LIEM, R. K. 2005a. Microtubule actin crosslinking factor 1b: a novel plakin that localizes to the Golgi complex. *J Cell Sci*, 118, 3727-38.
- LIN, S. Y., PAN, H. W., LIU, S. H., JENG, Y. M., HU, F. C., PENG, S. Y., LAI, P. L. & HSU, H. C. 2008. ASPM is a novel marker for vascular invasion, early recurrence, and poor prognosis of hepatocellular carcinoma. *Clin Cancer Res*, 14, 4814-20.
- LIN, S. Y., RAI, R., LI, K., XU, Z. X. & ELLEDGE, S. J. 2005b. BRIT1/MCPH1 is a DNA damage responsive protein that regulates the Brca1-Chk1 pathway, implicating checkpoint dysfunction in microcephaly. *Proc Natl Acad Sci U S A*, 102, 15105-9.
- LIN, Y. C., CHIANG, T. C., LIU, Y. T., TSAI, Y. T., JANG, L. T. & LEE, F. J. 2011. ARL4A acts with GCC185 to modulate Golgi complex organization. *J Cell Sci*, 124, 4014-26.
- LIZARRAGA, S. B., MARGOSSIAN, S. P., HARRIS, M. H., CAMPAGNA, D. R., HAN, A.-P., BLEVINS, S., MUDBHARY, R., BARKER, J. E., WALSH, C. A. & FLEMING, M. D. 2010. Cdk5rap2 regulates centrosome function and chromosome segregation in neuronal progenitors. *Development*, 137, 1907-1917.
- LOFFLER, H., FECHTER, A., MATUSZEWSKA, M., SAFFRICH, R., MISTRİK, M., MARHOLD, J., HORNUNG, C., WESTERMANN, F., BARTEK, J. & KRAMER, A. 2011. Cep63 recruits Cdk1 to the centrosome: implications for regulation of mitotic entry, centrosome amplification, and genome maintenance. *Cancer Res*, 71, 2129-39.
- LU, B., JAN, L. & JAN, Y. N. 2000. Control of cell divisions in the nervous system: symmetry and asymmetry. *Annu Rev Neurosci*, 23, 531-56.
- LUERS, G. H., MICHELS, M., SCHWAAB, U. & FRANZ, T. 2002. Murine calmodulin binding protein 1 (Calmbp1): tissue-specific expression during development and in adult tissues. *Mechanisms of Development*, 118, 229-232.
- LYDERSEN, B. K. & PETTIJOHN, D. E. 1980. Human-specific nuclear protein that associates with the polar region of the mitotic apparatus: distribution in a human/hamster hybrid cell. *Cell*, 22, 489-99.
- MADAULE, P., EDA, M., WATANABE, N., FUJISAWA, K., MATSUOKA, T., BITO, H., ISHIZAKI, T. & NARUMIYA, S. 1998. Role of citron kinase as a target of the small GTPase Rho in cytokinesis. *Nature*, 394, 491-494.
- MADAULE, P., FURUYASHIKI, T., REID, T., ISHIZAKI, T., WATANABE, G., MORII, N. & NARUMIYA, S. 1995. A novel partner for the GTP-bound forms of rho and rac. *FEBS Lett*, 377, 243-8.

- MAHMOOD, S., AHMAD, W. & HASSAN, M. J. 2011. Autosomal recessive primary microcephaly (MCPH): clinical manifestations, genetic heterogeneity and mutation continuum. *Orphanet J Rare Dis*.
- MANNING, B. D.; CANTLEY, L. C. 2007. AKT/PKB signaling: navigating downstream. ISSN 0092-8674
- MATOV, A. et al. 2010. Analysis of microtubule dynamic instability using a plus-end growth marker. *Nat Methods*, ISSN 1548-7091
- MARTIN, C. A., MURRAY, J. E., CARROLL, P., LEITCH, A., MACKENZIE, K. J., HALACHEV, M., FETIT, A. E., KEITH, C., BICKNELL, L. S., FLUTEAU, A., GAUTIER, P., HALL, E. A., JOSS, S., SOARES, G., SILVA, J., BOBER, M. B., DUKER, A., WISE, C. A., QUIGLEY, A. J., PHADKE, S. R., WOOD, A. J., VAGNARELLI, P. & JACKSON, A. P. 2016. Mutations in genes encoding condensin complex proteins cause microcephaly through decatenation failure at mitosis. *Genes Dev*, 30, 2158-2172.
- MATSUZAKI, F. & SHITAMUKAI, A. 2015. Cell Division Modes and Cleavage Planes of Neural Progenitors during Mammalian Cortical Development. *Cold Spring Harb Perspect Biol*.
- McIntyre RE, Lakshminarasimhan Chavali P, Ismail O, Carragher DM, Sanchez-Andrade G, Forment JV, Fu B, Del Castillo Velasco-Herrera M, Edwards A, van der Weyden L, Yang F; Sanger Mouse Genetics Project, Ramirez-Solis R, Estabel J, Gallagher FA, Logan DW, Arends MJ, Tsang SH, Mahajan VB, Scudamore CL, White JK, Jackson SP, Gergely F, Adams DJ. 2012. Disruption of mouse *Cenpj*, a regulator of centriole biogenesis, phenocopies Seckel syndrome. *PLoS Genet*. e1003022
- MCKEAN PG, BAINES A, VAUGHAN S, GULL K. 2003. Gamma-tubulin functions. in the nucleation of a discrete subset of microtubules in the eukaryotic flagellum. *Curr Biol*. 598-602
- MERDES, A., RAMYAR, K., VECHIO, J. D. & CLEVELAND, D. W. 1996. A complex of NuMA and cytoplasmic dynein is essential for mitotic spindle assembly. *Cell*, 87, 447-58.
- MI, Y., SUN, C., WEI, B., SUN, F., GUO, Y., HU, Q., DING, W., ZHU, L. & XIA, G. 2018. Coatamer subunit beta 2 (COPB2), identified by label-free quantitative proteomics, regulates cell proliferation and apoptosis in human prostate carcinoma cells. *Biochem Biophys Res Commun*, 495, 473-480.
- MING, G. & SONG, H. 2011. Adult Neurogenesis in the Mammalian Brain: Significant Answers and Significant Questions. *Neuron*, 70, 687-702.
- MOCHIDA, G. H.; PODURI, A.; WALSH, C. A. Genetic disorders of cerebral cortical development. *Emery and Rimoin's Essential Medical Genetics*, 1184, p. 438, 2013.
- MOOG, U. T. E., SMEETS, E. E. J., VAN ROOZENDAAL, K. E. P., SCHOENMAKERS, S., HERBERGS, J., SCHOONBROOD-LENSSEN, A. M. J. & SCHRANDER-STUMPEL, C. T. 2003. Neurodevelopmental

- disorders in males related to the gene causing Rett syndrome in females (MECP2). *European Journal of Paediatric Neurology*, 7, 5-12.
- MORALES-MULIA, S. & SCHOLEY, J. M. 2005. Spindle pole organization in *Drosophila* S2 cells by dynein, abnormal spindle protein (Asp), and KLP10A. *Mol Biol Cell*, 16, 3176-86.
- MOYNIHAN, L., JACKSON, A. P., ROBERTS, E., KARBANI, G., LEWIS, I., CORRY, P., TURNER, G., MUELLER, R. F., LENCH, N. J. & WOODS, C. G. 2000. A third novel locus for primary autosomal recessive microcephaly maps to chromosome 9q34. *Am J Hum Genet*, 66, 724-7.
- MOFFAT JJ,KA M, JUNG EM, SMITH AL, KIM WY,2017. The role of MACF1 in nervous system development and maintenance. *Semin Cell Dev Biol*.
- MUNRO, S. & NICHOLS, B. J. 1999. The GRIP domain - a novel Golgi-targeting domain found in several coiled-coil proteins. *Curr Biol*, 9, 377-80.
- NAIM, V., IMARISIO, S., DI CUNTO, F., GATTI, M. & BONACCORSI, S. 2004. *Drosophila* Citron Kinase Is Required for the Final Steps of Cytokinesis. In: GOLDSTEIN, L. (ed.) *Mol Biol Cell*.
- NAVEED, M., KAZMI, S. K., AMIN, M., ASIF, Z., ISLAM, U., SHAHID, K. & TEHREEM, S. 2018. Comprehensive review on the molecular genetics of autosomal recessive primary microcephaly (MCPH). *Genetics research*, 100.
- NICHOLAS, A. K., KHURSHID, M., DESIR, J., CARVALHO, O. P., COX, J. J., THORNTON, G., KAUSAR, R., ANSAR, M., AHMAD, W., VERLOES, A., PASSEMARD, S., MISSON, J. P., LINDSAY, S., GERGELY, F., DOBYNS, W. B., ROBERTS, E., ABRAMOWICZ, M. & WOODS, C. G. 2010. WDR62 is associated with the spindle pole and is mutated in human microcephaly. *Nat Genet*, 42, 1010-4.
- NICHOLAS, A. K., SWANSON, E. A., COX, J. J., KARBANI, G., MALIK, S., SPRINGELL, K., HAMPSHIRE, D., AHMED, M., BOND, J., DI BENEDETTO, D., FICHERA, M., ROMANO, C., DOBYNS, W. B. & WOODS, C. G. 2009. The molecular landscape of ASPM mutations in primary microcephaly. *Journal of Medical Genetics*, 46, 249-253.
- NIEUWENHUYNS, R.; HANS, J.; NICHOLSON, C.2014. The central nervous system of vertebrates. ISBN 3642182623.
- NOATYNSKA, A., GOTTA, M. & MERALDI, P. 2012. Mitotic spindle (DIS)orientation and DISease: cause or consequence? *J Cell Biol*, 199, 1025-35.
- NOVOROL, C., BURKHARDT, J., WOOD, K. J., IQBAL, A., ROQUE, C., COUTTS, N., ALMEIDA, A. D., HE, J., WILKINSON, C. J. & HARRIS, W. A. 2013. Microcephaly models in the developing zebrafish retinal neuroepithelium point to an underlying defect in metaphase progression. *Open Biol*, 3, 130065.

- ODE, H., MATSUYAMA, S., HATA, M., NEYA, S., KAKIZAWA, J., SUGIURA, W. & HOSHINO, T. 2007. Computational characterization of structural role of the non-active site mutation M36I of human immunodeficiency virus type 1 protease. *J Mol Biol*, 370, 598-607
- O'DRISCOLL, M., JACKSON, A. P. & JEGGO, P. A. 2006. Microcephalin: a causal link between impaired damage response signalling and microcephaly. *Cell Cycle*, 5, 2339-44.
- ODE, H., MATSUYAMA, S., HATA, M., NEYA, S., KAKIZAWA, J., SUGIURA, W. & HOSHINO, T. 2007. Computational characterization of structural role of the non-active site mutation M36I of human immunodeficiency virus type 1 protease. *J Mol Biol*, 370, 598-607.
- OHSHIMA, S. 2008. Abnormal mitosis in hypertetraploid cells causes aberrant nuclear morphology in association with H₂O₂-induced premature senescence. *Cytometry A*, 73, 808-15.
- OHTA, T., ESSNER, R., RYU, J. H., PALAZZO, R. E., UETAKE, Y. & KURIYAMA, R. 2002. Characterization of Cep135, a novel coiled-coil centrosomal protein involved in microtubule organization in mammalian cells. *J Cell Biol*, 156, 87-99.
- ONO, T., LOSADA, A., HIRANO, M., MYERS, M. P., NEUWALD, A. F. & HIRANO, T. 2003. Differential contributions of condensin I and condensin II to mitotic chromosome architecture in vertebrate cells. *Cell*, 115, 109-21.
- OPITZ, J. M. & HOLT, M. C. 1990. Microcephaly: general considerations and aids to nosology. *J Craniofac Genet Dev Biol*, 10, 175-204.
- PAI, V. C., HSU, C.-C., CHAN, T.-S., LIAO, W.-Y., CHUU, C.-P., CHEN, W.-Y., LI, C.-R., LIN, C.-Y., HWANG, S.-P., CHEN, L.-T. & TSAI, K. K. 2018. ASPM promotes prostate cancer stemness and progression by augmenting Wnt–Dvl-3– β -catenin signaling. *Oncogene*.
- PALASTANGA, N. P.; FIELD, D.; SOAMES, R. 2006. *Anatomy and Human Movement: Structure and Function*. 5th. London: Butterworth Heinemann Inc, 717 ISBN 0-7506-8814-9.
- PANCHAUD, A., STOJANOV, M., AMMERDORFFER, A., VOUGA, M. & BAUD, D. 2016. Emerging Role of Zika Virus in Adverse Fetal and Neonatal Outcomes. *Clin Microbiol Rev*. 1752 N St., N.W., Washington, DC.
- PAPARI, E., BASTAMI, M., FARHADI, A., ABEDINI, S. S., HOSSEINI, M., BAHMAN, I., MOHSENI, M., GARSHASBI, M., MOHEB, L. A., BEHJATI, F., KAHRIZI, K., ROPERS, H. H. & NAJMABADI, H. 2013. Investigation of primary microcephaly in Bushehr province of Iran: novel STIL and ASPM mutations. *Clin Genet*, 83, 488-90.

- PARAMASIVAM, M., CHANG, Y. J. & LOTURCO, J. J. 2007. ASPM and citron kinase co-localize to the midbody ring during cytokinesis. *Cell Cycle*, 6, 1605-1612.
- PARENT, J.-S., JAUVION, V., BOUCHÉ, N., BÉCLIN, C., HACHET, M., ZYTNICKI, M. & VAUCHERET, H. 2015. Post-transcriptional gene silencing triggered by sense transgenes involves uncapped antisense RNA and differs from silencing intentionally triggered by antisense transgenes. *Nucleic acids research*, 43, 8464-8475
- PARIDAEN, J. & HUTTNER, W. B. 2014. Neurogenesis during development of the vertebrate central nervous system. *EMBO Rep*, 15, 351-64.
- PASCUAL, J. M., WANG, D., LECUMBERRI, B., YANG, H., MAO, X., YANG, R. & DE VIVO, D. C. 2004. GLUT1 deficiency and other glucose transporter diseases. *Eur J Endocrinol*, 150, 627-33.
- PASSEMARD, S., KAINDL, A. M. & VERLOES, A. 2013. Microcephaly. *Handb Clin Neurol*, 111, 129-41.
- PATTISON, L., CROW, Y. J., DEEBLE, V. J., JACKSON, A. P., JAFRI, H., RASHID, Y., ROBERTS, E. & WOODS, C. G. 2000a. A fifth locus for primary autosomal recessive microcephaly maps to chromosome 1q31. *Am J Hum Genet*, 67, 1578-80.
- PATTISON, L., CROW, Y. J., DEEBLE, V. J., JACKSON, A. P., JAFRI, H., RASHID, Y., ROBERTS, E. & WOODS, C. G. 2000b. A fifth locus for primary autosomal recessive microcephaly maps to chromosome 1q31. *American Journal of Human Genetics*, 67, 1578-1580.
- PAWLOWSKI, A., RIEDEL, K. U., KLIPP, W., DREISKEMPER, P., GROß, S., BIERHOFF, H., DREPPER, T. & MASEPOHL, B. 2003. Yeast Two-Hybrid Studies on Interaction of Proteins Involved in Regulation of Nitrogen Fixation in the Phototrophic Bacterium *Rhodobacter capsulatus*. *J Bacteriol*.
- PENG, G., YIM, E. K., DAI, H., JACKSON, A. P., BURGT, I., PAN, M. R., HU, R., LI, K. & LIN, S. Y. 2009. BRIT1/MCPH1 links chromatin remodelling to DNA damage response. *Nat Cell Biol*, 11, 865-72.
- PICHON, B., VANKERCKHOVE, S., BOURROUILLOU, G., DUPREZ, L. & ABRAMOWICZ, M. J. 2004. A translocation breakpoint disrupts the ASPM gene in a patient with primary microcephaly. *Eur J Hum Genet*, 12, 419-21.
- PILZ, D. T., KUC, J., MATSUMOTO, N., BODURTHA, J., BERNADI, B., TASSINARI, C. A., DOBYNS, W. B. & LEDBETTER, D. H. 1999. Subcortical band heterotopia in rare affected males can be caused by missense mutations in DCX (XLIS) or LIS1. *Hum Mol Genet*, 8, 1757-60.
- POLIAKOVA, K., ADEBOLA, A., LEUNG, C. L., FAVRE, B., LIEM, R. K. H., SCHEPENS, I. & BORRADORI, L. 2014. BPAG1a and b Associate with EB1 and EB3 and Modulate Vesicular Transport, Golgi Apparatus Structure, and Cell Migration in C2.7 Myoblasts. *PLOS ONE*, 9, e107535.

- PORTEGIJS V, FIELMICH LE, GALLI M, SCHMIDTR, Muñoz J, van Mourik T, Akhmanova A, Heck AJ, Boxem M, van den Heuvel S. 2016. Multisite Phosphorylation of NuMA-Related LIN-5 Controls Mitotic Spindle Positioning in *C. elegans*. *PLoS genetics*, ISSN 1553-7404.
- PONTING, C. P. 2006. A novel domain suggests a ciliary function for ASPM, a brain size determining gene. *Bioinformatics*, ISSN 1460-2059.
- PULVERS, J. N., BRYK, J., FISH, J. L., WILSCH-BRÄUNINGER, M., ARAI, Y., SCHREIER, D., NAUMANN, R., HELPPI, J., HABERMANN, B., VOGT, J., NITSCH, R., TÓTH, A., ENARD, W., PÄÄBO, S. & HUTTNER, W. B. 2010. Mutations in mouse *Aspm* (abnormal spindle-like microcephaly associated) cause not only microcephaly but also major defects in the germline. *Proceedings of the National Academy of Sciences*, 107, 16595.
- PULVERS, J. N., JOURNIAC, N., ARAI, Y. & NARDELLI, J. 2015. MCPH1: a window into brain development and evolution. *Front Cell Neurosci*, 9.
- QAZI, Q. H. & REED, T. E. 1973. A problem in diagnosis of primary versus secondary microcephaly. *Clin Genet*, 4, 46-52.
- RAGKOUSI, K.; GIBSON, M. C. 2014. Cell division and the maintenance of epithelial order. *J Cell Biol*, ISSN 0021-9525.
- RAO, V. S., SRINIVAS, K., SUJINI, G. N. & KUMAR, G. N. S. 2014. Protein-Protein Interaction Detection: Methods and Analysis. *Int J Proteomics*, 2014.
- REILING, J. H., CLISH, C. B., CARETTE, J. E., VARADARAJAN, M., BRUMMELKAMP, T. R. & SABATINI, D. M. 2011. A haploid genetic screen identifies the major facilitator domain containing 2A (MFSD2A) transporter as a key mediator in the response to tunicamycin. *Proc Natl Acad Sci U S A*, 108, 11756-65.
- RHOADS, A. & KENGUELE, H. 2005. Expression of IQ-motif genes in human cells and ASPM domain structure. *Ethnicity & Disease*, 15, S88-S91.
- RIPARBELLI, M. G., CALLAINI, G., GLOVER, D. M. & AVIDES MDO, C. 2002. A requirement for the Abnormal Spindle protein to organise microtubules of the central spindle for cytokinesis in *Drosophila*. *J Cell Sci*, 115, 913-22.
- RIPOLL, P., PIMPINELLI, S., VALDIVIA, M. M. & AVILA, J. 1985. A cell division mutant of *Drosophila* with a functionally abnormal spindle. *Cell*, 41, 907-12.
- ROBERTS, E., HAMPSHIRE, D. J., PATTISON, L., SPRINGELL, K., JAFRI, H., CORRY, P., MANNON, J., RASHID, Y., CROW, Y., BOND, J. & WOODS, C. G. 2002. Autosomal recessive primary microcephaly: an analysis of locus heterogeneity and phenotypic variation. *Journal of Medical Genetics*, 39, 718-721.
- ROLLS, M. M., ALBERTSON, R., SHIH, H. P., LEE, C. Y. & DOE, C. Q. 2003. *Drosophila* aPKC regulates cell polarity and cell proliferation in neuroblasts and epithelia. *J Cell Biol*, 163, 1089-98.

- ROPER, K., GREGORY, S. L. & BROWN, N. H. 2002. The 'spectraplakins': cytoskeletal giants with characteristics of both spectrin and plakin families. *J Cell Sci*, 115, 4215-25.
- ROQUE, H., WAINMAN, A., RICHENS, J., KOZYRSKA, K., FRANZ, A. & RAFF, J. W. 2012. Drosophila Cep135/Bld10 maintains proper centriole structure but is dispensable for cartwheel formation. *J Cell Sci*, 125, 5881-6.
- ROSENBERG, M. J., AGARWALA, R., BOUFFARD, G., DAVIS, J., FIERMONTE, G., HILLIARD, M. S., KOCH, T., KALIKIN, L. M., MAKALOWSKA, I., MORTON, D. H., PETTY, E. M., WEBER, J. L., PALMIERI, F., KELLEY, R. I., SCHAFFER, A. A. & BIESECKER, L. G. 2002. Mutant deoxynucleotide carrier is associated with congenital microcephaly. *Nat Genet*, 32, 175-9.
- SAAR, K., CHRZANOWSKA, K. H., STUMM, M., JUNG, M., NURNBERG, G., WIENKER, T. F., SEEMANOVA, E., WEGNER, R. D., REIS, A. & SPERLING, K. 1997. The gene for the ataxia-telangiectasia variant, Nijmegen breakage syndrome, maps to a 1-cM interval on chromosome 8q21. *Am J Hum Genet*, 60, 605-10.
- SAJID HUSSAIN, M., MARRIAM BAKHTIAR, S., FAROOQ, M., ANJUM, I., JANZEN, E., REZA TOLIAT, M., EIBERG, H., KJAER, K. W., TOMMERUP, N., NOEGEL, A. A., NURNBERG, P., BAIG, S. M. & HANSEN, L. 2013. Genetic heterogeneity in Pakistani microcephaly families. *Clin Genet*, 83, 446-51.
- SARKISIAN, M. R., LI, W., DI CUNTO, F., D'MELLO, S. R. & LOTURCO, J. J. 2002. Citron-Kinase, A Protein Essential to Cytokinesis in Neuronal Progenitors, Is Deleted in the Flathead Mutant Rat. *Journal of Neuroscience*, 22, RC217-RC217.
- SANTORO A, VIACHOU T, CARMINATI M, PELICCI PG, MAPELLI M. 2016. Molecular mechanisms of asymmetric divisions in mammary stem cells. *EMBO Rep*, ISSN 1469-221X
- SAUNDERS, R. D., AVIDES, M. C., HOWARD, T., GONZALEZ, C. & GLOVER, D. M. 1997. The Drosophila gene abnormal spindle encodes a novel microtubule-associated protein that associates with the polar regions of the mitotic spindle. *J Cell Biol*, 137, 881-90.
- SCHMIDT, T. I., KLEYLEIN-SOHN, J., WESTENDORF, J., LE CLECH, M., LAVOIE, S. B., STIERHOF, Y. D. & NIGG, E. A. 2009. Control of centriole length by CPAP and CP110. *Curr Biol*, 19, 1005-11.
- SCHMIESING, J. A., GREGSON, H. C., ZHOU, S. & YOKOMORI, K. 2000. A human condensin complex containing hCAP-C-hCAP-E and CNAP1, a homolog of Xenopus XCAP-D2, colocalizes with phosphorylated histone H3 during the early stage of mitotic chromosome condensation. *Mol Cell Biol*, 20, 6996-7006.

- SCHOU KB, MORTHORST SK, CHIRSTENSEN ST, PEDERSEN LB. 2014. Identification of conserved, centrosome-targeting ASH domains in TRAPP II complex subunits and TRAPPC8. *Cilia*, 2014, 25:30-36.
- SCHNEIDER, C. A., RASBAND, W. S. & ELICEIRI, K. W. 2012. NIH Image to ImageJ: 25 years of image analysis. *Nat Methods*, 9, 671-5.
- SCHOBORG, T., ZAJAC, A. L., FAGERSTROM, C. J., GUILLEN, R. X. & RUSAN, N. M. 2015. An Asp-CaM complex is required for centrosome-pole cohesion and centrosome inheritance in neural stem cells. *J Cell Biol*, 211, 987-98.
- SELDIN, L., POULSON, N. D., FOOTE, H. P. & LECHLER, T. 2013. NuMA localization, stability, and function in spindle orientation involve 4.1 and Cdk1 interactions. *Mol Biol Cell*, 24, 3651-62.
- SHEN, J., EYAD, W., MOCHIDA, G. H., AL-MOAYYAD, F., BODELL, A., WOODS, C. G. & WALSH, C. A. 2005. ASPM mutations identified in patients with primary microcephaly and seizures. *J Med Genet*. England.
- SHI, L., LI, M. & SU, B. 2012. MCPH1/BRIT1 represses transcription of the human telomerase reverse transcriptase gene. *Gene*, 495, 1-9.
- SHUBBAR, E., KOVÁCS, A., HAJIZADEH, S., PARRIS, T. Z., NEMES, S., GUNNARSDÓTTIR, K., EINBEIGI, Z., KARLSSON, P. & HELOU, K. 2013. Elevated cyclin B2 expression in invasive breast carcinoma is associated with unfavorable clinical outcome. *BMC Cancer*, 13, 1.
- SIDMAN, R. L.; RAKIC, P. 1973. Neuronal migration, with special reference to developing human brain: a review. *Brain research*, ISSN 0006-8993.
- SILK, A. D., HOLLAND, A. J. & CLEVELAND, D. W. 2009. Requirements for NuMA in maintenance and establishment of mammalian spindle poles. *J Cell Biol*.
- SINGHMAR, P. & KUMAR, A. 2011. Angelman syndrome protein UBE3A interacts with primary microcephaly protein ASPM, localizes to centrosomes and regulates chromosome segregation. *PLoS One*, 6, e20397.
- SIR, J. H., BARR, A. R., NICHOLAS, A. K., CARVALHO, O. P., KHURSHID, M., SOSSICK, A., REICHEL, S., D'SANTOS, C., WOODS, C. G. & GERGELY, F. 2011. A primary microcephaly protein complex forms a ring around parental centrioles. *Nat Genet*, 43, 1147-53.
- SMITH, T. C., FANG, Z. & LUNA, E. J. 2010. Novel interactors and a role for supervillin in early cytokinesis. *Cytoskeleton (Hoboken)*, 67, 346-64.
- SONNEN, K. F., GABRYJONCZYK, A. M., ANSELM, E., STIERHOF, Y. D. & NIGG, E. A. 2013. Human Cep192 and Cep152 cooperate in Plk4 recruitment and centriole duplication. *J Cell Sci*, 126, 3223-33.
- SPORNY, M., GUEZ-HADDAD, J., KREUSCH, A., SHAKARTZI, S., NEZNANSKY, A., CROSS, A., ISUPOV, M. N., QUALMANN, B., KESSELS, M. M. & OPATOWSKY, Y. 2017. Structural History of Human SRGAP2 Proteins. *Molecular Biology and Evolution*, 34, 1463-1478.

- STYNEN, B., TOURNU, H., TAVERNIER, J. & VAN DIJCK, P. 2012. Diversity in Genetic In Vivo Methods for Protein-Protein Interaction Studies: from the Yeast Two-Hybrid System to the Mammalian Split-Luciferase System. *Microbiol Mol Biol Rev.* 1752 N St., N.W., Washington, DC.
- SUMIYOSHI, E. & SUGIMOTO, A. 2012. Cell Polarity: Centrosomes Release Signals for Polarization. *Current Biology*, 22, R281-R283.
- SUN, Q. Y. & SCHATTEN, H. 2006. Role of NuMA in vertebrate cells: review of an intriguing multifunctional protein. *Front Biosci*, 11, 1137-46.
- TANG, C. J., LIN, S. Y., HSU, W. B., LIN, Y. N., WU, C. T., LIN, Y. C., CHANG, C. W., WU, K. S. & TANG, T. K. 2011. The human microcephaly protein STIL interacts with CPAP and is required for procentriole formation. *EMBO J*, 30, 4790-804.
- TEWARI, R., BAILES, E., BUNTING, K. A. & COATES, J. C. 2010. Armadillo-repeat protein functions: questions for little creatures. *Trends Cell Biol*, 20, 470-81.
- TIEDE, S., CANTZ, M., SPRANGER, J. & BRAULKE, T. 2006. Missense mutation in the N-acetylglucosamine-1-phosphotransferase gene (GNPTA) in a patient with mucopolipidosis II induces changes in the size and cellular distribution of GNPTG. *Hum Mutat*, 27, 830-1.
- TILLEMENT, V., REMY, M. H., RAYNAUD-MESSINA, B., MAZZOLINI, L., HAREN, L. & MERDES, A. 2009. Spindle assembly defects leading to the formation of a monopolar mitotic apparatus. *Biol Cell*, 101, 1-11.
- TRIMBORN, M., BELL, S. M., FELIX, C., RASHID, Y., JAFRI, H., GRIFFITHS, P. D., NEUMANN, L. M., KREBS, A., REIS, A., SPERLING, K., NEITZEL, H. & JACKSON, A. P. 2004. Mutations in microcephalin cause aberrant regulation of chromosome condensation. *Am J Hum Genet*, 75, 261-6.
- TUNGADI, E. A., ITO, A., KIYOMITSU, T. & GOSHIMA, G. 2017. Human microcephaly ASPM protein is a spindle pole-focusing factor that functions redundantly with CDK5RAP2. *J Cell Sci*, 130, 3676-3684.
- TWEEDELL, K. S. 2017. The Adaptability of Somatic Stem Cells: A Review. *J Stem Cells Regen Med*.
- URBÁN, N. & GUILLEMOT, F. 2014. Neurogenesis in the embryonic and adult brain: same regulators, different roles. *Front Cell Neurosci*, 8.
- UZQUIANO, A., GLADWYN-NG, I., NGUYEN, L., REINER, O., GÖTZ, M., MATSUZAKI, F. & FRANCIS, F. 2018. Cortical progenitor biology: key features mediating proliferation versus differentiation. *Journal of Neurochemistry*, 0.
- VAN DER VOET, M., BERENDS, C. W., PERREAULT, A., NGUYEN-NGOC, T., GONCZY, P., VIDAL, M., BOXEM, M. & VAN DEN HEUVEL, S. 2009. NuMA-related LIN-5, ASPM-1, calmodulin and dynein promote meiotic

- spindle rotation independently of cortical LIN-5/GPR/Galpha. *Nat Cell Biol*, 11, 269-77.
- VERDIER, P.; MORTHORST, S. K.; PEDERSEN, L. B. 2016. Targeting of ASH Domain-Containing Proteins to the Centrosome. ISSN 1064-3745.
- VERLOES, A., DRUNAT, S., GRESSENS, P. & PASSEMARD, S. 2013. Primary autosomal recessive microcephalies and Seckel syndrome spectrum disorders.
- VERSTRAETEN, V., PECKHAM, L. A., OLIVE, M., CAPELL, B. C., COLLINS, F. S., NABEL, E. G., YOUNG, S. G., FONG, L. G. & LAMMERDING, J. 2011. Protein farnesylation inhibitors cause donut-shaped cell nuclei attributable to a centrosome separation defect. *Proc Natl Acad Sci U S A*
- VERMEULEN, R. J., WILKE, M., HORBER, V. & KRAGELOH-MANN, I. 2010. Microcephaly with simplified gyral pattern: MRI classification. *Neurology*, 74, 386-91.
- VINKEN, P. & BRUYN, G. 1969. Handbook of clinical neurology.
- WAKEFIELD, J. G., BONACCORSI, S. & GATTI, M. 2001. The drosophila protein asp is involved in microtubule organization during spindle formation and cytokinesis. *J Cell Biol*, 153, 637-48.
- WALSH, C. A. 1999. Genetic malformations of the human cerebral cortex. *Neuron*, 23, 19-29.
- WANG, D., KRANZ-EBLE, P. & DE VIVO, D. C. 2000. Mutational analysis of GLUT1 (SLC2A1) in Glut-1 deficiency syndrome. *Human Mutation*, 16, 224-231.
- WANG, F., WANG, R., LI, Q., QU, X., HAO, Y., YANG, J., ZHAO, H., WANG, Q., LI, G., ZHANG, F., ZHANG, H., ZHOU, X., PENG, X., BIAN, Y. & XIAO, W. 2017. A transcriptome profile in hepatocellular carcinomas based on integrated analysis of microarray studies. *Diagn Pathol*. London.
- WATANABE, S., DE ZAN, T., ISHIZAKI, T. & NARUMIYA, S. 2013. Citron kinase mediates transition from constriction to abscission through its coiled-coil domain. *J Cell Sci*, 126, 1773-84.
- WEEMAES, C. M. R., HUSTINX, T. W. J., SCHERES, J., VANMUNSTER, P. J. J., BAKKEREN, J. & TAALMAN, R. 1981. A NEW CHROMOSOMAL INSTABILITY DISORDER - THE NIJMEGEN BREAKAGE SYNDROME. *Acta Paediatrica Scandinavica*, 70, 557-564.
- WELLS, R. A., CATZAVELOS, C. & KAMEL-REID, S. 1997. Fusion of retinoic acid receptor alpha to NuMA, the nuclear mitotic apparatus protein, by a variant translocation in acute promyelocytic leukaemia. *Nat Genet*, 17, 109-13.
- WILLARDSSEN, M. I. & LINK, B. A. 2011. Cell biological regulation of division fate in vertebrate neuroepithelial cells. *Dev Dyn*, 240, 1865-79.

- WINDER, S. J. & KENDRICK-JONES, J. 1995. Calcium/calmodulin-dependent regulation of the NH₂-terminal F-actin binding domain of utrophin. *FEBS letters*, 357, 125-128.
- WINDER, S. J. & WALSH, M. P. 1993. Calponin: thin filament-linked regulation of smooth muscle contraction. *Cellular signalling*, 5, 677-686.
- WOLF, A., KEIL, R., GOTZL, O., MUN, A., SCHWARZE, K., LEDERER, M., HUTTELMAIER, S. & HATZFELD, M. 2006. The armadillo protein p0071 regulates Rho signalling during cytokinesis. *Nat Cell Biol*, 8, 1432-40.
- WOODS, C. G. 2004. Human microcephaly. *Current Opinion in Neurobiology*, 14, 112-117.
- WOODS, C. G., BOND, J. & ENARD, W. 2005. Autosomal recessive primary microcephaly (MCPH): A review of clinical, molecular, and evolutionary findings. *American Journal of Human Genetics*, 76, 717-728.
- WOOLNER, S., BRIEN, L. L., WIESE, C. & BEMENT, W. M. 2008. Myosin-10 and actin filaments are essential for mitotic spindle function. *The Journal of Cell Biology*, 182, 77.
- XIE, J.-J., ZHUO, Y.-J., ZHENG, Y., MO, R.-J., LIU, Z.-Z., LI, B.-W., CAI, Z.-D., ZHU, X.-J., LIANG, Y.-X., HE, H.-C. & ZHONG, W.-D. 2017. High expression of ASPM correlates with tumor progression and predicts poor outcome in patients with prostate cancer. *International Urology and Nephrology*, 49, 817-823.
- XING, S., WALLMERTH, N., BERENDZEN, K. W. & GREFEN, C. 2016. Techniques for the Analysis of Protein-Protein Interactions in Vivo. *Plant Physiol.*
- XU, D., ZHANG, F., WANG, Y., SUN, Y. & XU, Z. 2014. Microcephaly-associated protein WDR62 regulates neurogenesis through JNK1 in the developing neocortex. *Cell Rep*, 6, 104-16.
- XU, W., LAKSHMAN, N. & MORSHEAD, C. M. 2017. Building a central nervous system: The neural stem cell lineage revealed. *Neurogenesis (Austin)*.
- XU, X. L., MA, W., ZHU, Y. B., WANG, C., WANG, B. Y., AN, N., AN, L., LIU, Y., WU, Z. H. & TIAN, J. H. 2012. The microtubule-associated protein ASPM regulates spindle assembly and meiotic progression in mouse oocytes. *PLoS One*, 7, e49303.
- YAMAGUCHI, M. & MORI, K. 2014. Critical periods in adult neurogenesis and possible clinical utilization of new neurons. *Frontiers in Neuroscience*, 8, 177.
- YAMAMOTO, A. & SIMONSEN, A. 2011. Alfy-dependent elimination of aggregated proteins by macroautophagy: can there be too much of a good thing? *Autophagy*, 7, 346-50.

- YANG, C. H. & SNYDER, M. 1992. The nuclear-mitotic apparatus protein is important in the establishment and maintenance of the bipolar mitotic spindle apparatus. *Mol Biol Cell*, 3, 1259-67.
- YANG, Y. J., BALTUS, A. E., MATHEW, R. S., MURPHY, E. A., EVRONY, G. D., GONZALEZ, D. M., WANG, E. P., MARSHALL-WALKER, C. A., BARRY, B. J., MURN, J., TATARAKIS, A., MAHAJAN, M. A., SAMUELS, H. H., SHI, Y., GOLDEN, J. A., MAHAJNAH, M., SHENHAV, R. & WALSH, C. A. 2012. Microcephaly gene links trithorax and REST/NRSF to control neural stem cell proliferation and differentiation. *Cell*, 151, 1097-112.
- YOSHINO, A., BIELER, B. M., HARPER, D. C., COWAN, D. A., SUTTERWALA, S., GAY, D. M., COLE, N. B., MCCAFFERY, J. M. & MARKS, M. S. 2003. A role for GRIP domain proteins and/or their ligands in structure and function of the trans Golgi network. *J Cell Sci*, 116, 4441-54.
- YU, T. W., MOCHIDA, G. H., TISCHFIELD, D. J., SGAIER, S. K., FLORES-SARNAT, L., SERGI, C. M., TOPCU, M., MCDONALD, M. T., BARRY, B. J., FELIE, J. M., SUNU, C., DOBYNS, W. B., FOLKERTH, R. D., BARKOVICH, A. J. & WALSH, C. A. 2010. Mutations in WDR62, encoding a centrosome-associated protein, cause microcephaly with simplified gyri and abnormal cortical architecture. *Nat Genet*, 42, 1015-20.
- ZAQOUT, S., MORRIS-ROSENDAHL, D. & KAINDL, A. M. 2017. Autosomal Recessive Primary Microcephaly (MCPH): An Update. *Neuropediatrics*, 48, 135-142.
- ZHANG, J. 2003. Evolution of the human ASPM gene, a major determinant of brain size. *Genetics*, 165, 2063-70.
- ZHANG, S. C., LI, X. J., AUSTIN JOHNSON, M. & PANKRATZ, M. T. 2008. Human embryonic stem cells for brain repair? *Philos Trans R Soc Lond B Biol Sci*. London.
- ZHANG, X., LIU, D., LV, S., WANG, H., ZHONG, X., LIU, B., WANG, B., LIAO, J., LI, J., PFEIFER, G. P. & XU, X. 2009. CDK5RAP2 is required for spindle checkpoint function. *Cell Cycle*, 8, 1206-16.
- ZHONG, X., LIU, L., ZHAO, A., PFEIFER, G. P. & XU, X. 2005. The abnormal spindle-like, microcephaly-associated (ASPM) gene encodes a centrosomal protein. *Cell Cycle*, 4, 1227-9.
- ZHANG, Z., MITEVA, M. A., WANG, L. & ALEXOV, E. 2012. Analyzing effects of naturally occurring missense mutations. *Comput Math Methods Med*, 2012, 805827.
- ZUCCOLO, L., DEROO, L. A., WILLS, A. K., DAVEY SMITH, G., SUREN, P., ROTH, C., STOLTENBERG, C. & MAGNUS, P. 2016. Pre-conception and prenatal alcohol exposure from mothers and fathers drinking and head circumference: results from the Norwegian Mother-Child Study (MoBa). *Sci Rep*, 6.

Chapter 8 : Appendix

Appendix 1: Primary Antibodies employed in this project.

Antibody	Type	Epitope	Host Species	Clonality	Dilution for IF	Dilution for WB
ASPM 216-1	Primary	Base pairs 1117-1158 KDN YGLN QDLESESC	rabbit	polyclonal	1/2000	Not used
ASPM 217-2	Primary	PEDWRKSEVSPRIPEC	rabbit	polyclonal	1/250	1/200
GCC2	Primary	Internal region C-QKLTNKNNKIED	goat	polyclonal	Not used	1/1500
SRGAP2	Primary	Not published on website	rabbit	polyclonal	Not used	1/1000
MACF1	Primary	Amino acids 1-95	mouse	polyclonal	1/1000	1/500
β -Actin	Primary	Not published on website	mouse	monoclonal	Not used	1/2500
GST	Primary	Not published on website	mouse	polyclonal	Not used	1/500

Appendix 2: Secondary Antibodies employed in this project

Antibody	Dilution used for IF	Dilution used for WB
Polyclonal Rabbit Anti-Goat Immunoglobulins/HRP	Not used	1/2500
Polyclonal Swine Anti-Rabbit Immunoglobulins/HRP	Not used	1/2500
Polyclonal Rabbit Anti Mouse Immunoglobulins/HRP	Not used	1/2500
Alexa Fluor 488 goat anti-rabbit IgG	1/500	Not used
Alexa Fluor 594 goat anti-rat IgG	1/500	Not used
Alexa Fluor 489 Chicken anti-goat IgG	1/500	Not used
Alexa Fluor 594 donkey anti-rabbit IgG	1/500	Not used
DAPI	1/2000	Not used
Phalloidin- 488	1/1000	Not used

Appendix 3: The expression of ASPM in paraformaldehyde fixed cell.

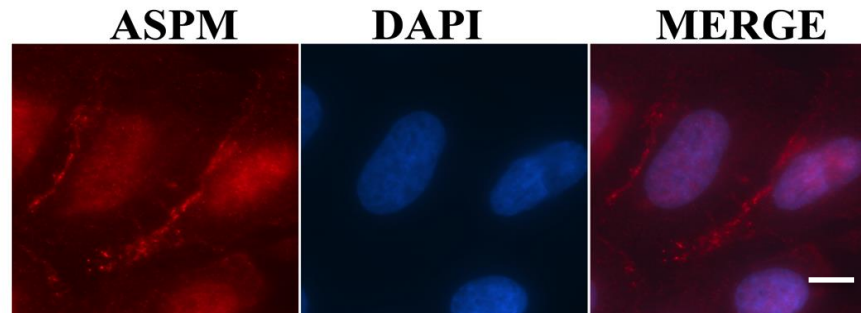


Figure 8.1: ASPM is expressed at the periphery of a proportion of PFA fixed interphase U2OS cells. ASPM 216-1P antibody is red, actin is green and DNA is stained with DAPI (blue). Scale bar = 5 μ m.(This data is unverified)

Appendix 4: Homo sapiens - abnormalspindles vs Human Fetal Brain_RP1 Results Summary.

Screen Parameters

Nature	cDNA
Reference Bait Fragment	Homo sapiens - abnormalspindles (3226-3477) ; hgx2510v1
Prey Library	Human Fetal Brain_RP1
Vector(s)	pB66 (N-GAL4-bait-C fusion)
Processed Clones	91 (pB66) + 92 (pB66)
Analyzed Interactions	20.3 millions (pB66) + 31.4 millions (pB66)
3AT Concentration	0.0 mM (pB66) + 0.0 mM (pB66)

Global PBS®
















Global PBS (for Interactions represented in the Screen)		Nb	%
A	Very high confidence in the interaction	1	1.0%
B	High confidence in the interaction	3	3.1%
C	Good confidence in the interaction	2	2.1%
D	Moderate confidence in the interaction This category is the most difficult to interpret because it mixes two classes of interactions : - False-positive interactions - Interactions hardly detectable by the Y2H technique (low representation of the mRNA in the library, prey folding, prey toxicity in yeast)	86	89.6%
E	Interactions involving highly connected prey domains, warning of non-specific interaction. The threshold for high connectivity is 10 for screens with Human, Mouse, Drosophila and Arabidopsis and 6 for all other organisms. They can be classified in different categories: - Prey proteins that are known to be highly connected due to their biological function - Proteins with a prey interacting domain that contains a known protein interaction motif or a biochemically promiscuous motif	4	4.2%
F	Experimentally proven technical artifacts	0	0.0%
Non Applicable			
N/A	The PBS is a score that is automatically computed through algorithms and cannot be attributed for the following reasons : - All the fragments of the same reference CDS are antisense - The 5p sequence is missing - All the fragments of the same reference CDS are either all OOF1 or all OOF2		

	- All the fragments of the same reference CDS lie in the 5' or 3' UTR
--	---

Prey Fragment Analysis


Symbols	Means
*	The fragment contains the full length CDS
↳	Fragment is fully in 5' UTR
↪	Fragment is fully in 3' UTR
x	Fragment contains at least one In Frame STOP codon
[NR]	Fragment was found to be non relevant (poor quality, high N density)
IF OOF1 OOF2	With regard to the theoretical frame of each corresponding CDS (GeneBank), fragments are cloned in frame (IF) if they are in the same frame as Gal4AD. In general, polypeptides synthesized from OOF fragments are not considered of biological interest, unless found together with another frame. However, some of the proteins expressed from an OOF fragment can be translated in the correct frame, due to the existence of natural frame-shift events during translation in yeast
??	Unidentified frame when : - The clone sequence is antisense - The 5p sequence is missing










N	Antisense
Start...Stop	Position of the 5p and 3p prey fragment ends, relative to the position of the ATG start codon (A=0)



Clone Name	Type Seq	Gene Name (Best Match)	Start..Stop (nt)	Frame	Sense	%Id 5p	%Id 3p	PBS
pB66_B-104	5p/3p	Homo sapiens - AHSA1	889..348	??	N	97.4	95.4	N/A
pB66_B-149	5p/3p	Homo sapiens - AKAP9	6730..5540	??	N	100.0	75.0	N/A
pB66_B-155	5p/3p	Homo sapiens - APBB2	1719..2630  	IF		97.6	97.1	N/A
pB66_A-40	5p/3p	Homo sapiens - ATRX	8927..9309  	OOF2		96.9	96.9	N/A
pB66_B-146	5p/3p	Homo sapiens - ATRX	8927..9309  	OOF2		96.9	96.9	N/A
pB66_A-7	5p/3p	Homo sapiens - ATRX	8927..9309  	OOF2		96.9	96.9	N/A
pB66_B-147	5p/3p	Homo sapiens - ATRX	8927..9309  	OOF2		96.9	96.9	N/A
pB66_A-52	5p/3p	Homo sapiens - BACH2	1716..2161	IF		99.8	89.0	
pB66_A-77	5p/3p	Homo sapiens - BITE	993..2154 	IF		99.6	98.3	
pB66_A-9	5p/3p	Homo sapiens - C7orf60	-10..688	IF		99.3	99.6	
pB66_A-41	5p/3p	Homo sapiens - CEP170 variant beta	3495..4284	IF		98.7	98.4	









pB66_A-81	5p/3p	Homo sapiens - CEP170 variant gamma	3441..5115 ✖	IF			99.9	99.6	D
pB66_A-66	3p	Homo sapiens - CLIP2	1098..1601	IF				100.0	D
pB66_B-108	5p/3p	Homo sapiens - CLIP2	1098..1601	IF			100.0	100.0	D
pB66_B-148	3p	Homo sapiens - COG4	..1286	??				94.7	N/A
pB66_A-29	5p/3p	Homo sapiens - DIO2	3232..2679	??	N		98.7	83.8	N/A
pB66_A-93	5p/3p	Homo sapiens - DNAJC7	48..899	IF			99.7	99.1	E
pB66_A-75	5p/3p	Homo sapiens - DST	8157..10147	IF			98.5	100.0	D
pB66_A-2	5p/3p	Homo sapiens - DYNC1H1	10053..10467	IF			99.8	99.8	D
pB66_A-53	5p/3p	Homo sapiens - EB-1	219..1076	IF			97.7	96.9	D
pB66_A-44	5p/3p	Homo sapiens - EPIM	177..1019 ✖	IF			93.4	88.6	D
pB66_B-152	5p/3p	Homo sapiens - FRY	5169..6128	IF			99.6	99.1	D
pB66_A-83	5p/3p	Homo sapiens - GCC2	558..1629	IF			98.8	98.8	B
pB66_A-42	5p/3p	Homo sapiens - GCC2	1494..2334	IF			96.6	96.8	B
pB66_A-12	5p/3p	Homo sapiens - GCC2	1494..2334	IF			99.2	99.1	B
pB66_A-31	5p/3p	Homo sapiens - GCC2	1512..2352	IF			96.5	98.4	B










pB66_A-95	5p/3p	Homo sapiens - HERC2	10185..9785	??	N	100.0	100.0	N/A
-----------	-------	----------------------	-------------	----	---	-------	-------	-----















Clone Name	Type Seq	Gene Name (Best Match)	Start..Stop (nt)	Frame	Sense	%Id 5p	%Id 3p	PBS
pB66_B-113	5p/3p	Homo sapiens - HNRNPH3	1927..877	??	N	98.2	98.4	N/A
pB66_A-49	5p/3p	Homo sapiens - HNRNPH3	1927..877	??	N	98.9	98.7	N/A
pB66_B-123	5p/3p	Homo sapiens - IMAGE:5296963	1403..2138 ✖	OOF2		95.8	98.0	N/A
pB66_A-84	3p	Homo sapiens - KIAA1078	12..593	IF			99.8	D
pB66_B-25	5p/3p	Homo sapiens - KIF1A	5131..5483  ✖	OOF2		97.0	100.0	N/A
pB66_A-86	5p/3p	Homo sapiens - KIF5C	1860..2465	IF		100.0	100.0	D
pB66_B-99	5p/3p	Homo sapiens - KLHL7	2146..1198	??	N	98.7	98.2	N/A
pB66_A-76	3p	Homo sapiens - MACF1	..12545	??			99.6	D
pB66_A-90	5p/3p	Homo sapiens - MACF1	9972..10697	IF		98.8	99.7	D
pB66_A-85	5p/3p	Homo sapiens - MACF1	10851..12545	IF		99.6	99.9	D
pB66_B-93	5p/3p	Homo sapiens - MACF1	10851..12545	IF		99.5	99.9	D
pB66_A-56	5p/3p	Homo sapiens - MACF1	10851..12545	IF		98.1	98.9	D
pB66_B-45	5p/3p	Homo sapiens - MACF1	10851..12545	IF		98.1	99.3	D

pB66_A-91	5p/3p	Homo sapiens - MACF1	13377..14276		IF		98.8	98.9	D
pB66_A-19	5p/3p	Homo sapiens - MEF2C	3699..2970 		??	N	97.2	98.9	N/A
pB66_B-142	5p/3p	Homo sapiens - MEF2C	3699..2970 		??	N	94.5	99.8	N/A
pB66_B-102	5p/3p	Homo sapiens - NAA25	5158..4386 		??	N	95.2	97.8	N/A
pB66_B-110	5p/3p	Homo sapiens - NEDD9	2466..2842 		IF		98.9	99.2	E
pB66_B-35	5p/3p	Homo sapiens - NIPBL	6722..6080		??	N	99.8	99.4	N/A
pB66_A-80	5p/3p	Homo sapiens - PDCD6IP	1053..2036		IF		98.7	98.7	D
pB66_B-27	5p	Homo sapiens - PDZK4	3347 		??	N	97.8		N/A
pB66_A-27	5p/3p	Homo sapiens - PDZK4	3347..2986 		??	N	100.0	100.0	N/A
pB66_B-137	5p/3p	Homo sapiens - PRO1633	-604..-1284 		??	N	96.6	98.3	N/A
pB66_A-37	5p/3p	Homo sapiens - PRPF31	772..441		??	N	100.0	100.0	N/A
pB66_A-69	5p/3p	Homo sapiens - PTPRD	4671..5382  		IF		98.8	99.5	N/A
pB66_A-4	5p/3p	Homo sapiens - Proteic Match 60S ribosomal protein L19	1015..-9		??	N	97.9	98.9	N/A
pB66_B-141	5p/3p	Homo sapiens - Proteic Match 60S ribosomal protein L19	1015..-9		??	N	97.8	97.9	N/A

pB66_A-24	5p/3p	Homo sapiens - Proteic Match RecName: Full=Putative uncharacterized protein LOC65996	-6..205	✘	OOF1		100.0	100.0	N/A
pB66_A-70	5p/3p	Homo sapiens - Proteic Match RecName: Full=Putative uncharacterized protein LOC65996	-6..205	✘	OOF1		100.0	100.0	N/A
pB66_A-50	5p/3p	Homo sapiens - Proteic Match RecName: Full=Putative uncharacterized protein LOC65996	-6..205	✘	OOF1		100.0	100.0	N/A
pB66_A-73	5p/3p	Homo sapiens - Proteic Match RecName: Full=Putative uncharacterized protein LOC65996	-6..205	✘	OOF1		100.0	100.0	N/A
pB66_B-126	5p/3p	Homo sapiens - Proteic Match translocase of inner mitochondrial membrane 8 homolog A (yeast), isoform CRA_a	641..-105		??	N	98.6	99.2	N/A
pB66_B-129	5p/3p	Homo sapiens - SLC25A40	1537..2281	 ✘	OOF1		99.1	96.7	N/A
pB66_A-43	5p/3p	Homo sapiens - SLC25A40	1537..2281	 ✘	OOF1		99.6	98.3	N/A

pB66_A-59	5p/3p	Homo sapiens - SOX9	1829..2864  	OOF2		98.9	96.3	N/A
pB66_A-72	5p/3p	Homo sapiens - SPTAN1	486..1011	IF		100.0	100.0	
pB66_A-87	5p/3p	Homo sapiens - SPTAN1	3795..4562	IF		99.6	99.1	
pB66_A-5	5p/3p	Homo sapiens - SRGAP2	534..872	IF		99.7	99.7	
pB66_A-16	5p/3p	Homo sapiens - SRGAP2	534..872	IF		99.7	99.7	
pB66_A-51	5p/3p	Homo sapiens - SRGAP2	549..1153	IF		99.5	99.0	
pB66_A-20	5p/3p	Homo sapiens - SRGAP2	552..1013	IF		99.8	99.8	

Clone Name	Type Seq	Gene Name (Best Match)	Start..Stop (nt)	Frame	Sense	%Id 5p	%Id 3p	PBS
pB66_A-33	5p/3p	Homo sapiens - SRGAP2	552..1021	IF		99.6	99.6	
pB66_B-23	5p/3p	Homo sapiens - SUN1	1020..1526	IF		100.0	100.0	
pB66_A-47	5p/3p	Homo sapiens - SYNE2	15501..16057	IF		99.6	99.6	
pB66_A-62	5p/3p	Homo sapiens - TMPO	3622..3136 	??	N	59.5	100.0	N/A
pB66_B-100	5p/3p	Homo sapiens - TRIM2	4089..4607  	IF		100.0	99.8	N/A
pB66_A-38	5p/3p	Homo sapiens - TRIOBP	6381..6924	IF		99.8	99.8	
pB66_B-140	5p/3p	Homo sapiens - TULP4	4472..4739  	OOF2		100.0	100.0	N/A









pB66_A-68	5p/3p	Homo sapiens - WDR52	6856..7846  	OOF1		95.9	99.2	N/A
pB66_A-65	5p/3p	Homo sapiens - pleckstrin homology domain containing, family A (phosphoinositide binding specific) member 1 variant	1474..2306  	OOF1		99.0	86.7	N/A
pB66_A-55	5p/3p	Homo sapiens - GenMatch GID: 300116183	-1..1237 	IF		97.3	98.3	
pB66_B-22	5p	Homo sapiens - GenMatch GID: 300116183	6	IF		98.5		
pB66_A-46	5p/3p	Homo sapiens - GenMatch GID: 1621245	-1	IF		100.0	72.9	
pB66_A-32	5p/3p	Homo sapiens - GenMatch GID: 20087107	-1..812 	IF		100.0	98.6	
pB66_A-28	5p/3p	Homo sapiens - GenMatch GID: 16445199	-1..530 	IF		100.0	67.3	
pB66_A-21	5p/3p	Homo sapiens - GenMatch GID: 21165982	-1..1245 	IF		100.0	85.2	

pB66_A-14	5p/3p	Homo sapiens - GenMatch GID: 27436781	-1..1249	✘	IF		100.0	83.3	D
pB66_B-156	5p/3p	Homo sapiens - GenMatch GID: 11597140	-1..1088	✘	IF		98.3	100.0	D
pB66_B-151	5p/3p	Homo sapiens - GenMatch GID: 11121000	-1..592	✘	IF		100.0	100.0	D
pB66_B-10	5p/3p	Homo sapiens - GenMatch GID: 289177246	-1..1085	✘	IF		99.2	98.4	D
pB66_B-144	5p/3p	Homo sapiens - GenMatch GID: 14270149	-1..781	✘	IF		98.1	99.3	D
pB66_B-133	5p/3p	Homo sapiens - GenMatch GID: 29243147	-1..1081	✘	IF		96.1	100.0	D
pB66_B-132	5p/3p	Homo sapiens - GenMatch GID: 17985915	-1..573	✘	IF		99.8	100.0	D
pB66_B-130	5p/3p	Homo sapiens - GenMatch GID: 28394260	-1..306	✘	IF		100.0	100.0	D
pB66_B-128	5p/3p	Homo sapiens - GenMatch GID:	-1..939	✘	IF		96.9	96.7	D

		3132348							
pB66_B-127	5p/3p	Homo sapiens - GenMatch GID: 14669244	-1..1186	✘	IF		95.1	99.6	D
pB66_B-48	5p	Homo sapiens - GenMatch GID: 14669244	-1		IF		85.3		D
pB66_B-125	5p/3p	Homo sapiens - GenMatch GID: 21530897	-1..476	✘	IF		98.8	98.0	D
pB66_B-117	5p/3p	Homo sapiens - GenMatch GID: 27764209	-1..757	✘	IF		97.0	99.6	D
pB66_B-115	5p/3p	Homo sapiens - GenMatch GID: 13435199	-1..392	✘	IF		92.9	98.0	D
pB66_B-94	5p/3p	Homo sapiens - GenMatch GID: 10716638	-1..430	✘	IF		100.0	100.0	D
pB66_B-112	5p/3p	Homo sapiens - GenMatch GID: 10716638	-1..430	✘	IF		100.0	100.0	D
pB66_B-150	3p	Homo sapiens - GenMatch GID: 10716638	-1..430	✘	IF			100.0	D

Clone Name	Type Seq	Gene Name (Best Match)	Start..Stop (nt)	Frame	Sense	%Id 5p	%Id 3p	PBS
pB66_B-109	5p/3p	Homo sapiens - GenMatch GID: 3789713	-1..793 ×	IF		91.1	89.6	D
pB66_B-107	5p/3p	Homo sapiens - GenMatch GID: 28006935	-1..538 ×	IF		100.0	100.0	C
pB66_B-135	5p/3p	Homo sapiens - GenMatch GID: 28006935	3..774 ×	IF		99.9	99.0	C
pB66_B-106	5p/3p	Homo sapiens - GenMatch GID: 19071705	-1..1280 ×	IF		97.9	96.1	D
pB66_A-89	5p/3p	Homo sapiens - GenMatch GID: 19071705	1277..1096	??	N	98.3	98.3	N/A
pB66_B-103	5p/3p	Homo sapiens - GenMatch GID: 9713008	-1..1070 ×	IF		96.6	99.4	D
pB66_B-101	5p/3p	Homo sapiens - GenMatch GID: 29243376	-1..235 ×	IF		100.0	100.0	D
pB66_B-97	5p/3p	Homo sapiens - GenMatch GID:	-1..590 ×	IF		100.0	100.0	D

		18464324							
pB66_B-86	5p/3p	Homo sapiens - GenMatch GID: 13443261	-1..691	✘	IF		98.5	99.9	D
pB66_B-85	5p/3p	Homo sapiens - GenMatch GID: 4809347	-1..375	✘	IF		100.0	100.0	D
pB66_B-73	5p/3p	Homo sapiens - GenMatch GID: 2897864	-1..452	✘	IF		100.0	100.0	D
pB66_B-70	5p/3p	Homo sapiens - GenMatch GID: 13751950	-1..989	✘	IF		96.5	99.6	D
pB66_B-61	5p/3p	Homo sapiens - GenMatch GID: 4508112	-1..1079	✘	IF		98.4	99.9	D
pB66_B-60	5p/3p	Homo sapiens - GenMatch GID: 27413192	-1..901	✘	IF		99.2	99.9	D
pB66_B-47	5p/3p	Homo sapiens - GenMatch GID: 22531390	-1..197	✘	IF		100.0	100.0	D
pB66_B-20	5p/3p	Homo sapiens - GenMatch GID: 18464324	-1..1018	✘	IF		96.7	99.7	D

		4128007						
pB66_B-14	5p/3p	Homo sapiens - GenMatch GID: 9857582	-1..640	✘	IF		100.0	99.4 
pB66_B-122	5p/3p	Homo sapiens - GenMatch GID: 9857582	-1..947	✘	IF		100.0	77.8 
pB66_B-12	5p/3p	Homo sapiens - GenMatch GID: 16303557	-1..497	✘	IF		100.0	100.0 
pB66_B-11	5p/3p	Homo sapiens - GenMatch GID: 15145528	-1..451	✘	IF		97.6	97.6 
pB66_B-120	5p/3p	Homo sapiens - GenMatch GID: 15145528	-1..561	✘	IF		100.0	100.0 
pB66_B-9	5p/3p	Homo sapiens - GenMatch GID: 14277249	-1..623	✘	IF		99.8	99.8 
pB66_B-145	5p/3p	Homo sapiens - GenMatch GID: 55925155	-1..445	✘	IF		100.0	100.0 
pB66_B-8	5p/3p	Homo sapiens - GenMatch GID: 55925155	-1..445	✘	IF		100.0	100.0 

		55925155							
pB66_B-2	5p/3p	Homo sapiens - GenMatch GID: 15887284	-1..808	×	IF		98.7	99.6	D
pB66_B-1	5p/3p	Homo sapiens - GenMatch GID: 20066282	-1..1036	×	IF		99.1	100.0	D
pB66_A-74	5p/3p	Homo sapiens - GenMatch GID: 20377046	-1..349	×	IF		99.4	100.0	B
pB66_B-71	5p/3p	Homo sapiens - GenMatch GID: 20377046	9..349	×	IF		99.7	100.0	B
pB66_B-84	5p/3p	Homo sapiens - GenMatch GID: 20377046	9..349	×	IF		99.4	100.0	B
pB66_B-98	5p/3p	Homo sapiens - GenMatch GID: 20377046	9..349	×	IF		99.4	100.0	B

Clone Name	Type Seq	Gene Name (Best Match)	Start..Stop (nt)	Frame	Sense	%Id 5p	%Id 3p	PBS	
pB66_A-71	5p/3p	Homo sapiens - GenMatch GID:	-1..836	×	IF		96.7	98.5	D

		24796735							
pB66_A-67	5p/3p	Homo sapiens - GenMatch GID: 22417440	-1..374	✘	IF		94.3	54.6	B
pB66_B-143	5p/3p	Homo sapiens - GenMatch GID: 22417440	-1..703	✘	IF		93.9	54.3	B
pB66_A-92	5p/3p	Homo sapiens - GenMatch GID: 22417440	535..892	✘	OOF1		100.0	100.0	B
pB66_A-64	5p/3p	Homo sapiens - GenMatch GID: 22417440	550..1320	✘	OOF1		84.7	94.9	B
pB66_B-153	5p/3p	Homo sapiens - GenMatch GID: 11067121	-1		IF		100.0	65.0	D
pB66_B-81	5p/3p	Homo sapiens - GenMatch GID: 14916216	-1..869	✘	IF		98.9	99.7	D
pB66_A-61	5p/3p	Homo sapiens - GenMatch GID: 14916216	-1..869	✘	IF		99.2	100.0	D
pB66_A-79	3p	Homo sapiens - GenMatch GID:	..869		??			99.6	D

		14916216						
pB66_A-58	5p/3p	Homo sapiens - GenMatch GID: 20486432	-1..332	✘	IF		100.0	100.0 D
pB66_B-114	5p/3p	Homo sapiens - GenMatch GID: 14718390	-1..1182	✘	IF		95.5	99.3 D
pB66_A-57	5p/3p	Homo sapiens - GenMatch GID: 14718390	-1..403	✘	IF		100.0	100.0 D
pB66_A-82	5p/3p	Homo sapiens - GenMatch GID: 14718390	-1..1182	✘	IF		92.2	99.6 D
pB66_B-139	5p/3p	Homo sapiens - GenMatch GID: 3688077	-1..558	✘	IF		100.0	94.3 D
pB66_B-138	5p/3p	Homo sapiens - GenMatch GID: 28144489	-1..503	✘	IF		100.0	82.2 D
pB66_B-136	5p	Homo sapiens - GenMatch GID: 25446596	-2..460	✘	IF		100.0	D
pB66_B-131	5p	Homo sapiens - GenMatch GID:	-1		IF		100.0	D

		157074332							
pB66_B-121	5p/3p	Homo sapiens - GenMatch GID: 26892320	-1..805	✘	IF		100.0	97.3	D
pB66_A-48	5p/3p	Homo sapiens - GenMatch GID: 28827889	-1..260	✘	IF		100.0	100.0	E
pB66_A-88	5p/3p	Homo sapiens - GenMatch GID: 28827889	-1..260	✘	IF		100.0	100.0	E
pB66_A-54	5p/3p	Homo sapiens - GenMatch GID: 17530779	-1..1051	✘	IF		97.7	71.7	D
pB66_A-45	5p/3p	Homo sapiens - GenMatch GID: 17530779	-1..1051	✘	IF		96.2	70.9	D
pB66_A-8	5p/3p	Homo sapiens - GenMatch GID: 16973212	-1..730	✘	IF		97.0	97.0	D
pB66_A-6	5p/3p	Homo sapiens - GenMatch GID: 4926893	-1..944	✘	IF		98.4	99.9	D
pB66_A-35	5p/3p	Homo sapiens - GenMatch GID:	-1..618	✘	IF		100.0	99.8	D

		29029215							
pB66_A-34	5p/3p	Homo sapiens - GenMatch GID: 14010934	-1..562	✘	IF		100.0	99.8	D
pB66_B-111	5p/3p	Homo sapiens - GenMatch GID: 60391308	-1..121	✘	IF		100.0	77.9	D
pB66_B-157	5p/3p	Homo sapiens - GenMatch GID: 24111040	-1..685	✘	IF		95.6	95.3	D
pB66_B-154	5p/3p	Homo sapiens - GenMatch GID: 24111040	945..92		??	N	97.6	59.8	N/A
pB66_B-95	5p/3p	Homo sapiens - GenMatch GID: 18997213	-1..752	✘	IF		100.0	97.3	D
Clone Name	Type Seq	Gene Name (Best Match)	Start..Stop (nt)		Frame	Sense	%Id 5p	%Id 3p	PBS
pB66_B-83	5p/3p	Homo sapiens - GenMatch GID: 5454237	-1..1264	✘	IF		100.0	75.4	D
pB66_B-74	5p/3p	Homo sapiens - GenMatch GID: 29124050	-1..1264	✘	IF		100.0	70.2	D

pB66_A-26	5p/3p	Homo sapiens - GenMatch GID: 14010905	-1..1180	✘	IF		95.8	99.7	D
pB66_A-25	5p/3p	Homo sapiens - GenMatch GID: 21263157	-1..725	✘	IF		100.0	98.3	D
pB66_A-63	5p/3p	Homo sapiens - GenMatch GID: 21263157	-1..725	✘	IF		98.8	96.6	D
pB66_A-23	5p/3p	Homo sapiens - GenMatch GID: 2133862	-1..395	✘	IF		100.0	99.7	D
pB66_B-124	5p/3p	Homo sapiens - GenMatch GID: 5918011	-1..498	✘	IF		100.0	100.0	D
pB66_A-22	5p/3p	Homo sapiens - GenMatch GID: 5918011	-1..498	✘	IF		100.0	100.0	D
pB66_A-13	5p/3p	Homo sapiens - GenMatch GID: 11386322	-1..380	✘	IF		100.0	100.0	E
pB66_A-78	3p	Homo sapiens - GenMatch GID: 11386322	-1..380	✘	IF			100.0	E

pB66_A-11	5p/3p	Homo sapiens - GenMatch GID: 21217405	-1..448	✘	IF		100.0	100.0	D
pB66_B-59	5p/3p	Homo sapiens - GenMatch GID: 14670071	-1..1283	✘	IF		100.0	89.8	D
pB66_A-10	5p/3p	Homo sapiens - GenMatch GID: 23343644	-1..444	✘	IF		100.0	100.0	D
pB66_B-32	5p/3p	Homo sapiens - GenMatch GID: 254939586	-1..1331	✘	IF		100.0	89.9	D
pB66_A-94	5p/3p	Homo sapiens - GenMatch GID: 12584366	-1..1006	✘	IF		100.0	79.8	D
pB66_A-60	5p/3p	Homo sapiens - unknown GID: 31874075	3185..4469	✘	OOF2		82.1	92.9	N/A
pB66_B-105	5p/3p	Homo sapiens - unknown GID: 31874075	3185..4469	✘	OOF2		90.3	99.9	N/A
pB66_A-3	5p/3p	Homo sapiens - unknown GID: 50505696	199..1161	✘	OOF1		98.9	98.8	N/A

pB66_A-18	5p/3p	Homo sapiens - unknown GID: 50505696	199..1161	✘	OOF1		98.4	84.7	N/A
pB66_A-17	5p/3p	Homo sapiens - unknown GID: 50505696	223..1064	✘	OOF1		98.5	98.8	N/A
pB66_A-15	5p/3p	Homo sapiens - unknown GID: 50505696	223..1064	✘	OOF1		97.5	97.7	N/A
pB66_B-119	5p/3p	Homo sapiens - unknown GID: 21756253	2675..2203		??	N	100.0	100.0	N/A
pB66_B-134	5p/3p	Homo sapiens - unnamed protein product	1185..314		??	N	99.8	100.0	N/A

